

Dynamic Stability of Suddenly Loaded Structures

@Seismicisolation

George J. Simitses

Dynamic Stability of Suddenly Loaded Structures

With 120 Figures



Springer-Verlag New York Berlin Heidelberg
London Paris Tokyo Hong Kong

@Seismicisolation

George J. Simitses
School of Aerospace Engineering
Georgia Institute of Technology
Atlanta, GA 30332
USA

Current address
George J. Simitses
Department of Aerospace Engineering
and Engineering Mechanics
University of Cincinnati
Cincinnati, OH 45221
USA

Library of Congress Cataloging-in-Publication Data
Simitses, George J., 1932-

Dynamic stability of suddenly loaded structures/George J. Simitses.

p. cm.

Includes bibliographies and index.

ISBN-13:978-1-4612-7932-7

1. Structural dynamics. 2. Structural stability. 3. Buckling
(Mechanics) I. Title.

TA654.S56 1989

624.1'7—dc20

89-32860

© 1990 by Springer-Verlag New York Inc.

Softcover reprint of the hardcover 1st edition 1990

All rights reserved. This work may not be translated or copied in whole or in part without the written permission of the publisher (Springer-Verlag, 175 Fifth Avenue, New York, NY 10010, USA), except for brief excerpts in connection with reviews or scholarly analysis. Use in connection with any form of information storage and retrieval, electronic adaptation, computer software, or by similar or dissimilar methodology now known or hereafter developed is forbidden.

The use of general descriptive names, trade names, trademarks, etc. in this publication, even if the former are not especially identified, is not to be taken as a sign that such names, as understood by the Trade Marks and Merchandise Marks Act, may accordingly be used freely by anyone.

Typeset by Thomson Press (India) Limited, New Delhi.

9 8 7 6 5 4 3 2 1

ISBN-13:978-1-4612-7932-7 e-ISBN-13:978-1-4612-3244-5

DOI: 10.1007/978-1-4612-3244-5

@Seismicisolation

Preface

Dynamic instability or dynamic buckling as applied to structures is a term that has been used to describe many classes of problems and many physical phenomena. It is not surprising, then, that the term finds several uses and interpretations among structural mechanicians. Problems of parametric resonance, follower-force, whirling of rotating shafts, fluid–solid interaction, general response of structures to dynamic loads, and several others are all classified under dynamic instability. Many analytical and experimental studies of such problems can be found in several books as either specialized topics or the main theme. Two such classes, parametric resonance and stability of nonconservative systems under static loads (follower-force problems), form the main theme of two books by V.V. Bolotin, which have been translated from Russian. Moreover, treatment of aeroelastic instabilities can be found in several textbooks. Finally, analytical and experimental studies of structural elements and systems subjected to intense loads (of very short duration) are the focus of the recent monograph by Lindberg and Florence.

The first chapter attempts to classify the various “dynamic instability” phenomena by taking into consideration the nature of the cause, the character of the response, and the history of the problem. Moreover, the various concepts and methodologies as developed and used by the various investigators for estimating critical conditions for suddenly loaded elastic systems are fully described.

Chapter 2 demonstrates the concepts and criteria for dynamic stability through simple mechanical models with one and two degrees of freedom. The emphasis here is on loads applied suddenly with constant magnitude and infinite duration or extremely small duration (ideal impulse).

The concepts and methodologies are extended in Chapter 3 for the more general case of constant load of finite duration, and they are also demonstrated through the same simple mechanical models used in Chapter 2.

The influence of static preloading is fully assessed in Chapter 4, and the proper modification of the methodology for estimating critical conditions is described.

Chapters 5 through 10 deal with applications to structural elements and

systems such as the two-bar simple frame, the shallow arch, the shallow spherical cap, the thin cylindrical shell of various constructions (metallic with and without stiffening and laminated composite), and finally beams and bars. Chapter 5 extends the concept of dynamic instability to the continuum, and the remaining chapters cover strictly the applications. For each configuration discussed, a fairly complete bibliography is presented. Finally, some specialized topics are presented in three appendices for the sake of self-containment. Appendix A discusses parametric resonance with applications to a simple mechanical model and the Euler column. Appendix B presents a brief treatise on brachistochrone problems, and Appendix C deals with the influence of small damping on the critical conditions under sudden application of the loads. This is demonstrated through application to the one- and two-degree-of-freedom models treated in Chapter 2.

At the end of the first few chapters are several suggested problems to be assigned when the book is used as a text.

Having had the experience of publishing another text before this one, I expect that several misprints and errors will be present in the book. I welcome notification of such errors from the readers and users of the monograph. Errata sheets will be forwarded periodically to those who request them.

I wish to express my gratitude to Professor William Nachbar for introducing me to the field of dynamic buckling. The many discussions on the subject with Professor Nicholas J. Hoff are gratefully acknowledged. Special thanks are due to my coworkers, research collaborators, and former students, who made substantial contributions that can be found in different chapters. This book could not be possible without the help of Dr. Charles M. Blackmon, Dr. Jaganath Giri, Professor Antonios N. Kounadis, Professor Izhak Sheinman, Dr. Costas Lazopoulos, and Dr. Dein Shaw. Special thanks are due to the Georgia Tech Foundation for providing tangible support toward the completion of the project. Mrs. Vivian Tucker, Mrs. Betty Mitchell, Mrs. Martha Young, and Mrs. Julia Roach worked with great dedication in typing the manuscript.

Cincinnati, Ohio

George J. Simitses

Contents

Preface	v
-------------------	---

Part I *Concepts and Criteria*

CHAPTER 1 Introduction and Fundamental Concepts	3
CHAPTER 2 Simple Mechanical Models	24
CHAPTER 3 Dynamic Stability Under Constant Load of Finite Duration.	54
CHAPTER 4 The Influence of Static Preloading	68

Part II *Structural Applications*

CHAPTER 5 The Concept of Dynamic Stability	95
CHAPTER 6 Two-Bar Simple Frames	101
CHAPTER 7 The Shallow Arch.	117
CHAPTER 8 The Shallow Spherical Cap	154
CHAPTER 9 Thin Cylindrical Shells	176
CHAPTER 10 Other Structural Systems	245

APPENDIX A	
Parametric Resonance	260
APPENDIX B	
Brachistochrone Problems.	269
APPENDIX C	
The Influence of Small Damping	274
Index	289

Part I Concepts and Criteria

1

Introduction and Fundamental Concepts

1.1 Dynamic Stability

Dynamic stability or instability of elastic structures has drawn considerable attention in the past 30 years. The beginning of the subject can be traced to the investigation of Koning and Taub [1], who considered the response of an imperfect (half-sine wave), simply supported column subjected to a sudden axial load of specified duration. Since then, many studies have been conducted by various investigators on structural systems that are either suddenly loaded or subjected to time-dependent loads (periodic or nonperiodic), and several attempts have been made to find common response features and to define critical conditions for these systems. As a result of this, the term *dynamic stability* encompasses many classes of problems and many different physical phenomena; in some instances the term is used for two distinctly different responses for the same configuration subjected to the same dynamic loads. Therefore, it is not surprising that there exist several uses and interpretations of the term.

In general, problems that deal with the stability of motion have concerned researchers for many years in many fields of engineering. Definitions for stability and for the related criteria and estimates of critical conditions as developed through the years are given by Stoker [2]. In particular, the contributions of Thompson and Tait [3] and Routh [4] deserve particular attention. Some of these criteria find wide uses in problems of control theory [5], of stability and control of aircraft [6], and in other areas [7].

The class of problems falling in the category of parametric excitation, or parametric resonance, includes the best defined, conceived, and understood problems of dynamic stability. An excellent treatment and bibliography can be found in the book by Bolotin [8]. Another reference on the subject is Stoker's book [9]. More details and references are given in Appendix A.

The problem of parametric excitation is best defined in terms of an example. Consider an Euler column, which is loaded at one end by a periodic axial force. The other end is immovable. It can be shown that, for certain relationships between the exciting frequency and the column natural frequency of transverse vibration, transverse vibrations occur with rapidly

increasing amplitudes. This is called parametric resonance and the system is said to be dynamically unstable. Moreover, the loading is called parametric excitation.

Other examples of parametric resonance include (1) a thin flat plate parametrically loaded by in-plane forces, which may cause transverse plate vibrations; (2) parametrically loaded shallow arches (symmetric loading), which under certain conditions vibrate asymmetrically with increasing amplitude; and (3) long cylindrical, thin shells (or thin rings) under uniform but periodically applied pressure, which can excite vibrations in an asymmetric mode. Thus, it is seen that, in parametric excitation, the loading is parametric with respect to certain deformation forms. This makes parametric resonance different from the usual forced vibration resonance. In addition, from these few examples of parametric excitation, one realizes that systems that exhibit bifurcational buckling under static conditions (regardless of whether the bifurcating static equilibrium branch is stable or unstable) are subject to parametric excitation. More details are presented in Appendix A.

Moreover, there exists a large class of problems for which the load is applied statically but the system is nonconservative. An elastic system is conservative when subjected to conservative loads [10]; the reader is also referred to Ziegler's book [11] for a classification of loads and reactions. An excellent review on the subject of stability of elastic systems under nonconservative forces is given by Herrmann [12]. He classifies all problems of nonconservative systems into three groups. The first group deals with follower-force problems, the second with problems of rotating shafts (whirling), and the third with aeroelasticity (fluid–solid interaction; flutter). All of these groups, justifiably or not, are called problems of dynamic stability. In the opinion of the author, justification is needed only for the first group. Ziegler [13] has shown that critical conditions for this group of nonconservative systems can be obtained only through the use of the dynamic or kinetic approach to stability problems. The question of applicability of the particular approach was clearly presented by Herrmann and Bungay [14] through a two-degree-of-freedom model. They showed that in some nonconservative systems, there exist two instability mechanisms, one of divergence (large deflections may occur) and one of flutter (oscillations of increasing amplitude). They further showed that the critical load for which the flutter type of instability occurs can be determined only through the kinetic approach, while the divergence type of critical load can be determined by employing any one of the three approaches (classical, potential energy, or kinetic [10]). It is understandable, then, why many authors refer to problems of follower-forced systems as dynamic stability problems. Furthermore, the problem of flow-induced vibrations in elastic pipes is another fluid–solid interaction problem that falls under the general heading of dynamic stability. The establishment of stability concepts, as well as of estimates for critical conditions, is an area of great practical importance. A few references [15–29]

are provided for the interested reader. In addition, a few studies have been reported that deal with the phenomenon of parametric resonance in a fluid–structure interaction problem [30–33]. For completeness, one should refer to a few studies of aeroelastic flutter [34–38].

Finally, a large class of structural problems that has received considerable attention and does qualify as a category of dynamic stability is that of impulsively loaded configurations and configurations that are suddenly loaded with loads of constant magnitude and infinite duration. These configurations under static loading are subject to either limit point instability or bifurcational instability with an unstable postbuckling branch (violent buckling). The two types of loads may be thought of as mathematical idealizations of blast loads of (1) large decay rates and small decay times and (2) small decay rates and large decay times, respectively. For these loads, the concept of dynamic stability is related to the observation that for sufficiently small values of the loading, the system simply oscillates about the near static equilibrium point and the corresponding amplitudes of oscillation are sufficiently small. If the loading is increased, some systems will experience large-amplitude oscillations or, in general, a divergent type of motion. For this phenomenon to happen, the configuration must possess two or more static equilibrium positions, and escaping motion occurs by having trajectories that can pass near an unstable static equilibrium point. Consequently, the methodologies developed by the various investigators are for structural configurations that exhibit snap-through buckling when loaded quasi-statically.

Solutions to such problems started appearing in the open literature in the early 1950s. Hoff and Bruce [39] considered the dynamic stability of a pinned half-sine arch under a half-sine distributed load. Budiansky and Roth [40], in studying the axisymmetric behavior of a shallow spherical cap under suddenly applied loads, defined the load to be critical when the transient response increases suddenly with very little increase in the magnitude of the load. This concept was adopted by numerous investigators [41–48] in subsequent years, because it is tractable to computer solutions. Finally, the concept was generalized in a paper by Budiansky [44] in attempting to predict critical conditions for imperfection-sensitive structures under time-dependent loads.

Conceptually, one of the best efforts in the area of dynamic buckling under suddenly applied loads is the work of Hsu and his collaborators [45–49]. Hsu defined sufficiency conditions for stability and sufficiency conditions for instability, thus finding upper and lower bounds for the critical impulse or critical sudden load. Independently, Simitses [50], in dealing with the dynamic buckling of shallow arches and spherical caps, termed the lower bound a minimum possible critical load (MPCL) and the upper bound a minimum guaranteed critical load (MGCL). Some interesting comments on dynamic stability are given by Hoff [51]. Finally, Thompson [52] presented a criterion for estimating critical conditions for suddenly loaded systems.

The totality of concepts and methodologies used by the various investigators in estimating critical conditions for suddenly loaded elastic systems (of the last category) can be classified in the following three groups:

1. Equations of motion approach (Budiansky–Roth [40]). The equations of motion are (numerically) solved for various values of the load parameter (ideal impulse, or sudden load), thus obtaining the system response. The load parameter at which there exists a large (finite) change in the response is called critical.
2. Total energy–phase plane approach (Hoff–Hsu [45–49]). Critical conditions are related to characteristics of the system’s phase plane, and the emphasis is on establishing sufficient conditions for stability (lower bounds) and sufficient conditions for instability (upper bounds).
3. Total potential energy approach (Hoff–Simitses [50]). Critical conditions are related to characteristics of the system’s total potential. Through this approach also, lower and upper bounds of critical conditions are established. This last approach is applicable to conservative systems only. The concepts and procedure related to the last approach are explained next in some detail.

1.2 The Total Potential Energy Approach: Concepts and Procedure

The concept of dynamic stability is best explained through a single-degree-of-freedom system. First, the case of ideal impulse is treated and then the case of constant load of infinite duration.

1.2.1 Ideal Impulse

Consider a single-degree-of-freedom system for which the total potential (under zero load) curve is plotted versus the generalized coordinate (independent variable) (see Figure 1.1). Clearly, points *A*, *B*, *C* denote static equilibrium points and point *B* denotes the initial position ($\theta = 0$) of the system.

Since the system is conservative, the sum of the total potential \bar{U}_T^0 (under “zero” load) and the kinetic energy T^0 is a constant C , or

$$\bar{U}_T^0 + T^0 = C. \quad (1)$$

Moreover (see Figure 1.1), since \bar{U}_T^0 is zero at the initial position ($\theta = 0$), the constant C can be related to some initial kinetic energy T_i^0 . Then

$$\bar{U}_T^0 + T^0 = T_i^0. \quad (2)$$

Next, consider an ideal impulse applied to the system. Through the

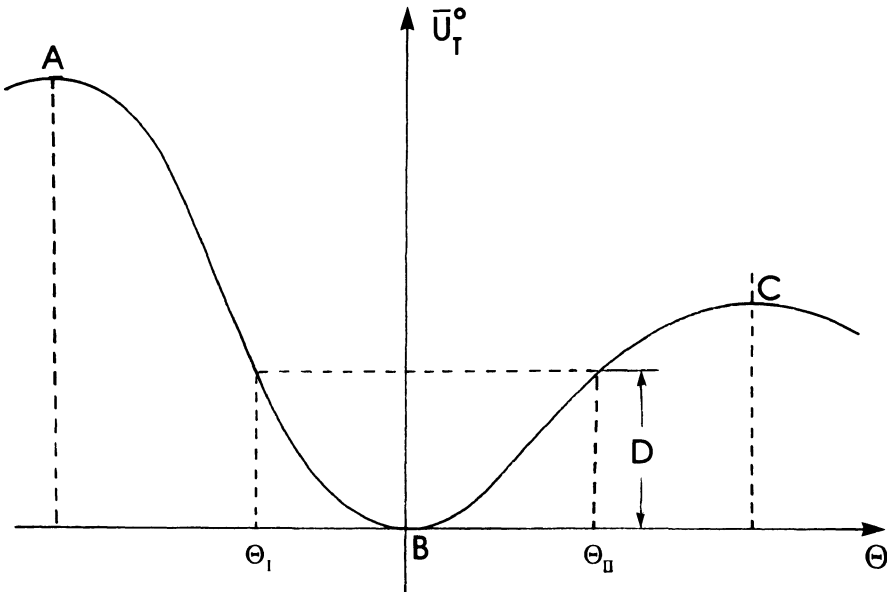


FIGURE 1.1. Total potential curve (zero load, one degree of freedom).

impulse-momentum theorem, the impulse is related to the initial kinetic energy T_i^0 . Clearly, if T_i^0 is equal to D (see Figure 1.1) or $\bar{U}_T^0(\Theta_{II})$, the system will simply oscillate between Θ_I and Θ_{II} . On the other hand, if the initial kinetic energy T_i^0 is equal to the value of the total potential at the unstable static equilibrium point C , $\bar{U}_T^0(C)$, then the system can reach point C with zero velocity ($T^0 = 0$), and there exists a possibility of motion escaping (passing position C) or becoming unbounded. Such a motion is termed *buckled motion*. In the case for which motion is bounded and the path may include the initial point (B), the motion is termed *unbuckled motion*.

Through this, a concept of dynamic stability is presented and the necessary steps for estimating critical impulses are suggested. Note that once the unstable static equilibrium positions (points A and C) are established, the critical initial kinetic energy is estimated by

$$T_{i_{cr}}^0 = \bar{U}_T^0(C). \quad (3)$$

Moreover, since T_i^0 is related to the ideal impulse, the critical impulse is estimated through eq. (3). Observe that an instability of this type can occur only when the system, under zero load, possesses unstable static equilibrium points. Furthermore, if position C corresponds to a very large and thus unacceptable position θ (from physical considerations), one may still use this concept and estimate a maximum allowable (and therefore critical) ideal impulse. For instance, if one restricts motion to the region between Θ_I and Θ_{II} , the maximum allowable ideal impulse is obtained from eq. (3), but with

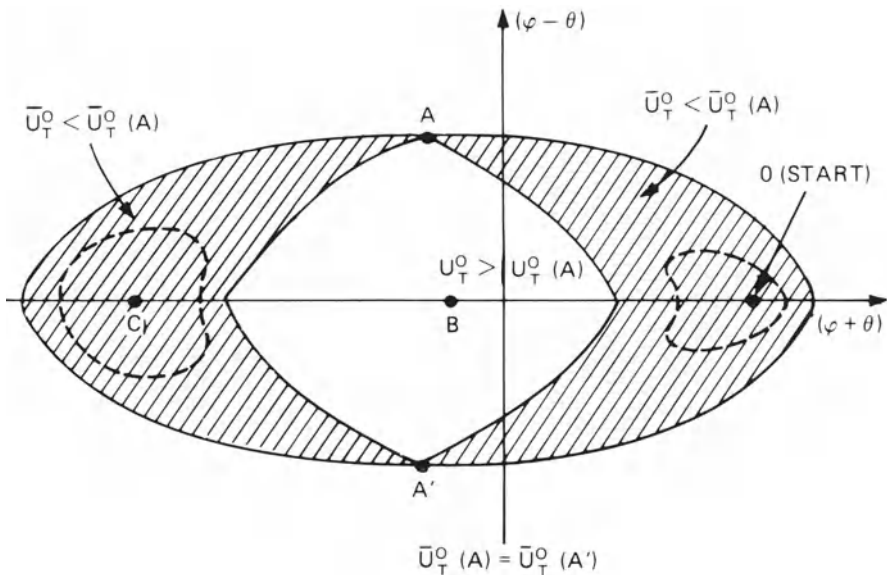


FIGURE 1.2. Curves of constant total potential (zero load, two degrees of freedom).

D or $\bar{U}_T^0(\Theta_{II})$ replacing $\bar{U}_T^0(C)$. Because of this, a critical or an allowable ideal impulse can be obtained for all systems (including those that are not subject to buckling under static conditions such as beams, shafts, etc.).

A similar situation exists for a two-degree-of-freedom system. Figure 1.2 depicts curves of total potential lines corresponding to the value of the total potential at points A and A' , in the space of $(\phi + \theta)$ and $(\phi - \theta)$. Note that ϕ and θ denote the two generalized coordinates. The total potential curves are typical for the mechanical model shown in Figure 1.3. Further, note that $\phi = 0$ denotes symmetric behavior (this model is analyzed in detail in a later section). Returning to Figure 1.2, points O , A , A' , B , and C denote static equilibrium under zero load. The value of the total potential in the shaded area is smaller than the value of the total potential at points A and A' . Everywhere else the total potential is larger than that at points A and A' .

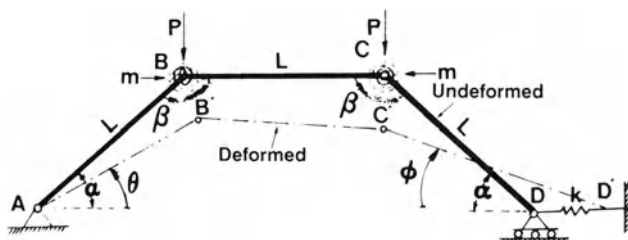


FIGURE 1.3. A two-degree-of-freedom mechanical model (rigid bars).

Positions O and C correspond to stable static equilibrium positions, while positions A and A' (saddle points) and B correspond to unstable ones. Point O is the starting or natural unloaded position.

Here also, as in the case of the one-degree-of-freedom system, the work done by the ideal impulsive load is imparted into the system instantaneously as initial kinetic energy. Through the impulse–momentum theorem, the ideal impulse can be related to the initial kinetic energy. For small values of the initial kinetic energy, motion is confined to some small area surrounding the starting (stable) static point, O . In this case, there is no possibility of buckled motion. If the kinetic energy value is equal to the value of the total potential at point A (or A'), then there exists a possibility of the system reaching either position A or A' with zero kinetic energy and motion to take place toward point C (buckled motion). Note that if the value of the initial kinetic energy is equal to the value of the total potential at the unstable static position B (top of the hill), $U_T^0(B)$, then motion toward the far stable position C (buckled) is guaranteed. Thus, in the first case a possibility of escaping motion exists, while in the latter case escaping motion is guaranteed.

On the basis of the above explanations for both systems, the following definitions may now be given:

Possible locus or path. A possible locus or path on the total potential surface is one that corresponds at every point of the locus or path to a nonnegative kinetic energy.

Unbuckled motion. Unbuckled motion of the system is defined as any possible locus or path on the total potential surface that passes through or completely encloses only the near equilibrium point.

Note that for the case of the ideal impulse, the near static equilibrium point is also the starting point.

Buckled motion. If the possible locus or path passes through or encloses other static equilibrium points (stable or unstable), then the motion is defined as buckled.

Note that buckled motion may also be referred to as escaping motion, and the phenomenon as dynamic snap-through buckling.

Minimum possible critical load (MPCL). The least upper bound of loads for which all possible loci correspond only to unbuckled motion. At the MPCL there exists at least one possible locus on the potential surface that the structure can follow to dynamically snap-through.

Note that Hsu [45–49] refers to this bound as a sufficiency condition for stability (dynamic).

Minimum guaranteed critical load (MGCL). The greatest lower bound of loads for which no possible loci correspond to unbuckled motion.

Note that, in this case, dynamic snap-through will definitely happen. This bound is termed by Hsu a sufficiency condition for instability (dynamic).

From the above definitions, it is evident that for one-degree-of-freedom systems, the two critical loads are coincident. On the other hand, for

multi-degree-of-freedom systems, the critical load can only be bracketed between an upper bound (MGCL) and a lower bound (MPCL).

These concepts are applied to continuous structural systems in later sections.

One final comment for the case of ideal impulse: Note from Figure 1.1, in the absence of damping (as assumed), the direction of the ideal impulse is immaterial. If the system is loaded in one direction (say that the resulting motion corresponds to positive θ), then a critical condition exists when the system reaches position C with zero kinetic energy. If the system is loaded in the opposite direction, then some negative position will be reached with zero kinetic energy; after that the direction of the motion will reverse, and finally the system will reach position C with zero kinetic energy. Both of these phenomena occur for the same value of the ideal impulse. This is also true for the two-degree-of-freedom system (see Figures 1.2 and 1.3). The critical load (ideal impulse) is not affected by the direction of the loading. (Starting at point O , the system will initially move along the $\theta + \phi$ axis, to the right or to the left.)

1.2.2 Constant Load of Infinite Duration

Consider again a single-degree-of-freedom system. Total potential curves are plotted versus the generalized coordinate on Figure 1.4. Note that the various curves correspond to different load values P_i . The index i varies from 1 to 5, and the magnitude of the load increases with increasing index value. These curves are typical of systems that, for each load value, contain at least two static equilibrium points A_i and B_i . This is the case when the system is subject to limit point instability and/or bifurcational buckling with unstable branching, under static application of the load (shallow arches and spherical caps, perfect or imperfect cylindrical and spherical shells, two-bar frames, etc.).

Given such a system, one applies a given load suddenly with constant magnitude and infinite duration. For a conservative system,

$$\bar{U}_T^P + T^P = C. \quad (4)$$

The potential may be defined in such a way that it is zero at the initial position ($\theta = 0$). In such a case, the constant is zero, or

$$\bar{U}_T^P + T^P = 0. \quad (5)$$

Since the kinetic energy is a positive definite function of the generalized velocity, motion is possible when the total potential is nonpositive (shaded area, in Figure 1.4, for P_2). From this it is clear that for small values of the applied load, the system simply oscillates about the near static equilibrium position (point A_2). This is also an observed physical phenomenon. As the load increases, the total potential at the unstable point B_i decreases, it becomes zero (point B_3), and then it increases negatively until points A_i and

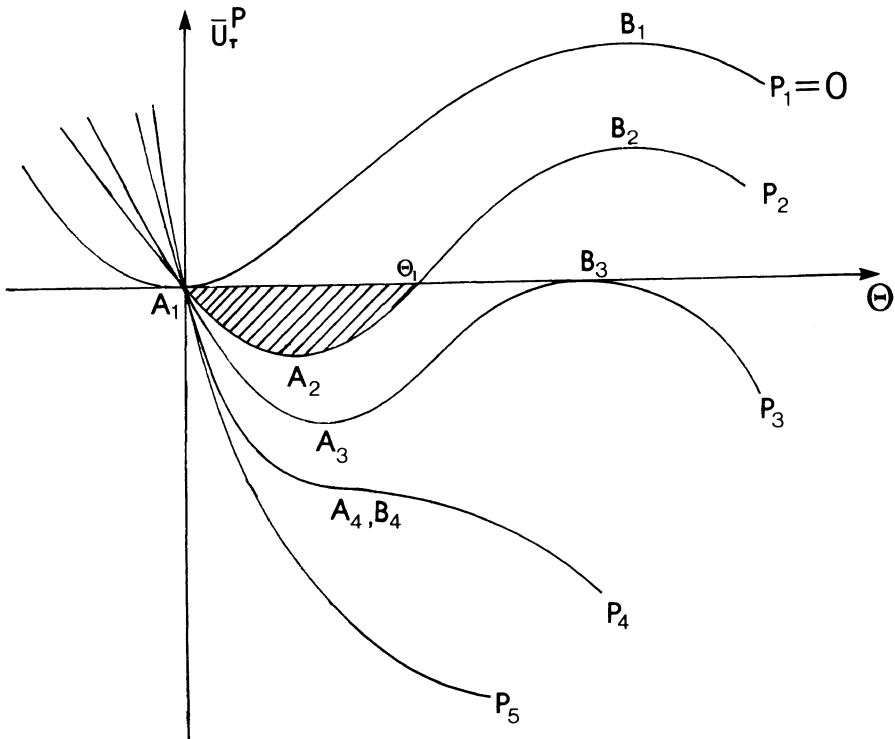


FIGURE 1.4. Total potential curves (one degree of freedom).

B_i (A_4, B_4) coincide (the corresponding load P_4 denotes the limit point under static loading). For loads higher than this (P_4), the stationary points (static equilibrium positions) disappear from the neighborhood. When the sudden load reaches the value corresponding to P_3 , a critical condition exists, because the system can reach position B_3 with zero kinetic energy and then move toward larger θ values (buckled motion can occur). Thus, P_3 is a measure of the critical condition. Note that the value of P_3 is smaller than the value of the limit point P_4 . This implies that the critical load under sudden application (infinite duration) is smaller than the corresponding static critical load.

In this case, also, one may wish to limit the dynamic response of the system to a value smaller than B_3 (see Figure 1.4), say, Θ_1 . Then in such a case, the maximum allowable and consequently the critical dynamic load is denoted by P_2 .

As in the case of the ideal impulse, for systems of two or more degrees of freedom, upper and lower bounds of critical conditions can be established.

Figure 1.5 shows typical constant-potential (zero) lines in the space of the generalized coordinates $\phi + \theta$ and $\phi - \theta$ (see Figure 1.3). In this case, the total potential is defined such that the constant in eq. (4) is zero (in the

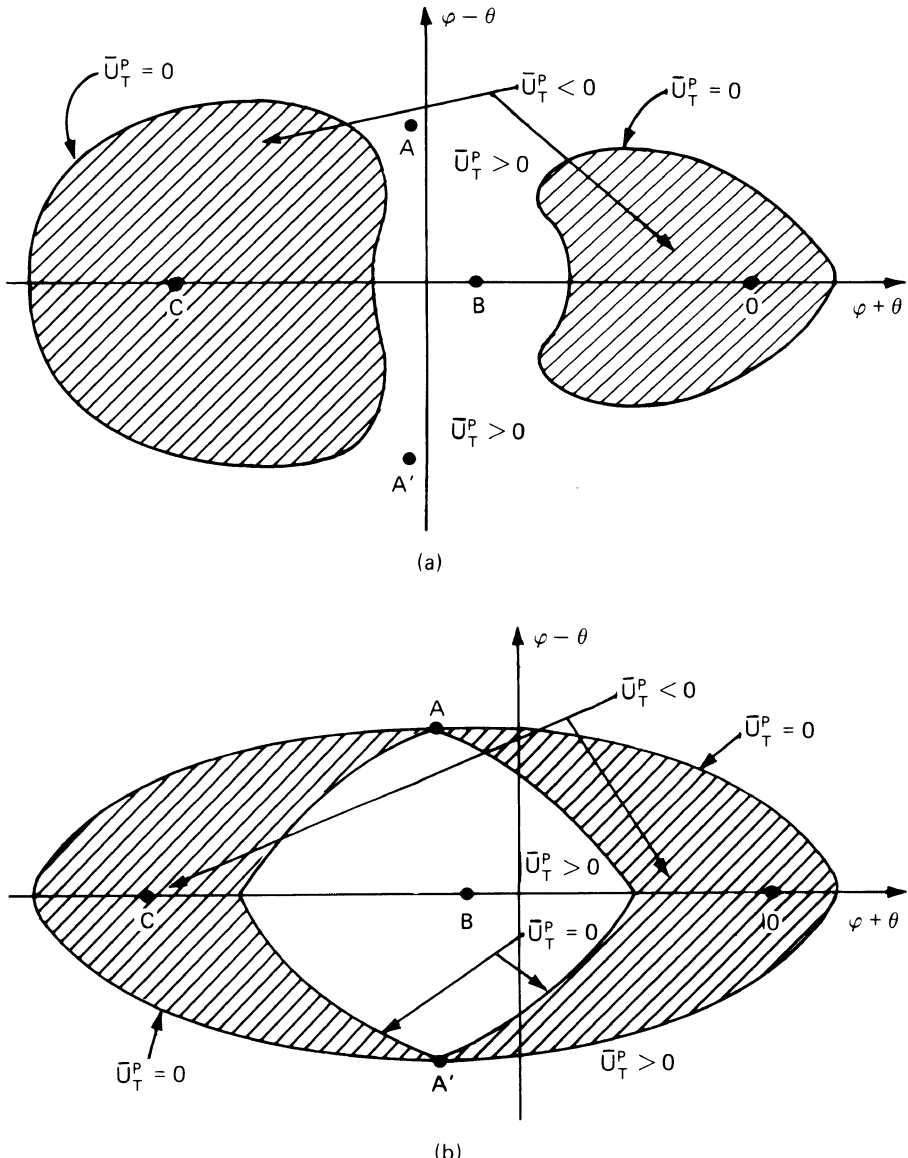


FIGURE 1.5. Curves of constant (zero) total potential (two degrees of freedom). (a) $|P_I| < |P_{cr_\infty}|$ (MPCL). (b) $|P_{II}| > |P_I|$, $P_{II} = P_{cr_\infty}$ (MPCL).

absence of initial kinetic energy). Points O , A , A' , B , and C denote the same static equilibrium positions as in Figure 1.2. Note that in the shaded areas the total potential is nonpositive, and everywhere else the total potential is nonnegative. In Figure 1.5a, the motion is confined to the shaded area enclosing point O (starting point) and the motion is unbuckled. As the value of the load increases, the value of the total potential at A and A' continuously

decreases until it becomes zero at load P_{II} (Figure 1.5b). At this load the system can possibly snap-through toward the far equilibrium position C and either oscillate about C or return to region (OAA') and oscillate about O , and so on. Load P_{II} denotes the lower bound for a critical condition (MPLC) because there exists at least one path through which the system can reach position A or A' with zero kinetic energy and possibly escape toward (snap-through) position C . As the value of the applied load is further increased, buckled motion will always occur at some value P_{III} (larger than P_{II}). This load denotes the upper bound. The system shown on Figure 1.3 is analyzed in detail in a later section. For this load case also, the concepts of dynamic stability are applied to continuous structural systems in later sections.

Moreover, these concepts and the related methodologies for estimating critical conditions are modified and applied to the case of suddenly loaded systems with constant loads of finite duration. These modifications are also presented in a later section. In addition, since most structural configurations, in service, are subject to static loads, the effect of static preloading on the critical dynamic conditions is presented by similar concepts. An example of this would be a submarine resting at a depth of 1,000 feet (static preloading) and subjected to a blast loading (dynamic) of small decay rate and large decay time (sudden load of constant magnitude and infinite duration).

1.3 Extension of the Dynamic Stability Concept

The concept of dynamic stability, discussed in the previous section, is developed primarily for structural configurations that are subject to violent buckling under static loading. It is also observed that the concept can be extended, even for these systems, when one limits the maximum allowable deflection resulting from the sudden loads. This being the case, then, the extended and modified concept can be used for all structural configurations (at least in theory).

This is demonstrated in this section through a simple model. First, though, some clarifying remarks are in order.

All structural configurations, when acted on by quasi-static loads, respond in a manner described in one of Figures 1.6 to 1.10. These figures characterize equilibrium positions (structural responses) as plots of a load parameter P versus some characteristic displacement θ . The solid curves denote the response of systems that are free of imperfections, and the dashed curves denote the response of the corresponding imperfect systems.

Figure 1.6 shows the response of such structural elements as columns, plates, and unbraced portal frames. The perfect configuration is subject to bifurcational buckling, while the imperfect configuration is characterized by stable equilibrium (unique), for elastic material behavior.

Figure 1.7 typifies the response of some simple trusses and two-bar frames.

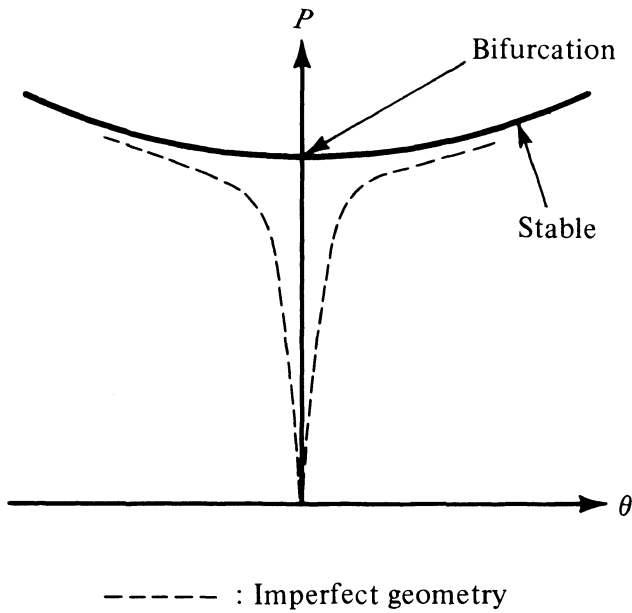


FIGURE 1.6. Bifurcated equilibrium paths with stable branching.

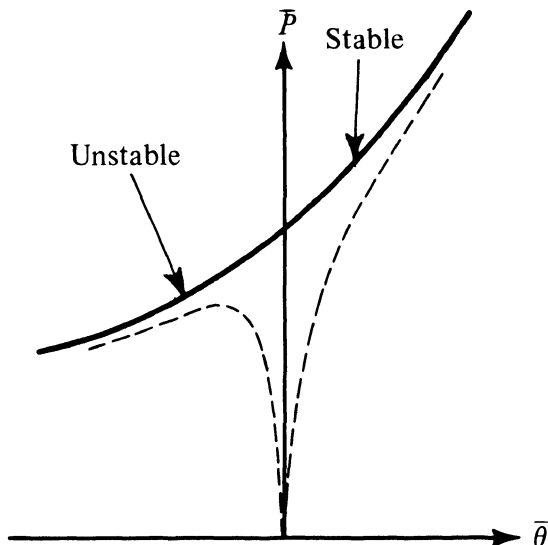


FIGURE 1.7. Bifurcated equilibrium paths with stable and unstable branches.

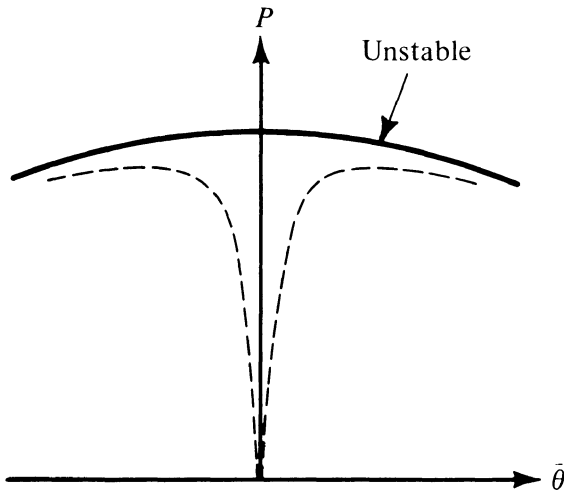


FIGURE 1.8. Bifurcated equilibrium paths with unstable branching.

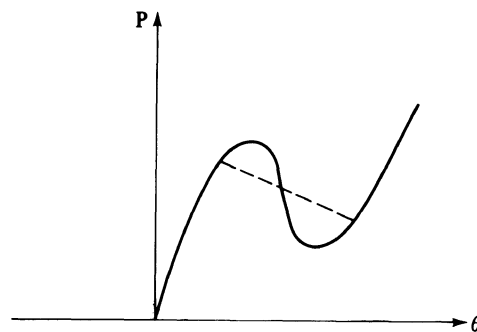


FIGURE 1.9. Snap-through buckling paths (through limit point or unstable branching).

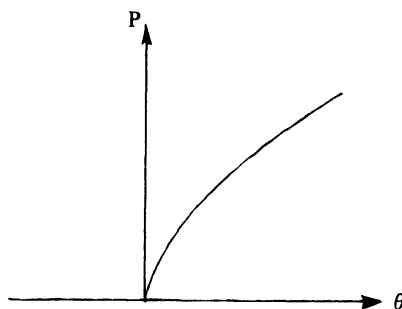


FIGURE 1.10. Unique stable equilibrium path.

The perfect configuration is subject to bifurcational buckling, with a smooth (stable) branch in one direction of the response and a violent (unstable) branch in the other. Correspondingly, the response of the imperfect configuration is characterized by stable equilibrium (unique) for increasing load in one direction, while in the other, the system is subject to limit point instability.

Figure 1.8 typifies the response of troublesome structural configurations such as cylindrical shells (especially under uniform axial compression and of isotropic construction), pressure-loaded spherical shells, and some simple two-bar frames. These systems are imperfection-sensitive systems and are subject to violent buckling under static loading.

A large class of structural elements is subject to limit point instability. In some cases, unstable bifurcation is present in addition to the limit point. The response of such systems is shown in Figure 1.9. Two structural elements that behave in this manner are the shallow spherical cap and the low arch. Both elements have been used extensively in practice.

Finally, there is a very large class of structural elements that are always in stable equilibrium for elastic behavior and for all levels of the applied loads. These systems are not subject to instability under static conditions. Typical members of this class are beams and transversely loaded plates. For this class of structural elements, the load-displacement curve is unique and monotonically increasing (Figure 1.10).

The concept of dynamic stability, as developed and discussed (see also [41, 45–50]), is always with reference to systems that are subject to violent buckling under static loading. This implies that dynamic buckling has been discussed for systems with static behavior shown in Figures 1.7 (to the left), 1.8, and 1.9.

In developing concepts and the related criteria and estimates for dynamic buckling, it is observed that, even for systems that are subject to violent (static) buckling, critical dynamic loads can be associated with *limitations* in deflectional response rather than escaping motion through a static unstable point. This is especially applicable to the design of structural members and configurations, which are deflection limited. From this point of view, then, the concept of dynamic stability can be extended to all structural systems.

The extended concepts are demonstrated through the simple mass-spring (linear) system shown in Figure 1.11.

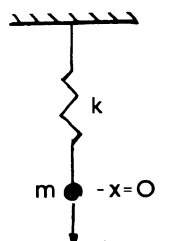


FIGURE 1.11. The mass-spring system.

1.3.1 The Mass-Spring System

Consider the mass-spring (linear) system shown in Figure 1.11. Consider a suddenly applied load $P(t)$ applied at $t = 0$. This load may, in general, include the weight (mg). In the case of finite duration, consider the weight to be negligible.

First, the problem of constant load suddenly applied with infinite duration is considered.

For this case, one may write the equation of motion and solve for the response by imposing the proper initial conditions:

$$\ddot{x} + \frac{k}{m}x = \frac{P}{m} \quad (6)$$

subject to

$$\dot{x}(0) = x(0) = 0 \quad (7)$$

where the dot denotes differentiation with respect to time.

By changing the dependent variable to

$$y = x + C \quad (8)$$

where C is a constant, the equation of motion and initial conditions become

$$\ddot{y} + \frac{k}{m}y = 0, \quad (9)$$

$$y(0) = -\frac{P}{K} \quad \text{and} \quad \dot{y}(0) = 0. \quad (10)$$

The solution is

$$y = \frac{P}{k} \cos \sqrt{\frac{k}{m}} t$$

and

$$x = \frac{P}{k} \left(1 - \cos \sqrt{\frac{k}{m}} t \right). \quad (11)$$

Note that

$$x_{\max} = \frac{2P}{k} \quad (12)$$

and it occurs at

$$\sqrt{\frac{k}{m}} t = \pi \quad \text{or at} \quad t = \pi \sqrt{\frac{m}{k}} = \frac{T_0}{2} \quad (13)$$

where T_0 is the period of vibration.

Note that if the load is applied quasi-statically, then

$$P_{st} = kx_{st}. \quad (14)$$

From eqs. (12) and (14), it is clear that if the maximum dynamic response x_{\max} and maximum static deflection $x_{st,\max}$ are to be equal and no larger than a specified value X (deflection-limited response), then

$$P_{st} = 2P_{dyn}. \quad (15)$$

Because of this, many systems for which the design loads are dynamic in nature (suddenly applied of constant magnitude and infinite duration) are designed in terms of considerations but with design (static) loads twice as large as the dynamic loads, eq. (15). Note that both loads (P_{st}, P_{dyn}) correspond to the same maximum (allowable) deflection X .

Next, the same problem is viewed in terms of energy considerations.

First, the total potential U_T^P for the system is given by

$$U_T^P = \frac{1}{2}kx^2 - Px, \quad (16)$$

and the kinetic energy T^P by

$$T^P = \frac{1}{2}m(\dot{x})^2. \quad (17)$$

Note that the system is conservative, the kinetic energy is a positive definite function of the velocity (for all t), and $U_T^P = 0$ when $x = 0$. Then,

$$U_T^P + T = 0, \quad (18)$$

and motion is possible only in the range of x values for which U_T is nonpositive (see shaded area of Figure 1.12).

It is also seen from eq. (16) that the maximum x value corresponds to $2P/k$.

Note that the static deflection is equal to P/k , eq. (14) and point A on Figure 1.12. Therefore, if the maximum dynamic response and maximum static deflection are to be equal to X , eq. (15) must hold.

Now, one may develop a different viewpoint for the same problem. Suppose that a load P is to be applied suddenly to the mass-spring system with the condition that the maximum deflectional response cannot be larger than a

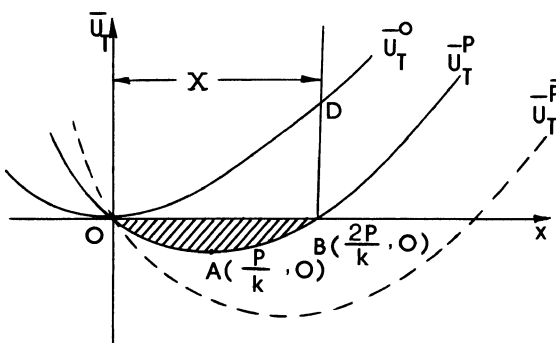


FIGURE 1.12. Total potential curves (suddenly loaded mass-spring system).

specified value X . If the magnitude of the load is such that

$$\frac{2P}{k} < X, \quad (19)$$

we shall call the load dynamically subcritical.

When the inequality becomes an equality, we shall call the corresponding load dynamically critical. This implies that the system cannot withstand a dynamic load $P > kX/2$ without violating the kinematic constraint. Therefore,

$$P_{\text{dyn,cr}} = \frac{kX}{2}. \quad (20)$$

Moreover, on the basis of this concept, one may find a critical ideal impulse. The question, in this load case, is to find the ideal impulse such that the system response does not exceed a prescribed value X . From Figure 1.12 and conservation of energy,

$$U_T^0 + T^0 = T_i^0, \quad (21)$$

and T_i^0 is critical if the system can reach position D with zero velocity (kinetic energy). Thus,

$$T_{\text{icr}}^0 = U_T^0(D) = U_T^0(X). \quad (22)$$

From the impulse-momentum theorem, the ideal impulse, Imp , is related to the initial velocity and consequently to the initial kinetic energy:

$$\text{Imp} = \lim_{t \rightarrow 0} (Pt_0) = m\dot{x}_i \quad (23)$$

where \dot{x}_i is the initial velocity magnitude (unidirectional case) and t_0 is the duration time of a square pulse.

From eq. (23),

$$\dot{x}_i = \frac{\text{Imp}}{m}, \quad (24)$$

and use of eq. (17) yields

$$\dot{x}_i = \left(\frac{2T_i^0}{m} \right)^{1/2}. \quad (25)$$

Since the critical initial kinetic energy is given by eq. (22),

$$\text{Imp}_{\text{cr}} = (mk)^{1/2} X. \quad (26)$$

Next, the following nondimensionalized parameters are introduced:

$$\begin{aligned} p &= \frac{2P}{kX}, & \xi &= \frac{x}{X}, & \tau &= t \sqrt{\frac{k}{m}} \\ \bar{U}_T &= \frac{2U_T}{kX^2}, & T &= \frac{2T}{kX^2}, & \text{Imp} &= \frac{2 \text{Imp}}{X \sqrt{km}}. \end{aligned} \quad (27)$$

On the basis of this, eq. (26) becomes

$$\bar{\text{Imp}}_{\text{cr}} = 2. \quad (28)$$

Similar examples, as well as this one, are treated in a later section for the case of a step load of finite duration.

1.4 Behavior of Suddenly Loaded Systems

So far, from the discussion of the subject of dynamic stability of suddenly loaded structural configurations, it is seen that the following phenomena are possible:

1. *Parametric resonance.* Systems that are subject to bifurcational buckling under static conditions are subject to parametric resonance if the loading is sudden (ideal impulse or constant load of infinite duration) and certain conditions are met.

For example, a perfectly straight column [53] loaded suddenly without eccentricity is subject to parametric resonance if the in-plane motion is accounted for. What happens in this case (it is shown in [53] and in a later section) is that the in-plane motion is periodic, which leads to a periodic axial force and yields a Mathieu–Hill type of equation for transverse motion and therefore a possibility of parametric resonance.

Similarly, a perfectly symmetric shallow arch loaded by a sudden symmetric loading may lead to parametric resonance in an antisymmetric mode because of the coupling between symmetric and antisymmetric modes.

Parametric resonance for suddenly loaded systems is more of a theoretical possibility than an actual physical phenomenon, because neither the structural system nor the external (sudden) loading is free of imperfections.

More details are presented in Appendix A. The material presented is by no means complete, but it suffices to make the discussion self-contained.

2. *Escaping motion type of instability.* Systems that are subject to the violent type of buckling under static loading can and do experience an escaping motion type of instability when suddenly loaded (Figures 1.7 [to the left], 1.8, and 1.9). Examples of these include shallow arches, shallow spherical caps, certain two-bar frames, and imperfect cylindrical shells. The concepts discussed in Section 1.2 are for these systems. Moreover, the Budiansky–Roth criterion and the concepts developed by Hsu and his collaborators were developed for these systems. The physical phenomenon for this case is as follows: For small values of the load (suddenly applied) parameter, the system simply oscillates (linearly or nonlinearly) about the near static equilibrium point. As the load parameter is increased, a value is reached for which an escaping or large-amplitude motion is observed. This phenomenon is demonstrated through several examples in later sections.

3. *Linear or nonlinear oscillatory motion.* Systems that under static loading

are subject either to bifurcational (smooth) buckling with stable postbuckling branch (Figures 1.7 [to the right] and 1.6) or are not subject to buckling at all (Figure 1.10) do not experience any type of dynamic instability. These systems, when suddenly loaded, simply oscillate about the stable static equilibrium position. Examples of these systems include the imperfect column, unbraced portal frames, and transversely loaded (suddenly) beams and thin plates.

Note that, through the application of the extended concept of dynamic stability (Section 1.3), critical conditions (loads) may be found for these systems by imposing limitations on the dynamic response characteristics of the system (either a maximum allowable amplitude of vibrations, a maximum allowable in-plane strain, or some other constraint).

References

1. Koning, C., and Taub, J. Impact buckling of thin bars in the elastic range hinged at both ends. *Luftfahrtforschung*, 10, 2, 1933, 55–64 (translated as NACA TM 748 in 1934).
2. Stoker, J.J. On the stability of mechanical systems. *Commun. Pure Appl. Math.*, VIII, 1955, 133–142.
3. Thompson, W., and Tait, P.G. *Treatise on Natural Philosophy*, part I. Cambridge University Press, Cambridge, England, 1923. (It was first published in 1867.)
4. Routh, E.J. *Stability of Motion* (edited by A.T. Fuller). Taylor & Francis, Halsted Press, New York, 1975. (Originally it appeared in 1877.)
5. Lefschetz, S. *Stability of Nonlinear Control Systems*. Academic Press, New York, 1965.
6. Seckel, E. *Stability and Control of Airplanes and Helicopters*. Academic Press, New York, 1964.
7. Crocco, L., and Cheng, S.I. *Theory of Combustion Instability in Liquid Propellant Rocket Motors*, AGARD Monograph No. 8. Butterworths, London, 1956.
8. Bolotin, V.V. *The Dynamic Stability of Elastic Systems* (translated by V.I. Weingarten et al.). Holden-Day, San Francisco, 1964.
9. Stoker, J.J. *Non-Linear Vibrations in Mechanical and Electrical Systems*, vol. II. Interscience, London, 1950.
10. Simitses, G.J. *Elastic Stability of Structures*. Prentice-Hall, Englewood Cliffs, N.J., 1976 (second printing, R.E. Krieger, Melbourne, Fla., 1985).
11. Ziegler, H. *Principles of Structural Stability*. Blaisdell, Waltham, Mass., 1968.
12. Herrmann, G. Stability of equilibrium of elastic systems subjected to nonconservative forces. *Appl. Mech. Rev.*, 20, 2, Feb. 1967, 103–108.
13. Ziegler, H. On the concept of elastic stability. *Advances in Applied Mechanics*, vol. 4, pp. 351–403. Academic Press, New York, 1956.
14. Herrmann, G., and Bungay, R.W. On the stability of elastic systems subjected to nonconservative forces. *J. Appl. Mech.*, 31, 3, 1964, 435–440.
15. Benjamin, T.B. Dynamics of a system of articulated pipes conveying fluid. *Proc. R. Soc. London Ser. A*, 261, 1961, 452–486.
16. Gregory, R.W., and Paidoussis, M.P. Unstable oscillation of tubular cantilevers conveying fluid. *Prod. R. Soc. London Ser. A*, 293, 1966, 512–527.

22 1. Introduction and Fundamental Concepts

17. Paidoussis, M.P., and Deksnis, B.E. Articulated models of cantilevers conveying fluid: The study of a paradox. *J. Mech. Eng. Sci.*, 42, 4, 1970, 288–300.
18. Paidoussis, M.P. Dynamics of tubular cantilevers conveying fluid. *J. Mech. Sci.*, 12, 2, 1970, 85–103.
19. Hill, J.L., and Swanson, C.P. Effects of lumped masses on the stability of fluid conveying tubes. *J. Appl. Mech.*, 37, 2, 1970, 494–497.
20. Junger, M., and Feit, D. *Sound, Structures and Their Interaction*. MIT Press, Cambridge, Mass., 1972.
21. Blevins, R.D. *Flow-Induced Vibration*. Van Nostrand-Reinhold, New York, 1977.
22. Scanlan, R.H., and Simin, E. *Wind Effects on Structures: An Introduction to Wind Engineering*. Wiley, New York, 1978.
23. King, R. A review of vortex shedding research and its applications. *Ocean Eng.*, 4, 1977, 141–171.
24. Chen, S.S. Vibration of nuclear fuel bundles. *Nucl. Eng. Des.*, 35, 3, 1975, 399–422.
25. Chen, S.S. Vibration of a row of circular cylinders in a liquid. *J. Eng. Ind., Trans. ASME*, 91, 4, 1975, 1212–1218.
26. Chen, S.S. Crossflow-induced vibrations of heat exchanger tube banks. *Nucl. Eng. Des.*, 47, 1, 1978, 67–86.
27. Reusselet, J., and Herrmann, G. Flutter of articulated pipes at finite amplitude. *Trans. ASME*, 99, 1, 1977, 154–158.
28. Au-Yang, M.K., and Brown, S.J., Jr. (editors). *Fluid Structure Interaction Phenomena in Pressure Vessel and Piping Systems*, PVP-PB-026. ASME, New York, 1977.
29. Chen, S.S. Fluid damping for circular cylindrical structures. *Nucl. Eng. Des.*, 63, 1, 1981, 81–100.
30. Ginsberg, J.H. The dynamic stability of a pipe conveying a pulsatile flow. *Int. J. Eng. Sci.*, 11, 1973, 1013–1024.
31. Bohn, M.P., and Herrmann, G. The dynamic behavior of articulated pipes conveying fluid with periodic flow rate. *J. Appl. Mech.*, 41, 1, 1974, 55–62.
32. Paidoussis, M.P., and Issid, N.T. Experiments on parametric resonance of pipes containing pulsatile flow. *J. Appl. Mech., Trans. ASME*, 98, 1976, 198–202.
33. Paidoussis, M.P., and Sundararajan, C. Parametric and combination resonances of a pipe conveying pulsating fluid. *J. Appl. Mech.*, 42, 4, 1975, 780–784.
34. Dowell, E. Nonlinear flutter of curved plates, *AIAA J.*, 7, 3, March 1969, 424–431.
35. Morino, L. Perturbation method for treating nonlinear panel flutter problems. *AIAA J.*, 7, 3, March 1969, 405–411.
36. Kornecki, A. Traveling wave-type flutter of infinite elastic plates. *AIAA J.*, 8, 7, July 1970, 1342–1344.
37. Dowell, E. Panel flutter, a review of the aeroelastic stability of plates and shells. *AIAA J.*, 8, 3, March 1970, 385–399.
38. Kuo, G.C., Morino, L., and Dugundji, J. Perturbation and harmonic balance methods of nonlinear panel flutter. *AIAA J.*, 10, 11, Nov. 1972, 1479–1484.
39. Hoff, N.J., and Bruce, V.C. Dynamic analysis of the buckling of laterally loaded flat arches. *Q. Math. Phys.*, 32, 1954, 276–388.
40. Budiansky, B., and Roth, R.S. Axisymmetric dynamic buckling of clamped shallow spherical shells. Collected Papers on Instability of Shell Structures. NASA TN D-1510, 1962.
41. Budiansky, B., and Hutchinson, J.W. Dynamic buckling of imperfection-sensitive structures. *Proc. XI International Congress of Applied Mechanics*, Munich, 1964.

42. Simitses, G.J. On the dynamic buckling of shallow spherical caps. *J. Appl. Mech.*, 41, 1, 1974, 299–300.
43. Tamura, Y.S., and Babcock, C.D. Dynamic stability of cylindrical shells under step loading. *J. Appl. Mech.*, 42, 1, 1975, 190–194.
44. Budiansky, B. Dynamic buckling of elastic structures: Criteria and estimates. *Dynamic Stability of Structures* (edited by G. Herrmann). Pergamon, New York, 1967.
45. Hsu, C.S. The effects of various parameters on the dynamic stability of a shallow arch. *J. Appl. Mech.*, 34, 2, 1967, 349–356.
46. Hsu, C.S. Stability of shallow arches against snap-through under timewise step loads. *J. Appl. Mech.*, 35, 1, 1968, 31–39.
47. Hsu, C.S. Equilibrium configurations of a shallow arch of arbitrary shape and their dynamic stability character. *Int. J. Nonlinear Mech.*, 3, June 1968, 113–136.
48. Hsu, C.S. On dynamic stability of elastic bodies with prescribed initial conditions. *Int. J. Nonlinear Mech.*, 4, 1, 1968, 1–21.
49. Hsu, C.S., Kuo, C.T., and Lee, S.S. On the final states of shallow arches on elastic foundations subjected to dynamic loads. *J. Appl. Mech.*, 35, 4, 1968, 713–723.
50. Simitses, G.J. Dynamic snap-through buckling of low arches and shallow spherical caps. Ph.D. Dissertation, Department of Aeronautics and Astronautics, Stanford University, June 1965.
51. Hoff, N.J. Dynamic stability of structures. *Dynamic Stability of Structures* (edited by G. Herrmann). Pergamon, New York, 1967.
52. Thompson, J.M.T. Dynamic buckling under step loading. *Dynamic Stability of Structures* (edited by G. Herrmann). Pergamon, New York, 1967.
53. Wauer, J. Über Kinetische Verweigungs Probleme Elastischer Strukturen unter Stosseblastung. *Ingenieur-Arch.*, 49, 1980, 227–233.

2

Simple Mechanical Models

Two single-degree-of-freedom mechanical models and one two-degree-of-freedom model are employed in this chapter to demonstrate the concept of dynamic stability for the extreme cases of the ideal impulse and sudden constant load of infinite duration. These models are typical of imperfection-sensitive structural configurations. They are kept as simple as possible, so that the emphasis can easily be placed on the concepts rather than on complex mathematical theories. For each model, the static stability analysis, based on the total potential energy approach, is given in detail. In addition, the total energy-phase plane approach is used for one model. For the same model, the equations of motion approach is also used, for demonstration and comparison purposes. The main emphasis, though, is placed on the total potential energy approach.

Finally, a few observations are presented that result from these simple studies but are general in applicability.

2.1 Model A: A Geometrically Imperfect Model

Consider the model shown in Figure 2.1. This model consists of two rigid bars of equal length L pinned together. The left bar is pinned on an immovable support A , while the right end of the second bar is pinned on a movable support C and loaded by a horizontal constant-directional force P . A linear spring of stiffness k connects the common pin B to an immovable support D , which is L units directly below support A . The initial geometric imperfection θ_0 is an angle between the horizontal line joining supports A and C and bar AB (or BC). The deformed position is characterized by angle θ as shown (in its positive direction). For simplicity, the two rigid bars are assumed to be weightless, and the mass m of the system is concentrated at joint B .

2.1.1 Static Stability Analysis of Model A

The stability analysis of this model under quasi-static application of the load P is performed by employing the energy approach. Through this approach,

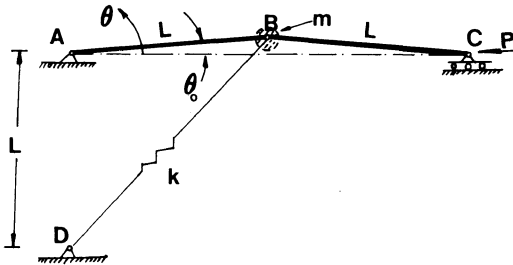


FIGURE 2.1. Geometry and sign convention for model A.

equilibrium is characterized by

$$\frac{dU_T^P}{d\theta} = 0 \quad (1)$$

where U_T is the total potential, and the character of equilibrium (stable or unstable) by the sign of the second derivative.

The total potential is

$$\bar{U}_T^P = \frac{U_T^P}{kL^2} = [\sqrt{1 + \sin \theta} - \sqrt{1 + \sin \theta_0}]^2 - p(\cos \theta_0 - \cos \theta) \quad (2)$$

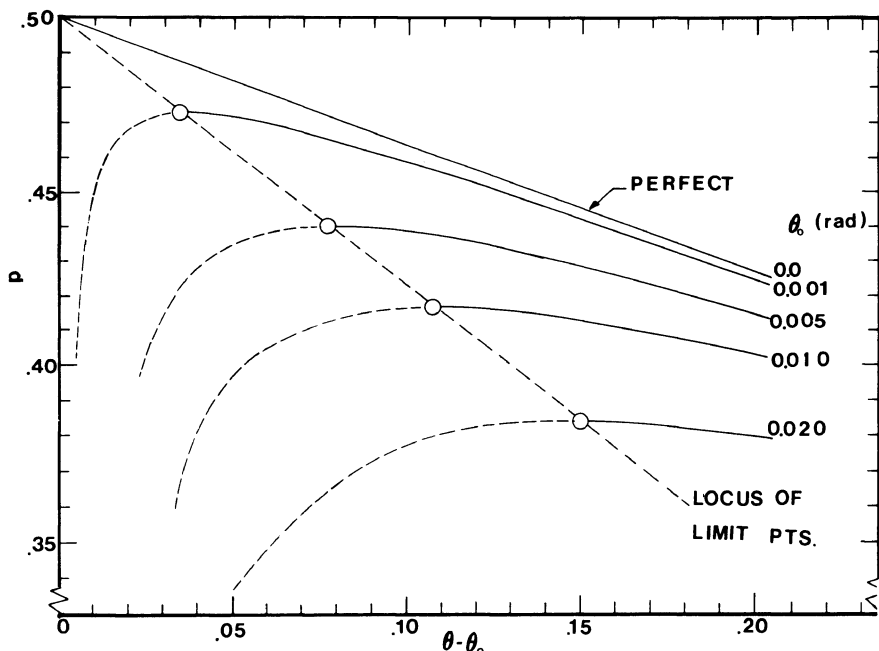


FIGURE 2.2 Load-displacement curves (model A).

where $p = 2P/kL$ and \bar{U}_T^P denotes the nondimensionalized total potential. The superscript P implies “under load P .”

The static equilibrium points are characterized by

$$p = [\sqrt{1 + \sin \theta} - \sqrt{1 + \sin \theta_0}] \frac{\cot \theta}{\sqrt{1 + \sin \theta}} \quad \text{for } \theta_0 \neq 0. \quad (3)$$

Note that, for $\theta_0 = 0$ equilibrium is characterized by

$$\text{either } \theta = 0$$

$$\text{or } p = \cot \theta (\sqrt{1 + \sin \theta} - 1) / \sqrt{1 + \sin \theta}. \quad (4)$$

Equilibrium positions are plotted in Figure 2.2 as p versus $\theta - \theta_0$ for various values of the geometric imperfection θ_0 . The stability test reveals that the dashed line positions are stable, while the solid line positions are unstable and snapping (violent buckling) takes place through the existence of a limit point. Also note that positions characterized by negative values for $\theta - \theta_0$ (not shown here) are stable and there is no possibility of buckling. Therefore, our interest lies in the area of $\theta_0 > 0$ and $\theta > \theta_0$.

2.1.2 Dynamic Analysis: Ideal Impulse

Assume that the load P is suddenly applied with a very short duration time T_0 and that the impulse (PT_0) is imparted instantaneously into the system as initial kinetic energy.

Through impulse–momentum, one obtains the following relation:

$$(PT_0) = \frac{1}{2} \left(\frac{mL\dot{\theta}_0}{\sin \theta_0} \right) \quad (5)$$

where $\dot{\theta}_0 = d\theta/dt$ at $\theta = \theta_0$.

Since the system is conservative,

$$U_T^0 + T^0 = \text{const.} = T_i^0 \quad (6)$$

where U_T^0 denotes the total potential “under zero load” and T^0 is the kinetic energy, given by

$$T^0 = \frac{1}{2} mL^2 \dot{\theta}^2. \quad (7)$$

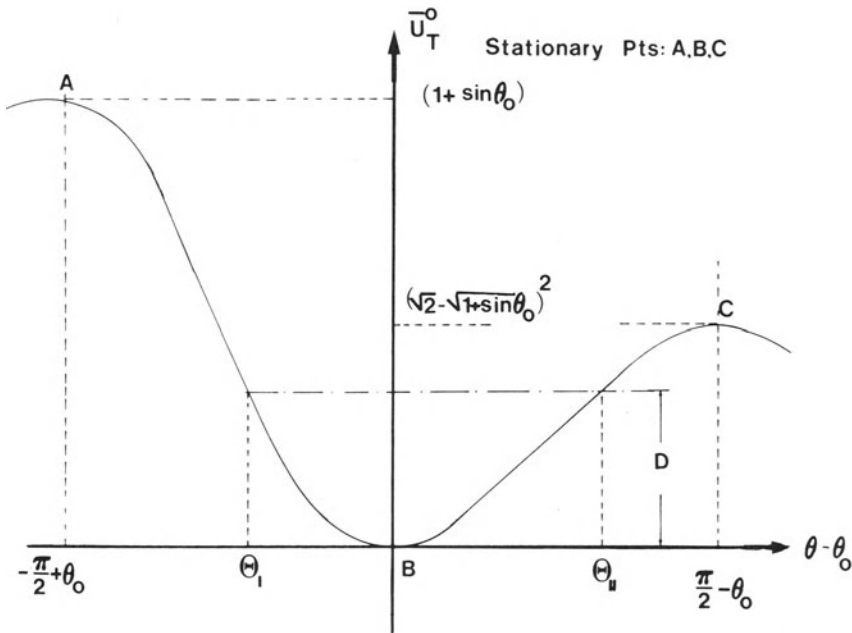
Note that T_i^0 is the initial kinetic energy imparted instantaneously by the impulsive load.

The expression for \bar{U}_T^0 is given by

$$\bar{U}_T^0 = [\sqrt{1 + \sin \theta} - \sqrt{1 + \sin \theta_0}]^2. \quad (8)$$

Figure 2.3 is a plot of \bar{U}_T^0 versus $\theta - \theta_0$.

According to eq. (6), and since T^0 is positive definite, motion is possible

FIGURE 2.3. “Zero-load” total potential versus $\theta - \theta_0$ (model A).

if and only if

$$T_i^0 - U_T^0 \geq 0. \quad (9)$$

This implies that, for a given initial kinetic energy, eq. (7), and consequently a given impulse, say $T_i^0 = D$ (see Figure 2.3—total potential presented in nondimensionalized form), motion is confined in the region $\Theta_1 < \theta - \theta_0 < \Theta_2$. It is clearly seen then that, as long as $T_i^0 = D < \bar{U}_T^0(C)$, the motion of the system is bounded and it contains only the stable zero-load static equilibrium point B . Such a motion is termed *unbuckled*. For the motion to cease to be unbuckled, that is, to become unbounded, and cease to include only the initial stable static equilibrium point B , D must be at least equal to the value of \bar{U}_T^0 at the unstable static point C . Then that point (C) can be reached with zero velocity and the motion can become unbounded. Clearly, if D is even slightly higher than the \bar{U}_T^0 value at point C , the motion does become unbounded, and it can contain other static equilibrium points, such as point C . Such a motion is called *buckled*, and a critical condition exists when the impulse is large enough to satisfy the relation

$$T_{i_{cr}}^0 = U_T^0(C). \quad (10)$$

Introducing nondimensionalized time and load parameters

$$\tau = t(2k/m)^{1/2}, \quad \tau_0 = T_0(2k/m)^{1/2}, \quad p = 2P/kL, \quad (11)$$

then

$$\bar{T}_i^0 = \frac{T^0}{kL^2} = \frac{1}{2} \left(\frac{m}{k} \right) (\dot{\theta}^2)_{\theta_0} = \left(\frac{d\theta}{d\tau} \right)_{\theta_0}^2 \quad (12)$$

where $(\dot{\theta})_{\theta_0}$ is the initial angular speed.

From eq. (5) one obtains

$$(p\tau_0) = \frac{2}{\sin \theta_0} \left(\frac{d\theta}{d\tau} \right)_{\theta_0}. \quad (13)$$

The zero-load static equilibrium positions are obtained by requiring the total potential, eq. (8), to have a stationary value, or

$$\frac{d\bar{U}_T^0}{d\theta} = 0 = [\sqrt{1 + \sin \theta} - \sqrt{1 + \sin \theta_0}] \cot \theta / \sqrt{1 + \sin \theta} \quad \text{for } \theta_0 \neq 0. \quad (14)$$

This requirement yields

$$\theta = \theta_0 \quad \text{and} \quad \theta = \pm \pi/2. \quad (15)$$

Through the second derivative (variation) of \bar{U}_T^0 with respect to θ , it can easily be shown that position $\theta = \theta_0$ is a stable one (point *B* on Figure 2.3) whereas positions $\theta = \pm \pi/2$ (points *C* and *A* on Figure 2.3) are unstable.

A critical condition exists when $\bar{T}_i^0 = \bar{U}_T^0(\theta = \pi/2)$, or

$$\bar{T}_{icr}^0 = [\sqrt{2} - \sqrt{1 + \sin \theta_0}]^2. \quad (16)$$

From eqs. (12) and (13),

$$(p\tau_0)_{cr} = \frac{2}{\sin \theta_0} \bar{T}_{icr}^{1/2} = 2[\sqrt{2} - \sqrt{1 + \sin \theta_0}] / \sin \theta_0. \quad (17)$$

Two observations are worth mentioning at this point: (1) Because this is a one-degree-of-freedom model, the critical impulse $(p\tau_0)_{cr}$ given by eq. (17) represents both the minimum possible (MPCL) and minimum guaranteed (MGCL) critical load. Although the concept presented so far is clear and it leads to a criterion and estimate of the critical condition, it might be impractical when applied to real structures. In the particular example shown so far, it is clear that, according to the presented concept of dynamic instability, buckled motion is possible if the system is allowed to reach the position $\theta = \pi/2$. In many cases such positions may be considered excessive, especially in deflection-limited designs. In such cases, if θ cannot be larger than a specified value, then the allowable impulse is smaller and its value can be found from eq. (10), if C is replaced by the maximum allowable value of θ , say Θ_L . In this case,

$$(p\tau_0)_{cr} = 2[\sqrt{1 + \sin \Theta_L} - \sqrt{1 + \sin \theta_0}] / \sin \theta_0. \quad (18)$$

Related to this discussion is the broad definition of stability proposed by Hoff [1]: "A structure is in a stable state if admissible finite disturbances of

its initial state of static or dynamic equilibrium are followed by displacements whose magnitudes remain within allowable bounds during the required lifetime of the structure.” (2) Finally, as already mentioned in Chapter 1 (Section 1.2), the sense of the impulsive load (in the absence of damping) has no effect on the critical condition.

If the load is applied (extremely short duration) to the right instead of the left (see Figure 2.1), then the system tends to move with negative values for $\theta - \theta_0$ (see Figure 2.3; the system would move toward Θ_1). The critical value for the initial kinetic energy is still given by eq. (16), because the system would reach position E (see Figure 2.3) with zero velocity, reverse its motion, pass through the stable static equilibrium position B , and then reach the unstable static equilibrium point C with zero kinetic energy (buckled motion, thus, is possible).

2.1.3 Dynamic Analysis: Sudden Constant Load of Infinite Duration

For this case, the sum of the total potential and kinetic energy is zero:

$$\bar{U}_T^P + \bar{T} = 0. \quad (19)$$

Figure 2.4 shows plots of \bar{U}_T^P versus $\theta - \theta_0$ (in radians) for various values of the applied load p . It is seen from this figure that for $p < 0.432$ motion is confined between the origin and $\theta - \theta_0 < A$, or the motion is unbuckled. A critical condition exists when the motion can become unbounded by including position A'' (buckled motion).

Thus, the critical load is found by requiring [see eq. 19)] that \bar{U}_T^P be zero at the unstable static equilibrium position, A'' (see Figure 2.4; the curves on this figure correspond to $\theta_0 = 0.005$).

Numerically, the critical dynamic load is found by solving the following two equations simultaneously:

$$[\sqrt{1 + \sin \theta} - \sqrt{1 + \sin \theta_0}]^2 - p(\cos \theta_0 - \cos \theta) = 0 \quad (20)$$

$$p = [\sqrt{1 + \sin \theta} - \sqrt{1 + \sin \theta_0}] \cot \theta / \sqrt{1 + \sin \theta} \quad (21)$$

subject to the condition $d^2 \bar{U}_T^P / d\theta^2 < 0$, at the solution of eqs. (20) and (21).

The inequality condition ensures that $\bar{U}_T^P = 0$, eq. (20), at an unstable static equilibrium position. The simultaneous solution of eqs. (20) and (21) (two equations in the unknowns θ and p) yields the dynamic critical load and the corresponding position of the unstable static equilibrium point A'' (see Figure 2.4).

Values of critical dynamic loads for the case of suddenly applied constant loads of infinite duration are shown graphically in Figure 2.5, for various small imperfection angles θ_0 , and they are compared to the corresponding static critical loads (see Figure 2.2).

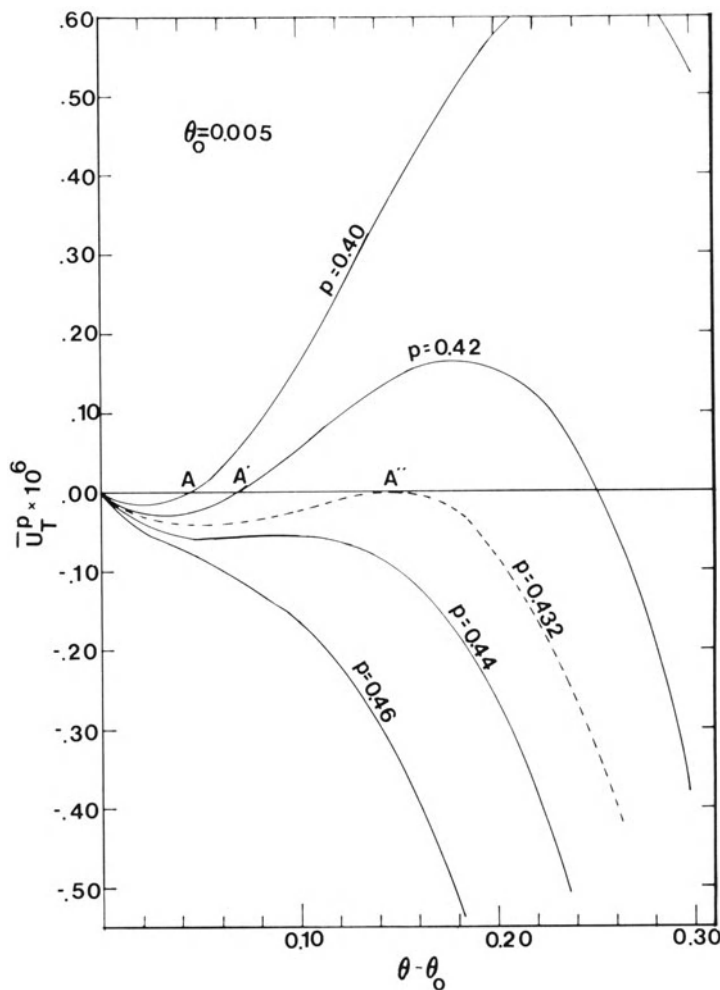


FIGURE 2.4. Total potential versus displacement for various loads (model A).

For this load case also, since the system is a single-degree-of-freedom system, the minimum possible (MPCL) and minimum guaranteed (MGCL) critical loads are one and the same. Furthermore, if the value of θ is limited by other considerations (say the maximum allowable θ value is such that $\theta - \theta_0$ is equal to the value denoted by A' on Figure 2.4), then there is no escaping motion type of instability, but the value $p = 0.42$ (see Figure 2.4) would be a measure of the maximum allowable sudden (dynamic) load and therefore critical (in the sense that the kinematic constraint is not violated for loads smaller than $p = 0.42$).

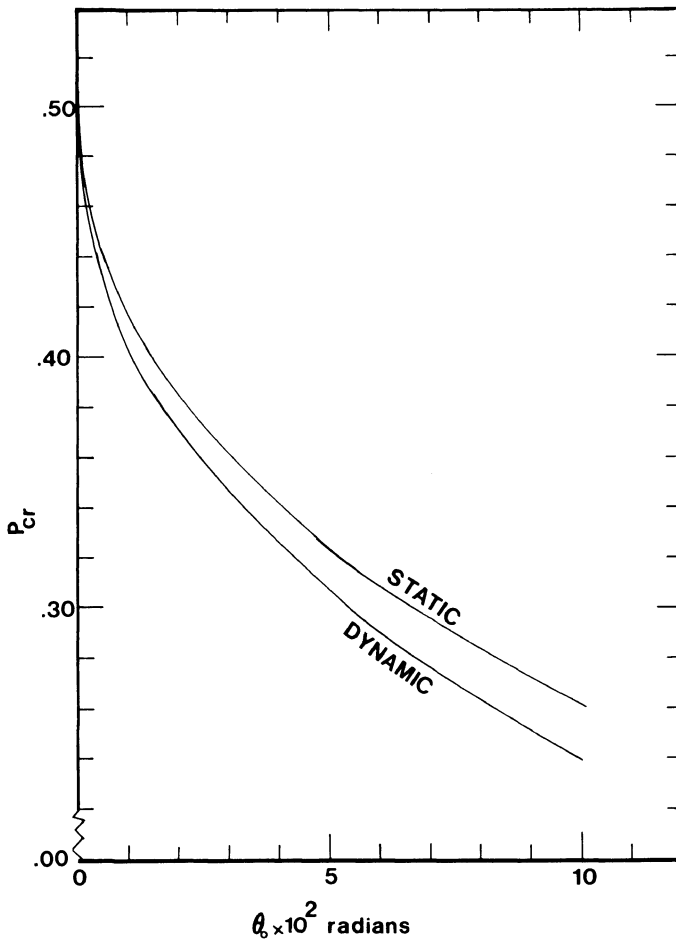


FIGURE 2.5. Static and dynamic critical loads (model A).

2.2 Model B: A Load Imperfection Model

Model B, shown in Figure 2.6, is representative of eccentrically loaded structural systems, exhibiting limit point instability. The bar is rigid and of length L ; the spring is linear of stiffness k , and the load eccentricity is denoted by e . The bar is assumed to be weightless, and the mass m of the system is concentrated on the top of the rod, point B .

2.2.1 Static Stability Analysis of Model B

For this model also, the energy approach is employed in the static stability analysis.

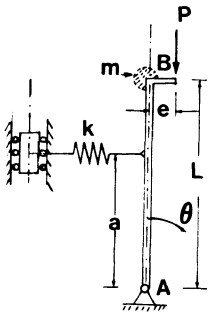


FIGURE 2.6. Geometry and sign convention for model B.

The total potential is given by

$$U_T^P = \frac{1}{2}ka^2 \sin^2 \theta - PL \left(1 - \cos \theta + \frac{e}{L} \sin \theta \right). \quad (22)$$

First, nondimensionalized parameters are introduced:

$$\bar{e} = \frac{e}{L}, \quad p = \frac{PL}{ka^2}, \quad \bar{U}_T^P = \frac{2U_T^P}{ka^2}. \quad (23)$$

With the aid of eqs. (23), the expression for the total potential becomes

$$\bar{U}_T^P = \sin^2 \theta - 2p(1 - \cos \theta + \bar{e} \sin \theta). \quad (24)$$

For equilibrium,

$$\frac{d\bar{U}_T^P}{d\theta} = 0 = 2 \sin \theta \cos \theta - 2p(\sin \theta + \bar{e} \cos \theta). \quad (25)$$

From this equation, one obtains all of the static equilibrium positions. These are plotted in Figure 2.7 for both positive eccentricity (as shown in Figure 2.6) and negative eccentricity. The positions (of static equilibrium) corresponding to zero eccentricity are also shown.

If $\bar{e} = 0$, the static equilibrium positions are characterized by [see eq. (25)]

$$\sin \theta = 0 \rightarrow \theta = 0 \quad \text{and} \quad p = \cos \theta. \quad (26)$$

On the other hand, if $\bar{e} \neq 0$, the static equilibrium positions are characterized by

$$p = \sin \theta / (\tan \theta + \bar{e}). \quad (27)$$

Note that if \bar{e} is replaced by $-\bar{e}$ and θ by $-\theta$, the load deflection relation, eq. (27), does not change. This is reflected in Figure 2.7 by the two curves, one corresponding to $\bar{e} = A^2$ and the other to $\bar{e} = -A^2$.

The stability or instability of the static equilibrium positions, eq. (27), is next established through use of the second variation. If we restrict the range of θ values to $0 < \theta < \pi/2$, we study the sign of the second derivative of the

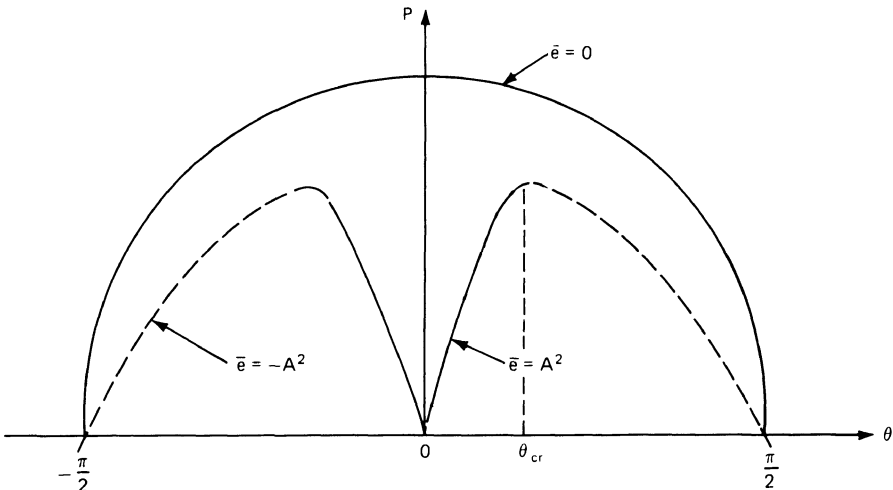


FIGURE 2.7. Positions of static equilibrium for model B.

total potential evaluated at static equilibrium points:

$$\frac{d^2 \bar{U}_T^P}{d\theta^2} = \cos 2\theta - p(\cos \theta - \bar{e} \sin \theta) \quad (28)$$

and

$$\left. \frac{d^2 \bar{U}_T^P}{d\theta^2} \right|_{\text{equil. pts.}} = \frac{\cos^2 \theta}{\tan \theta + \bar{e}} (\bar{e} - \tan^3 \theta). \quad (29)$$

It is clearly seen from eq. (29) that the sign of the second derivative (evaluated at static equilibrium points) depends on the sign of $\bar{e} - \tan^3 \theta$. Thus

$$\begin{aligned} &\text{if } \tan^3 \theta < \bar{e}, \text{ we have stability,} \\ &\text{and if } \tan^3 \theta > \bar{e}, \text{ we have instability.} \end{aligned} \quad (30)$$

The stable positions correspond to the solid lines of the $\bar{e} = \pm A^2$ curves of Figure 2.7, while the dashed lines characterize unstable static positions. When $\tan^3 \theta = \bar{e}$, $p = p_{cr}$ and substitution for this θ into eq. (27) yields

$$p_{cr} = (1 + \bar{e}^{2/3})^{-3/2}. \quad (31)$$

Similar arguments can be used for $-\pi/2 < \theta < 0$ and the results are the same.

2.2.2 Dynamic Analysis: Ideal Impulse

Following the same procedure as for model A, one can easily establish critical conditions for this load case.

The expressions for the zero-load total potential and kinetic energy are

given by

$$\bar{U}_T^0 = \sin^2 \theta \quad (32)$$

$$\bar{T}^0 = \frac{2T^0}{ka^2} = \frac{2I}{2ka^2} \left(\frac{d\theta}{dt} \right)^2 \quad (33)$$

where I is the moment of inertia of the mass of the system about the hinge A (see Figure 2.6).

Introducing a nondimensionalized time parameter τ , where

$$\tau = t(ka^2/I)^{1/2}, \quad (34)$$

the expression for the kinetic energy becomes

$$\bar{T}^0 = \left(\frac{d\theta}{d\tau} \right)^2. \quad (35)$$

Use of the impulse (angular)-momentum (moment of) theorem yields

$$\left[\lim_{T_0 \rightarrow 0} (PT_0) \right] e = I \left(\frac{d\theta}{dt} \right)_i, \quad (36)$$

and in terms of nondimensionalized parameters [T_0 and τ_0 are taken as small as one wishes and therefore the limit sign is dropped (but implied)]

$$(p\tau_0) = \frac{1}{\bar{e}} \left(\frac{d\theta}{d\tau} \right)_i \quad (37)$$

where i implies *initial* velocity and/or kinetic energy.

Note from eq. (32) that there exist three static equilibrium points under zero load. These correspond to $\theta = 0$ and $\theta = \pm \pi/2$ (see Figure 2.7). Thus, a critical condition exists if the ideal impulse is instantaneously imparted into the system as initial kinetic energy, \bar{T}_i^0 , of sufficient magnitude for the system to reach the unstable static points ($\pm \pi/2$; see Figure 2.7 for stability or instability) with zero kinetic energy. In such a case, buckled motion is possible, and

$$\bar{T}_{i_{cr}}^0 = \sin^2(\pm \pi/2) = 1. \quad (38)$$

From eqs. (35) and (37),

$$(p\tau_0)_{cr} = 1/\bar{e}. \quad (39)$$

It is observed for this model also that the sense of the impulsive load does not affect the critical condition. The only difference is that dynamic instability can take place by escaping motion either through unstable position $\theta = \pi/2$ or $\theta = -\pi/2$.

Moreover, in deflection-limited situations, say $|\theta| < |\Theta_L|$ where $|\Theta_L| < \pi/2$, the maximum allowable (and therefore critical) impulse is given by

$$(p\tau_0)_{cr} = \frac{\sin \Theta_L}{\bar{e}}. \quad (40)$$

2.2.3 Dynamic Analysis: Sudden Constant Load of Infinite Duration

In a similar manner as for model A, a critical condition exists if buckled motion can take place. This is possible if the total potential is zero at an unstable static equilibrium position. The critical condition is obtained through the simultaneous solution of the following two equations (in two unknowns p and θ):

$$\bar{U}_T^P = 0 = \sin^2 \theta - 2p(1 - \cos \theta + \bar{e} \sin \theta) \quad (41)$$

and

$$p = \sin \theta / (\tan \theta + \bar{e}) \quad (42)$$

subject to the condition

$$\left. \frac{d^2 \bar{U}_T^P}{d\theta^2} \right|_{\text{equil. pt.}} < 0. \quad (43)$$

Note that eq. (42) characterizes static equilibrium positions.

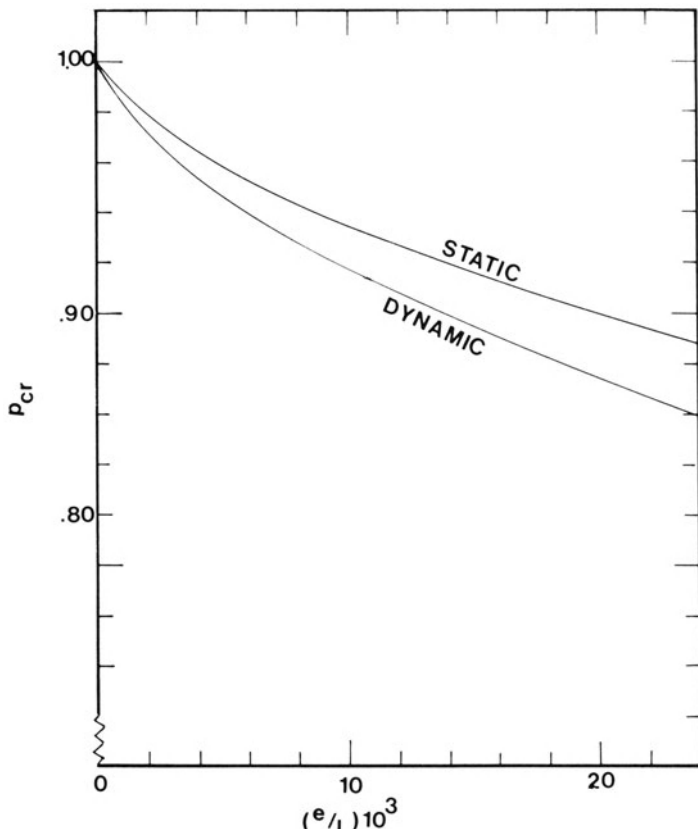


FIGURE 2.8. Static and dynamic critical loads (model B).

Results are presented graphically in Figure 2.8 for several values of the load eccentricity, and they are compared to the static (critical) conditions. Note that the static curve represents a plot of eq. (31).

It is important to note that for both models A and B the total potential, \bar{U}_T^P , is defined in such a way that it is zero at the initial (unloaded) position. Thus, in the absence of initial kinetic energy, the energy balance for both models is given by eq. (5) of Chapter 1, or

$$\bar{U}_T^P + \bar{T}^P = 0. \quad (44)$$

Before proceeding with the analysis of other mechanical models, model B is used to demonstrate the other two approaches that are discussed in Chapter 1.

2.2.4 The Total Energy–Phase Plane Approach

First the case of the ideal impulse is treated. This approach is also based on the total energy balance (conservation of energy), but instead of associating critical conditions with characteristics of the total potential surface (under “zero load” for the ideal impulse), the critical condition is associated with characteristics of the system phase plane.

Conservation of energy requires

$$\bar{U}_T^0 + \bar{T}^0 = \bar{T}_i^0. \quad (45)$$

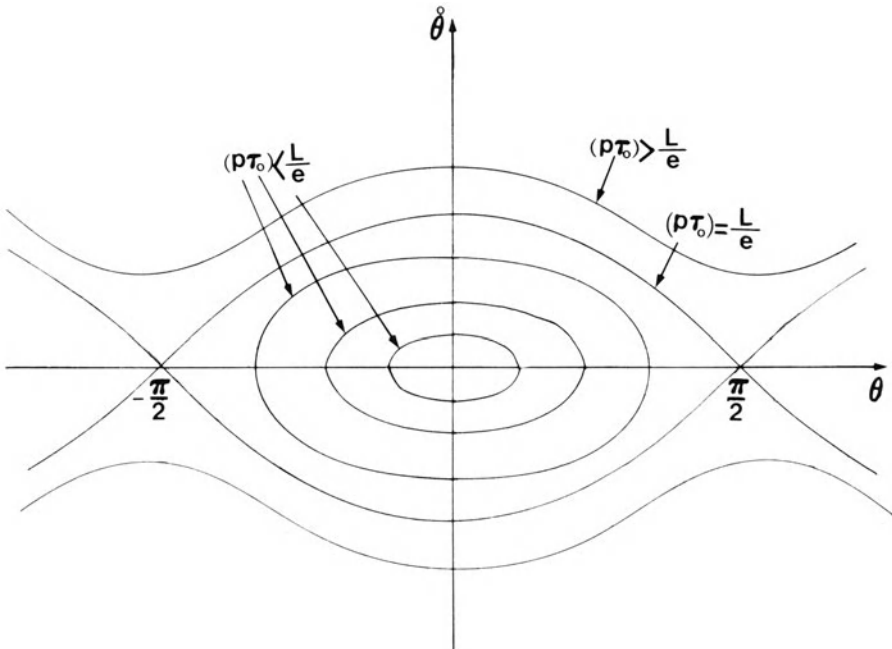


FIGURE 2.9. Phase plane curves for model B.
@Seismicisolation

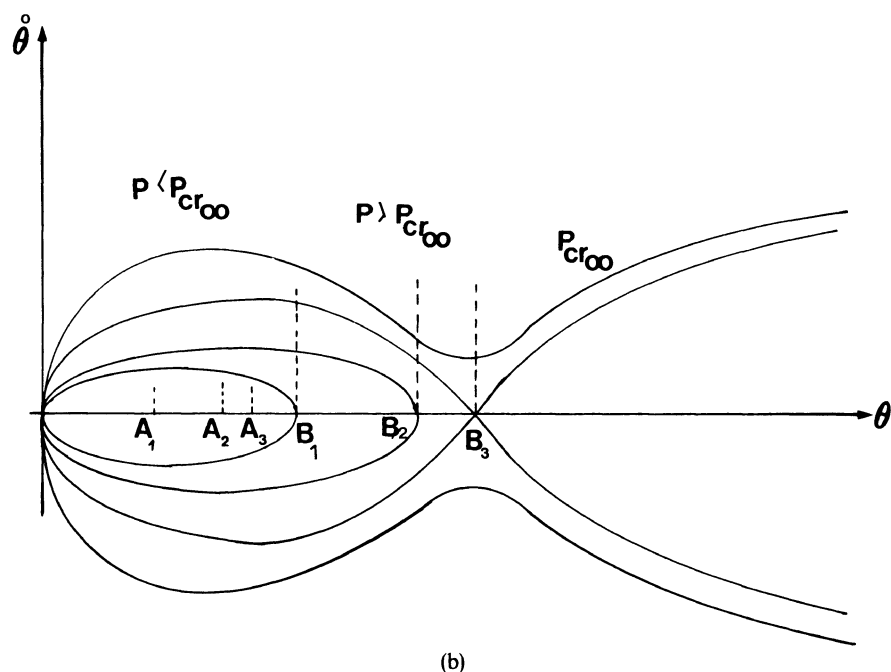
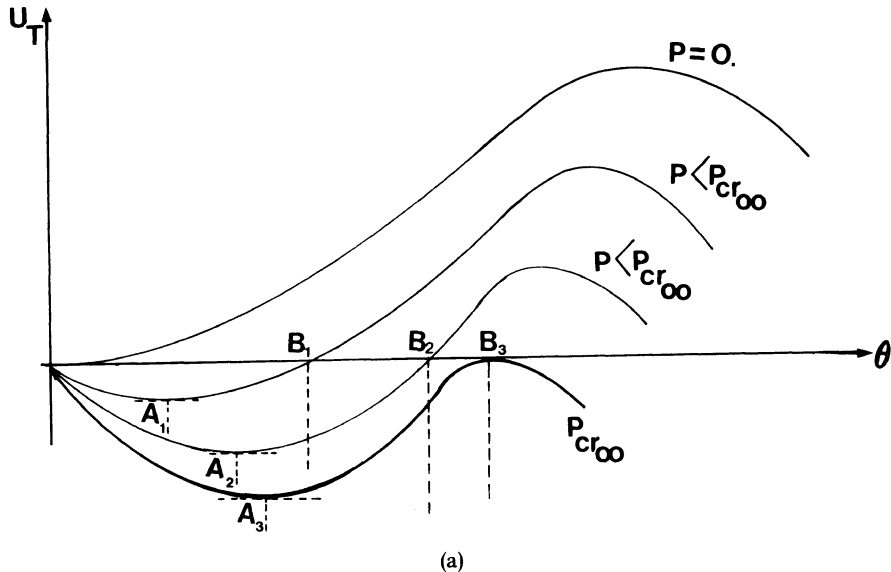


FIGURE 2.10. Critical conditions for model B: constant load of infinite duration.
(a) Total potential curves. (b) The phase plane.

Use of eqs. (32), (35), and (37) yields

$$\sin^2 \theta + \left(\frac{d\theta}{d\tau} \right)^2 = [(p\tau_0)\bar{e}]^2. \quad (46)$$

This equation is plotted on the phase plane ($\dot{\theta} = d\theta/d\tau$ versus θ curves) for various values of the right-hand side (Figure 2.9, p. 36).

Clearly, if

$$[(p\tau_0)\bar{e}]^2 < 1 \quad (47)$$

eq. (46) denotes a closed curve about the null position ($\dot{\theta} = \theta = 0$) in the phase plane. In this case the motion is called unbuckled (see Figure 2.9). When $[(p\tau_0)\bar{e}]^2 = 1$, eq. (46) denotes a curve that can escape the closed loop and thus the motion becomes buckled. Therefore,

$$(p\tau_0)_{cr} = \frac{L}{e} = \frac{1}{\bar{e}}. \quad (48)$$

Clearly, the result is the same as before, eq. (39).

Next, the case of a sudden constant load of infinite duration is considered.

Use of eqs. (41) and (35) yields the following expression for the total energy:

$$\dot{\theta}^2 + \sin^2 \theta - 2p(1 - \cos \theta + \bar{e} \sin \theta) = 0. \quad (49)$$

This equation is shown qualitatively on Figure 2.10b (p. 37) for different values of the sudden load. Figure 2.10a shows total potential curves for various values of the applied load starting from zero. The two figures are shown together and clearly demonstrate the applicability of both concepts in establishing critical conditions. The symbol p_{cr} is used on Figure 2.10 to denote the critical load for the case of suddenly applied loads with infinite duration.

Note on Figure 2.10 that for sudden loads smaller than the critical, the system simply oscillates about the near static equilibrium position A_i . At the critical load, escaping (buckled) motion is possible through the unstable static equilibrium position B_3 .

For two-degree-of-freedom systems, dealing with phase plane curves is considerably more complex. As the number of degrees of freedom increases, the complexity increases exponentially to the point of virtual impossibility (of using this approach). As far as the continuum is concerned, this approach can be used only by reducing the phase space to a finite-dimensional space by constraining the motion. This means that the deformation of the continuum is represented by a finite number of degrees of freedom (Ritz method, Galerkin procedure, finite-element and finite-difference methods).

2.2.5 The Equations of Motion Approach

As stated in Chapter 1, this approach was first applied by Budiansky and Roth [2] in finding critical conditions for a pressure-loaded, clamped, shallow,

thin, spherical shell. The pressure was assumed to be applied suddenly with constant magnitude and infinite duration. The equations of motion are solved for several values of the load parameter, starting from a small value and incrementing it. At low values of the load parameter, the system experienced small oscillations. The maximum response amplitude, w_{\max} , increased smoothly with λ . Figure 2.11 gives a qualitative description of the phenomenon. At some level of λ , the maximum response amplitude experienced a large jump. The λ value at which this jump took place was identified as the critical dynamic load, λ_{cr} .

For model B (see Figure 2.6), the equation of motion is given by

$$I \frac{d^2\theta}{dt^2} + M(\theta) = 0 \quad (50)$$

where $M(\theta)$ is the restoring moment, which can be expressed in terms of the contributions of the spring force and the externally applied force, or

$$M(\theta) = ka^2 \sin \theta \cos \theta - PL \left(\sin \theta + \frac{e}{L} \cos \theta \right). \quad (51)$$

Note that θ is a function of time, and the sudden force P is a step function of time.

Substitution of the expression for $M(\theta)$, eq. (51), into the equation of motion, eq. (50), and use of the nondimensionalized parameters, eqs. (23) and (34), yields

$$\frac{d^2\theta}{d\tau^2} + \sin \theta \cos \theta - p(\sin \theta + \bar{e} \cos \theta) = 0. \quad (52)$$

This equation is solved numerically (using a finite-difference scheme), for $\bar{e} = 0.02$ and several values of the load parameter p : $p = 0.1, 0.5, 0.8, 0.85$, and 0.9 . The results are presented graphically on Figures 2.12 and 2.13. Figure 2.13 shows plots of $\theta(\tau)$ versus time τ for various values of the load parameter. Note that for $p < p_{cr_\infty}$ (see Figure 2.8), the motion is simply oscillatory. The oscillations are between zero and a maximum amplitude that is much smaller than $\pi/2$. They seem to take place about the near static stable equilibrium position. For $p > p_{cr_\infty}$ ($p = 0.9$, Figure 2.13), the motion has a very large amplitude ($\theta_{\max} > \pi/2$) and it appears to be oscillating about the value of π . The important observation here is that if the range of allowable θ values is extended beyond $\pm\pi/2$, then $\theta = \pm\pi$ is a stable static equilibrium position, and the system tends to oscillate about this far ($\theta = \pi$) static position. Moreover, the amplitude decreases with time, because the force p yields restoring moments about the hinge, and the position $\theta = \pi$ is an asymptotically stable position (even in the absence of damping). Asymptotically stable means that for $t \rightarrow \infty$ the system will come to rest at this position. Figure 2.13 shows a plot of the maximum response amplitude versus the load parameter. Clearly, there is a large jump in the maximum

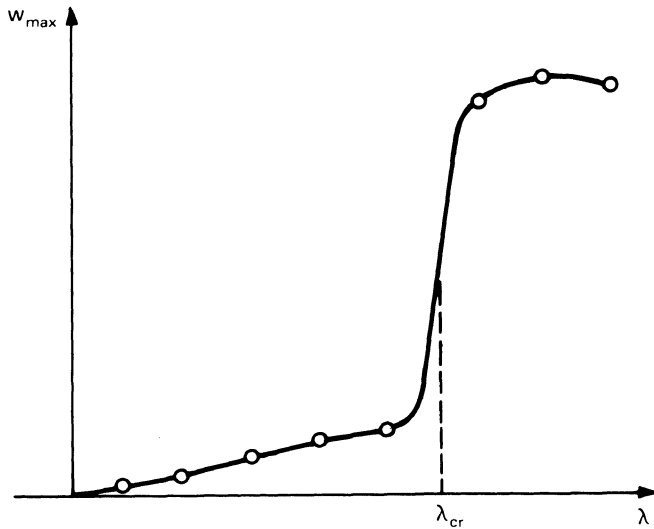
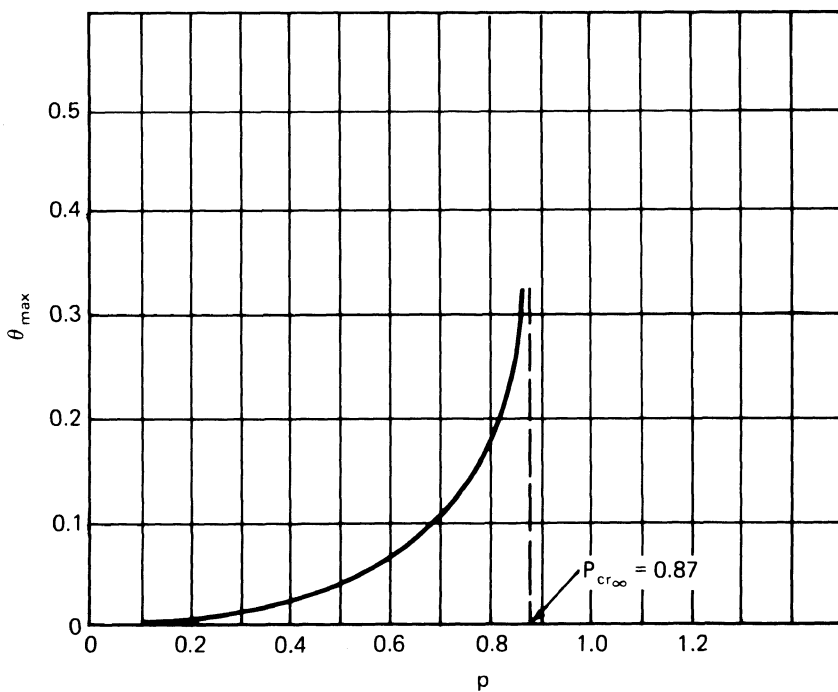


FIGURE 2.11. Description of the Budiansky–Roth criterion of dynamic stability.

FIGURE 2.12. A plot of θ_{\max} versus p (model B).

@Seismicisolation

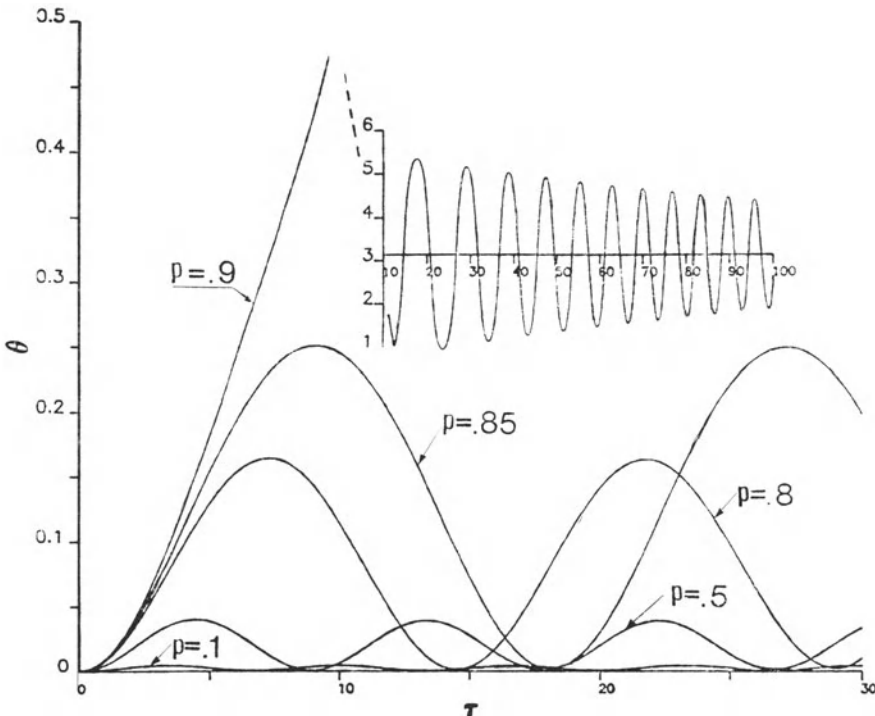


FIGURE 2.13. Plots of θ versus time τ for various load values p (model B).

amplitude of oscillation, θ_{\max} , between $p = 0.85$ and $p = 0.90$. According to the Budiansky–Roth criterion, p_{cr} is estimated to be 0.87, which is in excellent agreement (as expected for a single-degree-of-freedom system) with the value obtained from energy considerations.

2.3 Model C: A Snap-Through Model

Consider the model shown on Figure 2.14, which consists of three equal-length rigid bars. The three bars are pinned to each other, and they are connected with (linear) rotational springs of stiffness β . The left bar is pinned onto an immovable support, while the right bar is pinned onto a movable support, which in turn is connected to a wall through a (horizontal) linear extensional spring of stiffness k . The middle bar is originally horizontal, and the loading consists of two equal concentrated forces P applied at the ends of the middle bar and remaining vertical. The original angle between the horizontal line joining the supports and the end bars is α . The angle between the horizontal and the left bar in a deformed state is θ , while the angle between the horizontal and the right bar is ϕ .

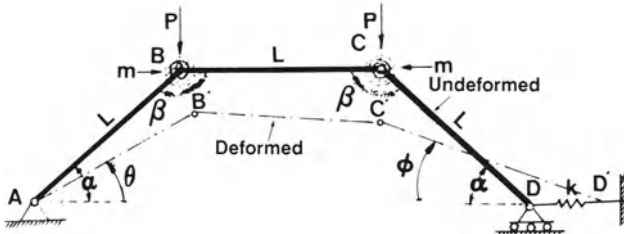


FIGURE 2.14. Geometry and sign convention for model C.

This is a two-degree-of-freedom model, and as will be seen from the ensuing discussion, certain new features enter into the solution.

Again, for the sake of simplicity, the rigid bars are assumed to be weightless and the mass of the system, $2m$, is assumed to be concentrated at joints B and C (m at each joint).

Assuming that α , θ , and ϕ are small angles such that their sine can be well approximated by the angle itself and the cosine by one minus half of the angle squared, the expression for the total potential is approximated by

$$\begin{aligned} U_T^P = & \frac{1}{2}\beta[5\theta + 5\phi^2 - 2\alpha^2 - 8\phi\theta - 2\theta\alpha - 2\phi\alpha] \\ & + \frac{kL^2}{2}(\alpha^2 - \theta^2 - \phi^2 + \phi\theta)^2 - PL(2\alpha - \theta - \phi). \end{aligned} \quad (53)$$

Note that for the above equation to be dimensionally correct the following order of magnitude must apply to the various terms. If α , θ , and ϕ are taken to be small numbers (of order δ), then β must be of order $\delta^2(kL^2)$, PL of order $\delta^3(kL^2)$, and U_T^P of order $\delta^4(kL^2)$.

The independent variables are ϕ and θ , and the symmetric response mode is characterized by $\theta = \phi$.

New variables r and s are introduced such that the symmetric response is characterized by $s = 0$. These are

$$\begin{aligned} \theta &= \sqrt{\bar{\beta}}(r - s) \\ \phi &= \sqrt{\bar{\beta}}(r + s) \end{aligned} \quad (54)$$

or

$$\begin{aligned} r &= (\theta + \phi)/2\sqrt{\bar{\beta}} \\ s &= (\phi - \theta)/2\sqrt{\bar{\beta}} \end{aligned} \quad (55)$$

where $\bar{\beta} = \beta/kL^2$ is a nondimensionalized rotational spring stiffness parameter. Through introduction of additional nondimensionalized parameters

$$\bar{U}_T^P = \frac{U_T^P}{\bar{\beta}^2 k L^2}, \quad p = \frac{P}{k L \bar{\beta}^{3/2}} \quad (56)$$

and by letting

$$\alpha^2 = \bar{\beta}\Lambda, \quad (57)$$

the following expression for the total potential is obtained:

$$\bar{U}_T^P = (r^2 + 9s^2 - 2\sqrt{\Lambda}r + \Lambda) + \frac{1}{2}(\Lambda - r^2 - 3s^2)^2 - 2p(\sqrt{\Lambda} - r). \quad (58)$$

Note that, on the basis of the nondimensionalization, the order of magnitude of the new parameters is as follows: (1) $\bar{\beta}$ is of order δ^2 , (2) \bar{U}_T^P is of order one, (3) r and s are of order one, (4) Λ is of order one, and (5) p is of order one.

2.3.1 Static Stability Analysis of Model C

It can easily be shown that if $\bar{\beta} = 0$ (no rotational springs), the system is unstable for zero load, $p = 0$, and thus the $\bar{\beta} = 0$ case is excluded from the present discussion, which also allows the nondimensionalization given by eqs. (56) and (57) (division by a nonzero number). In the case $\bar{\beta} = 0$, upon the application of a very small load P , the system snaps through an asymmetric mode ($s \neq 0$). Note also that unless $\bar{\beta} \neq 0$, the new coordinates, r and s , could not be defined.

The static analysis is performed by employing the energy approach.

The equilibrium equations are

$$\frac{\partial \bar{U}_T^P}{\partial r} = 0 = 2(r - \sqrt{\Lambda}) - (\Lambda - r^2 - 3s^2)2r + 2p \quad (59)$$

$$\frac{\partial \bar{U}_T^P}{\partial s} = 0 = 18s - (\Lambda - r^2 - 3s^2)6s. \quad (60)$$

By introducing a new load parameter

$$Q = p - \sqrt{\Lambda}, \quad (61)$$

the equilibrium equations, eqs. (59) and (60), become

$$\begin{aligned} (\Lambda - 1 - r^2 - 3s^2)r &= Q \\ s(\Lambda - 3 - r^2 - 3s^2) &= 0. \end{aligned} \quad (62)$$

There are two possible solutions to eqs. (62):

1. symmetric response $s \equiv 0$, and

$$(\Lambda - 1 - r^2)r = Q; \quad (63)$$

2. existence of asymmetric response, $s \neq 0$,

$$\Lambda - 3 = r^2 + 3s^2, \quad 2r = Q. \quad (64)$$

The equilibrium positions, eqs. (62), are plotted on Figure 2.15 for all Q and on Figure 2.16 as a load-deflection, $Q-r$, curve.

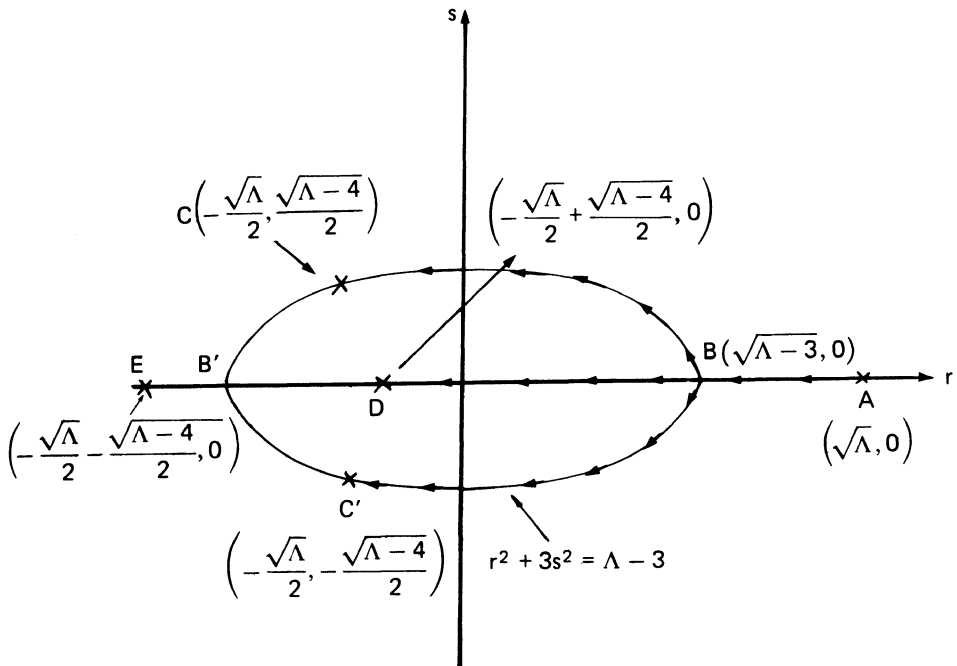


FIGURE 2.15. Locus of static equilibrium positions (model C).

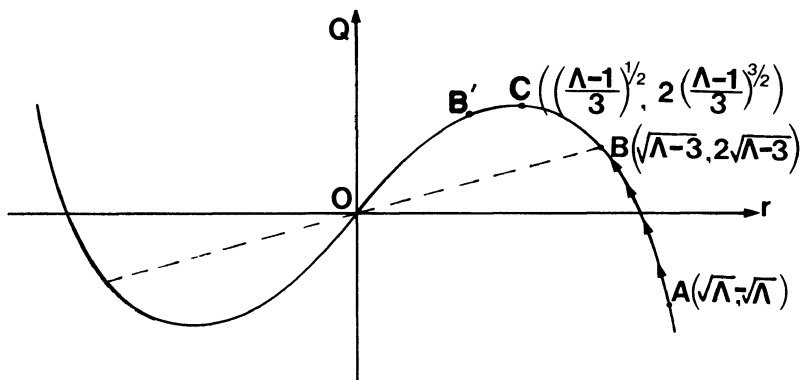


FIGURE 2.16. Load-displacement curve for model C.

On the basis of the above results and by performing the stability test (second derivatives), the following conclusions are drawn (for details see [3], in particular sections 2.3 and 7.5).

1. For $\Lambda < 1$ there is no possibility of buckling. Moreover, an asymmetric response ($s \neq 0$) cannot exist.
2. For $1 \leq \Lambda < 3$ the response is symmetric ($s = 0$) and buckling occurs

through the limit point (point *C* on Figure 2.16). Positions between *A* and *C* are stable, and the critical load is given by

$$\begin{aligned}\frac{1}{2}Q_{\text{cr}} &= \sqrt{\frac{\Lambda - 1}{3}}, \\ p_{\text{cr}} &= \sqrt{\Lambda} + 2\sqrt{\frac{\Lambda - 1}{3}}.\end{aligned}\tag{65}$$

3. For $3 < \Lambda < 4$ there is a possibility of asymmetric modes, but for this range of Λ values, point *B* is to the left of point *C* (shown as point *B'* on Figure 2.16),

$$\sqrt{\frac{\Lambda - 1}{3}} < \sqrt{\Lambda - 3},\tag{66}$$

and buckling still occurs through the existence of a limit point. Therefore, p_{cr} is given by eq. (65).

4. For $\Lambda > 4$ buckling occurs through the existence of an unstable bifurcation point (point *B*). Positions *A* to *B* are stable (see Figure 2.16), positions *BCO* and *BO* are unstable, and the critical load is given by

$$\begin{aligned}Q_{\text{cr}} &= 2\sqrt{\Lambda - 3} \quad \text{or} \\ p_{\text{cr}} &= \sqrt{\Lambda} + 2\sqrt{\Lambda - 3}.\end{aligned}\tag{67}$$

2.3.2 Dynamic Analysis: Ideal Impulse

In this case the procedure is the same as before, but since we are dealing with a two-degree-of-freedom system, special care is needed.

First, recall that it is assumed that the three bars are weightless and that the impulse is imparted into the system through two masses m at points *B* and *C*. This is also used in determining the initial kinetic energy. Next, through the impulse (moment of)-momentum theorem,

$$\lim_{T_0 \rightarrow 0} (2PT_0 L \cos \alpha) = mL \left(\frac{d\theta}{dt} \Big|_{\theta=\alpha} + \frac{d\phi}{dt} \Big|_{\phi=\alpha} \right).\tag{68}$$

Since α is very small, $\cos \alpha = 1$, and the expression for the ideal impulse, Imp , is

$$\text{Imp} = \lim_{T_0 \rightarrow 0} (2PT_0) = m \frac{d(\theta + \phi)}{dt} \Big|_{\theta=\phi=\alpha}.\tag{69}$$

In terms of the symmetric mode coordinate r [see eqs. (55)], and by making use of eq. (57), the expression for the impulse, eq. (69), becomes

$$\lim_{T_0 \rightarrow 0} (2PT_0) = 2mL \sqrt{\bar{\beta}} \frac{dr}{dt} \Big|_{r=\sqrt{\Lambda}}.\tag{70}$$

Next, we introduce a nondimensionalized time parameter τ by

$$\tau = t \left(\frac{\bar{\beta}k}{2m} \right)^{1/2}. \quad (71)$$

Finally, by dropping the designation *lim* from the expression for the ideal impulse and by using nondimensionalized parameters, eqs. (56) and (71), we may write

$$(2p\tau_0) = \left. \frac{dr}{d\tau} \right|_{r=\sqrt{\Lambda}}. \quad (72)$$

Similarly, the initial kinetic energy is given by

$$T_i^0 = \frac{1}{2}mL^2 \left(\left. \frac{d\theta}{dt} \right|_{\theta=\alpha}^2 + \left. \frac{d\phi}{dt} \right|_{\phi=\alpha}^2 \right) \quad (73)$$

or

$$T_i^0 = mL^2 \bar{\beta} \left(\left. \frac{dr}{dt} \right|_{r=\sqrt{\Lambda}}^2 \right),$$

and the nondimensionalized expression becomes

$$\bar{T}_i^0 = T_i^0 / \bar{\beta}^2 k L^2 = \frac{1}{2} \left(\left. \frac{dr}{d\tau} \right|_{r=\sqrt{\Lambda}}^2 \right). \quad (74)$$

The concept of dynamic stability is similar to the one used for models A and B:

$$\bar{U}_T^0 + \bar{T}_i^0 = \bar{T}_i^0. \quad (75)$$

A critical condition exists if the impulse $(2p\tau_0)$ imparts sufficient kinetic energy into the system so it can reach, with zero velocity, an unstable static equilibrium point on the zero-load total potential \bar{U}_T^0 , and thus the motion can become unbounded (buckled). Clearly, then, use of eqs. (75), (72), and (74) yields

$$(2p\tau_0)_{cr} = (2\bar{T}_i^0)^{1/2} = -[2\bar{U}_T^0 (\text{unstable static point})]^{1/2}. \quad (76)$$

Thus, before $(2p\tau_0)_{cr}$ can be found, one must have knowledge of all stationary points and of their character (stable, unstable, etc.). Starting with the expression for \bar{U}_T^0 [eq. (58) with $p = 0$], requiring equilibrium, and performing a stability analysis, the following results are obtained:

Stationary points and their character:

Point 1 at $(\sqrt{\Lambda}, 0)$	Stable (relative minimum)
Point 2 at $[(-\sqrt{\Lambda} + \sqrt{\Lambda - 4})/2, 0]$	Unstable (relative maximum)
Point 3 at $[(-\sqrt{\Lambda} - \sqrt{\Lambda - 4})/2, 0]$	Stable (relative minimum)

Point 4 at $[-\sqrt{\Lambda}/2, \sqrt{\Lambda - 4}/2]$ Unstable (saddle point)

Point 5 at $[-\sqrt{\Lambda}/2, -\sqrt{\Lambda - 4}/2]$ Unstable (saddle point).

It is seen from these results that regardless of the character (relative maximum or saddle points), unstable static equilibrium points exist only for $\Lambda \geq 4$. This implies that a critical ideal impulse exists (in the sense of escaping or buckled motion) only for $\Lambda \geq 4$.

Moreover, the value of the total potential at the static equilibrium points under zero load is given by

$$\begin{aligned} \text{At point 1} \quad & \bar{U}_T^0 = 0 \\ \text{At point 2} \quad & \bar{U}_T^0 = \frac{1}{2}[5\Lambda - 2 - 3\sqrt{\Lambda(\Lambda - 4)} + \frac{1}{4}(\Lambda + 2 + \sqrt{\Lambda(\Lambda - 4)})^2] \\ \text{At points 4 and 5} \quad & U_T^0 = \frac{9}{2}(\Lambda - 1) \\ \text{At point 3} \quad & U_T^0 = \frac{5}{2}\Lambda - 1 + \frac{3}{2}\sqrt{\Lambda(\Lambda - 4)} + \frac{1}{8}(\Lambda + 2 - \sqrt{\Lambda(\Lambda - 4)})^2. \end{aligned} \tag{77}$$

We observe that there are two possibilities for the motion to become unbounded: (1) Motion can become unbounded by reaching point 2 with zero velocity, in which case the system will definitely move toward point 3 (far stable point). In this case the corresponding critical impulse is termed (MGCL) because U_T^0 (point 2) is the largest of all \bar{U}_T^0 (stationary points) and

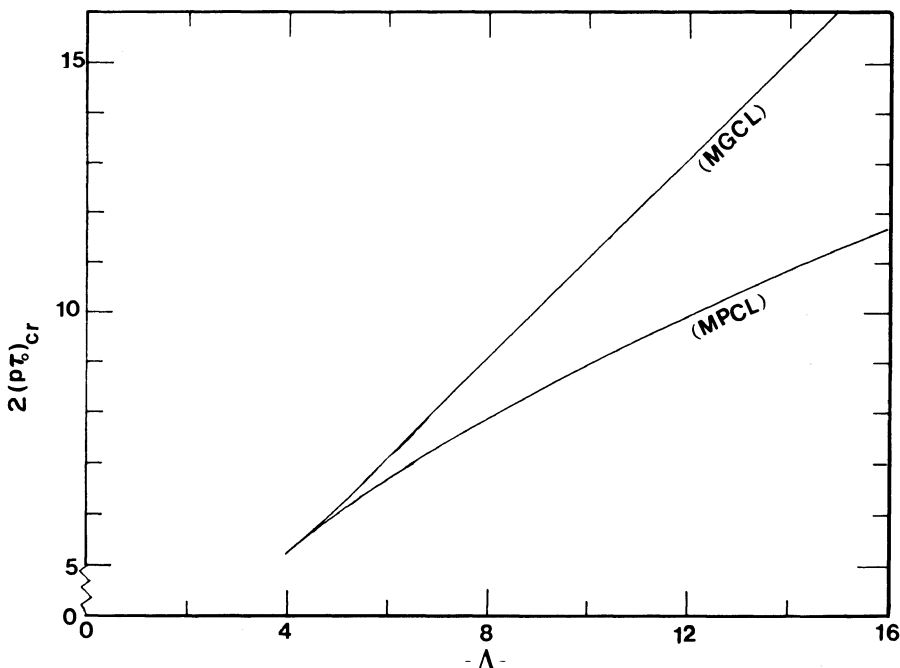


FIGURE 2.17. Upper and lower bounds for the critical ideal impulse (model C).

thus, regardless of the path of motion in the (r, s) space, starting from $(\Lambda, 0)$ the motion will enclose at least one unstable point and will become either large or unbounded. (2) Motion can also become unbounded by reaching either point 4 or point 5, in which case there exists a possibility of motion becoming either large or unbounded and enclosing one unstable point. Note that, in this case, there is a possibility of escaping motion, but this is not guaranteed, because the system can simply oscillate in the (r, s) space bounded by lines of equal potential [to \bar{U}_T^0 (point 4)] enclosing only the near static stable point, point 1, and neither of the “saddle” points, point 4 or point 5; thus, the corresponding critical impulse is called (MPCL).

(MPCL) and (MGCL) denote upper and lower bounds of $2(p\tau_0)_{cr}$. By eq. (76),

$$(MPCL) \quad 2(p\tau_0)_{cr} = 3\sqrt{\Lambda - 1} \quad (78)$$

$$(MGCL) \quad 2(p\tau_0)_{cr} = [5\Lambda - 2 - 3\sqrt{\Lambda^2 - 4\Lambda} + \frac{1}{4}(\Lambda + 2 + \sqrt{\Lambda^2 - 4\Lambda})^2]^{1/2}.$$

Note that critical conditions can exist only for $\Lambda \geq 4$. If $\Lambda = 4$, the relative maximum and the two saddle points coincide, and the upper and lower bounds for the critical impulse coincide. The results are plotted on Figure 2.17.

2.3.3 Dynamic Analysis: Sudden Constant Load of Infinite Duration

The concept of dynamic stability is similar to the one used for one-degree-of-freedom models. The only difference is that, in this case also, there are a lower bound (MPCL) and an upper bound (MGCL). The lower bound corresponds to loads for which there is a possibility of buckled motion, while the upper bound corresponds to loads for which the motion will definitely be buckled. Because the existence of bounds is dependent on the value of Λ , the discussion will be based on the range of Λ values. Each range of Λ values is discussed separately.

1. For $\Lambda < 3$, there are no saddle points and the system behaves as a one-degree-of-freedom system. Therefore, for this case the governing equations are

$$\bar{U}_T^P = 0, \quad (\Lambda - 1 - r^2)r = Q \quad (79)$$

and

$$\frac{d^2 \bar{U}_T^P}{dr^2} < 0 \quad \text{at the solution.}$$

Note that, for this case, buckled motion is both possible and guaranteed. Thus, the upper and lower bounds are coincident.

2. For $\Lambda > 3$, there exist saddle points on the total potential, in addition to

the relative maximum point. All three are unstable static equilibrium points (stationary points). Therefore, the motion can become buckled either through a saddle point or through the relative maximum point. It will be shown next that, in certain instances, buckled motion is possible and in others, guaranteed (corresponding to lower and upper bounds of critical conditions). Before proceeding with the analysis, the following observations are made:

Parenthesis 1. For a specified load the total potential has a lower value at a saddle point than at a relative maximum point. This can be proved through computation of \bar{U}_T^P at the corresponding points.

Parenthesis 2. Regardless of the values of p and Λ (for $\Lambda > 3$), the total potential at any s position, but a fixed r position ($r = \bar{r} < \Lambda - 3$), has a higher potential than that of a position characterized by $r = \bar{r}$ and an s position on the ellipse

$$r^2 + 3s^2 = \Lambda - 3. \quad (80)$$

Note that the ellipse, eq. (80), defines the locus of static equilibrium points [saddle points; see eqs. (64)].

Proof. Let $\Delta\bar{U}_T^P$ denote the difference in total potential between any s position and that of an s position on the ellipse ($r = \bar{r}$). Then, from eqs. (58) and (60),

$$\begin{aligned} \Delta\bar{U}_T^P &= [\bar{r}^2 + 9s^2 - 2\sqrt{\Lambda}\bar{r} + \Lambda + \frac{1}{2}(\Lambda - r^2 - 3s^2)^2 - 2p(\sqrt{\Lambda} - r)] \\ &\quad - [4\Lambda - \frac{9}{2} - 2\bar{r}^2 - 2\sqrt{\Lambda}\bar{r} - 2p(\sqrt{\Lambda} - \bar{r})] \\ &= 3(\bar{r}^2 + 3s^2 - \Lambda) + \frac{9}{2} + \frac{1}{2}(\Lambda - \bar{r}^2 - 3s^2)^2 \\ &= \frac{1}{2}(\Lambda - 3 - \bar{r}^2 - 3s^2)^2 \geq 0, \quad \text{Q.E.D.} \end{aligned} \quad (81)$$

Clearly, the difference is zero when s is on the ellipse and positive for all other s .

Parenthesis 3. For $p \geq \sqrt{\Lambda} + 2\sqrt{\Lambda - 3}$ [loads higher than the static critical load—see eq. (67)], if $r_1 < r_2 \leq \sqrt{\Lambda - 3}$, then the total potential on the ellipse, eq. (80), is higher at r_2 than at r_1 .

Let

$$\Delta\bar{U}_T^P = \bar{U}_T^P(r_2) - \bar{U}_T^P(r_1). \quad (82)$$

Then, by eqs. (58) and (82),

$$\Delta\bar{U}_T^P = 2(r_2 - r_1)[p - \sqrt{\Lambda} - (\bar{r}_2 + \bar{r}_1)]. \quad (83)$$

Since $r_2 - r_1$ is positive, $\Delta\bar{U}_T^P$ is positive if $p > \sqrt{\Lambda} + (\bar{r}_2 + \bar{r}_1)$. But since $p \geq \sqrt{\Lambda} + 2\sqrt{\Lambda - 3}$, if $\sqrt{\Lambda} + 2\sqrt{\Lambda - 3} > \sqrt{\Lambda} + (\bar{r}_2 + \bar{r}_1)$ then definitely $p > \sqrt{\Lambda} + (\bar{r}_2 + \bar{r}_1)$. Clearly, from the statement of this parenthesis $2\sqrt{\Lambda - 3} > r_2 + r_1$, which concludes the proof.

As the load is increased from zero, at low values of p , the zero potential

lines in the (r, s) space enclose only the near static equilibrium point and the motion is unbuckled (see Figure 1.5). At some value of the load, the first unstable point(s), at which the total potential can become zero, is the saddle point(s) according to Parenthesis 1. At this load there exists a possibility of buckled motion through the saddle point. This load, then, is called (MPCL). The governing equations for finding this critical load, as well as the corresponding position (s, r coordinates) of the saddle point, are

$$\begin{aligned} \bar{U}_T^P = & (r^2 + 9s^2 - 2\sqrt{\Lambda}r + \Lambda) + \frac{1}{2}(\Lambda - r^2 - 3s^2)^2 - 2p(\sqrt{\Lambda} - r) = 0 \\ (\Lambda - 1 - r^2 - 3s^2)r = & p - \sqrt{\Lambda} \\ \Lambda - 3 - r^2 - 3s^2 = & 0. \end{aligned} \quad (84)$$

Note that saddle points are unstable; thus, there is no need to apply the stability requirements. The solution of eqs. (84) yields

$$(\text{MPCL}) \quad p_{cr,\infty} = 3(\sqrt{\Lambda} - 1)$$

and saddle points at $r = \sqrt{\Lambda} - \frac{3}{2}$, $s = \pm(\sqrt{\Lambda} - \frac{7}{4})^{1/2}$. The solutions to eqs. (79) and (84) are plotted on Figure 2.18.

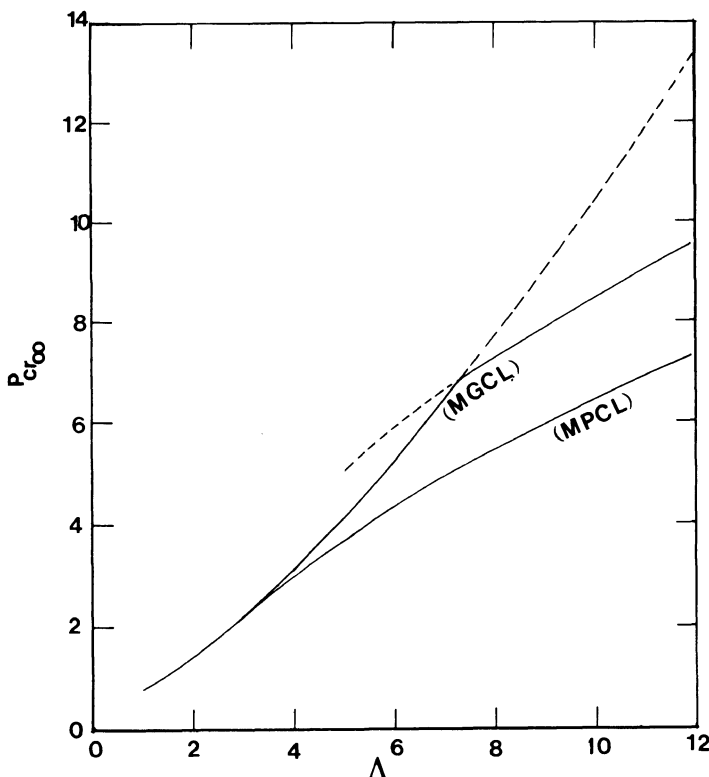


FIGURE 2.18. Upper and lower bounds for the critical load (infinite duration, model C).

As far as the case of the upper bound is concerned, (MGCL), there are two ways through which a guaranteed buckled motion can be achieved. One way is to require \bar{U}_T^P at the relative maximum unstable static point to be zero. In this case the motion is definitely buckled and the critical load can be obtained from the solution of eqs. (79). The second way is for loads that are equal to the static critical load for asymmetric buckling ($\sqrt{\Lambda} + 2\sqrt{\Lambda - 3}$). In this case, although the total potential at the relative maximum point is higher than zero, guaranteed buckled motion can be achieved, because of Parentheses 2 and 3. In this latter case, p_{cr} (MGCL) is given by the expression for the static load. Both results are shown graphically on Figure 2.18.

Note that the upper bound is the smallest load computed, either by the solutions of eqs. (79) (for $\frac{7}{4} \leq \Lambda \leq 7.3$) or by the static critical load (for $\Lambda \geq 7.3$). Moreover, for very large Λ values the upper and lower bounds approach each other ($3\sqrt{\Lambda}$).

Problems

- Consider the model shown on Figure 2.19. The bars are rigid and hinged. For simplicity, assume the mass of the system to be concentrated at the hinge between the two bars. Find (numerically) for the entire range of α values ($0^\circ \leq \alpha < 90^\circ$)
 - Values for the critical ideal impulse.
 - Values for the critical dynamic load for the case of infinite duration. Compare these values to the static critical load values.
 For this problem use (i) the total potential energy approach and (ii) the total energy-phase plane approach.

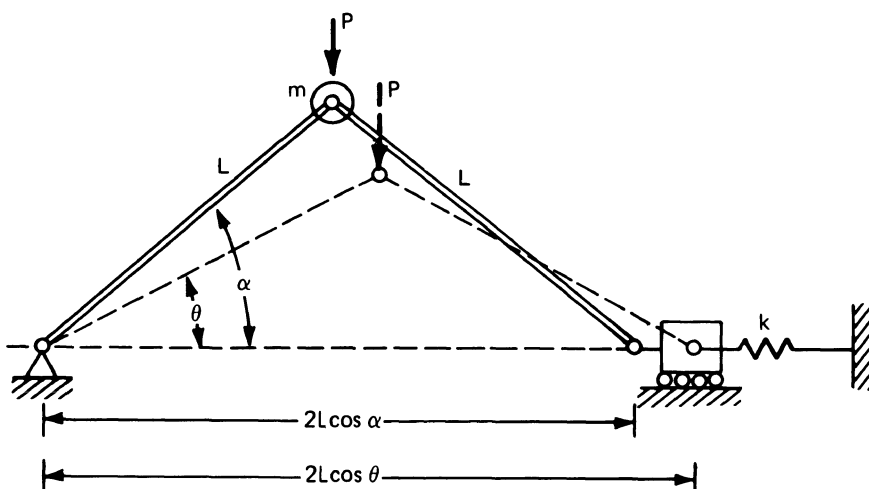


FIGURE 2.19. Problem 1 model.

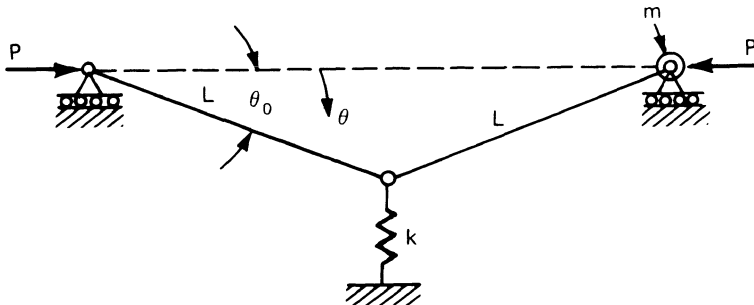


FIGURE 2.20. Problem 2 model.

2. Consider the mechanical model shown in Figure 2.20. The two bars are rigid and the spring stiffness is constant, k . Assume that the mass of the system is concentrated at the right-end hinge.
 - a. Give a complete static analysis.
 - b. Find (numerically), for $\theta_0 = 0.01$, $\theta_0 = 0.05$, and $\theta_0 = 0.10$, (i) values for the critical ideal impulse and (ii) values for the critical dynamic load (constant magnitude of infinite duration). Use the potential energy approach.
3. Consider the mechanical model shown in Figure 2.21. The two bars are rigid and the rotational spring stiffness is constant, β . The constant k may be determined from geometric considerations and θ_0 is some small geometric imperfection. Assume that the system mass is concentrated at the right-end hinge.
 - a. Give a complete static analysis.
 - b. Find (numerically) for $\theta_0 = 0.01$, 0.05 , 0.10 , and 0.20 (i) values for the critical ideal impulse and (ii) values for the critical dynamic load (constant load of infinite duration). Use the potential energy approach.
4. Model C, Figure 2.14, was analyzed by assuming that θ and ϕ are small angles (say $\theta, \phi \leq 0.2$ radians). Also note that there is no restriction on the Λ values, other than that they must be greater than one to yield instability. Perform an order analysis and investigate if the following geometries can be represented by the model (C):

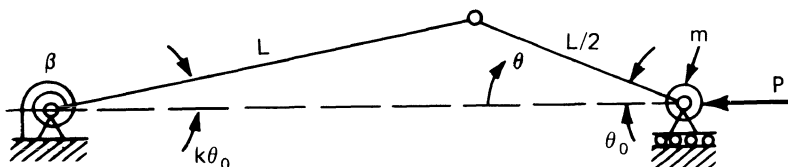


FIGURE 2.21. Problem 3 model.

- a. $L = 12$ in., $k = 10$ lb/in.; $\beta = 200$ lb-in./rad.
 - b. $L = 100$ in., $k = 100$ lb/in.; $\beta = 4,000$ lb-in./rad.
 - c. $L = 20$ in., $k = 2$ lb/in.; $\beta = 1,000$ lb-in./rad.
 - d. $L = 10$ in., $k = 10$ lb/in.; $\beta = 100$ lb-in./rad.
5. For model C, find critical dynamic loads (in pounds) for the geometries of problem 4 (whenever possible) and $\alpha = 7^\circ$.

References

1. Hoff, N.J. Dynamic stability of structures. *Dynamic Stability of Structures* (edited by G. Herrmann). Pergamon, New York, 1967.
2. Budiansky, B., and Roth, R.S. Axisymmetric dynamic buckling of clamped shallow spherical shells. Collected Papers on Instability of Shell Structures. NASA TN D-1510, 1962.
3. Simitses, G.J. *An Introduction to the Elastic Stability of Structures*. Prentice-Hall, Englewood Cliffs, N.J., 1976.

3

Dynamic Stability Under Constant Load of Finite Duration

3.1 Statement of the Problem

Consider a system (model) at its natural (unloaded) position. At time $t = 0$ a constant load P is suddenly applied to the system and it acts only for a finite duration, time $t = T_0$ (Figure 3.1). After the release of the force P , the system moves because of the energy imparted, during the action of the load P . The concept of dynamic stability for this particular load case is similar to the concept used in the cases of the ideal impulse and of the constant load of infinite duration. Thus, for all three cases the concept of dynamic stability is based on the definition of *buckled* and *unbuckled* motion.

If the energy imparted (into the system) through the load P is insufficient for the system to reach the unstable static equilibrium point on the “zero-load” total potential with zero velocity (zero kinetic energy), the motion is called unbuckled. In this case, the system is dynamically stable. Consequently, the criterion for dynamic stability requires that the dynamically stable system possess total energy (at the release time T_0) at a level below the level of the potential at its unstable static equilibrium point for the zero-load system. This is fully substantiated by mathematical arguments in the next section.

The concept and the related procedure for finding critical conditions are demonstrated through application to the same three simple mechanical models (models A, B, and C) employed in Chapter 2. The extreme cases of the duration time T_0 approaching zero (ideal impulse) and infinity (constant load of infinite duration) are special cases of the present one.

3.2 Criterion for Critical Conditions

First the criterion is presented for a single-degree-of-freedom system and then it is extended to a two-degree-of-freedom system. Finally, some commentary is given concerning multi-degree-of-freedom systems.

Consider a single-degree-of-freedom system (θ is the generalized coordinate) subjected to a sudden load of constant magnitude and finite

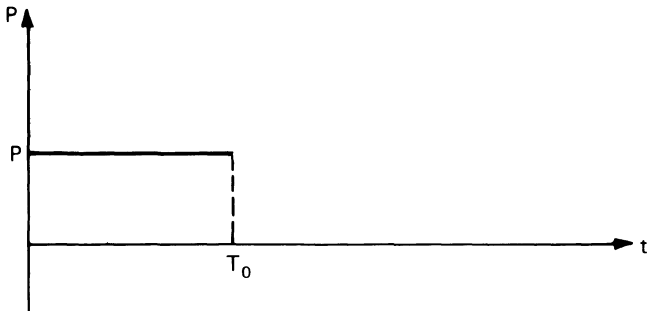


FIGURE 3.1. A step load.

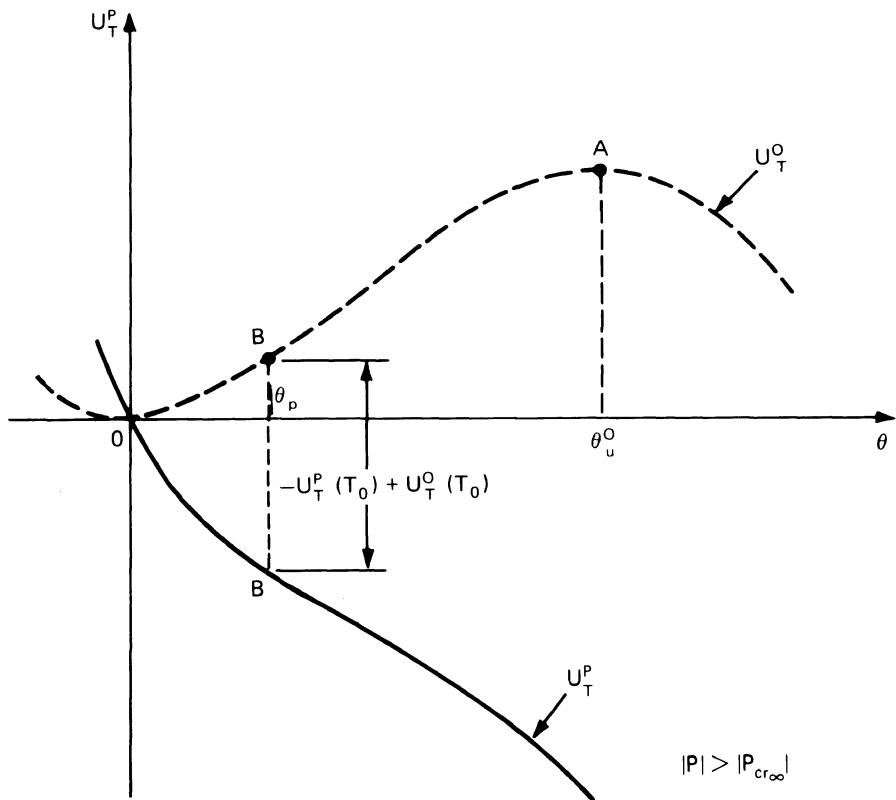


FIGURE 3.2. Total potential curves for a single-degree-of-freedom system.

duration T_0 (see Figure 3.1). T_0 is also referred to as the time of release. Let U_T^P and T^P denote the system total potential and kinetic energies, respectively.

Two total potential curves are shown on Figure 3.2, one corresponding to zero load and one to a load P with magnitude larger than the critical dynamic load for infinite duration, $P_{cr,\infty}$. It can be shown that for finite values of T_0 the critical load is larger than $P_{cr,\infty}$. As T_0 approaches infinity, the critical load approaches (asymptotically) $P_{cr,\infty}$.

Since the system is conservative,

$$U_T^P + T^P = 0 \quad \text{for } 0 \leq t < T_0, \quad (1)$$

and

$$U_T^0 + T^0 = C = U^0(T_0) + T^0(T_0) \quad \text{for } t > T_0. \quad (2)$$

These two equations express conservation of energy for $0 \leq t < T_0$ and $t > T_0$. According to eq. (2), the constant C must equal the total energy at the instant of release of the sudden load P .

The continuity of the kinetic energy at the time of release T_0 is expressed by

$$T^0(T_0) = T^P(T_0). \quad (3)$$

Use of eqs. (1) and (3) in eq. (2) yields

$$U_T^0 + T^0 = U_T^0(T_0) - U_T^P(T_0) \quad \text{for } t \leq T_0. \quad (4)$$

If θ_u^0 indicates the position of the unstable static equilibrium point for $P = 0$ (see Figure 3.2), the critical condition is met (buckled motion is possible) if the load P , acting for time T_0 , imparts sufficient energy to the system to equal the potential $U_T^0(\theta_u^0)$ of the zero-load system at the unstable position θ_u^0 . Thus, the stability criterion is expressed by

$$U_T^0(T_0) - U_T^P(T_0) \leq U_T^0(\theta_u^0). \quad (5)$$

The equality sign implies a critical condition, while the inequality refers to a dynamically stable situation.

Note that eq. (5) relates the applied load P and the release position θ_p (one equation in two unknown quantities, if one views the release position θ_p at time T_0 as one quantity). In addition, through eq. (1), one may relate the applied load P , the release position θ_p , and the release time T_0 for a specified path of motion. For one-degree-of-freedom systems there is only one path. With the aid of Figure 3.2, eqs.(3), (4), and (5) are first explained. The system is suddenly loaded and the load is released at time T_0 . The system, at that instant, has reached position θ_p . During this time, the system traverses the curve U_T^P , and the system kinetic energy at $t = T_0$ is given by eq. (1) as $-U_T^P(\theta_p)$. This value must be equal to $T^0(\theta_p)$ or $T^0(T_0)$ because of kinematic continuity, eq. (3). For $t > T_0$, the system traverses the U_T^0 curve (see Figure 3.2), and a dynamic instability is possible if the system can reach point A with zero kinetic energy, eq. (5) with the equality sign. This clearly explains the concept of dynamic stability of a one-degree-of-freedom system.

Next, the numerical procedure for estimating critical conditions is outlined.

For this load case, a critical condition consists of finding a P_{cr} for a given value of T_0 , or a $T_{0,cr}$ for a given value of P (greater than the one corresponding to infinite duration). Thus, either T_0 is given and the unknown is P , or P is given and the unknown is T_0 . According to eq. (5), which can be written as

$$U_T^0(\theta_p) - U_T^P(\theta_p) = U_T^0(\theta_u^0), \quad (6)$$

we have one equation relating two unknowns, θ_p and either P or T_0 . Next, eq. (1) can be written as

$$T^P = \bar{C} \left(\frac{d\theta}{dt} \right)^2 = -U_T^P \quad (7)$$

where \bar{C} is a known constant. Then from eq. (7),

$$dt = [-U_T^P/\bar{C}]^{-1/2} d\theta, \quad (8)$$

and integration from zero to T_0 yields

$$T_0 = \int_0^{\theta_p} \frac{d\theta}{[-U_T^P/\bar{C}]^{1/2}}. \quad (9)$$

This equation, eq. (9), yields a second equation in the same two unknowns (θ_p and either P or T_0). The simultaneous solution of the two equations, eqs. (6) and (9), yields the critical condition for this load case. As is shown in later sections, computationally it is much simpler (in many cases) to assign (small) values of θ_p and solve eqs. (6) and (9) for T_0 and the corresponding P .

Note that for a single-degree-of-freedom system the critical condition is uniquely determined (the lower and upper bounds are one and the same).

For a system of two or more degrees of freedom, a similar procedure is needed to establish either the lower bound (MPCL) or the upper bound (MGCL).

For the case of the lower bound, one of the equations needed for estimating the (possible) critical load is eq. (6). In eq. (6), $\underline{\theta}_u^0$ denotes the static unstable equilibrium position, which yields the lowest value for the total potential (note that $\underline{\theta}_u^0$ is the vector of all generalized coordinates). But the second equation is obtained from the energy balance (conservation of energy) for the initial length of time ($0 < t < T_0$), or

$$U_T^P + T^P = 0 \quad \text{for } 0 \leq t < T_0. \quad (1)$$

In the above equation, both the total potential U_T^P and the kinetic energy T^P are functions of all the generalized coordinates (degrees of freedom). Clearly then, in order to define critical conditions uniquely, the path of motion should also be known. In other words, one should determine how the system moves in the space of the generalized coordinates during the application ($0 < t < T_0$) of the sudden load. In many structural problems this is a very difficult task. Then one has three choices: (1) Assume the path; that is, on the basis of physical arguments, assume some path. An example of

this would be that for model C and relatively small values of the duration time T_0 , the path may be assumed to be symmetric ($s \equiv 0$). (2) Numerically solve the equations of motion for $t < T_0$, so that one can establish the true path. Of course, this approach is somehow defeating the purpose of relating critical conditions to characteristics of the system total potential and thus avoiding the solution of complicated coupled nonlinear partial differential equations; thus, this second choice is a poor one for use in connection with the total potential energy approach. (3) Establish the path of motion by solving the related “brachistochrone” problem. This can be accomplished if one is interested in finding only a lower bound for the minimum possible critical load (MPCL), which denotes a lower bound of critical loads itself; the entire problem is then viewed as follows: find the smallest time T_0 (and the related path) for a given load P such that the motion can possibly become buckled (in the sense that sufficient energy is imparted to the system that it can reach the static unstable position θ_u^0 with zero kinetic energy—note that after the release of the load the path of motion is irrelevant, in the sense that it does not enter into the calculations).

The extended concept and related procedure for estimating critical conditions are demonstrated through the same three mechanical models as in Chapter 2 (models A, B, and C).

3.3 Application to Model A

For this particular model, the static and dynamic analyses with all the necessary equations are presented in Chapter 2. According to the static analysis of the model [Figure 2.3 and eqs. (2), (8), and (15) of Chapter 2], the unstable static equilibrium positions are located at $\theta = \pm \pi/2$. Furthermore, the first of the two needed equations, eq. (6), becomes

$$p(\cos \theta_0 - \cos \theta_p) = [\sqrt{2} - \sqrt{1 + \sin \theta_0}]^2. \quad (10)$$

Next, by eqs. (7) and (12) of Chapter 2, the expression for the kinetic energy [in terms of nondimensionalized parameters—see eqs. (11) of Chapter 2] is

$$\bar{T}^0 = \left(\frac{d\theta}{d\tau} \right)^2. \quad (11)$$

Therefore, the second needed equation, eq. (9), expressed in terms of nondimensionalized parameters, is given by

$$\tau_0 = \int_{\theta_0}^{\theta_p} \frac{d\theta}{\sqrt{-U_T^P}}$$

or

$$\tau_0 = \int_{\theta_0}^{\theta_p} \left[-(\sqrt{1 + \sin \theta} - \sqrt{1 + \sin \theta_0})^2 + p(\cos \theta_0 - \cos \theta) \right]^{-1/2} d\theta. \quad (12)$$

Note that for a given P , the simultaneous solution of eqs. (10) and (12) yields $\tau_{0,\text{cr}}$ and θ_{cr} . As already discussed, a critical condition may also be characterized by a p_{cr} for a given τ_0 . It is easily seen, though, from eqs. (10) and (12) that computationally it is more convenient to assign values of θ_p , calculate p [from eq. (10)], and then compute τ_0 by numerical integration [from eq. (12)]. The pair of p , τ_0 denotes a critical condition for the employed value of θ_p . This is repeated for higher values of θ_p and the entire curve of p versus $\tau_{0,\text{cr}}$ (or p_{cr} versus τ_0) is produced (starting with $\theta = \theta_0 + \theta_1$, where θ_1 is a small increment, and increasing θ_1 to values approaching the angle corresponding to the infinite-duration case—see point A on Figure 2.4).

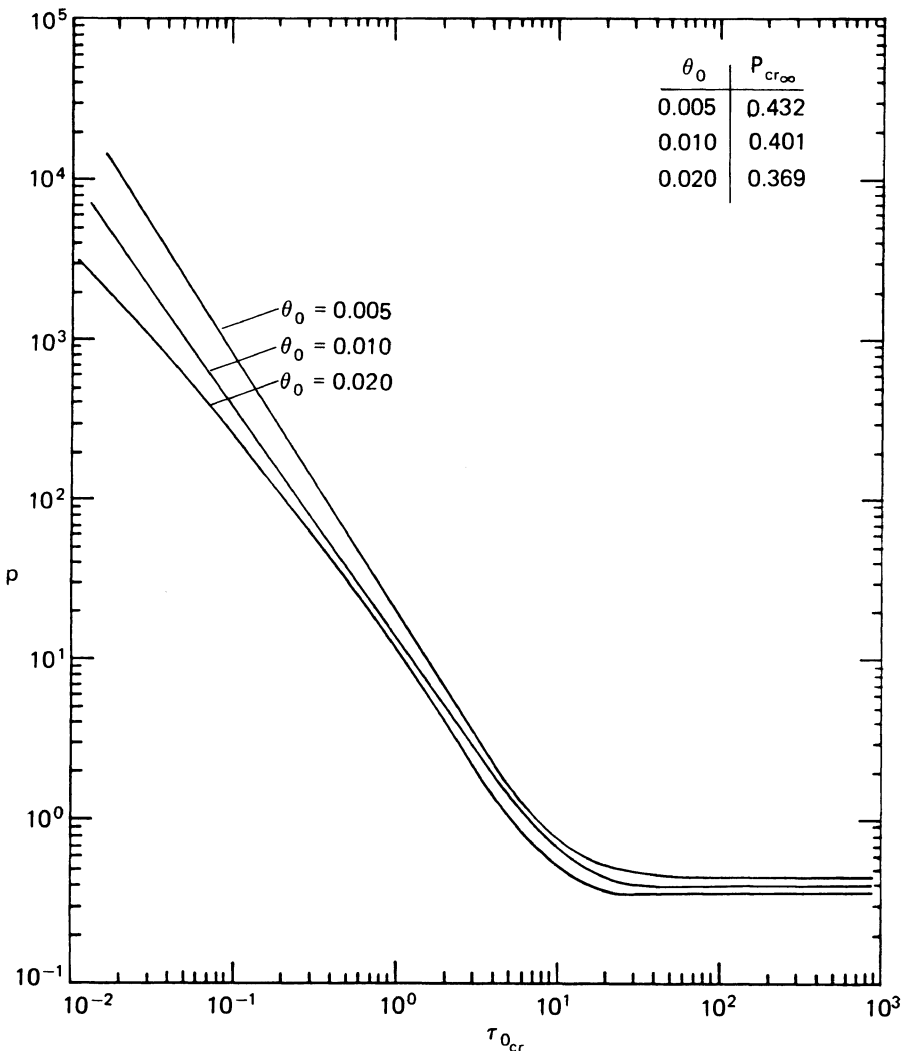


FIGURE 3.3 Constant load p versus critical duration time $\tau_{0,\text{cr}}$ (model A).

Results are presented graphically on Figure 3.3 as plots of p versus $\tau_{0_{cr}}$ for three values of θ_0 ($\theta_0 = 0.005, 0.10$, and 0.20) and on Figure 3.4 as plots of critical impulse (defined as the product of p and $\tau_{0_{cr}}$) versus $\tau_{0_{cr}}$ for the same three values of θ_0 .

Two observations are important. First, as $\tau_{0_{cr}}$ becomes very large, the corresponding load asymptotically approaches the value corresponding to p_{cr_∞} (Figure 3.3) (constant load of infinite duration). Second, as $\tau_{0_{cr}}$ approaches zero, the value of $(p\tau_0)$ approaches the value of the critical ideal impulse (Figure 3.4). For this particular model (see Figure 3.4), it appears that there exists a minimum value for $(p\tau_0)$ corresponding to a value for τ_0 approximately equal to 10. This seems to be true for all θ_0 values.

Before closing, it is shown that the closed-form expression for the ideal impulse, eq. (17) of Chapter 2, can be obtained from eqs. (10) and (12) by assuming that θ_p (or θ_{cr}) is equal to θ_0 , plus a very small angle $\hat{\theta}$.

Note that the expression for the ideal impulse (from Chapter 2) is given by

$$(p\tau_0)_{cr} = \frac{2(\sqrt{2} - \sqrt{1 + \sin \theta_0})}{\sin \theta_0}. \quad (13)$$

By letting $\theta_p = \theta_{cr} = \theta_0 + \hat{\theta}$, eq. (10) yields

$$p_{cr} = \frac{(\sqrt{2} - \sqrt{1 + \sin \theta_0})^2}{\hat{\theta} \sin \theta_0} \quad (14)$$

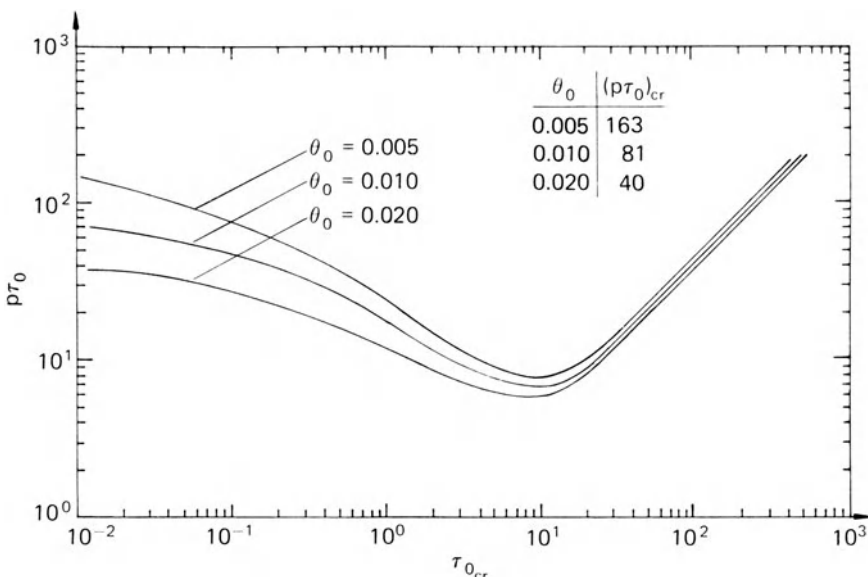


FIGURE 3.4. Impulse $(p\tau_0)$ versus critical duration time $\tau_{0_{cr}}$ (model A).

where the denominator is obtained from

$$\cos \theta_0 - \cos \theta_p = \cos \theta_0 - \cos(\theta_0 + \hat{\theta}) = \sin \theta_0 \sin \hat{\theta} = \hat{\theta} \sin \theta_0. \quad (15)$$

The integrand of eq. (12) contains an angle θ , which varies from θ_0 to θ_p (limits of integration). If a new variable (angle) is introduced, say $\delta\theta$, such that $\theta = \theta_0 + \delta\theta$, then $\delta\theta$ varies between zero and $\hat{\theta}$, and $\delta\theta$ is thus a very small angle (also). Then eq. (12) becomes (through an order of magnitude analysis)

$$\tau_0 = \int_{\theta_0}^{\theta_0 + \hat{\theta}} \frac{d\theta}{\sqrt{p\delta\theta \sin \theta_0}} \quad (16)$$

or

$$\tau_{0_{cr}} = \int_0^{\hat{\theta}} \frac{d(\delta\theta)}{\sqrt{p \sin \theta_0} \sqrt{\delta\theta}} = \frac{2\sqrt{\hat{\theta}}}{p \sin \theta_0}. \quad (17)$$

Finally, from eqs. (14) and (17) one can obtain the following:

$$(p\tau_0) = \frac{2\sqrt{p_{cr}}\sqrt{\hat{\theta}}}{\sqrt{\sin \theta_0}} = \frac{2(\sqrt{2} - \sqrt{1 + \sin \theta_0})\sqrt{\hat{\theta}}}{\sqrt{\hat{\theta}}\sqrt{\sin \theta_0}\sqrt{\sin \theta_0}}$$

or

$$(pr_0)_{cr} = \frac{2(\sqrt{2} - \sqrt{1 + \sin \theta_0})}{\sin \theta_0}, \quad (18)$$

which is identical to the previously obtained closed-form solution, eq. (13).

3.4 Application to Model B

For this particular model the unstable stationary points on the zero-load total potential are also located at $\theta = \pm \pi/2$ (see Figure 2.7). Then eq. (6) becomes (for this model)

$$2p(1 - \cos \theta_{cr} + \bar{e} \sin \theta_{cr}) = 1 \quad (19)$$

where $\bar{e} = e/L$, $p = PL/ka^2$, and θ_{cr} is the position of the system at the critical time of release, $\tau_{0_{cr}}$.

According to the nondimensionalization employed for this model in Chapter 2, the kinetic energy and time parameters are [see eqs. (34) and (35) of Chapter 2]

$$\bar{T} = (d\theta/d\tau)^2, \quad \tau = (ka^2/I)^{1/2}t. \quad (20)$$

For this model, eq. (1) becomes

$$\bar{U}_T^P + \dot{\theta}^2 = 0. \quad (21)$$

From eq. (21) one may solve for the critical duration time $\tau_{0_{cr}}$, or

$$\tau_{0_{cr}} = \int_0^{\theta_{cr}} \frac{d\theta}{\sqrt{-\bar{U}_T^P}} \quad (22)$$

where the \bar{U}_T^P expression for model B is given by eq. (24) of Chapter 2:

$$\bar{U}_T^P = \sin^2 \theta - 2p(1 - \cos \theta + \bar{e} \sin \theta). \quad (23)$$

For this model, as in the case of model A, critical conditions are obtained by solving simultaneously eqs. (19) and (22). Again, computationally it is more

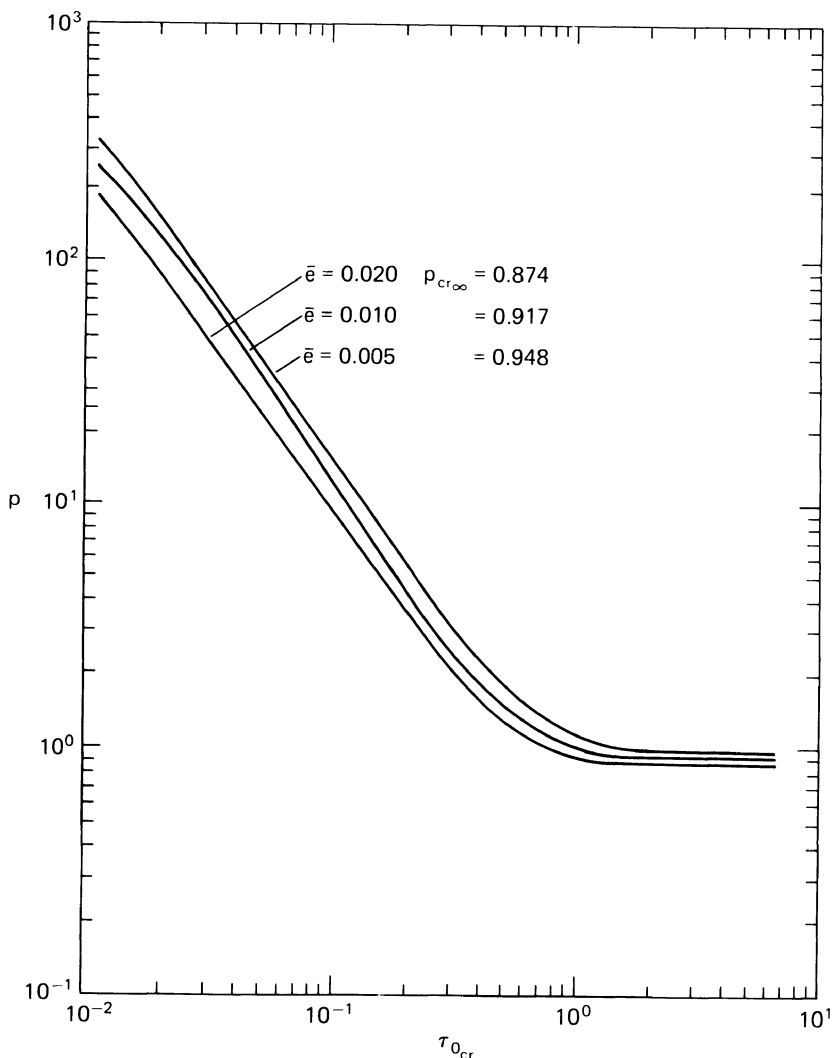


FIGURE 3.5. Constant load p_{cr} versus critical duration time $\tau_{0_{cr}}$ (model B).

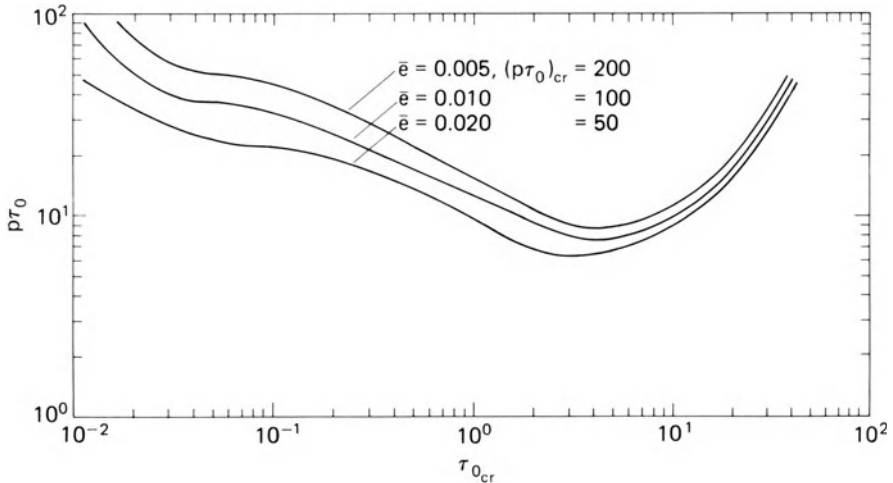


FIGURE 3.6. Impulse ($p\tau_0$) versus critical time $\tau_{0_{cr}}$ (model B).

convenient to assign small values for θ_{cr} (starting from an extremely small angle and increasing it to the value corresponding to the case of sudden constant load of infinite duration), solve for p_{cr} from eq. (19), and then solve for $\tau_{0_{cr}}$ from eq. (22) (through numerical integration). Results are presented graphically on Figures 3.5 and 3.6 for three values of the load eccentricity parameter ($\bar{e} = 0.005, 0.010$, and 0.020).

As the release time τ_0 approaches infinity (becomes very large), the corresponding load approaches the critical value for a sudden constant load with infinite duration (see Figure 3.5). Similarly, as the duration time approaches zero, the critical impulse approaches the value for the critical ideal impulse [$(p\tau_0)_{cr} = 1/\bar{e}$]. This expression is derived analytically by assuming that τ_0 is a very small number and, consequently, θ_{cr} is as small as we wish it to be.

Therefore eq. (19) yields

$$p_{cr} = \frac{1}{2\bar{e}\theta_{cr}}, \quad (24)$$

and eq. (22) yields

$$\begin{aligned} \tau_{0_{cr}} &= \int_0^{\theta_{cr}} \frac{d\theta}{\sqrt{2p(\frac{1}{2}\theta^2 + \bar{e}\theta) - \theta^2}} \\ &= \int_0^{\theta_{cr}} \frac{d\theta}{\sqrt{2p\bar{e}\theta}} = \frac{2\sqrt{\theta_{cr}}}{\sqrt{2p\bar{e}}}. \end{aligned} \quad (25)$$

Use of eqs. (24) and (25) gives us the following expression for the ideal

impulse:

$$(p\tau_0)_{cr} = \sqrt{\frac{p_{cr}}{2\bar{e}}} 2\sqrt{\theta_{cr}} = \frac{1}{\sqrt{(2\bar{e}\theta_{cr})2\bar{e}}} 2\sqrt{\theta_{cr}} \\ = \frac{1}{\bar{e}}, \quad (26)$$

which is identical to the closed-form solution obtained in Chapter 2.

Note that, for this model also, there exists a minimum value for $(p\tau_0)_{cr}$ (see Figure 3.6). The minimum occurs at $\tau_0 = 4$. The time parameter is a nondimensionalized one, and the two models are different. Thus, one has no reason to expect the minimum to occur at the same value for τ_0 .

For both models, because they are single-degree-of-freedom models, the upper and lower bounds are one and the same. Therefore, the critical conditions are the measures of dynamic instability for step loads.

3.5 Application to Model C

A complete static analysis for this model is presented in Chapter 2. Certain expressions are repeated here for continuity. The reader is also reminded that, for simplicity, it is assumed that the three bars are weightless and that the mass of the system is concentrated at the two interior joints (see Figure 2.14).

The expression for the zero-load total potential is given by

$$\bar{U}_T^0 = (r^2 + 9s^2 - 2\sqrt{\Lambda r + \Lambda}) + \frac{1}{2}(\Lambda - r^2 - 3s^2)^2. \quad (27)$$

Starting with \bar{U}_T^0 , requiring equilibrium, and performing a static stability analysis, the following stationary points are obtained (see Chapter 2 for details):

Point 1 at $(\Lambda, 0)$	Stable (relative minimum)
Point 2 at $[-(\sqrt{\Lambda} - \sqrt{\Lambda - 4})/2, 0]$	Unstable (relative maximum)
Point 3 at $[-(\sqrt{\Lambda} + \sqrt{\Lambda - 4})/2, 0]$	Stable (relative minimum)
Point 4 at $[-\sqrt{\Lambda}/2, \sqrt{\Lambda - 4}/2]$	Unstable (saddle point)
Point 5 at $[-\sqrt{\Lambda}/2, -\sqrt{\Lambda - 4}/2]$	Unstable (saddle point).

The nondimensionalized kinetic energy is expressed by $\bar{T} = T/\bar{\beta}^2 \Lambda L^2$, where T characterizes the kinetic energy and

$$\bar{T} = \frac{1}{2} \left[\left(\frac{dr}{d\tau} \right)^2 + \left(\frac{ds}{d\tau} \right)^2 \right] = \frac{1}{2} [1 + s'^2] \left(\frac{dr}{ds} \right)^2$$

where

$$(\quad)' = \frac{\partial}{\partial r} \quad \text{and} \quad \tau = t \left(\frac{\bar{\beta}k}{2m} \right)^{1/2}. \quad (28)$$

Clearly, saddle points exist for $\Lambda > 4$. For this range of Λ values, the zero-load total potential value at the saddle points, points 4 and 5, is smaller than the corresponding value at the relative maximum, point 2. On the basis of this observation, the motion can possibly become buckled through the saddle points, 4 and 5. The corresponding condition for this case is a *possible critical condition*. On the other hand, if the energy imparted by the applied force at the release time is sufficient to reach the relative maximum (unstable) static equilibrium point, point 2, buckled motion is guaranteed and the corresponding critical condition is a guaranteed one.

Next, the computational procedure for finding the possible critical condition is outlined (MPCL).

Through eq. (6) (in a nondimensionalized form) one obtains

$$2p(\sqrt{\Lambda} - r)_{\tau=\tau_0} = \frac{9}{2}(\Lambda - 1) \quad (29)$$

where τ_0 is the release time.

Moreover, eq. (1) in nondimensionalized form holds for $0 < \tau \leq \tau_0$. For a given path of motion, integration of eq. (1) yields a relation between the time of release and the position at the instant. Note that the problem has been cast in the following terms: for a given load p , find the smallest release time $\tau_{0,c}$, such that the system may reach an unstable point (saddle point for the minimum possible critical condition) with zero velocity, eq. (29). Since one is interested in obtaining the smallest release time $\tau_{0,c}$, and since the position at the time of release is path dependent, one can solve the problem by considering the associated brachistochrone problem. The brachistochrone problem makes use of eq. (1), for this system, and through its solution one obtains the relation between the smallest release time $\tau_{0,c}$ and the position at the instant of release, as well as the path that yields $\tau_{0,c}$.

As already mentioned, another approach is to assume that the motion (during the duration time) is axisymmetric. For this model, this assumption is very reasonable, especially for small values of the duration time. This can be verified by studying the characteristics of the total potential surface close to the starting point. For values of r larger than $\sqrt{\Lambda - 3}$ and close to $\sqrt{\Lambda}$ (see Figure 2.15, points *B* and *A*; *A* is the starting or initial point), the total potential is smaller at positions corresponding to $(r, s \equiv 0)$ than at positions corresponding to $(r, s \neq 0)$. Then it is reasonable to expect the motion to be (at least initially, before the system reaches the position $r = \sqrt{\Lambda - 3}$) axisymmetric (think of a ball rolling on a downsloping groove).

If one assumes the motion to be axisymmetric during τ_0 , then the kinetic

energy, eq. (28), becomes

$$\bar{T} = \frac{1}{2} \left(\frac{dr}{d\tau} \right)^2, \quad (30)$$

and eq. (1) yields

$$T_{0_{cr}} = \int_{\sqrt{\Lambda}}^{r_{cr}} \frac{dr}{\sqrt{4\bar{p}(\sqrt{\Lambda}-r) - 2(r-\sqrt{\Lambda})^2 - (\Lambda-r^2)^2}}. \quad (31)$$

The simultaneous solution of eqs. (29) and (31) yields critical conditions. Computationally, it is simpler for one to assign values of r_{cr} (starting with values close to the initial position, $r = \sqrt{\Lambda}$ and $s = 0$), solve for p through eq. (29), and then solve for $\tau_{0_{cr}}$ through eq. (31).

Note that for the case of the minimum guaranteed critical condition eq. (29) is replaced by a comparable equation that employs the value of the zero-load total potential at the relative maximum unstable static point.

Numerical results are presented graphically on Figures 3.7 and 3.8 for the minimum possible critical condition only and for various values of Λ . The curves of Figure 3.7 depict critical conditions in terms of applied load p versus critical release time $\tau_{0_{cr}}$. One may observe that as $\tau_{0_{cr}}$ increases the corresponding load approaches, asymptotically, the value of $p_{cr\infty}$ for the infinite duration time. Figure 3.8 presents the same results as Figure 3.7, but in terms

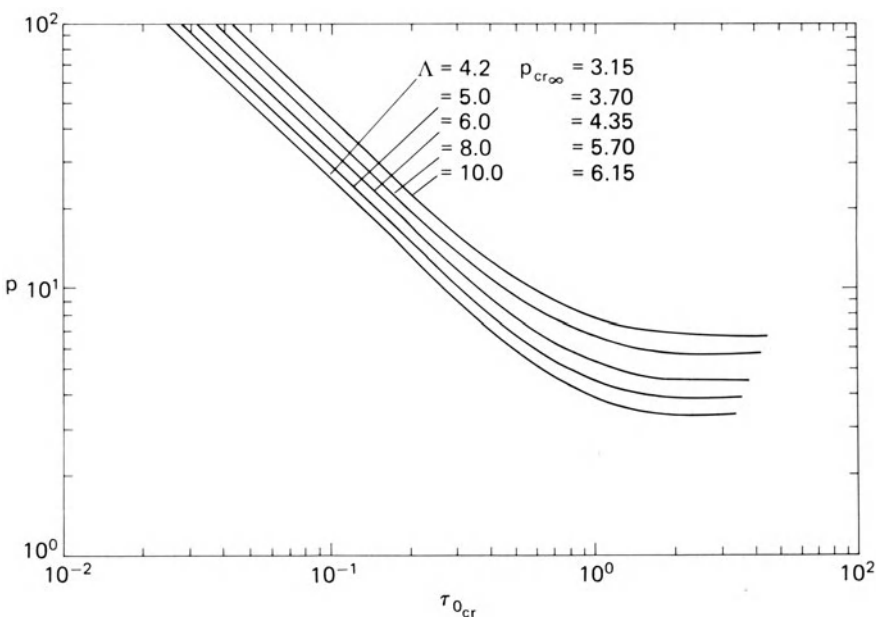


FIGURE 3.7. Load p versus critical duration time $\tau_{0_{cr}}$ (model C).

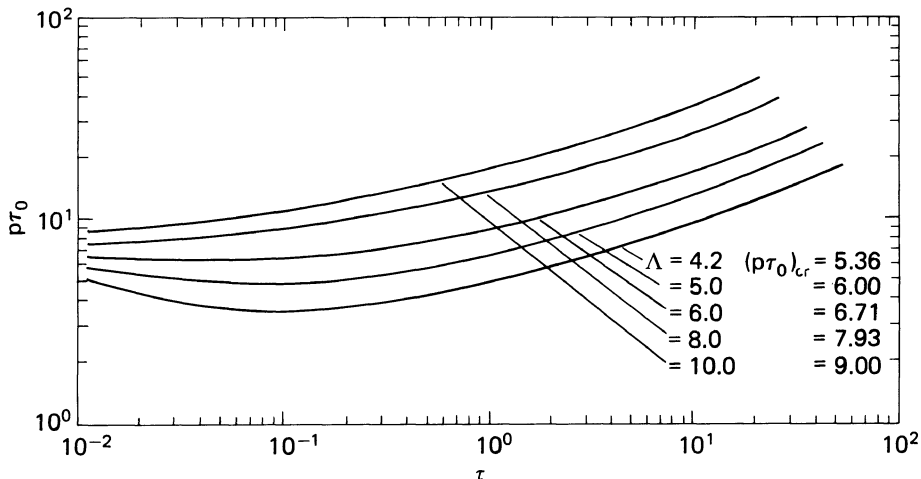


FIGURE 3.8. Impulse ($p\tau_0$) versus critical duration time $\tau_{0,cr}$ (model C).

of $(p\tau_0)_{cr}$ versus critical time $\tau_{0,cr}$. Note that as $\tau_{0,cr}$ approaches zero, the value of $(p\tau_0)_{cr}$ approaches that of the critical ideal impulse.

Problems

1. For the model shown in problem 1, Figure 2.19 of Chapter 2, consider sudden loads of finite duration and find critical conditions numerically as plots of p versus $\tau_{0,cr}$ for a given angle α . Use nondimensionalized parameters.
2. For the same problem as in 1, find the ideal critical impulse as a limiting case ($\tau_{0,cr} \rightarrow 0$) of the present load case.
3. Consider the mechanical model of problem 2, Figure 2.20, of Chapter 2. Let $\theta_0 = 0.05$ and 0.10 and find critical conditions numerically as plots of p versus τ_0 . Use nondimensionalized parameters.
4. For the same problem as in 3, find the critical ideal impulse as a limiting case of the present load case (for $\theta_0 = 0.05, 0.10$).
5. For model C, as treated in this chapter, find the critical ideal impulse as a special case of the present load case (for $\Lambda = 5, 6, 8, 10$).
6. For model C, find critical conditions, corresponding to the minimum guaranteed case (MGCL), as plots of p versus τ_0 for $\Lambda = 5, 6, 8$, and 10 .

4

The Influence of Static Preloading

4.1 Introduction

So far, in discussing the behavior of suddenly loaded structures, it has been assumed that the system is free of loading and that a step load is suddenly applied for a given time duration. The cases of finite duration T_0 , see Figure 3.1, as well as the extreme cases of ideal impulse ($T_0 \rightarrow 0$) and constant load of infinite duration ($T_0 \rightarrow \infty$), have been presented in the previous chapters. Although one may find several systems that fall in the category of initially load-free structures, in the world of structural configurations it is easier and more realistic to deal with initially preloaded structures. This means that the structure is first loaded quasi-statically and then is subjected to a dynamic load. Consider, for example, a submarine resting at the bottom of the ocean, at a reasonable depth. This implies that it is statistically preloaded by the ocean pressure at that depth. Then the submarine is subjected to a sudden blast load. This additional loading is the dynamic load, which can be idealized as an ideal impulse or a sudden load of finite duration T_0 . A similar example is an aircraft in a level unaccelerated flight (static preloading) subjected to a sudden blast load (dynamic). Finally, one can include in this broad class of problems bridges, buildings, and other standing structures that are already under load and then are subjected to earthquake loads; for all of these cases, the sudden load is idealized as a constant load of finite duration T_0 . The precise statement of the problem treated in this chapter is given below.

Consider a structural configuration at its stable equilibrium position $L_s^{P_0}$ when subjected to an initial static load P_0 . At time $t = 0$, an additional constant load P is suddenly applied to the system and acts only for finite duration time $t = T_0$. After the release of the force P , the system moves because of the total energy acquired during the action of the sudden load P . The system will be called dynamically stable if its motion is *unbuckled*, in the sense described in previous chapters. Since the systems under consideration exhibit either limit or unstable bifurcation point instability, the system is stable if the energy, imparted through the action of the load P , is insufficient.

for the system to reach the unstable static equilibrium point, corresponding to the P_0 -load total potential of the system with zero velocity (zero kinetic energy). For each individual model considered in this chapter, the criterion is invoked and estimates for critical conditions are found. The extreme cases of $T_0 \rightarrow \infty$ (constant load of infinite duration) and $T_0 \rightarrow 0$ (ideal impulse) are treated as special cases.

4.2 Criterion for Critical Conditions

The concept of dynamic stability and the general procedure, as well, are extensions of those used in the cases of constant load of finite duration. The equilibrium positions of the preloaded system are given as solutions to

$$\frac{\partial U_T^{P_0}(L)}{\partial L} = 0 \quad (1)$$

where L is the position of the system. Thus, one may find all the P_0 -load static equilibrium positions including the near stable position $L_S^{P_0}$, as well as the unstable position $L_u^{P_0}$, through which buckled motion can be realized (see Figure 4.1).

Keeping the same generalized coordinates for all models and the same expressions for the total potential and for the kinetic energy, one may apply the concepts already developed. These are next explained through the use of Figure 4.1, which holds for one-degree-of-freedom systems, but the explanation is applicable to all finite-degree-of-freedom systems. Moreover, the nondimensionalized parameters, p for loads, \bar{U}_T for the total potential, τ_0 for the duration time, etc., will be employed in the ensuing discussion.

The system is initially loaded quasi-statically by load p_0 , and it reaches point A ($L = L_S^{P_0}$; stable static equilibrium point). Then a load p is applied suddenly for a time τ_0 (finite duration). At τ_0 , the load p is removed.

A potential \bar{U}_T^P is defined such that $\bar{U}_T^P = \bar{U}_T^{P_0}$, at $\tau = 0$, or at $L = L_S^{P_0}$ (see Figure 4.1). Then

$$\bar{U}_T^P = \bar{U}_T^{P_0+P} + [\bar{U}_T^{P_0}(L_S^{P_0}) - \bar{U}_T^{P_0+P}(L_S^{P_0})]. \quad (2)$$

Since the system is conservative, during the action of p , one may write

$$\bar{U}_T^P + \bar{T}^{P_0+P} = \bar{U}_T^{P_0}(L_S^{P_0}) \quad \text{for } 0 \leq \tau < \tau_0 \quad (3)$$

where \bar{T}^{P_0+P} is the kinetic energy of the system. Making use of eq. (2), eq. (3) becomes

$$\bar{U}_T^{P_0+P} + \bar{T}^{P_0+P} = \bar{U}_T^{P_0+P}(L_S^{P_0}) \quad \text{for } 0 \leq \tau < \tau_0. \quad (4)$$

For times greater than τ_0 , the system is also conservative and conservation of energy yields

$$\bar{U}_T^P + \bar{T}^{P_0}(\tau) = \bar{U}_T^{P_0}(\tau_0) + \bar{T}^{P_0}(\tau_0) \quad \text{for } \tau > \tau_0 \quad (5)$$

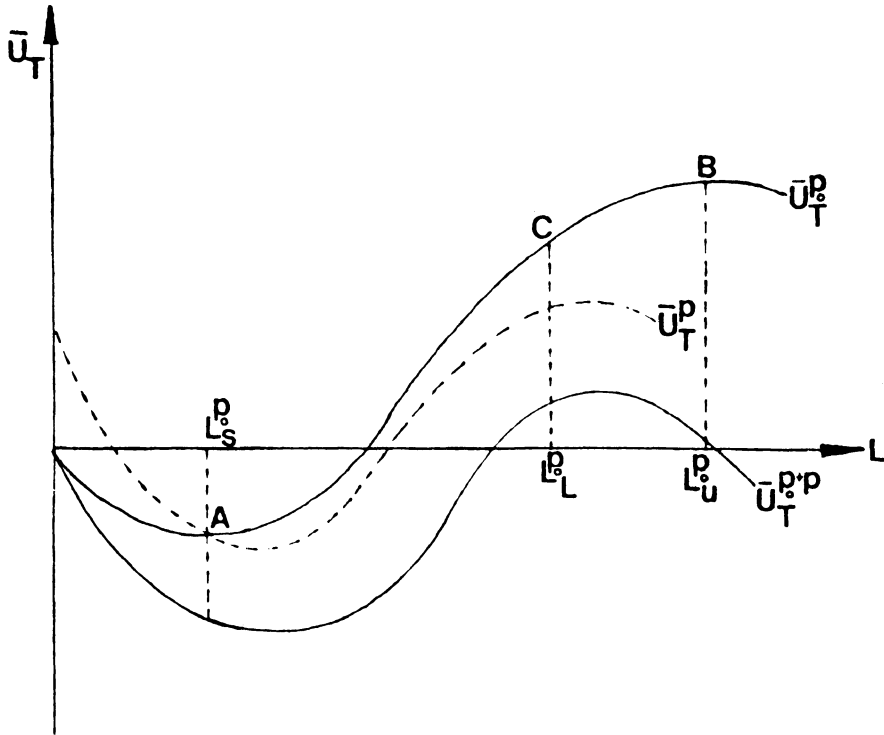


FIGURE 4.1. Definitions of total potentials (one-degree-of-freedom system).

where the right-hand side represents the level of the system energy at the release time τ_0 .

If the force p has imparted sufficient energy to the system, such that it can reach the unstable point B ($L = L_U^{P_0}$; see Figure 4.1) on the P_0 -load potential with zero kinetic energy (velocity), then buckled motion is possible, and the system becomes dynamically unstable.

The governing equations for predicting critical conditions are obtained from eqs. (4) and (5). This is explained below.

By requiring kinematic continuity at $\tau = \tau_0$, one may write

$$\bar{T}^{P_0+P}(\tau_0) = \bar{T}^{P_0}(\tau_0). \quad (6)$$

From eq. (4), then,

$$\bar{T}^{P_0+P}(\tau_0) = \bar{U}_T^{P_0+P}(L_S^{P_0}) - \bar{U}_T^{P_0+P}(\tau_0). \quad (7)$$

Substitution of eqs. (6) and (7) into eq. (5) yields

$$\bar{U}_T^{P_0} + \bar{T}^{P_0} = \bar{U}_T^{P_0}(\tau_0) - \bar{U}_T^{P_0+P}(\tau_0) + \bar{U}_T^{P_0+P}(L_S^{P_0}) \quad \text{for } \tau > \tau_0. \quad (8)$$

Next, a critical condition exists if the system can reach point B (see Figure 4.1)

with zero kinetic energy [$\bar{T}^{P_0}(L_u^{P_0}) = 0$]. Thus, denoting the critical condition by $p, \tau_{0_{cr}}$, one may write

$$\bar{U}_T^{P_0}(L_u^{P_0}) = \bar{U}_T^{P_0}(\tau_{0_{cr}}) - \bar{U}_T^{P_0+P}(\tau_{0_{cr}}) + \bar{U}_T^{P_0+P}(L_s^{P_0}). \quad (9)$$

Note that eq. (9) relates $p, \tau_{0_{cr}}$, and the position of the system, L_{cr} , at the instant of the release of the force p . Please observe (as also explained in Chapter 3) that the critical condition described above depends on the evaluation of two parameters, p and τ_0 . One approach is to prescribe τ_0 and find the corresponding p_{cr} , and the other is to prescribe p and find the corresponding $\tau_{0_{cr}}$. The two are equivalent. Regardless of the approach, eq. (9) relates three parameters $p, \tau_{0_{cr}}$ (or p_{cr}, τ_0), and L_{cr} (the position of the system taken as one parameter).

The second (needed) equation is obtained from eq. (4). This equation (see Chapter 3) is used to relate the load p , the duration time (or time of release) τ_0 , and the position of the system at the instant of release. In order to find, for a prescribed load, the position of the system at the instant of release, one must specify the path of motion. For one-degree-of-freedom systems there is only one path and this is easily accomplished. On the other hand, for a multi-degree-of-freedom system there are numerous possible paths leading to a multitude of positions for a given release time. In such cases, if one is interested in finding a lower bound for critical conditions, one may find the path that yields the smallest possible time. This may be accomplished by solving the corresponding brachistochrone problem (see Appendix B). The solution to the brachistochrone problem yields the path of motion that yields the smallest possible time. Thus, eq. (4), along with the path of motion, relates the release time τ_0 and system position L_{cr} at the instant of release. These steps are clearly demonstrated for each of the three models in the subsequent sections.

Moreover, if one is dealing with a deflection-limited design (the position of the system cannot exceed $L_L^{P_0}$ —see Figure 4.1), then $\bar{U}_T^{P_0}(L_u^{P_0})$ is replaced by $\bar{U}_T^{P_0}(L_L^{P_0})$, in the outlined computational procedure.

Parenthesis. The cases of ideal impulse and suddenly applied load of constant magnitude and infinite duration may be obtained as special cases of the present procedure.

However, critical conditions for these two load cases may also be obtained independently.

For the ideal impulse case, one may relate the impulse to an initial kinetic energy, and from conservation of energy

$$\bar{U}_T^{P_0} + \bar{T}^{P_0} = \bar{U}_T^{P_0}(L_s^{P_0}) + \bar{T}_i^{P_0}. \quad (10)$$

Then $\bar{T}_i^{P_0}$ is critical (related to the critical ideal impulse) if the system reaches position $L_u^{P_0}$ (point *B* of Figure 4.1) with zero kinetic energy. Thus,

$$\bar{T}_{i_{cr}}^{P_0} = \bar{U}_T^{P_0}(L_s^{P_0}) - \bar{U}_T^{P_0}(L_u^{P_0}). \quad (11)$$

For the second extreme case ($\tau_0 \rightarrow \infty$), P_{cr} may be obtained from eq. (3) or (4), which, for this case, holds true for all τ ($0 \leq \tau \leq \infty$). Thus, τ_{cr} corresponds to the solution of

$$\bar{U}_T^{P_0+P}(L_u^{P_0+P}) = \bar{U}_T^{P_0+P}(L_s^{P_0}) \quad (12)$$

where $L_u^{P_0+P}$ denotes the unstable equilibrium position of the system when the static load is equal to $p_0 + p$.

The procedure for establishing critical conditions is demonstrated through the three simple mechanical models described in Chapter 2. The analysis for each system is presented separately.

4.3 Application to Model A

For this particular model, the static stability analysis is presented in Chapter 2. The geometry of the model is given in Figure 2.1 and the static response in Figure 2.2.

In evaluating the effect of static preloading, three imperfection angles are chosen ($\theta_0 = 0.005, 0.010, 0.020$), and for each θ_0 value the system is initially loaded quasi-statistically with a p_0 load smaller than the p_{crs} static. Then the system is loaded dynamically. The following values are used in the dynamic analysis (values for p_{crs} are taken from Figure 2.2):

$$\theta_0 = 0.005, \quad p_{crs} = 0.440, \quad p_0 = 0.340, 0.380, \text{ and } 0.420$$

$$\theta_0 = 0.010, \quad p_{crs} = 0.415, \quad p_0 = 0.300, 0.360, \text{ and } 0.400$$

$$\theta_0 = 0.020, \quad p_{crs} = 0.384, \quad p_0 = 0.300, 0.340, \text{ and } 0.370.$$

First, the extreme cases ($\tau_0 \rightarrow 0$ and $\tau_0 \rightarrow \infty$) are analyzed by employing eqs. (11) and (12), respectively.

4.3.1 Ideal Impulse

The ideal impulse ($p\tau_0$) is related to the initial kinetic energy [in the nondimensionalized form; see eqs. (12) and (13) of Chapter 2] by the expression

$$(p\tau_0) = \frac{2}{\sin(\theta_s^{P_0})} [\bar{T}_i^{P_0}]^{1/2} \quad (13)$$

where $\theta_s^{P_0}$ is the stable static position (angle θ) under load p_0 .

The critical ideal impulse $(p\tau_0)_{cr}$ is obtained by substituting eq. (11) into eq. (13), or

$$(p\tau_0)_{cr} = \frac{2}{\sin(\theta_s^{P_0})} [\bar{U}_T^{P_0}(\theta_u^{P_0}) - \bar{U}_T^{P_0}(\theta_s^{P_0})]^{1/2} \quad (14)$$

where $\theta_u^{P_0}$ is the unstable static position under p_0 load, and the expression

TABLE 4.1. Critical ideal impulse $(p\tau_0)_{cr}$, model A.

$\theta_0 = 0.005$		$\theta_0 = 0.010$		$\theta_0 = 0.020$	
p_0	$(p\tau_0)_{cr}$	p_0	$(p\tau_0)_{cr}$	p_0	$(p\tau_0)_{cr}$
0	162.000	0	81.000	0	40.000
0.340	8.246	0.300	6.980	0.300	2.900
0.380	3.498	0.360	2.247	0.340	1.207
0.420	0.758	0.400	0.486	0.370	0.338
0.440	0	0.416	0	0.384	0

for the total potential is given by eq. (2) of Chapter 2, by using p_0 wherever p appears in the equation. The numerical results for all (θ_0, p_0) combinations are presented in tabular form in Table 4.1.

Note that the first-row results are obtained from eq. (17) of Chapter 2. Note also that as the value of p_0 approaches the value of the static critical load, the additionally imposed critical impulse tends to zero. This is reflected by the results of the last row (Table 4.1).

4.3.2 Constant Load of Infinite Duration

The critical load for the case of infinite duration, p_{cr_∞} , is obtained by the following steps, for a given (θ_0, p_0) combination:

- Solve eq. (3) of Chapter 2, given below, for $\theta_s^{p_0}$ (stable position):

$$p_0 = [\sqrt{1 + \sin \theta} - \sqrt{1 + \sin \theta_0}] \cot \theta / \sqrt{1 + \sin \theta}. \quad (15)$$

- Static equilibrium positions are also characterized by eq. (3) of Chapter 2 for the loading value of $(p_0 + p)$, or

$$p + p_0 = [\sqrt{1 + \sin \theta} - \sqrt{1 + \sin \theta_0}] \cot \theta / \sqrt{1 + \sin \theta}. \quad (16)$$

- Equation (12) for this model is given below:

$$\begin{aligned} &[\sqrt{1 + \sin \theta_u^{p_0+p}} - \sqrt{1 + \sin \theta_0}]^2 - (p_0 + p)(\cos \theta_0 - \cos \theta_u^{p_0+p}) \\ &= [\sqrt{1 + \sin \theta_s^{p_0}} - \sqrt{1 + \sin \theta_0}]^2 - p_0(\cos \theta_0 - \cos \theta_s^{p_0}). \end{aligned} \quad (17)$$

The simultaneous solution of eqs. (16) and (17) yields $\theta_u^{p_0+p}$ and p_{cr_∞} .

Note that since eq. (17) must be satisfied at an unstable point, $(\theta_u^{p_0+p})$, the stability test must be used to ensure this, or

$$\left. \frac{d^2 U_T^{p_0+p}}{d\theta^2} \right|_{\theta_u^{p_0+p}} < 0.$$

The numerical results for all (θ_0, p_0) combinations are presented in Table 4.2.

Note that the first-row results of Table 4.2 are taken from Chapter 2. The

TABLE 4.2. Critical load of infinite duration, $p_{cr,\infty}$, model A.

$\theta_0 = 0.005$			$\theta_0 = 0.010$			$\theta_0 = 0.020$		
p_0	$p_{cr,\infty}$	$p_0 + p_{cr,\infty}$	p_0	$p_{cr,\infty}$	$p_0 + p_{cr,\infty}$	p_0	$p_{cr,\infty}$	$p_0 + p_{cr,\infty}$
0	0.4320	0.4320	0	0.4010	0.4010	0	0.3690	0.3690
0.340	0.0940	0.4340	0.300	0.1090	0.4090	0.300	0.0751	0.3751
0.380	0.0560	0.4360	0.360	0.0517	0.4117	0.340	0.0396	0.3796
0.420	0.0165	0.4365	0.400	0.0136	0.4136	0.370	0.0116	0.3816
0.440	0	0.4400	0.416	0	0.4160	0.384	0	0.3840

results of the last row reflect the fact that if the system is loaded quasi-statically up to the limit point, then the additional suddenly applied load that the system can withstand tends to zero.

4.3.3 Constant Load of Finite Duration

Finally, for the case of constant load p applied suddenly for a finite duration τ_0 , critical conditions are obtained from the following steps:

1. From the static stability analysis obtain $\theta_s^{p_0}$ and $\theta_u^{p_0}$ for each p_0 .
2. Use of eq. (9) yields

$$\begin{aligned} P(\cos \theta_s^{p_0} - \cos \theta_{cr}) &= [\sqrt{1 + \sin \theta_u^{p_0}} - \sqrt{1 + \sin \theta_0}]^2 \\ &\quad - [\sqrt{1 + \sin \theta_s^{p_0}} - \sqrt{1 + \sin \theta_0}]^2 \\ &\quad + p_0(\cos \theta_u^{p_0} - \cos \theta_s^{p_0}) \end{aligned} \quad (18)$$

where θ_{cr} is the position θ at the instant of release of the force p ($\tau = \tau_0$).

In eq. (18), for a given p_0 , everything is known ($p_0, \theta_0, \theta_s^{p_0}$, and $\theta_u^{p_0}$), except p and θ_{cr} . Therefore, eq. (18) relates p and θ_{cr} for a critical condition to exist.

3. Since $\bar{T}^{p+p_0} = (d\theta/d\tau)^2$, from eq. (4) we may write

$$\begin{aligned} \frac{d\theta}{d\tau} &= [\bar{U}_T^{p_0+P}(\theta_s^{p_0}) - \bar{U}_T^{p_0+P}(\theta)]^{1/2}, \quad \text{or} \\ d\tau &= [\bar{U}_T^{p_0+P}(\theta_s^{p_0}) - \bar{U}_T^{p_0+P}(\theta)]^{-1/2} d\theta. \end{aligned} \quad (19)$$

Integration from $\tau = 0$ to $\tau = \tau_0$ and use of the expression for the total potential [see eq. (2) of Chapter 2] yields

$$\begin{aligned} \tau_0 &= \int_{\theta_s^{p_0}}^{\theta_{cr}} \{[\sqrt{1 + \sin \theta_s^{p_0}} - \sqrt{1 + \sin \theta_0}] - [\sqrt{1 + \sin \theta} - \sqrt{1 + \sin \theta_0}] \\ &\quad + (p_0 + p)(\cos \theta_s^{p_0} - \cos \theta)\}^{-1/2} d\theta. \end{aligned} \quad (20)$$

Note that eq. (20) also relates θ_{cr} to p .

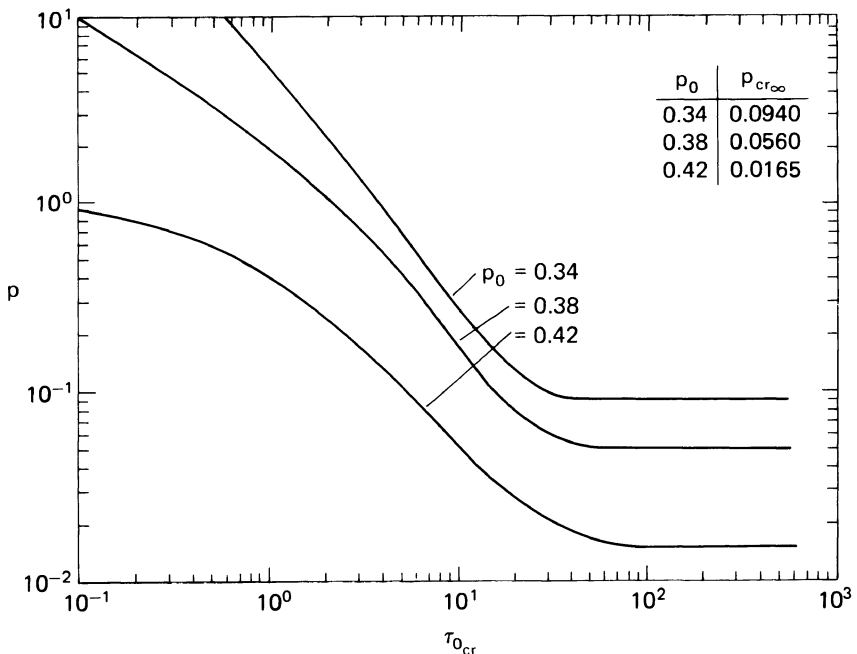


FIGURE 4.2. Superimposed load p versus critical finite time duration $\tau_{0_{cr}}$, prestressed model A, $\theta_0 = 0.005$.

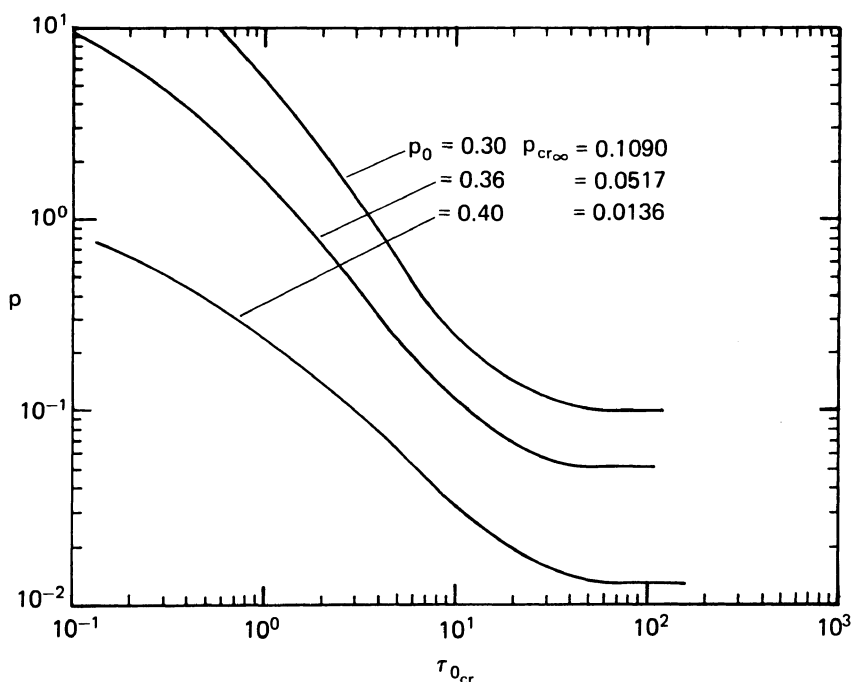


FIGURE 4.3. Superimposed load p versus critical time duration $\tau_{0_{cr}}$, prestressed model A, $\theta_0 = 0.01$.

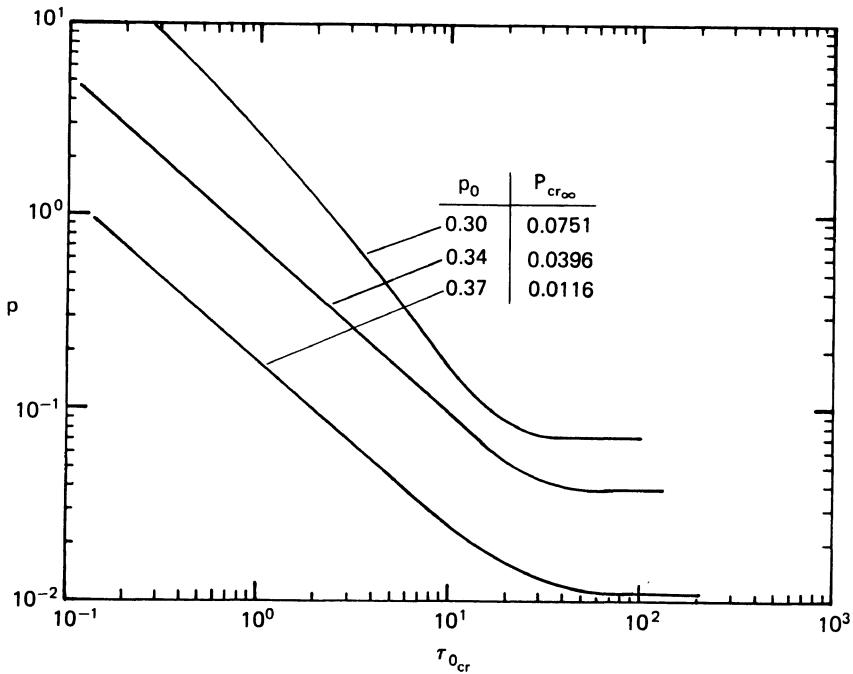


FIGURE 4.4. Superimposed load p versus critical time duration $\tau_{0,cr}$, prestressed model A, $\theta_0 = 0.02$.

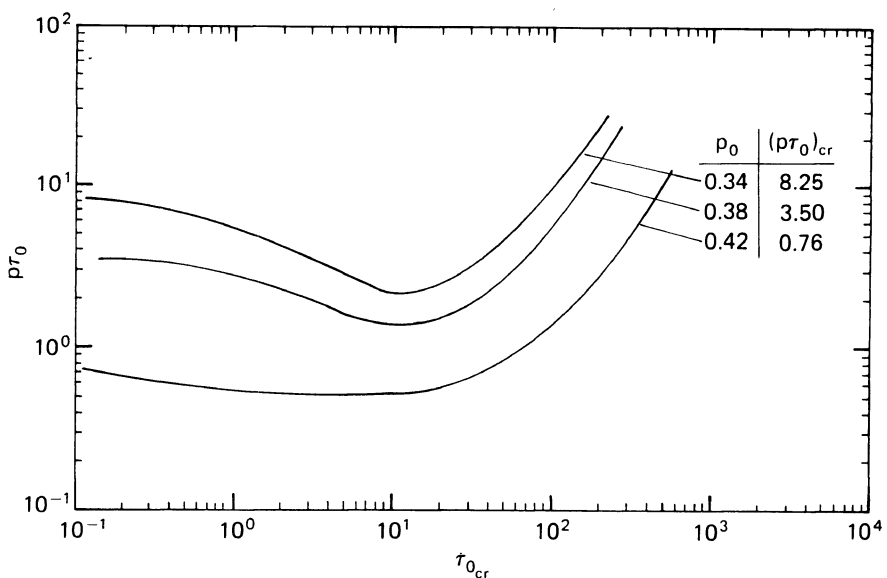


FIGURE 4.5. Superimposed impulse $(p\tau)$ versus critical duration time $\tau_{0,cr}$, prestressed model A, $\theta_0 = 0.005$.

A critical condition is characterized by a set of (p, τ_0) values that satisfies both equations, eqs. (18) and (20). This means that for a given release time τ_0 , find p_{cr} ; or for a given p , find $\tau_{0,cr}$. Computationally, though, it is easier to assign values of θ_{cr} , solve for p from eq. (18), and then solve for the corresponding value of τ_0 from eq. (20).

A simple computer program can be written for these computations. Values of θ_{cr} are assigned, starting with $\theta_s^{P_0} + \delta\theta$, where $\delta\theta$ is very small, and computing the corresponding values of p and τ_0 for each $\delta\theta$.

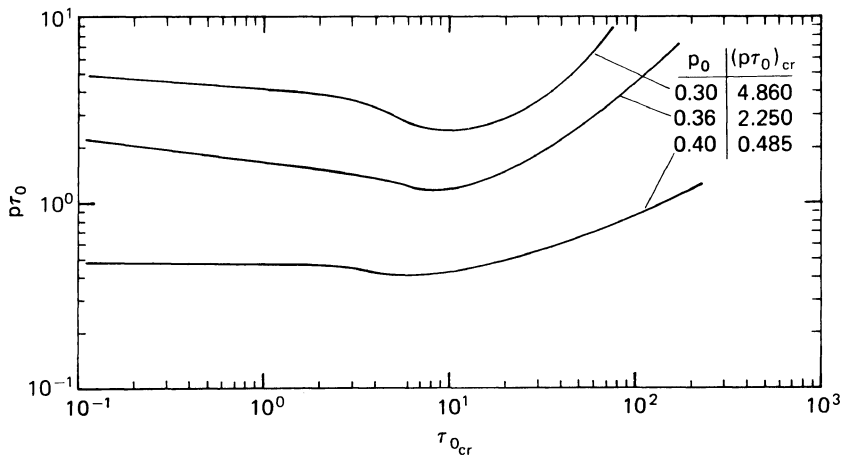


FIGURE 4.6. Superimposed impulse ($p\tau$) versus critical time duration $\tau_{0,cr}$, prestressed model A, $\theta_0 = 0.01$.

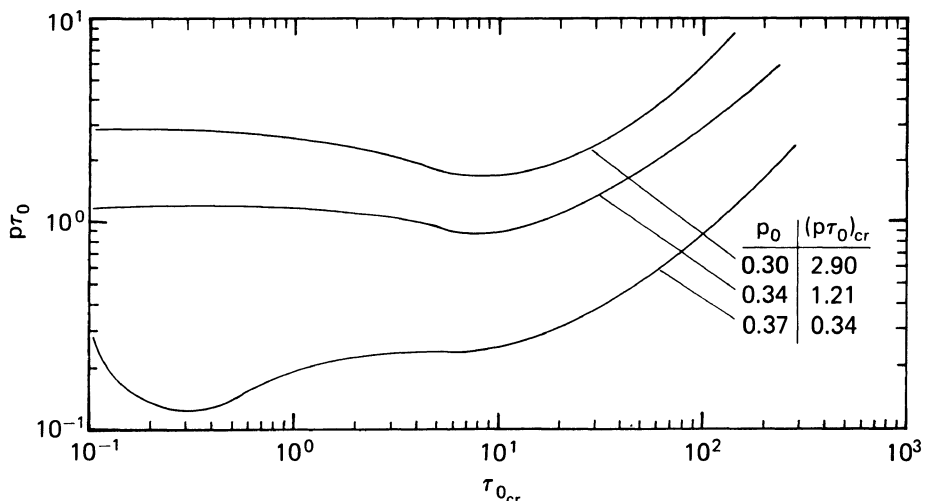


FIGURE 4.7. Superimposed impulse ($p\tau$) versus critical duration time $\tau_{0,cr}$, prestressed model A, $\theta_0 = 0.02$.

The results are presented graphically on Figures 4.2 to 4.7 (pp. 75–77) for the three values of θ_0 . On the first three figures, Figures 4.2 to 4.4, critical conditions appear as plots of p versus duration time $\tau_{0,\text{cr}}$. Note that as $\tau_{0,\text{cr}}$ becomes larger and larger, the corresponding value of p approaches $p_{\text{cr},\infty}$ (see Table 4.2). On the last three figures, Figures 4.5 to 4.7, critical conditions appear as plots of $(p\tau_0)_{\text{cr}}$ versus duration time $\tau_{0,\text{cr}}$. On these figures, as $\tau_{0,\text{cr}} \rightarrow 0$, the corresponding value of $(p\tau_0)_{\text{cr}}$ approaches the critical ideal impulse (see Table 4.1).

4.4 Application to Model B

For this particular model, the static stability analysis is presented in Chapter 2. The geometry of the model is given in Figure 2.3.

In evaluating the effect of static preloading, three eccentricities are chosen ($\bar{e} = 0.005, 0.010, 0.020$), and for each \bar{e} value, the system is initially loaded quasi-statically with a p_0 load smaller than $p_{\text{cr},\infty}$ static. Then the system is loaded dynamically. The following values are used in the dynamic analysis:

$$\begin{aligned}\bar{e} &= 0.005, & p_{\text{cr},\infty} &= 0.955, & p_0 &= 0.35, 0.40, \text{ and } 0.50; \\ \bar{e} &= 0.010, & p_{\text{cr},\infty} &= 0.932, & p_0 &= 0.30, 0.40, \text{ and } 0.50; \\ \bar{e} &= 0.020, & p_{\text{cr},\infty} &= 0.898, & p_0 &= 0.30, 0.40, \text{ and } 0.50.\end{aligned}$$

First, the extreme cases ($\tau_0 \rightarrow 0$ and $\tau_0 \rightarrow \infty$) are analyzed by employing eqs. (11) and (12), respectively.

4.4.1 Ideal Impulse

The ideal impulse $(p\tau_0)$ is related to the initial kinetic energy by the expression

$$(p\tau_0) = \frac{1}{\sin \theta_s^{p_0} + \bar{e} \cos \theta_s^{p_0}} [T_i^{p_0}]^{1/2} \quad (21)$$

where $\theta_s^{p_0}$ is the stable static position (angle θ) under p_0 load.

The critical ideal impulse $(p\tau_0)_{\text{cr}}$ is obtained by substituting eq. (11) into eq. (21), or

$$(p\tau_0)_{\text{cr}} = \frac{1}{\sin \theta_s^{p_0} + \bar{e} \cos \theta_s^{p_0}} [\bar{U}_T^{p_0}(\theta_s^{p_0}) - \bar{U}_T^{p_0}(\theta_u^{p_0})] \quad (22)$$

where $\theta_u^{p_0}$ is the unstable static position under p_0 load, and the expression for the total potential is given by eq. (24) of Chapter 2, by using p_0 wherever p appears in the equation. The numerical results for all (\bar{e}, p_0) combinations are presented in Table 4.3.

Note that the first-row results are obtained from eq. (39) of Chapter 2. Note also that as the value of p_0 approaches the value of the static critical load the additionally imposed critical impulse tends to zero. This is reflected by the results of the last row (Table 4.3).

TABLE 4.3. Critical ideal impulse $(p\tau_0)_{cr}$, model B.

$\bar{e} = 0.005$		$\bar{e} = 0.01$		$\bar{e} = 0.02$	
p_0	$(p\tau_0)_{cr}$	p_0	$(p\tau_0)_{cr}$	p_0	$(p\tau_0)_{cr}$
0	200	0	100	0	50
0.35	192	0.30	88	0.30	42
0.40	164	0.40	76	0.40	36
0.50	139	0.50	62	0.50	29
0.955	0	0.932	0	0.898	0

4.4.2 Constant Load of Infinite Duration

The critical load for the case of infinite duration, p_{cr_∞} , is obtained by the following steps, for a given (θ_0, p_0) combination.

1. Solve eq. (42) of Chapter 2, given below, for $\theta_s^{p_0}$ (stable position):

$$p_0 = \frac{\sin \theta_s^{p_0}}{\tan \theta_s^{p_0} + \bar{e}}. \quad (23)$$

2. Static equilibrium positions are also characterized by eq. (42) of Chapter 2 for the loading value of $(p_0 + p)$, or

$$p + p_0 = \frac{\sin \theta}{\tan \theta + \bar{e}}. \quad (24)$$

3. Equation (12) for this model is given below:

$$\begin{aligned} \sin^2 \theta_u^{p_0+p} - 2(p_0 + p)(1 - \cos \theta_u^{p_0+p} + \bar{e} \sin \theta_u^{p_0+p}) \\ = \sin^2 \theta_s^{p_0} - 2p_0(1 - \cos \theta_s^{p_0} + \bar{e} \sin \theta_s^{p_0}). \end{aligned} \quad (25)$$

The simultaneous solution of Eqs. (24) and (25) yields $\theta_u^{p_0+p}$ and p_{cr_∞} .

Note that since eq. (25) must be satisfied at an unstable point $(\theta_u^{p_0+p})$, the stability test may be used to ensure this, or

$$\left. \frac{d^2 \bar{U}_T^{p_0+p}}{d\theta^2} \right|_{\theta_u^{p_0+p}} < 0.$$

The numerical results for all (\bar{e}, p_0) combinations are presented in Table 4.4.

TABLE 4.4. Critical dynamic load of infinite duration, p_{cr_∞} , model B.

$\bar{e} = 0.0005$			$\bar{e} = 0.010$			$\bar{e} = 0.020$		
p_0	p_{cr_∞}	$p_0 + p_{cr_\infty}$	p_0	p_{cr_∞}	$p_0 + p_{cr_\infty}$	p_0	p_{cr_∞}	$p_0 + p_{cr_\infty}$
0	0.948	0.948	0	0.912	0.912	0	0.85	0.85
0.35	0.60	0.95	0.30	0.62	0.92	0.30	0.59	0.89
0.40	0.54	0.94	0.40	0.52	0.92	0.40	0.48	0.88
0.50	0.45	0.95	0.50	0.42	0.92	0.50	0.38	0.88
0.955	0	0.955	0.932	0	0.932	0.898	0	0.898

Note that the first-row results of Table 4.4 are taken from Chapter 2. The results of the last row reflect the fact that if the system is loaded quasi-statically up to the limit point, the additional suddenly applied load that the system can withstand tends to zero.

4.4.3 Constant Load of Finite Duration

Finally, for the case of constant load p applied suddenly for a finite duration τ_0 , critical conditions are obtained from the following steps:

1. From the static stability analysis, obtain $\theta_s^{P_0}$ and $\theta_u^{P_0}$ for each p_0 .
2. Use of eq. (9) yields

$$\begin{aligned} 2p(\cos \theta_s^{P_0} - \bar{e} \sin \theta_s^{P_0} - \cos \theta_{cr} + \bar{e} \sin \theta_{cr}) \\ = \sin^2 \theta_u^{P_0} - \sin^2 \theta_s^{P_0} - 2p_0(\cos \theta_s^{P_0} - \bar{e} \sin \theta_s^{P_0} - \cos \theta_u^{P_0} + \bar{e} \sin \theta_u^{P_0}) \end{aligned} \quad (26)$$

where θ_{cr} is the position θ at the instant of release of the force p ($\tau = \tau_0$).

In eq. (26) for a given geometry \bar{e} and static load p_0 , everything is known ($p_0, \bar{e}, \theta_s^{P_0}$, and $\theta_u^{P_0}$) except p and θ_{cr} . Therefore, eq. (26) relates p and θ_{cr} for a critical condition to exist.

3. $\bar{T}^{P_0+P} = (d\theta/d\tau)^2$; then from eq. (4) one may write

$$\begin{aligned} \frac{d\theta}{d\tau} &= [\bar{U}_T^{P_0+P}(\theta_s^{P_0}) - \bar{U}_T^{P_0+P}(\theta)]^{1/2}, \quad \text{or} \\ d\tau &= [\bar{U}_T^{P_0+P}(\theta_s^{P_0}) - \bar{U}_T^{P_0+P}(\theta)]^{-1/2} d\theta. \end{aligned} \quad (27)$$

Integration from $\tau = 0$ to $\tau = \tau_0$ and use of the expression for the total potential [see eq. (41) of Chapter 2] yields

$$\begin{aligned} \tau_0 = \int_{\theta_s^{P_0}}^{\theta_{cr}} \{ \sin^2 \theta_s^{P_0} - \sin^2 \theta \\ - 2(p_0 + p)(\bar{e} \sin \theta_s^{P_0} - \cos \theta_s^{P_0} - \bar{e} \sin \theta + \cos \theta) \}^{-1/2} d\theta. \end{aligned} \quad (28)$$

Note that eq. (28) also relates θ_{cr} to p .

A critical condition is characterized by a set of (p, τ_0) values that satisfies both eqs. (26) and (28). This means that for a given release time τ_0 , find p_{cr} ; or for a given p , find $\tau_{0,cr}$. Computationally, though, it is easier to assign values of θ_{cr} , solve for p from eq. (26), and then solve for the corresponding τ_0 from eq. (28).

A simple computer program can be written for these computations. Values of θ_{cr} are assigned, starting with $\theta_s^{P_0} + \delta\theta$, where $\delta\theta$ is very small, and the corresponding values of p and τ_0 for each $\delta\theta$ are computed.

The results are presented graphically on Figures 4.8–4.13 for the three values of θ_0 . On the first three figures, Figures 4.8–4.10, critical conditions

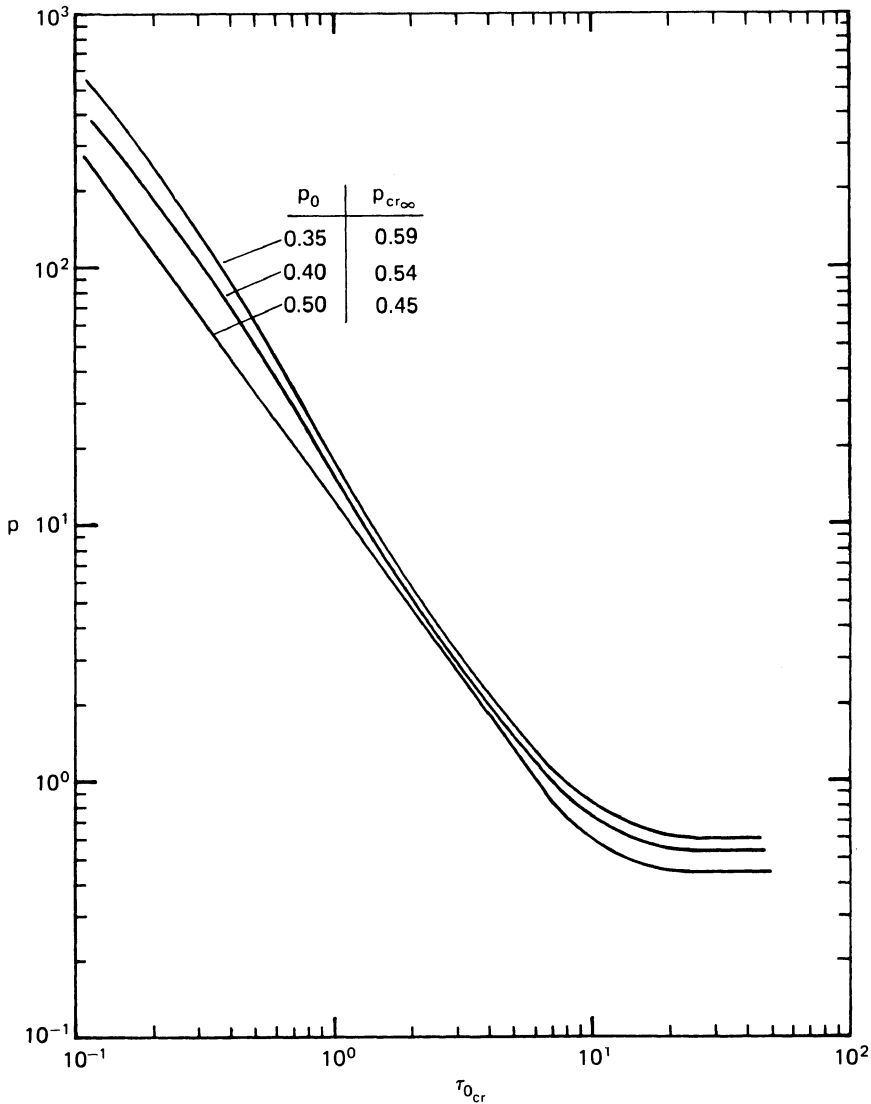


FIGURE 4.8. Superimposed load p versus critical duration time $\tau_{0\text{cr}}$, prestressed model B, $\bar{e} = 0.005$.

appear as plots of p versus duration time $\tau_{0\text{cr}}$. Note that as $\tau_{0\text{cr}}$ becomes larger and larger, the corresponding value of p approaches $p_{cr,\infty}$ (see Table 4.4). On the last three figures, Figures 4.11–4.13, critical conditions appear as plots of $(p\tau_0)_{\text{cr}}$ versus duration time $\tau_{0\text{cr}}$. On these figures, as $\tau_{0\text{cr}} \rightarrow 0$, the corresponding value of $(p\tau_0)_{\text{cr}}$ approaches the critical ideal impulse (see Table 4.3).

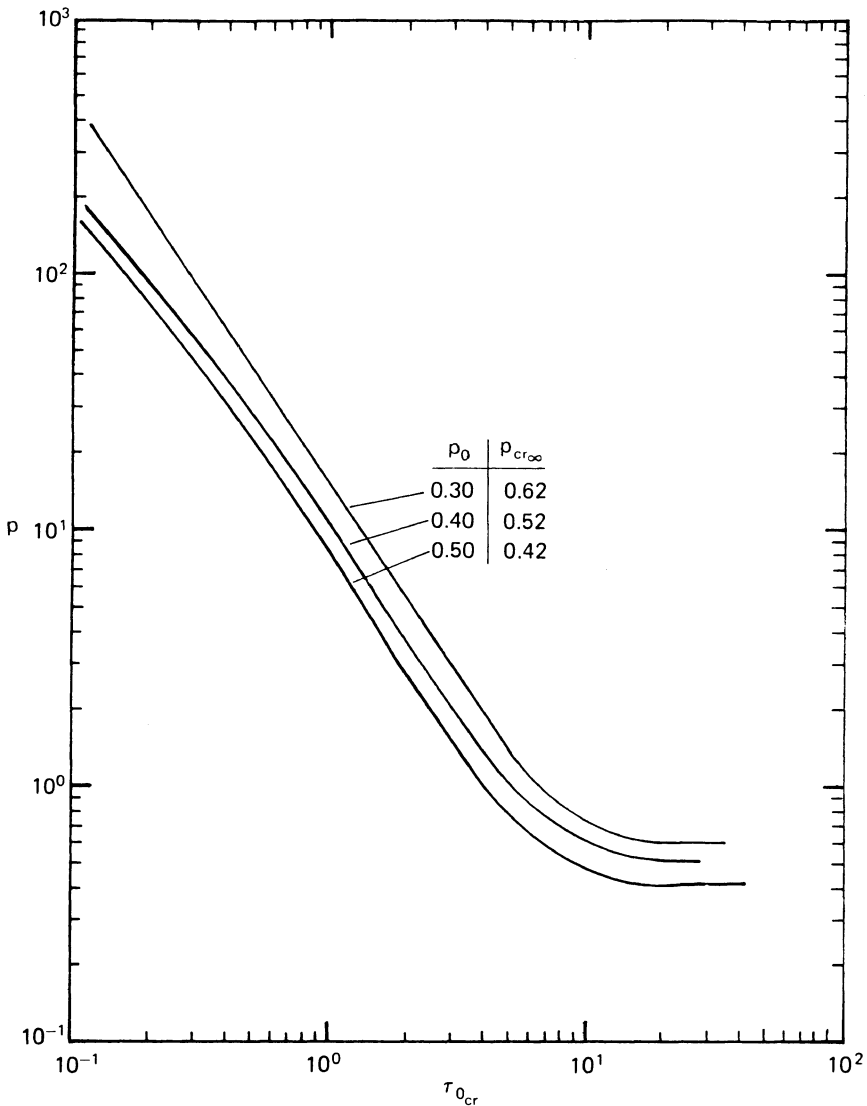


FIGURE 4.9. Superimposed load p versus critical duration time, prestressed model B, $\bar{\epsilon} = 0.01$.

4.5 Application to Model C

For this particular model, the static stability analysis is presented in Chapter 2. The geometry of the model is given on Figure 2.14 and the static response on Figure 2.16.

In evaluating the effect of static preloading, three Λ coefficients are chosen ($\Lambda = 5.0, 6.0, 8.0$), and for each Λ value the system is initially loaded

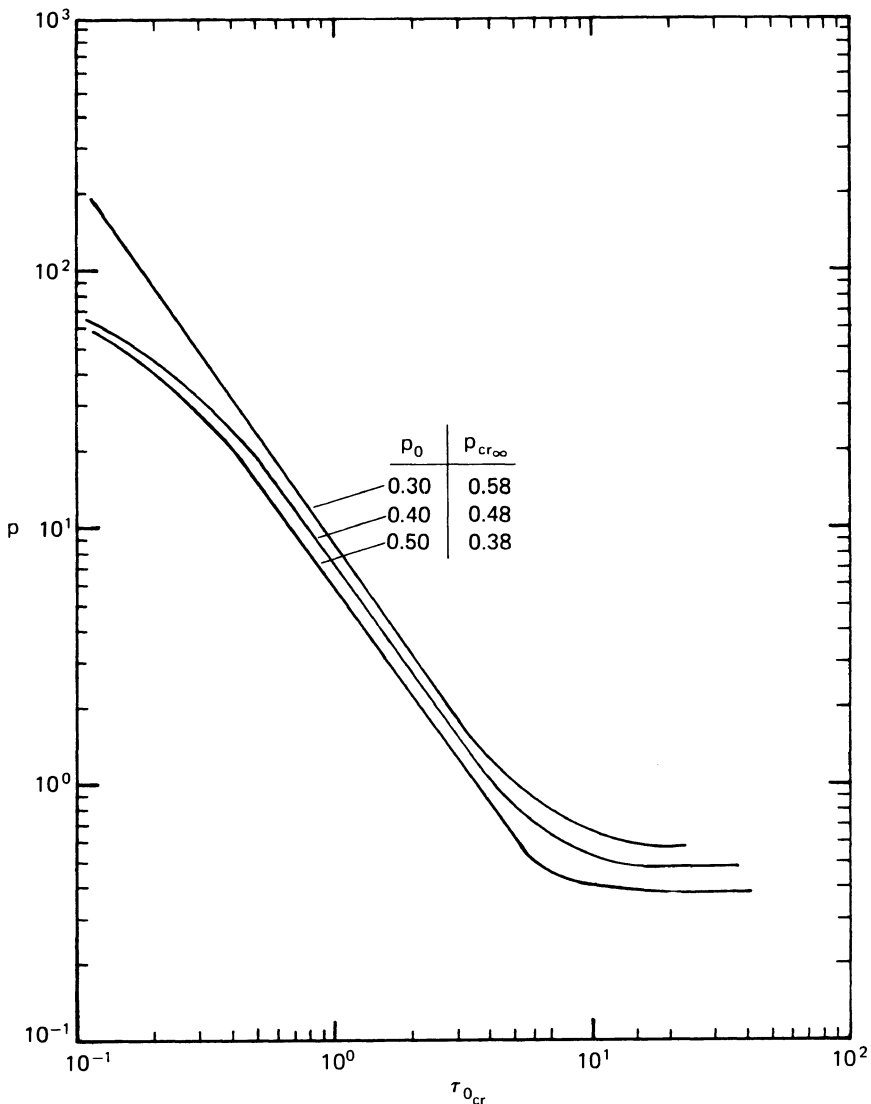


FIGURE 4.10. Superimposed load p versus critical duration time $\tau_{0_{cr}}$, prestressed model B, $\bar{e} = 0.02$.

quasi-statically with a p_0 load smaller than the p_{cr_s} static. Then the system is loaded dynamically (suddenly). The following values are used in the dynamic analysis:

$$\Lambda = 5.0, \quad p_{cr_s} = 5.154, \quad p_0 = 2.8, 3.4, 4.0$$

$$\Lambda = 6.0, \quad p_{cr_s} = 6.000, \quad p_0 = 3.2, 3.8, 4.2$$

$$\Lambda = 8.0, \quad p_{cr_s} = 7.310, \quad p_0 = 4.8, 5.4, 6.0$$

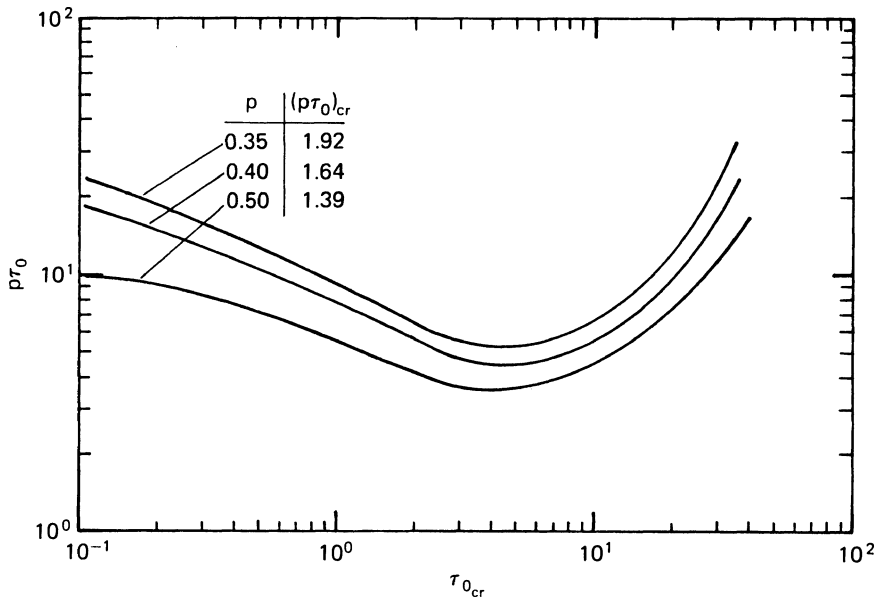


FIGURE 4.11. Superimposed impulse ($p\tau_0$) versus critical duration time $\tau_{0_{cr}}$, pre-stressed model B, $\bar{\epsilon} = 0.005$.

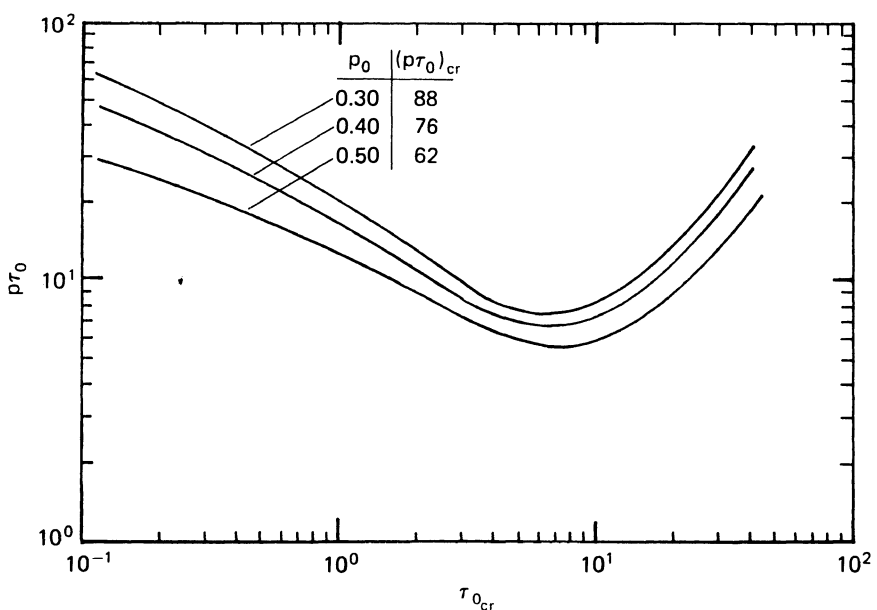


FIGURE 4.12. Superimposed impulse ($p\tau_0$) versus critical duration time $\tau_{0_{cr}}$, pre-stressed model B, $\bar{\epsilon} = 0.01$.

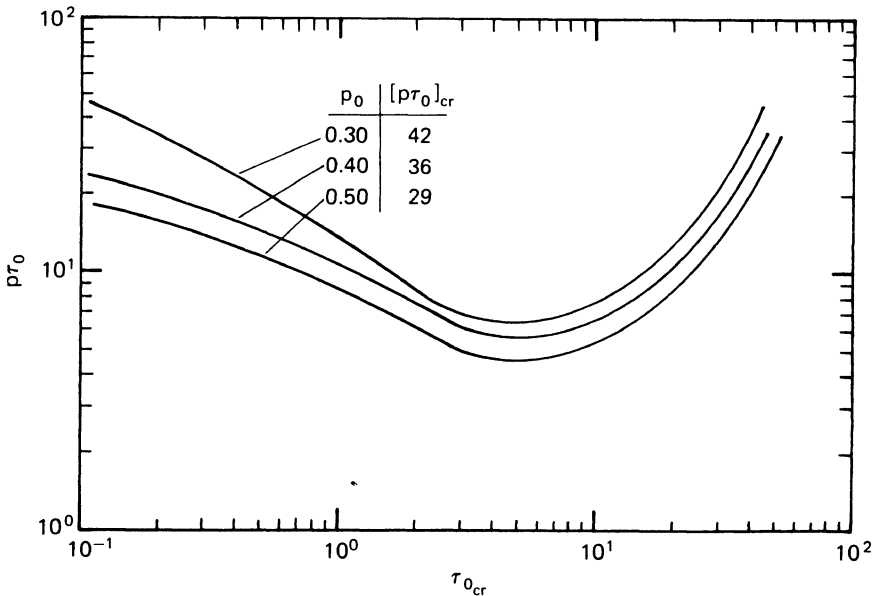


FIGURE 4.13. Superimposed impulse ($p\tau_0$) versus critical duration time $\tau_{0_{cr}}$, pre-stressed model B, $\bar{e} = 0.02$.

First, the extreme cases of ideal impulse and constant load of infinite duration are analyzed by employing eqs. (11) and (12), respectively.

4.5.1 Ideal Impulse

The ideal impulse ($p\tau_0$) is related to the initial kinetic energy in the non-dimensionalized form [see eq. (76) of Chapter 2] by the expression

$$2(p\tau_0)_{cr} = [2\bar{T}_i^{P_0}]^{1/2}. \quad (29)$$

The critical ideal impulse ($p\tau_0$)_{cr} is obtained by substituting eq. (11) into eq. (13), or

$$2(p\tau_0)_{cr} = \sqrt{2}[\bar{U}_T^{P_0}(\theta_s^{P_0}) - \bar{U}_T^{P_0}(\theta_u^{P_0})]^{1/2} \quad (30)$$

where $\theta_s^{P_0}$ is the stable static position (angle θ) under p_0 load, $\theta_u^{P_0}$ is the unstable static position under p_0 load, and the expression for the total potential is given by eq. (58) of Chapter 2, by using p_0 wherever p appears in the equation. The numerical results for all (Λ, p_0) combinations are presented in Table 4.5.

Note that the first-row results are obtained from eqs. (78) of Chapter 2. Note also that as the value of p_0 approaches the value of the static critical load, the additional imposed (critical) impulse tends to zero. This is reflected

TABLE 4.5. Critical ideal impulse ($p\tau_0$)_{cr} (MPCL).

$\Lambda = 5.0$		$\Lambda = 6.0$		$\Lambda = 8.0$	
p_0	$2(p\tau_0)_{cr}$	p_0	$2(p\tau_0)_{cr}$	p_0	$2(p\tau_0)_{cr}$
0	6.00	0	6.71	0	7.93
2.8	3.06	3.2	3.39	4.8	3.04
3.4	2.32	3.8	2.67	5.4	2.31
4.0	1.32	4.2	1.67	6.0	1.44
5.154	0	6.0	0	7.31	0

by the results of the last row (Table 4.5). Finally, the values for the critical ideal impulse in the table correspond to the lower bound values (MPCL).

4.5.2 Constant Load of Infinite Duration

The critical load for the case of infinite duration p_{cr_∞} , is obtained by the following steps for a given (Λ, p_0) combination.

1. Solve eq. (62) of Chapter 2, given below for $r_s^{P_0}$ (stable position) and $s = 0$, in terms of p_0 instead of Q .

$$p_0 = (\Lambda - 1 - [r_s^{P_0}]^2)r_s^{P_0} + \sqrt{\Lambda}. \quad (31)$$

2. Static saddle equilibrium positions are characterized by eq. (64) of Chapter 2 for loading $p_0 + p$, or

$$\begin{aligned} r &= \frac{p + p_0 - \sqrt{\Lambda}}{2} \\ r^2 + 3s^2 &= \Lambda - 3. \end{aligned} \quad (32)$$

3. Equation (12) for this model is given below:

$$\begin{aligned} (r^2 + 9s^2 - 2\sqrt{\Lambda}r + \Lambda) + \frac{1}{2}(\Lambda - r^2 - 3s^2)^2 - 2(p_0 + p)(\sqrt{\Lambda} - r) \\ = r_s^{P_0 2} + \frac{1}{2}(\Lambda - r_s^{P_0 2})^2 - 2p_0(\sqrt{\Lambda} - r_s^{P_0}). \end{aligned} \quad (33)$$

The simultaneous solution of eqs. (32) and (33) yields $r_u^{P_0 + P}$ and p_{cr_∞} .

TABLE 4.6. Critical dynamic loads of infinite duration, model C.

$\Lambda = 5.0$			$\Lambda = 6.0$			$\Lambda = 8.0$		
p_0	p_{cr_∞}	$p_0 + p_{cr_\infty}$	p_0	p_{cr_∞}	$p_0 + p_{cr_\infty}$	p_0	p_{cr_∞}	$p_0 + p_{cr_\infty}$
0	3.70	3.70	0	4.35	4.35	0	5.70	5.70
2.8	1.48	4.28	3.2	1.68	4.88	4.8	1.59	6.39
3.4	1.17	4.57	3.8	1.32	5.12	5.4	1.21	6.61
4.0	0.58	4.58	4.2	0.75	4.95	6.0	0.68	6.68
5.154	0	5.154	6.0	0	6.0	7.31	0	7.31

The numerical results for all (Λ, p_0) combinations are presented in Table 4.6.

Note that the first-row results of Table 4.6 are taken from Chapter 2. The results of the last row reflect the fact that if the system is loaded quasi-statically up to the limit point, then the additional suddenly applied load that the system can withstand tends to zero. The critical loads in Table 4.6 correspond to lower bound values (MPCL).

4.5.3 Constant Load of Finite Duration

Finally, for the case of constant load p applied suddenly for a finite duration τ_0 , critical conditions are obtained from the following steps:

1. From the static stability analysis, obtain $r_s^{p_0}$ and $r_u^{p_0}, s_u^{p_0}$ for each p_0 .
2. Use of eq. (9) yields

$$2p(r_s^{p_0} - r_{cr}) = (r_u^{p_0^2} + 9s_u^{p_0^2} - 2\sqrt{\Lambda}r_u^{p_0} + \Lambda) + \frac{1}{2}(\Lambda - r_u^{p_0})^2 - (r_s^{p_0} - \sqrt{\Lambda})^2 - \frac{1}{2}(\Lambda - r_s^{p_0})^2 + 2p_0(r_u^{p_0} - r_s^{p_0}) \quad (34)$$

where r_{cr} is the position r at the instant of the release of the force p ($\tau = \tau_0$). In eq. (34) for a given geometry, Λ , and static load p_0 , everything is known ($p_0, \Lambda, r_s^{p_0}, r_u^{p_0}$, and $s_u^{p_0}$), except p and r_{cr} . Therefore, eq. (34) relates p and r_{cr} for a critical condition to exist.

3. Since $\bar{T}^{p_0+p} = \frac{1}{2}[1 + (ds/dr)^2](dr/d\tau)^2$, from eq. (4) we may write

$$\begin{aligned} \frac{dr}{d\tau} &= [\bar{U}_T^{p_0+p}(r_s^{p_0}) - \bar{U}_T^{p_0+p}(r, s)]^{1/2}, \quad \text{or} \\ d\tau &= [\bar{U}_T^{p_0+p}(r_s^{p_0}) - \bar{U}_T^{p_0+p}(r, s)]^{-1/2} dr. \end{aligned} \quad (35)$$

Invoking the same techniques as the ones we used for the same problem but without static preloading in Chapter 3, the critical time τ_0 is computed by assuming the path to be symmetric ($s = 0$).

Integration from $\tau = 0$ to $\tau = \tau_0$ and use of the expression for the total potential [see eq. (58) of Chapter 2] yields

$$\begin{aligned} \tau_0 &= \int_{r_s^{p_0}}^{r_{cr}} [(r_s^{p_0} - \sqrt{\Lambda})^2 + \frac{1}{2}(\Lambda - r_s^{p_0})^2 - (r - \sqrt{\Lambda})^2 - \frac{1}{2}(\Lambda - r)^2 \\ &\quad - 2(p + p_0)(r - r_s^{p_0})]^{-1/2} dr. \end{aligned} \quad (36)$$

Note that eq. (34) also relates r_{cr} to p .

A critical condition is characterized by a set of (p, τ_0) values that satisfies both eqs. (34) and (36). This means that for a given release time τ_0 , find p_{cr} ; or for a given p , find $\tau_{0,cr}$. Computationally, though, it is easier to assign values of r_{cr} , solve for p from eq. (34), and then solve for the corresponding τ_0 from eq. (36).

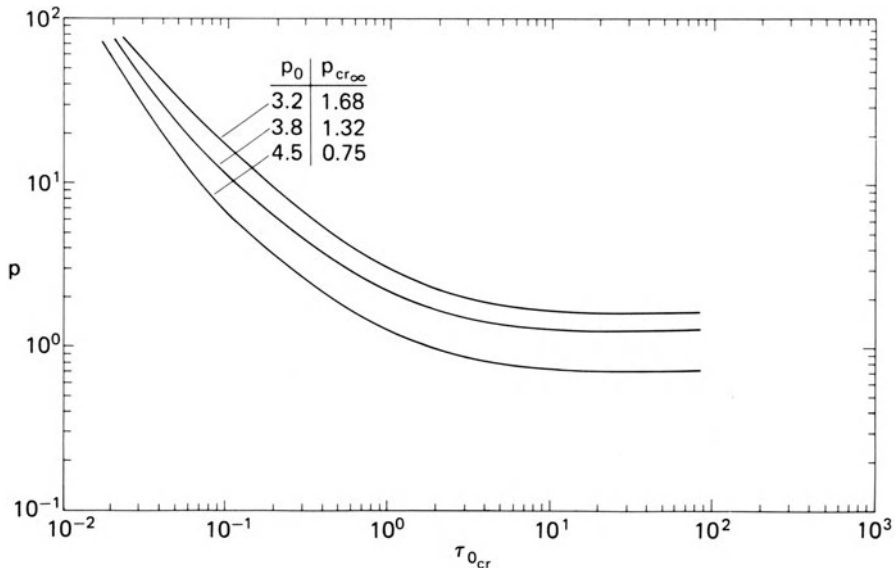


FIGURE 4.14. Constant load p versus critical duration time $\tau_{0_{cr}}$, prestressed model C, $\Lambda = 5.0$.

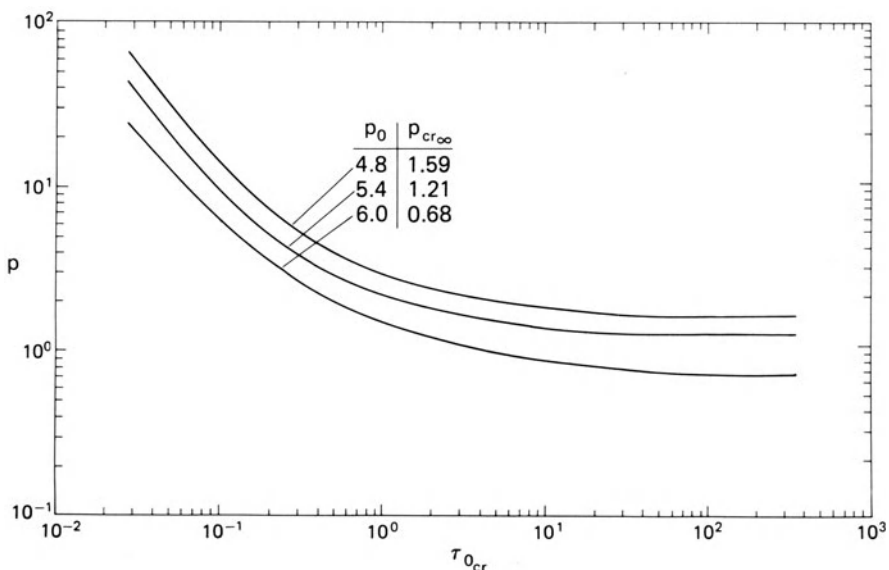


FIGURE 4.15. Constant load p versus critical duration time $\tau_{0_{cr}}$, prestressed model C, $\Lambda = 6.0$.

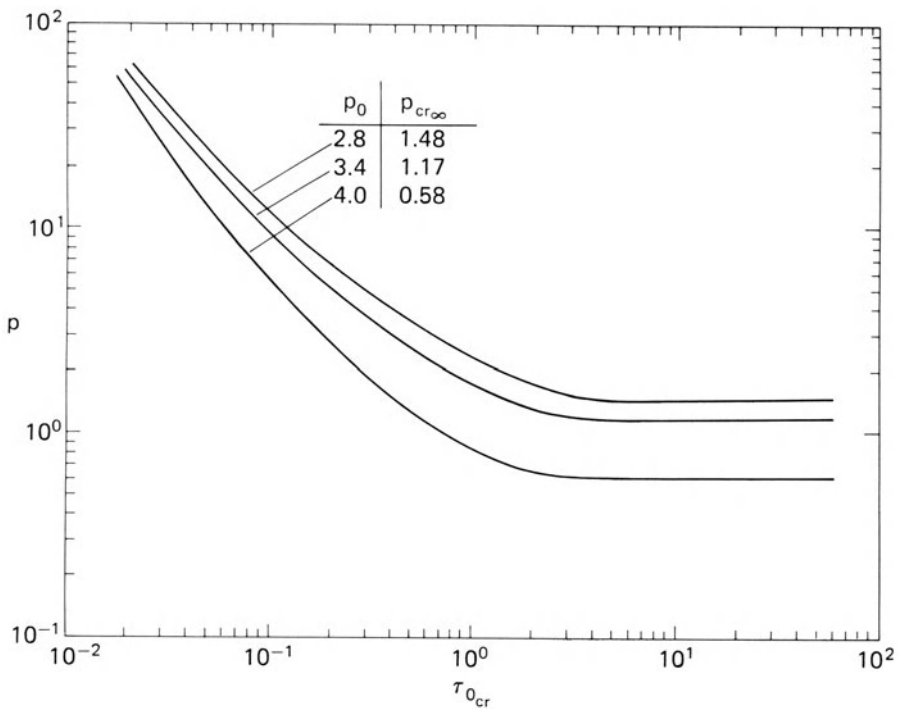


FIGURE 4.16. Constant load p versus critical duration time $\tau_{0_{cr}}$, prestressed model C, $\Lambda = 8.0$.

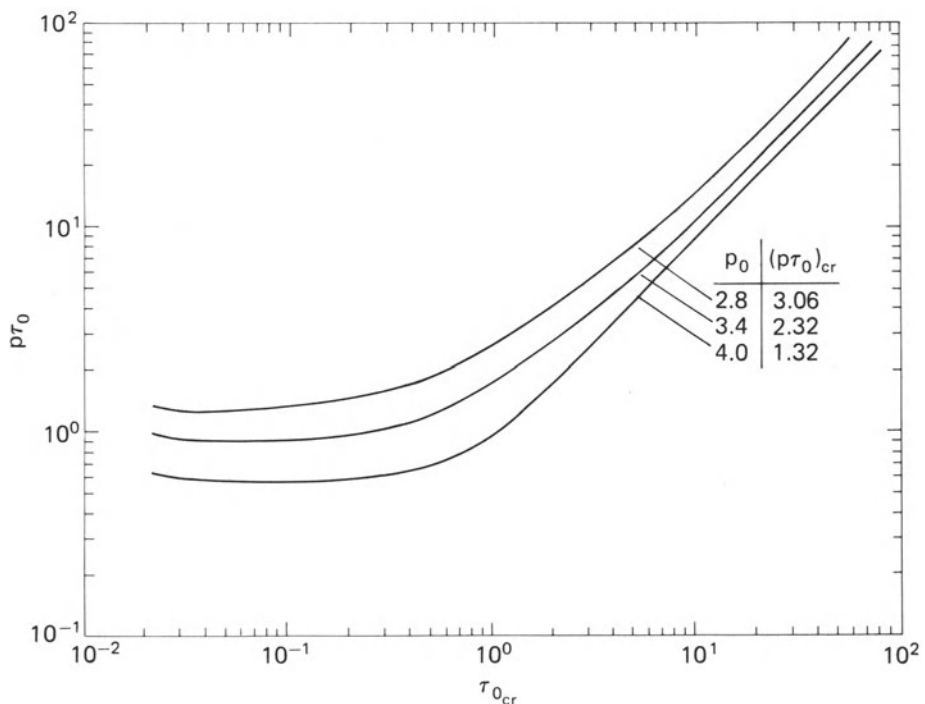


FIGURE 4.17. Impulse $(p\tau_0)$ versus critical time duration $\tau_{0_{cr}}$, preloaded model C, $\Lambda = 5.0$.

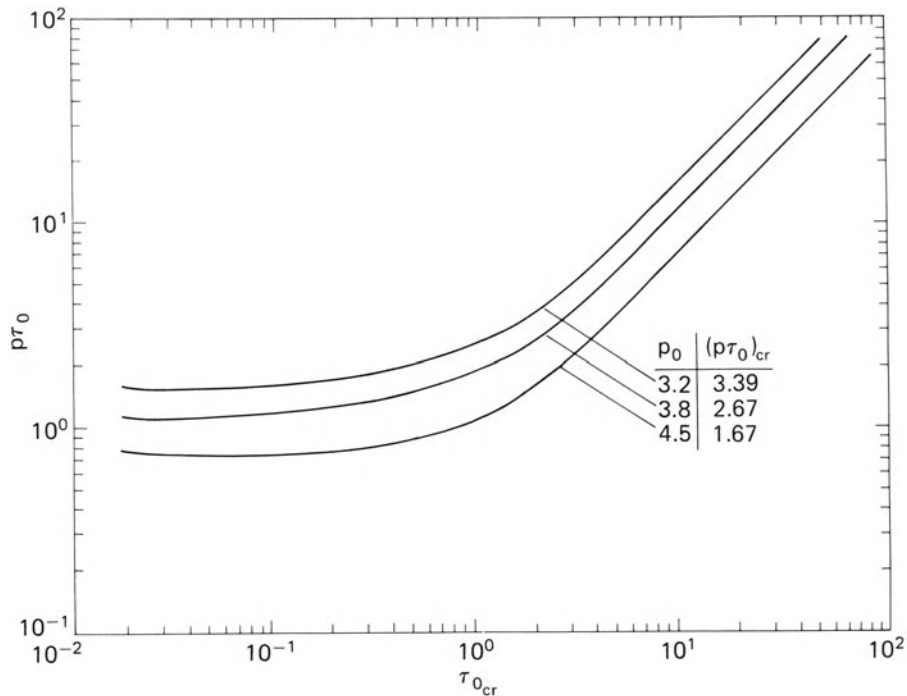


FIGURE 4.18. Impulse ($p\tau_0$) versus critical time $\tau_{0_{cr}}$, prestressed model C, $\Lambda = 6.0$.

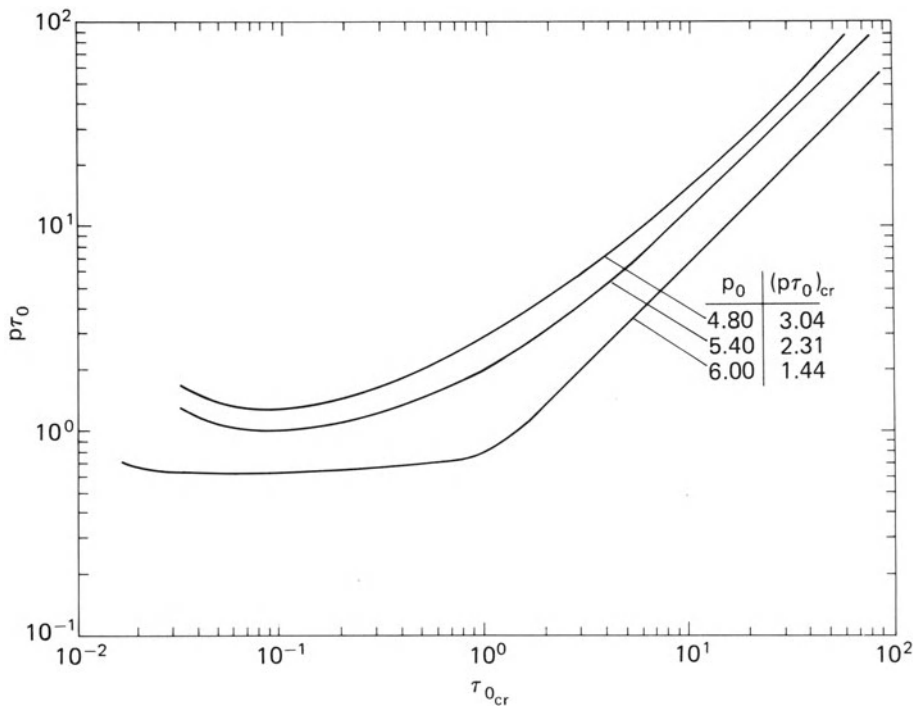


FIGURE 4.19. Impulse ($p\tau_0$) versus critical duration time $\tau_{0_{cr}}$, prestressed model C, $\Lambda = 8.0$.

A simple computer program can be written for these computations. Values of r_{cr} are assigned, starting with $r_s^{p_0} + \delta r$, where δr is very small, and computing the corresponding values of p and τ_0 for each δr .

The results are presented graphically on Figures 4.14 to 4.19 (pp. 88–90) for the three values of Λ . On the first three figures, Figures 4.14 to 4.16, critical conditions appear as plots of p versus duration time $\tau_{0,cr}$. Note that as $\tau_{0,cr}$ becomes larger and larger, the corresponding value of p approaches $p_{cr,\infty}$ (see Table 4.6). On the last three figures, Figures 6.17 to 6.19, critical conditions appear as plots of $(p\tau_0)_{cr}$ versus duration time $\tau_{0,cr}$. On these figures, as $\tau_{0,cr} \rightarrow 0$, the corresponding value of $(p\tau_0)_{cr}$ approaches the critical ideal impulse (see Table 4.5).

4.6 Remarks

The estimates in this chapter represent true critical conditions for one-degree-of-freedom systems. On the other hand, for the two-degree-of-freedom model, the estimates represent lower bounds for critical dynamic conditions (MPCL).

One important observation is that the effect of static preloading seems to be the same, regardless of the particular model. Specifically, (1) for the extreme case of the ideal impulse, the critical impulse decreases with increasing values of static preloading, and (2) for the other extreme case of constant load of infinite duration, the total load (the sum of the static preload and the critical dynamic load) increases with increasing values of static preloading. Both of these observations are very significant in the design of dynamically loaded systems. This is so because the “zero static preloading” analyses are much simpler in execution, but yet they provide a (lower) limit behavior for the cases of finite static preloading. Note that the amount of static preloading must be lower than the level of the static critical load.

Finally, it was mentioned in the analysis of model C that for multi-degree-of-freedom systems the path of motion is essential in establishing critical conditions. This path can influence the value of the critical load. If one wishes to be conservative, one must choose the path that yields the shortest time. This requires solving the related brachistochrone problem, discussed in Appendix B. For the model analyzed in this chapter, the critical condition is not that sensitive to the path, provided that a reasonable path is followed.

Problems

1. Consider the model shown in Figure 2.19 (Chapter 2). Find (numerically) for two α values, $\alpha = 30^\circ$ and $\alpha = 60^\circ$, (i) values of the critical ideal impulse, (ii) values for critical load of infinite duration, corresponding to several amounts of static preloading covering the entire permissible range from zero to the full value of the static critical load, $p_{cr,s}$ (use $p = \lambda p_{cr,s}$, and let $\lambda = 0, 0.25, 0.50, 0.75$, and 1.00)

2. For the same model (Figure 2.19 of Chapter 2), find critical conditions for the case of finite duration in the presence of static preloading. Let $p_0 = 0.50 p_{\text{crs}}$, $\alpha = 30^\circ$, and present the results as plots of p versus $\tau_{0,\text{cr}}$ only.
3. For model C with the case of constant load of finite duration, critical conditions were obtained by assuming the path to be symmetric [$s = 0$; see eq. (35)]. Find critical conditions for $\Lambda = 5$, by assuming the path $s = \sqrt{\Lambda - 4}(1 - r/\sqrt{\Lambda})/3$. Compare the results with those of Figure 4.14. Choose only one p_0 value (3.2, 3.8, or 4.5).
4. Repeat problem 3 by using the following path:

$$\begin{aligned}s &= 0 \quad \text{for } \sqrt{\Lambda - 3} \leq r \leq \sqrt{\Lambda} \\r^2 + 3s^2 &= \Lambda - 3 \quad \text{for } r < \sqrt{\Lambda - 3}.\end{aligned}$$

Here also use $\Lambda = 5$ and one p_0 value. Compare the results to those of Figure 4.14.

Part II Structural Applications

@Seismicisolation

5

The Concept of Dynamic Stability

5.1 Introduction

The beginning of dynamic instability and/or dynamic buckling can be traced to the investigation of Koning and Taub [1], who analyzed a suddenly loaded (in the axial direction) imperfect, simply supported column. Several studies followed in the 1940s and 1950s on the problem of dynamic column buckling. These studies [2–7] concentrated on such effects as those of axial inertia, of short and long duration of the load, of low- and high-velocity excitation, of in-plane inertia, of rotatory inertia, and of transverse shear. Similar studies continued into the 1970s [8–18] and the 1980s [19–20]. Moreover, non-deterministic consideration was included by Elishakoff [21–22] and extensions to plate geometries were reported by others [23–27]. A detailed discussion of geometries of this type is presented in Chapter 10. For these geometries, which under static conditions experience smooth buckling (the analysis shows that there exists a bifurcation point and the postbuckling branch corresponds to stable static equilibrium positions), there is no clear criterion of instability, although the criterion used for establishing critical conditions is very simple. When some characteristic deflection increases rapidly with time, we have a dynamically critical condition. In reality, the problem of suddenly loaded columns and plates is one of dynamic response rather than one that encounters escaping (buckled) motion of some type. Parametric resonance is a possible dynamic instability for these configurations (see [28]).

Note that these geometries can be analyzed by employing the Budiansky–Roth criterion as discussed in Chapter 1 (see [40] in Chapter 1) and extended to infinite-degree-of-freedom systems.

In this chapter, the concept of dynamic stability and the associated criterion for establishing critical conditions, based on the total potential energy approach, are extended to continuous systems. The extension is for the two extreme cases of sudden loads, the constant load of infinite duration and the ideal impulse. Once this has been accomplished, the dynamic stability of several structural configurations is discussed in subsequent chapters.

5.2 The Stability Criterion

Let us assume, for simplicity, that the kinematic state of all elements in a structural configuration is completely described by a displacement vector, which is a function of a single space coordinate (one dimension) and time t . Through this assumption, a large class of structural elements and configurations is covered. Bars, beams, arches, rings, and frames are examples of this class of systems. Extensions to two-dimensional (plates, shells, etc.) and three-dimensional configurations will follow.

5.2.1 Constant Load of Infinite Duration

For the case of a suddenly applied loading of constant magnitude and infinite duration, $P(t)$, one can write that

$$P(t) = H(t)P \quad (1)$$

where P is the magnitude and $H(t)$ is the Heaviside function.

Let the displacement components of the i th one-dimensional member of the structural configurations be denoted by $u_i(x, t)$ and $w_i(x, t)$. Moreover, define the total potential U_T in such a manner that its value is zero at $t = 0$. Since the system is at rest at $t = 0$ and only the loading $P(t)$ is suddenly applied, there is no initial velocity. Therefore, the kinetic energy is zero at $t = 0$. Finally, in dealing only with conservative systems, the total energy (Hamiltonian) is zero (constant) for all $t > 0$, in the absence of damping.

Therefore,

$$U_T \left[u_i, \frac{\partial u_i}{\partial x}, \frac{\partial^2 u_i}{\partial x^2}, \dots, w_i, \frac{\partial w_i}{\partial x}, \frac{\partial^2 w_i}{\partial x^2}, \dots, P \right] + T \left[\frac{\partial u_i}{\partial t}, \frac{\partial w_i}{\partial t} \right] = 0 \quad (2)$$

where U_T is the total potential and is a functional of u_i, w_i , their derivatives with respect to x , and P ; T is the kinetic energy and is a functional of the local displacement velocities $\partial u_i / \partial t$ and $\partial w_i / \partial t$. Note that if rotatory inertia effects are included, then the local angular velocity terms must be included in the kinetic energy functional.

For the systems under consideration, the kinetic energy T is a positive definite functional of the local material velocities, for all kinematically admissible trajectories. Then, according to eq. (2), motion is possible only when U_T is nonpositive, or

$$U_T \left[u_i, \frac{\partial u_i}{\partial x}, \frac{\partial^2 u_i}{\partial x^2}, \dots, w_i, \frac{\partial w_i}{\partial x}, \frac{\partial^2 w_i}{\partial x^2}, \dots, P \right] < 0. \quad (3)$$

Next, let us assume that at some level of the applied load $P = \bar{P}$, the ensuing motion is bounded for all possible, kinematically admissible trajectories. Then for each possible trajectory, regardless of whether it corresponds to a true trajectory of motion or not, there exists a set of displacement

components $[\bar{u}_i(x), \bar{w}_i(x)]$ such that

$$U_T \left[\bar{u}_i, \frac{\partial \bar{u}_i}{\partial x}, \dots, \bar{w}_i, \frac{\partial \bar{w}_i}{\partial x}, \frac{\partial^2 \bar{w}_i}{\partial x^2}, \dots, \bar{P} \right] = 0 \quad (4)$$

for all $t > 0$ (\bar{u}_i and \bar{w}_i are independent of t).

The collection of all such sets, corresponding to all possible, kinematically admissible trajectories, forms a boundary that is characterized by $U_T = 0$, and it separates the region of $U_T < 0$ from the region of $U_T > 0$. This boundary is dependent on the level of the applied load \bar{P} . Because of eq. (2), it has been established that motion can take place only in the region characterized by $U_T < 0$. At this point, note that, regardless of the trajectory, the velocities $\partial u_i / \partial t, \partial w_i / \partial t$ must be zero at the boundary characterized by $U_T = 0$, and a change in the motion takes place whenever the system reaches this boundary. Furthermore, the region characterized by $U_T < 0$ must contain at least one relative minimum position for U_T , with respect to functions u_i, w_i , regardless of trajectory and time. It may contain more than one relative minimum and some other stationary positions (saddle). These stationary positions are characterized by sets of displacement magnitudes and shapes $u_i(x), w_i(x)$ that, by definition, correspond to static equilibrium positions for the particular value \bar{P} of the applied load.

Having set the stage in this manner, we can now define unbuckled motion. If the bounded region ($U_T < 0$) contains only one stationary position (a minimum) then the motion for this \bar{P} is called *unbuckled*. The physical interpretation of unbuckled motion corresponds to the system performing nonlinear oscillations about the corresponding near stable static equilibrium position. This is indeed the case for small levels of the suddenly applied load. The only way the motion can become *buckled* (unbounded in the sense described above) is if the boundary characterized by the set of $[\bar{u}_i(x), \bar{w}_i(x)]$ contains an unstable static equilibrium position for the corresponding value of the applied load. This value of the load represents an upper bound of all loads for which the motion is unbuckled, and it is called herein the (minimum possible) critical dynamic load.

The definitions of critical dynamic load, buckled motion, and so forth are the same as in the case of finite-degree-of-freedom systems. The only difference is that generalized coordinates have been replaced by functions of position, and functions of the generalized coordinates by functionals of functions of position. Note that in the presence of even small damping, the system is asymptotically stable for loads smaller than the critical dynamic load. This is so because the system will eventually come to rest at the stable static equilibrium position, as $t \rightarrow \infty$.

Before closing, it suffices to say that if the system consists of either two-dimensional (plate and shell) elements or a combination of one- and two-dimensional elements, nothing changes except that the number of displacement components for each element increases from two to three (from u_i, w_i to u_i, v_i, w_i) and each displacement component is a function of two

coordinates instead of one (in an orthogonal cartesian system we have x and y instead of just x).

5.2.2 Ideal Impulse

For this case of the ideal impulse, the sum of the total potential and kinetic energy is a constant. By assuming that the ideal impulse is instantaneously imparted to the system as initial kinetic velocity, the constant is equal to the initial kinetic energy T_I . Here also we define U_T in such a manner that it is zero at $t = 0$. Thus, following the steps outlined for the case of constant load of infinite duration, we can write

$$U_T \left[u_i, \frac{\partial u_i}{\partial x}, \dots, w_i, \frac{\partial w_i}{\partial x}, \frac{\partial^2 w_i}{\partial x^2}, \dots \right] + T \left[\frac{\partial u_i}{\partial t}, \frac{\partial w_i}{\partial t} \right] = T_I \left[\frac{\partial u_i}{\partial t}, \frac{\partial w_i}{\partial t} \right]. \quad (5)$$

For the system under consideration, the kinetic energy T is a positive definite functional of the local material velocities, for all kinematically admissible trajectories. Then, according to eq. (5), motion is possible if U_T is no larger than the initial kinetic energy T_I imparted to the system at $t = 0$, or

$$U_T \left[u_i, \frac{\partial u_i}{\partial x}, \dots, w_i, \frac{\partial w_i}{\partial x}, \frac{\partial^2 w_i}{\partial x^2}, \dots \right] \leq T_I \left[\frac{\partial u_i}{\partial t}, \frac{\partial w_i}{\partial t} \right]. \quad (6)$$

Following the same steps as in the previous load case, we assume that for a given initial kinetic energy (corresponding to a given ideal impulse) the ensuing motion is bounded for all possible kinematically admissible trajectories. For each possible trajectory, regardless of whether it corresponds to a true trajectory or not, there exists a set of displacement components $[\bar{u}_i(x), \bar{w}_i(x)]$ such that

$$U_T \left[\bar{u}_i, \frac{\partial \bar{u}}{\partial x_i}, \dots, \bar{w}_i, \frac{\partial \bar{w}_i}{\partial x}, \frac{\partial^2 \bar{w}_i}{\partial x^2}, \dots \right] \leq T_I \left[\frac{\partial u_i}{\partial t}, \frac{\partial w_i}{\partial t} \right] \quad (7)$$

for $t > 0$ (\bar{u}_i and \bar{w}_i are independent of t). Note that the right-hand side does not contain “bar” quantities and it is the true initial kinetic energy.

The collection of all such sets forms a boundary, which is now characterized by $U_T = T_I$ and it separates the region of $U_T < T_I$ from the region of $U_T > T_I$ in the space of u_i and w_i . This boundary, clearly, is dependent on the level of the ideal impulse (value of T_I). Because of eq. (6), motion can take place only within the boundary characterized by eq. (7). Here, also, note that regardless of the trajectory, the velocities $\partial u_i / \partial t$, $\partial w_i / \partial t$ must be zero at the boundary characterized by eq. (7), and a change in the motion takes place whenever the system reaches this boundary. Furthermore, the region enclosed by this boundary already contains one relative minimum position of U_T with respect to u_i and w_i regardless of trajectory and time, corresponding to $P = 0$ (U_T is not explicitly a function of the load for the case of the ideal impulse). We'll say more about this relative minimum.

Now, as in the previous load case, we can define unbuckled motion. If the bounded region ($U_T < T_1$) contains only one stationary position (relative minimum with respect to functions u_i and w_i), then the corresponding motion is called unbuckled. The physical interpretation of unbuckled motion corresponds to the system performing nonlinear oscillations about the initial position, which also denotes a stable static equilibrium position under zero load. The only way that the motion can become buckled (unbounded or escaping motion) is if the boundary characterized by \bar{u}_i and \bar{w}_i [see eq. (7)] contains an unstable static equilibrium position under zero load. Thus, if the value of T_1 in eq. (7) is such that the value of U_T at an unstable static equilibrium position is equal to T_1 , then escaping motion is possible. In such a case the value of T_1 is critical and it corresponds to the (minimum possible) critical dynamic impulse.

Please note that the initial position (at $t = 0$) and the unstable position on the boundary are stable and unstable static positions with respect to functions $\bar{u}_i(x)$ and $\bar{w}_i(x)$ that correspond to zero loading.

Also note that the critical conditions, as defined in this section, correspond to minimum possible critical loads or necessary conditions for stability as defined and discussed in Chapter 1.

Finally, one must be reminded that the Budiansky–Roth criterion can and has been used in establishing critical conditions for structural elements and configurations.

References

1. Koning, C., and Taub, J. Impact buckling of thin bars in the elastic range hinged at both ends. *Luftfahrtforschung*, 10, 2, 1933, 55–64 (translated as NACA TM 748 in 1934).
2. Meier, J.H. On the dynamics of elastic buckling. *J. Aeronaut. Sci.*, 12, 4, 1945, 433–440.
3. Hoff, N.J. The dynamics of the buckling of elastic columns. *J. Appl. Mech.*, 18, 1, 1951, 68–74.
4. Gerard, G., and Becker, H. Column behavior under conditions of impact. *J. Aeronaut. Sci.*, 19, 1, 1952, 58–60.
5. Davidson, J.F. Buckling of struts under dynamic loading. *J. Mech. Phys. Solids*, 2, 1953, 54–66.
6. Schmitt, A.F. A method of stepwise integration in problems of impact buckling. *J. Appl. Mech.*, 23, 2, 1956, 291–294.
7. Sevin, E. On the elastic bending of columns due to dynamic axial forces including effects of axial inertia. *J. Appl. Mech.*, 27, 1, 1960, 125–131.
8. Housner, G.W., and Tso, W.K. Dynamic behavior of supercritically loaded struts. *J. Eng. Mech. Div., ASCE*, 88, Oct. 1962, 41–65.
9. Huffington, N.J., Jr. Response of elastic columns to axial pulse loading. *AIAA J.*, 1, 9, 1963, 2099–2104.
10. Hayashi, T., and Sano, Y. Dynamic buckling of elastic bars (the case of low velocity impact). *Bull. JSME*, 15, 88, 1972, 1167–1175.

11. Hayashi, T., and Sano, Y. Dynamic buckling of elastic bars (the case of high velocity impact). *Bull. JSME*, 15, 88, 1972, 1176–1184.
12. Holzer, S.M., and Eubanks, R.A. Stability of columns subject to impulsive loading. *J. Eng. Mech. Div., ASCE*, 95, EM4, 1969, 897–920.
13. Holzer, S.M. Response bounds for columns with transient loads. *J. Appl. Mech.*, 38, 1, 1971, 157–161.
14. Plaut, R.H. Displacement bounds for beam-columns with initial curvature subjected to transient loads. *Int. J. Solids Struct.*, 7, 9, 1971, 1229–1235.
15. McIvor, I.K., and Bernard, J.E. The dynamic response of columns under short duration axial loads. *J. Appl. Mech.*, 40, 3, 1973, 688–692.
16. Grybos, R. Impact stability of a bar. *Int. J. Eng. Sci.*, 13, 5, 1975, 463–477.
17. Malyi, V.I., and Efimov, A.B. Stability loss of a rod in longitudinal impact. *Sov. Phys.-Dokl.*, 17, 2, 1972, 176–177 (English translation).
18. Kiryukhin, L.V., and Malyi, V.I. Buckling of an elastic bar under longitudinal impact. *Moscow Univ. Mech. Bull.*, 29, 3, 1974, 14–28 (English translation).
19. Ari-Gur, J., Weller, T., and Singer, J. Experimental and theoretical studies of columns under axial impact. *Int. J. Solids Struct.*, 18, 7, 1982, 619–641.
20. Housner, J.M., and Knight, N.F., Jr. The dynamic collapse of a column impacting a rigid surface. *AIAA J.*, 21, 8, 1983, 1187–1195.
21. Elishakoff, J. Axial impact buckling of a column with random initial imperfections. *J. Appl. Mech.*, 45, 2, 1978, 361–365.
22. Elishakoff, I. Impact buckling of a thin bar via Monte Carlo method. *J. Appl. Mech.*, 45, 3, 1978, 586–590.
23. Zizicas, G.A. Dynamic buckling of thin elastic plates. *Trans. ASME*, 74, 7, 1952, 1257–1268.
24. Birkgau, A.Y., and Vol'mir, A.S. An investigation of the dynamic stability of plates using an electronic digital computer. *Sov. Phys.-Dokl.*, 5, 6, 1961, 1364–1366 (English translation).
25. Edstrom, R.E. Dynamic buckling of a rectangular orthotropic plate. *AIAA J.*, 11, 12, 1973, 1655–1659.
26. Ari-Gur, J., Singer, J., and Weller, T. Dynamic buckling of plates under longitudinal impact. *Israel J. Technol.*, 19, 1981, 57–64.
27. Wauer, J. Über Kinetische Verweigungs Problem Elastischer Strukturen under Stosseblastung. *Ingenieur-Arch.*, 49, 1980, 227–233.

6

Two-Bar Simple Frames

6.1 Introduction

The simple two-bar frame is a structural configuration that may or may not be imperfection-sensitive under static loading. This depends on the loading and boundary conditions. If both supports are immovable, and if the loading is a distributed load, the response is one of stable equilibrium and there is no possibility of static instability, either through the existence of a bifurcation point or through a limit point. Similarly, for the same supports, if the load is a concentrated one with a positive eccentricity (see Figure 6.1), the response is one of stable equilibrium (see [1–3]). On the other hand, if the eccentricity is zero or negative [1], the system is subject to limit point instability. For this case, the two-bar frame is sensitive to initial geometric imperfections and when the load is suddenly applied, critical conditions can easily be established by employing any of the three approaches discussed in Chapter 1. Moreover, if the support of the horizontal bar is movable along a vertical plane (Figure 6.1, model B), then the frame is imperfection sensitive for all loads. First the static analysis is presented and then the energy approach is employed for the estimation of critical conditions under sudden application of the load.

6.2 Static Analysis of the System

6.2.1 *The Mathematical Model*

Consider the simple two-bar frame shown on Figure 6.1. The two bars are of the same structural geometry (length l , cross-sectional area A , second moment of area I , and Young's modulus E). The vertical bar is supported by an immovable hinge, while the horizontal bar is supported by a hinge with three variations: immovable (model A), movable in a vertical direction (model B), and movable in a horizontal direction (model C). The external load P is applied vertically with a small eccentricity e . The transverse and axial displacement components are $w_i(x)$ and $u_i(x)$, respectively.

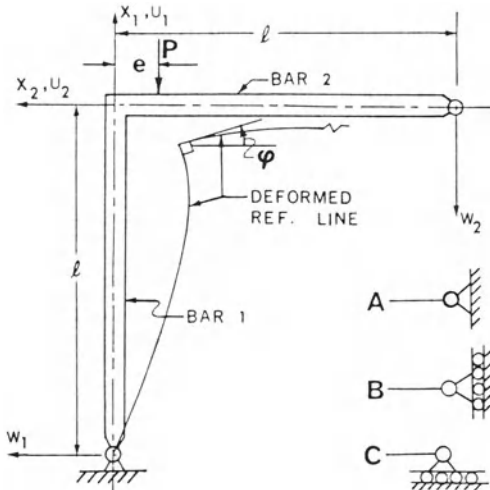


FIGURE 6.1. Geometry and sign convention.

By employing linear constitutive relations and nonlinear kinematic relations (those corresponding to moderate rotations, $w_{i,x}^2 \ll 1$), the total potential is given by

$$U_T = \frac{1}{2} \sum_{i=1}^2 \int_0^l [AE(u_{i,x} + \frac{1}{2}w_{i,x}^2)^2 + EIw_{i,xx}^2] dx + Pu_1(l) + Pew_{2,x}(l) \quad (1)$$

where a comma denotes differentiation with respect to the index that follows.

Through the principle of the stationary value of the total potential one may derive equilibrium equations and proper boundary conditions. The equilibrium equations are

$$\begin{aligned} S_{i,x} &= AE(u_{i,x} + \frac{1}{2}w_{i,x}^2)_{,x} = 0 \\ EIw_{i,xxxx} - AE(u_{i,x} + \frac{1}{2}w_{i,x}^2)w_{i,xx} &= 0 \end{aligned} \quad i = 1, 2 \quad (2)$$

where S_i is the axial force in bar i .

Use of the kinematic continuity conditions at the joint provides the proper expressions for the natural boundary conditions at $x = l$ for both bars. In addition, the support conditions are the same for all three models (A, B, and C) for the vertical bar but differ for the horizontal bar. The common conditions for all three models are listed first.

1. Continuity conditions:

$$w_1(l) = u_1(l), \quad w_2(l) = -u_1(l), \quad w_{1,x}(l) = w_{2,x}(l). \quad (3)$$

2. Natural boundary conditions at the joint:

$$\begin{aligned} AE[u_{1,x}(l) + \frac{1}{2}w_{1,x}^2(l)] + EIw_{2,xxx}(l) - AE[u_{2,x}(l) + \frac{1}{2}w_{2,x}^2(l)]w_{2,x}(l) + P &= 0 \\ AE[u_{1,x}(l) + \frac{1}{2}w_{1,x}^2(l)]w_{1,x}(l) - EIw_{1,xxx}(l) + AE[u_{2,x}(l) + \frac{1}{2}w_{2,x}^2(l)] &= 0 \\ EI[w_{1,xx}(l) + w_{2,xx}(l)] + Pe &= 0. \end{aligned} \quad (4)$$

3. Support conditions (vertical bar):

$$w_1(0) = u_1(0) = w_{1,xx}(0) = 0. \quad (5)$$

The support conditions for the horizontal bar are given below for each of the three models:

$$\text{Model A: } u_2(0) = w_2(0) = w_{2,xx}(0) = 0 \quad (6)$$

$$\begin{aligned} \text{Model B: } u_2(0) &= w_{2,xx}(0) = 0 \\ -EIw_{2,xxx}(0) + AE[u_{2,x}(0) + \frac{1}{2}w_{2,x}^2(0)] &= 0 \end{aligned} \quad (7)$$

$$\begin{aligned} \text{Model C: } AE[u_{2,x}(0) + \frac{1}{2}w_{2,x}^2(0)] &= 0 \\ w_2(0) = w_{2,xx}(0) &= 0. \end{aligned} \quad (8)$$

For convenience, all equations are cast in nondimensionalized form. In so doing it is recognized that the axial force in the vertical bar is always compressive, $-S_1$, where S_1 is the magnitude, while the axial force in the horizontal bar can be compressive, zero, or tensile, $\pm S_2$, where S_2 is its magnitude. The nondimensionalized parameters are

$$\begin{aligned} X &= x/l, & W_i &= w_i/l, & U_i &= u_i/l \\ \lambda &= l/\rho, & \rho^2 &= I/A, & \bar{e} &= e/l \\ \beta^2 &= \frac{Pl^2}{EI}, & k_i^2 &= \frac{S_i l^2}{EI}, & \lambda_c &= P/P_{cl} \end{aligned} \quad (9)$$

where P_{cl} is the linear theory critical load, ρ denotes the radius of gyration of the cross section, and λ denotes the bar slenderness ratio.

6.2.2 Solution Procedure

The solution procedure for each of the models is presented separately, and in each case a distinction is made for the two cases of compression and tension in the horizontal bar (whenever applicable).

Model A

First, the solution for the *compressive* case (compression in the horizontal bar) is given. This solution is obtained by writing the general solution to eqs. (2) and making use of the proper auxiliary conditions, eqs. (3), (4), (5), and (6), with the condition that the axial force in the horizontal bar is

compressive, therefore

$$EA[u_{2,x} + \frac{1}{2}w_{2,x}^2] = -S_2. \quad (10)$$

The solution for this case then is (in nondimensionalized form)

$$\begin{aligned} U_1(X) &= -\frac{k_1^2}{\lambda^2}X - B_1(X) \\ W_1(X) &= A_{11} \sin k_1 X + A_{13} X \\ U_2(X) &= -\frac{k_2^2}{\lambda^2}X - B_2(X) \\ W_2(X) &= A_{21} \sin k_2 X + A_{23} X \end{aligned} \quad (11)$$

where

$$\begin{aligned} B_1(X) &= \frac{1}{2} \left[A_{13}^2 X + 2A_{11}A_{13} \sin k_1 X + \frac{k_1^2 A_{11}^2}{2} \left(X + \frac{\sin 2k_1 X}{2k_1} \right) \right] \\ B_2 &= \frac{1}{2} \left[A_{23}^2 X + 2A_{21}A_{23} \sin k_2 X + \frac{k_2^2 A_{21}^2}{2} \left(X + \frac{\sin 2k_2 X}{2k_2} \right) \right] \\ A_{11} &= \frac{\beta^2 \bar{e} k_2 \cos k_2 + (k_1^4 + k_2^4 - k_1^2 \beta^2) \sin k_2 / k_2^2}{k_1 k_2 (k_1 \sin k_1 \cos k_2 + k_2 \cos k_1 \sin k_2)} \\ A_{21} &= \frac{\beta^2 \bar{e} k_1 \cos k_1 + (k_1^4 + k_2^4 - k_1^2 \beta^2) \sin k_1 / k_1^2}{k_1 k_2 (k_1 \sin k_1 \cos k_2 + k_2 \cos k_1 \sin k_2)} \\ A_{13} &= -k_2^2 / k_1^2, \quad A_{23} = (k_1^2 - \beta^2) / k_2^2 \end{aligned} \quad (13)$$

and k_1, k_2 , for every value of the applied load β^2 , load eccentricity \bar{e} , and slenderness ratio λ , are obtained from the simultaneous solution of the following two nonlinear equations:

$$\begin{aligned} A_{11} \sin k_1 + A_{13} + B_2(1) + \frac{k_2^2}{\lambda^2} &= 0 \\ A_{21} \sin k_2 + A_{23} - B_1(1) - \frac{k_1^2}{\lambda^2} &= 0. \end{aligned} \quad (14)$$

Note that once eqs. (14) are solved for each level of load for a given structural geometry (\bar{e}, λ), the complete response of the frame is known. This is so because knowledge of k_i implies knowledge of the A_{ij} and B_i , which in turn implies knowledge of the displacement components U_i and W_i . In addition, usually, equilibrium states are characterized by a plot of the external load β^2 versus some characteristic displacement. In this case, the joint rotation ϕ is chosen as the characteristic displacement (see Figure 6.1):

$$\phi = W_{1,x}(1) = A_{11} k_1 \cos k_1 + A_{13}. \quad (15)$$

In the case for which the force in the horizontal bar is *tensile*, the solution for model A is characterized by

$$\begin{aligned} U_1(X) &= -\frac{k_1^2}{\lambda^2}X - B_1(X) \\ W_1(X) &= A_{11} \sin k_1 X + A_{13}X \\ U_2(X) &= \frac{k_2^2}{\lambda^2}X - B_2(X) \\ W_2(X) &= A_{21} \sinh k_2 X + A_{23}X \end{aligned} \quad (16)$$

where B_1 is given by the first of eqs. (12) and

$$B_2 = \frac{1}{2} \left[A_{23}^2 X + 2A_{21}A_{23} \sinh k_2 X + \frac{k_2^2 A_{21}^2}{2} \left(X + \frac{\sinh 2k_2 X}{2k_2} \right) \right] \quad (17)$$

$$\begin{aligned} A_{11} &= \frac{\beta^2 \bar{e} k_2 \cosh k_2 + (k_1^4 + k_2^4 - k_1^2 \beta^2) \sinh k_2^2 / k_1^2}{k_1 k_2 (k_1 \sin k_1 \cosh k_2 - k_2 \cos k_1 \sinh k_2)} \\ A_{13} &= k_2^2 / k_1^2, \quad A_{23} = -(k_1^2 - \beta^2) / k_2^2, \end{aligned} \quad (18)$$

and the two nonlinear equations in k_1, k_2 are

$$\begin{aligned} A_{11} \sin k_1 + A_{13} + B_2(1) - k_2^2 / \lambda^2 &= 0 \\ A_{21} \sinh k_2 + A_{23} - B_1(1) - k_1^2 / \lambda^2 &= 0. \end{aligned} \quad (19)$$

The expression for the joint rotation ϕ is given by eq. (15) with A_{11} and A_{13} given by eqs. (18).

Model B

Again, as in model A, first the *compressive* case solution is obtained. Writing the general solution to eqs. (2), making use of the auxiliary conditions, eqs. (3), (4), (5), and (7), and

$$EA(u_{2,x} + \frac{1}{2}w_{2,x}^2) = -S_2, \quad (20)$$

one may write the following final solution:

$$\left. \begin{aligned} U_1(X) &= -\frac{k_1^2}{\lambda^2}X - B_1(X) \\ W_1(X) &= A_{11} \sin k_1 X + A_{13}X \\ U_2(X) &= -\frac{k_2^2}{\lambda^2}X - B_2(X) \\ W_2(X) &= A_{21} \sinh k_2 X + A_{24} \end{aligned} \right\} \quad (21)$$

where

$$\left. \begin{aligned} B_1 &= \frac{1}{2} \left[A_{13}^2 X + 2A_{11}A_{13} \sin k_1 X + \frac{k_1^2 A_{11}^2}{2} \left(X + \frac{\sin 2k_1 X}{2k_1} \right) \right] \\ B_2 &= \frac{k_2^2 A_{21}^2}{4} \left(X + \frac{\sin 2k_2 X}{2k_2} \right) \end{aligned} \right\} \quad (22)$$

$$\left. \begin{aligned} A_{11} &= \frac{\beta^2 \bar{e} k_2 \cos k_2 + k_2^4 \sin k_2 / k_1^2}{k_1 k_2 (k_1 \sin k_1 \cos k_2 + k_2 \cos k_1 \sin k_2)} \\ A_{21} &= \frac{\beta^2 \bar{e} k_1 \cos k_1 - k_2^2 \sin k_1}{k_1 k_2 (k_1 \sin k_1 \cos k_2 + k_2 \cos k_1 \sin k_2)} \\ A_{13} &= -k_2^2 / k_1^2, \quad k_1^2 = \beta^2 \\ A_{24} &= B_1(1) + k_1^2 / \lambda^2 - A_{21} \sin k_2 \end{aligned} \right\} \quad (23)$$

and k_2 (since for this case $k_1^2 = \beta^2$) for every value of the applied load β^2 and structural geometry \bar{e} , λ can be found from the solution of the following nonlinear equation:

$$k_2^2 A_{21} \left[A_{21} \frac{\beta^2}{4} \left(1 + \frac{\sin 2k_2}{2k_2} \right) - \sin k_2 \right] + \bar{e} \beta^2 + k_2^2 \left(\frac{\beta^2}{\lambda^2} - 1 \right) = 0. \quad (24)$$

Similarly, in the case of *tension* in the horizontal bar, the solution becomes

$$\left. \begin{aligned} U_1(X) &= -\frac{k_1^2}{\lambda^2} X - B_1(X) \\ W_1(X) &= A_{11} \sin k_1 X + A_{13} X \\ U_2(X) &= \frac{k_2^2}{\lambda^2} X - B_2(X) \\ W_2(X) &= A_{21} \sinh k_2 X + A_{24} \end{aligned} \right\} \quad (25)$$

where B_1 is given by the first of eqs. (22), and

$$B_2(X) = \frac{k_2^2 A_{21}^2}{4} X + \frac{\sinh 2k_2 X}{2k_2} \quad (26)$$

$$\left. \begin{aligned} A_{11} &= \frac{\beta^2 \bar{e} k_2 \cosh k_2 - k_2^4 \sinh k_2 / k_1^2}{k_1 k_2 (k_1 \sin k_1 \cosh k_2 - k_2 \cos k_1 \sinh k_2)} \\ A_{21} &= \frac{\beta^2 \bar{e} k_1 \cos k_1 + k_2^2 \sin k_1}{k_1 k_2 (k_1 \sin k_1 \cosh k_2 - k_2 \cos k_1 \sinh k_2)} \\ A_{13} &= k_2^2 / k_1^2, \quad k_1^2 = \beta^2 \\ A_{24} &= B_1(1) + \frac{k_1^2}{\lambda^2} - A_{21} \sinh k_2, \end{aligned} \right\} \quad (27)$$

and k_2 is obtained from the solution of the following nonlinear equation:

$$k_2^2 A_{21} \left[\frac{A_{21} \beta^2}{4} \left(1 + \frac{\sinh 2k_2}{2k_2} \right) + \sinh k_2 \right] + \bar{e} \beta^2 - k_2^2 \left(\frac{\beta^2}{\lambda^2} - 1 \right) = 0. \quad (28)$$

Model C

For this particular case, the axial force in the horizontal bar is zero (horizontally movable support) and thus there is only one solution to be considered. This solution is

$$\begin{aligned} U_1(X) &= -\frac{k_1^2}{\lambda^2} X - B_1(X) \\ W_1(X) &= A_{11} \sin k_1 X \\ U_2(X) &= A_{25} - B_2(X) \\ W_2(X) &= A_{21} X^3 + A_{23} X \end{aligned} \quad (29)$$

where

$$\begin{aligned} B_1(X) &= \frac{k_1^2 A_{11}^2}{4} \left(X + \frac{\sin 2k_1 X}{2k_1} \right) \\ B_2(X) &= \frac{1}{2} \left(\frac{9}{5} A_{21}^2 X^5 + 2A_{21} A_{23} X^3 + A_{23}^2 X \right) \\ A_{11} &= \frac{k_1^2 \beta^2 (\bar{e} - 1)}{k_1^2 \sin k_1} \\ A_{21} &= \frac{k_1^2 - \beta^2}{6} \\ A_{23} &= \frac{k_1^2 + \beta^2 (\bar{e} - 1)}{k_1} \cot k_1 + \frac{\beta^2 - k_1^2}{2} \\ A_{25} &= A_{11} \sin k_1 + B_2(1) \end{aligned} \quad (31)$$

and k_1 is the solution of the following nonlinear equation (for any β^2 , \bar{e} , and λ):

$$\frac{\beta^2 - k_1^2}{3} + \frac{k_1^2 + \beta^2 (\bar{e} - 1)}{k} \cot k_1 - \frac{k_1^2}{\lambda^2} - \frac{1}{4} \left[\frac{k_1^2 + \beta^2 (\bar{e} - 1)}{k_1 \sin k_1} \right]^2 \left(1 + \frac{\sin 2k_1}{2k_1} \right) = 0. \quad (32)$$

This particular configuration was investigated by Huddleston [4] by employing an inextensional large rotation theory (elastica type).

In order to establish equilibrium positions for all three models, it is necessary to solve the nonlinear (transcendental) equations that govern the response of each configuration. Note that for model A these are eqs. (14) or eqs. (19), for model B eq. (24) or eq. (28), and for model C eq. (32).

The primary interest herein is the estimation of critical loads (if one exists). This is accomplished by first establishing all equilibrium positions and

representing them as plots of load β_{cr}^2 versus some characteristic displacement ϕ . Once these plots are obtained, the critical load is determined either as a limit point (maximum on the load versus rotation curve) or as a bifurcation point. It is concluded from the generated data that limit point instability is the rule and bifurcational instability the exception.

The solution of the nonlinear equations is accomplished by employing optimization search techniques. Other methods are definitely acceptable [5]. Regardless of the model, at most two nonlinear equations need to be solved. These equations may be written as

$$f_i(k_1, k_2, \beta^2, \bar{e}, \lambda) = 0, \quad i = 1, 2 \quad (33)$$

where k_1 and k_2 are the unknowns and β^2 , \bar{e} , and λ are fixed.

Next, one can generate a new function $F(k_i, \beta^2, \bar{e}, \lambda)$ given by

$$F = f_1^2 + f_2^2.$$

Then it is observed that the minimum of F , in the space of k_i , corresponds to points that characterize the simultaneous solution of eqs. (33). Moreover, this minimum value is zero ($F_{min} = 0$). For the two-dimensional case (model A) the mathematical search technique of Nelder and Mead [6] is employed for finding the minimum of F and primarily the minimizing values k_i , which represent the solution of eqs. (33). For the one-dimensional cases (models B and C) the golden section search technique [7] is employed.

Once the solution to eqs. (33) is obtained, the complete response of the

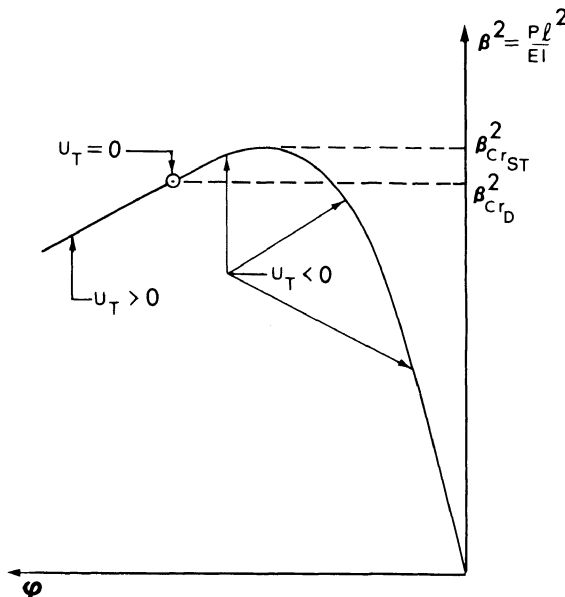


FIGURE 6.2. Typical load versus characteristic displacement (joint rotation) curve.

configuration is known, and equilibrium states are characterized by plots of load λ_c versus joint rotation ϕ . A typical plot is shown on Figure 6.2 for the cases for which the system exhibits limit point instability.

6.2.3 Numerical Results

Numerical results are computer generated for a single vertical load. These results consist of critical static (limit point) loads for several slenderness ratios ($\lambda = 40, 80, 120, \infty$) and for a wide range of small load eccentricities ($-0.01 \leq \bar{e} \leq 0.01$) for all three models. All equilibrium positions were obtained, regardless of whether the response is one of stable behavior for all loads or of limit point behavior. Only the critical loads are presented and discussed separately for each model.

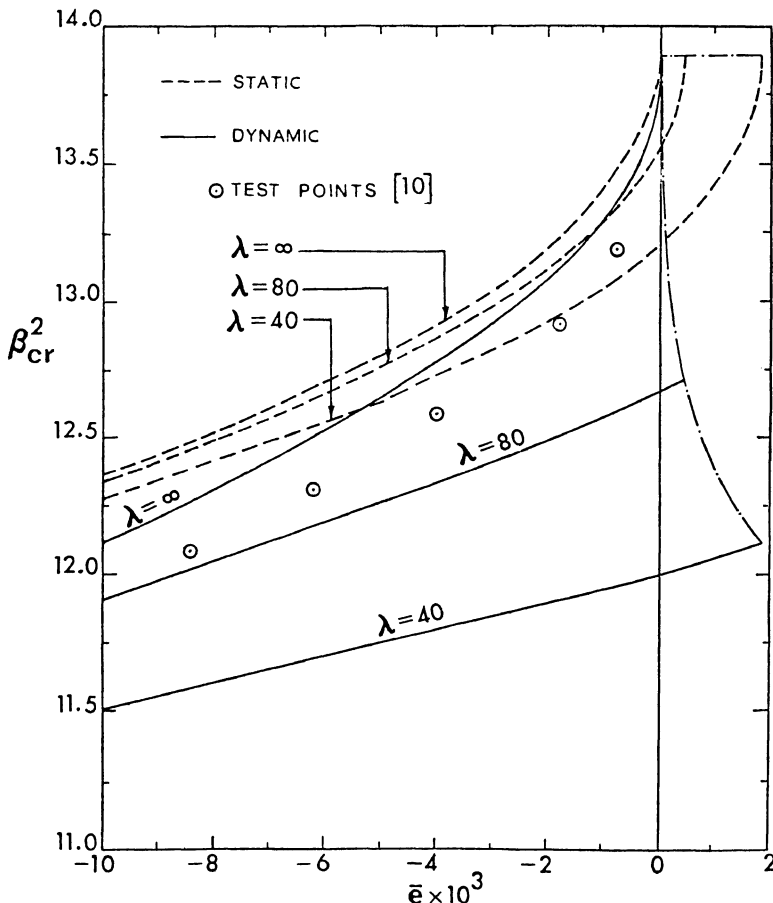


FIGURE 6.3. Effect of eccentricity \bar{e} and slenderness ratio λ on the static and dynamic critical loads β^2 (model A).

Model A

Some of the generated data are presented on Figure 6.3 as plots of β_{cr}^2 versus eccentricity \bar{e} for various values of the slenderness ratio λ (see dashed lines). Moreover, the experimental results of Roorda ([8], $\lambda = 1,275$) are included for comparison. It is seen from these results that (1) the test data are close to the theoretical predictions (the biggest difference is of the order of 2%) and (2) there exist limiting values of \bar{e} for which the response is one of limit point behavior. This value is zero for $\lambda \rightarrow \infty$ and it increases to 0.00182 as λ decreases to the value of 40. This means that for each λ value a critical load (limit point) exists for values of \bar{e} smaller than the corresponding limiting value. If \bar{e} is greater than this value the response is stable (see [1]).

Model B

This particular model is the only one, out of the three considered here, that exhibits bifurcational buckling. This occurs when $\bar{e} = 0$ and the postbuckling branches are unstable, which implies that the system is imperfection sensitive. As one can see from Figure 6.1, when $\bar{e} = 0$ as the load increases quasi-statically from zero the system preserves its shape (the two bars remain orthogonal), with the vertical bar experiencing compression while the horizontal bar simply translates in the vertical direction without deformation ($k_2 = 0$). A linear buckling analysis with a primary equilibrium path as described above reveals that there exists a bifurcation at $\beta^2 = \pi^2$. The nonlinear analysis employed here supports this result and $\beta_{cr}^2 = \pi^2$ for $\bar{e} = 0$, regardless of the value of the slenderness ratio λ . As a matter of fact, all generated results reveal that the critical loads, in their nondimensionalized form, are independent of λ value for all eccentricities. These results are plotted on Figure 6.4. Note that for this model, regardless of the sign of the load

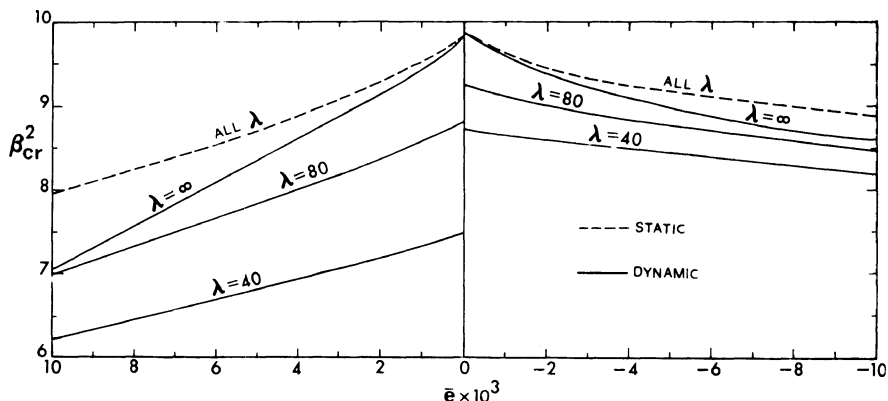


FIGURE 6.4. Effect of eccentricity \bar{e} and slenderness ratio λ on the static and dynamic critical loads β^2 (model B).

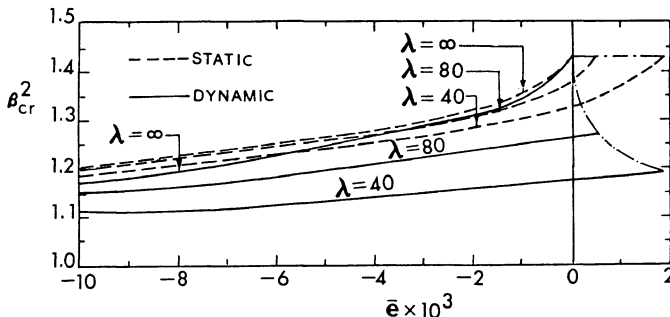


FIGURE 6.5. Effect of eccentricity \bar{e} and slenderness ratio λ on the static and dynamic critical loads β^2 (model C).

eccentricity, the behavior is one of limit point instability. The observation is that model B ($\bar{e} = 0$) and a simply supported column have the same bifurcation load ($\beta_{cr}^2 = \pi^2$). The only difference is that the column exhibits postbuckling strength, while model B exhibits unstable bifurcation and thus it is sensitive to small initial geometric imperfections.

Model C

The response of model C is very similar to that of model A. Critical loads β_{cr}^2 are plotted versus load eccentricity \bar{e} on Figure 6.5. The value reported by Huddleston [4] is taken to be the classical value. This value is $\beta_{cr}^2 = 1.4215$ ($\bar{e} = 0$) and it agrees well with the present result for $\bar{e} = 0$ and $\lambda \rightarrow \infty$. Moreover, the results presented on Figure 6.5 corresponding to the limiting values of load eccentricity are virtually the same for each λ value. The only thing that changes is the limiting value for \bar{e} ; that is, $\beta_{cr}^2 = 1.4215$ for $\lambda \rightarrow \infty$ and $\bar{e}_{cr} = 0$, $\beta_{cr}^2 = 1.4214$ for $\lambda = 80$ and $\bar{e}_{cr} = 0.00047$, and $\beta_{cr}^2 = 1.4206$ for $\lambda = 40$ and $\bar{e}_{cr} = 0.00187$.

6.3 Dynamic Stability Analysis

For the case of sudden application of the load one can write that

$$P(t) = PH(t) \quad (34)$$

where $H(t)$ is the Heaviside function and P is the magnitude of the eccentrically (\bar{e}) and vertically applied load (see Figure 6.1).

For this dynamic case, by employing Hamilton's principle one can obtain the equations of motion for the two-bar frame, or

$$\delta \int_{t_1}^{t_2} (T - U_T) dt = 0$$

where the functionals U_T (total potential) and T (kinetic energy) are given by

$$U_T[u_i, w_i; P] = \frac{1}{2} \sum_{i=1}^2 \int_0^l [AE(u_{i,x} + \frac{1}{2}w_{i,x}^2)^2 + EIw_{i,xx}^2] dx + H(t)[Pu_1(l) + Pe w_{2,x}(l)] \quad (35)$$

$$T[u_i, w_i; P] = \frac{1}{2} \sum_{i=1}^2 \int_0^l m(w_{i,t}^2 + u_{i,t}^2) dx \quad (36)$$

where the indices denote partial derivatives and m is the mass per unit length, the same for both bars. The equations of motion are

$$\begin{aligned} EA(u_{i,x} + \frac{1}{2}w_{i,x}^2)_x - mu_{i,tt} &= 0 \\ EIw_{i,xxxx} - EA[(u_{i,x} + \frac{1}{2}w_{i,x}^2)w_{i,x}]_x + mw_{i,tt} &= 0, \quad i = 1, 2. \end{aligned} \quad (37)$$

The kinematic continuity conditions at the joint are

$$w_1(l, t) = u_2(l, t), \quad w_2(l, t) = -u_1(l, t), \quad w_{1,x}(l, t) = w_{2,x}(l, t). \quad (38)$$

The force and moment balance conditions at the joint are obtained from the variational problem and by employing eqs. (38), which are independent of this formulation. These auxiliary conditions are

$$\begin{aligned} AE[u_{1,x}(l, t) + \frac{1}{2}w_{1,x}^2(l, t)] + EIw_{2,xxx}(l, t) - AE[u_{2,x}(l, t) + \frac{1}{2}w_{2,x}^2(l, t)]w_{2,x}(l, t) \\ + PH(t) = 0 \\ AE[u_{1,x}(l, t) + \frac{1}{2}w_{1,x}^2(l, t)]w_{1,x}(l, t) - EIw_{1,xxx}(l, t) \\ + AE[u_{2,x}(l, t) + \frac{1}{2}w_{2,x}^2(l, t)] = 0 \\ EI[w_{1,xx}(l, t) + w_{2,xx}(l, t)] + H(t)Pe = 0. \end{aligned} \quad (39)$$

Finally, the support conditions for the three models (A, B, and C) are listed below, as either common to all models or as those that are different.

Common

$$u_1(0, t) = w_1(0, t) = w_{1,xx}(0, t) = w_{2,xx}(0, t) = 0 \quad (40)$$

Model A

$$u_2(0, t) = 0, \quad w_2(0, t) = 0 \quad (41)$$

Model B

$$u_2(0, t) = EIw_{2,xxx}(0, t) - AE[u_{2,x}(0, t) + \frac{1}{2}w_{2,x}^2(0, t)]w_{2,x}(0, t) = 0 \quad (42)$$

Model C

$$w_2(0, t) = u_{2,x}(0, t) + \frac{1}{2}w_{2,x}^2(0, t) = 0. \quad (43)$$

The initial conditions must reflect the fact that the system is at rest initially ($t = 0$).

$$u_i(x, 0) = w_i(x, 0) = 0$$

$$u_{i,t}(x, 0) = w_{i,t}(x, 0) = 0, \quad i = 1, 2. \quad (44)$$

$$u_{i,t}(x, 0) = w_{i,t}(x, 0) = 0, \quad i = 1, 2. \quad (44)$$

The solution of the equations of motion, eqs. (37), a system of coupled nonlinear partial differential equations, subject to the auxiliary conditions, eqs. (38)–(40) and (41) or (42) or (43), and initial conditions, eqs. (44), is at best extremely difficult. Furthermore, even if the solution is possible, for various magnitudes of the applied force P , the eccentricity \bar{e} , and the slenderness ratio λ , a criterion for stability is still missing. One possibility here is to employ the criterion of Budiansky and Roth (see Chapter 1), which, in this particular case, requires a wise choice for a characteristic displacement response. Another possibility, of course, is to employ this criterion in conjunction with an approximate solution obtained on the basis of either direct variational methods or methods of weighted residuals [9]. In the latter approach, there is an uncertainty with both the direction and the estimation of the error involved in the approximation.

In the light of the above difficulties, a simpler approach giving accurate predictions is needed. Because of this, the energy approach as described for the continuum in Chapter 5 is employed.

By virtue of the initial conditions, eqs. (44), and the expressions for the total potential and kinetic energy, eqs. (35) and (36), both are zero at the initial point ($t = 0$).

According to the energy approach, one need only solve the corresponding static problem and compute the value of the total potential U_T at every static unstable equilibrium point. The load value P , for which the value of the total potential at this unstable static point becomes zero, is a measure of the critical dynamic load. Note that when this happens, there exists a possibility of escaping or buckled motion.

Specifically, the total potential U_T for the static problem may be expressed solely in terms of k_i , β^2 , \bar{e} , λ , that is,

$$U_T = U_T(k_i, \beta^2, \bar{e}, \lambda). \quad (45)$$

For any given geometry (\bar{e}, λ), static equilibrium positions are shown as plots of load parameter β^2 versus joint rotations ϕ (characteristic displacement—see Figure 6.2). At every point of this curve, the value of the total potential is computed. The value of β^2 at which U_T changes from negative to positive corresponds to the dynamic critical load β_{crD}^2 .

Another possible procedure for finding β_{crD}^2 is the simultaneous solution of the two nonlinear equilibrium equations

$$\frac{\partial U_T}{\partial k_i} = 0, \quad k_i = 1, 2 \quad (46)$$

along with

$$U_T = 0 \quad (47)$$

subject to the condition that the static equilibrium position, at which $U_T = 0$, is unstable, or

$$\left. \frac{\partial^2 U_T}{\partial k_i^2} \right|_{\text{equil}} \neq 0, \quad i = 1, 2 \quad (48)$$

and/or

$$\left(\frac{\partial^2 U_T}{\partial k_1^2} \right) \Big|_{\text{equil}} \left(\frac{\partial^2 U_T}{\partial k_2^2} \right) \Big|_{\text{equil}} > \left(\frac{\partial^2 U_T}{\partial k_1 \partial k_2} \right)^2 \Big|_{\text{equil}}$$

Note that eqs. (48) imply that the conditions for static stability are violated. This yields k_1 , k_2 , and β_{crD}^2 .

This alternative procedure needs special attention, because it can easily yield physically unacceptable solutions. These unacceptable solutions arise from the nonlinearity of the problem and do not belong on the load-displacement curve shown on Figure 6.2 (physically acceptable), which corresponds to dead weight loading.

The numerical results, presented here, are obtained from the first solution.

By employing the energy approach, critical dynamic loads (sudden loads) are computed for all three models. The results are presented on the same figures as the static critical loads, Figure 6.3, 6.4 and 6.5, and are discussed separately for each model.

TABLE 6.1. Critical conditions for $\lambda = 80$.

Model	\bar{e}	k_1	k_2	β_{crD}^2	$\beta_{\text{crD}}^2 / \beta_{\text{crst}}^2$
A	0.00047288	13.35030	0.701563	12.7054	0.915
	0.0000	13.31978	0.709696	12.6625	0.935
	0.0013	13.23990	0.732511	12.5486	0.948
	0.0025	13.17096	0.753974	12.4483	0.954
	0.0050	13.04018	0.799120	12.2528	0.961
	-0.0070	12.94609	0.834976	12.1081	0.963
	-0.0100	12.81903	0.887372	11.9077	0.965
B	0	8.77116	0.37756	8.7712	0.889
	0.002	8.37378	0.42278	8.3738	0.901
	0.004	7.99803	0.46167	7.9980	0.899
	0.008	7.31164	0.52393	7.3118	0.887
	0.010	7.00021	0.54887	7.0002	0.880
	0	9.24600	0.31035	9.2460	0.937
	-0.002	9.05455	0.34513	9.0546	0.955
	-0.004	8.88447	0.37852	8.8845	0.961
	-0.008	8.59210	0.43900	8.5921	0.959
	-0.010	8.46421	0.46605	8.4642	0.956
C	0.0004722	1.37022	0	1.27144	0.895
	0.0000	1.36547	0	1.26421	0.921
	-0.0013	1.35332	0	1.24523	0.939
	-0.0025	1.34319	0	1.22885	0.946
	-0.0050	1.32475	0	1.19771	0.953
	-0.0075	1.30910	0	1.16995	0.955
	-0.0100	1.29550	0	1.14492	0.956

Model A

The results for this model are presented graphically on Figure 6.3 and part of them in tabular form on Table 6.1. It is observed that, as in the static case, there is a small positive eccentricity \bar{e}_{cr} such that for $\bar{e} \leq \bar{e}_{cr}$ there is dynamic instability, while for $\bar{e} > \bar{e}_{cr}$ there is not. This \bar{e}_{cr} is λ dependent and identical to the corresponding static case. For all λ values considered, except $\lambda \rightarrow \infty$, the difference between $\beta_{cr_D}^2$ and $\beta_{cr_s}^2$ is the largest at $\bar{e} = \bar{e}_{cr}$ and it diminishes as \bar{e} increases negatively. On the contrary, for $\lambda \rightarrow \infty$ this effect is reversed and, more specifically, the difference is close to zero at $\bar{e} = \bar{e}_{cr}$ and increases as \bar{e} increases negatively. In addition, eccentricity has a destabilizing effect regardless of the value of the slenderness ratio. This effect is less pronounced for the static case.

Finally, dynamic instability, as defined in Chapter 5, takes place with a trajectory corresponding to a positive joint rotation ϕ . Because of this, of course, the compressive force in the vertical bar, k_1 , is higher than the applied load, β^2 , at the instant of possible buckled motion (trajectory possibly passing through the unstable static equilibrium point).

Note that the experimental results of Thompson ([10], $\lambda = 1,275$) agree very well with the $\lambda \rightarrow \infty$ theoretical predictions. The largest discrepancy between theory and experiment for the dynamic case is approximately 1.5%.

Model B

This is the only model that exhibits bifurcational buckling (through an unstable branch) under static application of the load. The results are presented graphically in Figure 6.4 and part of them in tabular form on Table 6.1.

It is seen from Figure 6.4 that the effect of slenderness ratio on the dynamic critical load is appreciable, while its effect on the static critical load (limit point load) is negligible. In addition, for all λ , except $\lambda \rightarrow \infty$, the difference between the static and dynamic critical loads is the largest at $\bar{e} = 0$ and decreases as $|\bar{e}|$ increases. Furthermore, at $\bar{e} = 0$ and for a given λ , except $\lambda \rightarrow \infty$, there are two dynamic critical loads, one corresponding to a negative rotation ϕ trajectory (the lower) and one corresponding to a positive ϕ trajectory (the upper). Probably the system for $\bar{e} = 0$ buckles in the mode associated with the lower load and it should be designed for this lower dynamic critical load. But the results indicate that a small positive eccentricity in this case has a stabilizing effect, because it forces the system to buckle dynamically through a positive rotation ϕ trajectory and therefore it can carry a higher load. In general, though, eccentricity has a destabilizing effect. This means that as $|\bar{e}|$ increases the dynamic critical load decreases.

Model C

The results for this model are presented graphically in Figure 6.5 and part of them in tabular form on Table 6.1. The observations for this model are very similar to those corresponding to model A.

6.4 Closing Remarks

For all three models, when the alternative method was employed for computing critical dynamic loads, eqs. (46)–(48), in some instances the results were unacceptable because of physical considerations.

Moreover, for all cases considered the critical dynamic load corresponds to a lower bound of loads for which buckled motion is possible. This implies that these loads are minimum possible critical loads (see Chapter 1) according to the total potential energy approach, or correspond to necessary conditions for stability according to the total energy-phase plane approach. In spite of this, the correlation between theoretical and experimental results is excellent.

There exist very few studies that have reported and that deal with the dynamic stability of two-bar frames. The only ones with the exception of the study of Thompson [10] are those of Simitses et al. [11] and of Kounadis [12].

Finally, from the generated results one sees that the critical dynamic load is at worst 70% of the corresponding static critical load. This means that if one is interested in designing the two-bar frame for sudden loads, then if one multiplies the dynamic loads by a factor of two (usual practice), uses this as an equivalent static load, and designs the frame for this static load, one will end up with a conservative design.

References

1. Kounadis, A.N., Giri, J., and Simitses, G.J. Nonlinear stability analysis of an eccentrically loaded two-bar frame. *J. Appl. Mech.*, 44, 4, 1977, 701–706.
2. Simitses, G.J., and Kounadis, A.N. Snap-through buckling of imperfect rigid-jointed frames. *J. Eng. Mech. Div., ASCE*, 104, EM 3, 1978, 569–586.
3. Simitses, G.J., and Vlahinos, A.S. Stability analysis of semi-rigidly connected simple frames. *J. Construct. Steel Res.*, 2, 3, 1982, 29–32.
4. Huddleston, J.V. Nonlinear buckling and snap-over of a two-member frame. *Int. J. Solids Struct.*, 3, 1967, 1023–1030.
5. Dennis, J.E., Jr., and Moore, J.J. Quasi-Newton methods; motivation and theory. *SIAM Rev.*, 19, 1, 1977.
6. Nelder, J.A., and Mead, R. A Simplex method of function minimization. *Comput. J.*, 7, 1964, 308–313.
7. Himmelblau, D.M. *Applied Nonlinear Programming*. McGraw-Hill, New York, 1972.
8. Roorda, J. Stability of structures with small imperfections. *J. Eng. Mech. Div., ASCE*, 91, EMI, 1965, 87–106.
9. Finlayson, B. *The Method of Weighted Residuals and Variational Principles*. Academic Press, New York, 1972.
10. Thompson, J.M.T. Dynamic buckling under step loading. *Dynamic Stability of Structures* (edited by G. Herrmann). Pergamon, New York, 1967.
11. Simitses, G.J., Kounadis, A.N., and Giri, J. Dynamic buckling of simple frames under a step load. *J. Eng. Mech. Div., ASCE*, 105, EM5, 1979, 896–900.
12. Kounadis, A. N. Dynamic snap-through buckling of a Timoshenko two-bar frame under a suddenly applied load. *Z. Angew. Math. Mech.*, 59, 1979, 523–531.

7

The Shallow Arch

7.1 Introduction

The first investigation of dynamic snap-through of shallow arches is due to Hoff and Bruce [1]. They considered the problem of a pinned arch with a half-sine-wave initial shape and a half-sine wave distributed lateral load. They treated the two extreme cases of sudden loads: that of constant magnitude and infinite duration and the ideal impulse case. Following this first paper, several studies are reported in the literature, in the middle to late 1960s, dealing with the arch configuration. These studies include the works of Lock [2], Hsu and his associates [3–6], and the Ph.D. thesis of the current author [7]. A short period after this, the arch problem was reinvestigated by employing the Budiansky–Roth [8] criterion. Please refer to Chapter 1 for a discussion of concepts, criteria, and estimates of critical conditions under suddenly applied loads. An attempt was made by Fulton and Barton [9] to introduce a different criterion for dynamic stability. The interested reader is also referred to the work of Lo and Masur [10] and of Huang and Nachbar [11], who added the effect of initial geometric imperfections and viscoelastic behavior. More recently, stability boundaries (interaction curves) were discussed by Gregory and Plaut [12] and Donaldson and Plaut [13] for arches that are loaded by two independent sets of dynamic loads applied in varying proportions to each other. The effect of damping on the dynamic buckling of low arches was investigated by Johnson [14]. Continuing with the historical development, one needs to mention the following three studies: first, Ariaratnam and Sankar's [15] investigation of dynamic buckling of arches with stochastic loads; next, Sundararajan and Kumani's [16] study of the effect of inclined loads; and finally, Huang and Plaut's [17; see also 13] work dealing with pulsating loads.

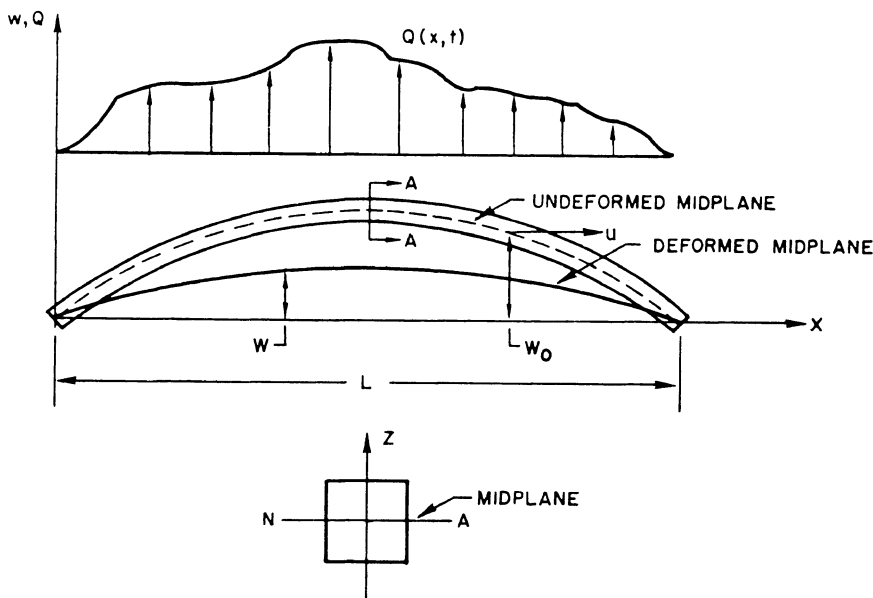
In this chapter, the complete analysis of a shallow pinned arch, loaded symmetrically by sudden step loads, is presented. The emphasis will be on the two extreme cases of step loads—but other results will be presented. These include results for sudden loads of finite duration and results addressing the effect of static preloading. Moreover, results are also presented for clamped arches under a symmetric concentrated load.

7.2 Static Stability Analysis

7.2.1 The Mathematical Model

Consider a slender arch of small initial curvature and symmetric cross section. Letting $w_0(x)$ denote the initial shape of the middle line, $w(x)$ the shape of the middle line after deformation, and $u(x)$ the horizontal displacement of any point of the midplane (see Figure 7.1), the following nonlinear strain-displacement relations hold:

$$\varepsilon_x = \varepsilon_{x_m} + z\kappa_x \quad (1)$$



Section A-A

(a)

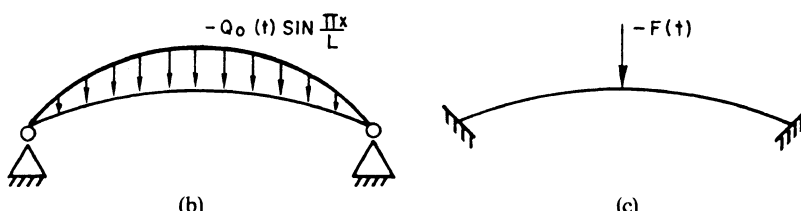


FIGURE 7.1. The low arch: geometry and sign convention. (a) Geometry. (b) The pinned arch. (c) The clamped arch.

where ε_{x_m} is the midplane strain given by

$$\varepsilon_{x_m} = \frac{\partial u}{\partial x} + \frac{1}{2} \left(\frac{\partial w}{\partial x} \right)^2 - \frac{1}{2} \left(\frac{dw_0}{dx} \right)^2 \quad (2)$$

and κ_x is the change in curvature of the midplane given by

$$\kappa_x = - \left(\frac{\partial^2 w}{\partial x^2} - \frac{d^2 w_0}{dx^2} \right). \quad (3)$$

Denoting by P and M the axial force and bending moment, respectively,

$$P = \int_A \sigma_x dA,$$

and for linear elasticity (Hooke's law),

$$\begin{aligned} P &= \int_A E \varepsilon_m dA = E \int_A (\varepsilon_{x_m} + z \kappa_x) dA \\ P &= e A \varepsilon_{x_m}. \end{aligned} \quad (4)$$

Similarly,

$$M = EI \kappa_x \quad (5)$$

where I is the cross-sectional area moment of inertia about the neutral axis. Next, letting U_b^* , U_m^* , and U_p^* denote the bending energy density, the stretching energy density, and the potential density of the external forces per unit length of underdeformed arch, respectively, one may write the following expression:

$$U_m^* = \frac{EA\varepsilon_{x_m}^2}{2} = \frac{P^2}{2EA}, \quad (6a)$$

$$U_b^* = \frac{EI\kappa_x^2}{2} = \frac{M^2}{2EI}, \quad (6b)$$

$$U_p^* = -Q^*(w - w_0). \quad (6c)$$

After integration over the entire length of the arch, the total energies are obtained:

$$U_{m_T}^* = \int_0^L \frac{1}{2} EA \varepsilon_{x_m}^2 dx = \int_0^L \frac{1}{2} \frac{P^2}{EA} dx, \quad (7)$$

$$U_{b_T}^* = \int_0^L \frac{1}{2} EI \kappa_x^2 dx = \int_0^L \frac{1}{2} \frac{M^2}{EI} dx, \quad (8)$$

and

$$U_{p_T}^* = - \int_0^L Q^*(w - w_0) dx. \quad (9)$$

Upon neglect of the rotatory and in-plane (in the longitudinal direction) kinetic energies, the expression for the kinetic energy T^* may be written

$$T^* = \int_V \frac{1}{2} \sigma \left(\frac{\partial w}{\partial t} \right)^2 dA dx$$

or

$$T^* = \frac{\sigma A}{2} \int_0^L \left(\frac{\partial w}{\partial t} \right)^2 dx \quad (10)$$

where σ is the density of the material and V the volume.

Denoting by U_T^* the total potential, L the Lagrangian, and I Hamilton's integral, one may write

$$U_T^* = U_{b_T}^* + U_{m_T}^* + U_{p_T}^*, \quad (11)$$

$$L = T^* - U_T^*, \quad (12)$$

and

$$I = \int_{t_1}^{t_2} L dt = \int_{t_1}^{t_2} (T^* - U_T^*) dt. \quad (13)$$

With use of Hamilton's principle, extremization of I with respect to the in-plane displacement u yields the in-plane equation of motion (equilibrium equation), which is

$$\frac{\partial P}{\partial x} = 0. \quad (14)$$

This equation implies that the axial force P is independent of the spatial coordinates, and by making use of the stress-displacement relations and the boundary conditions, P may be expressed in terms of the normal displacement w and its space-dependent derivatives alone:

$$P = EA\varepsilon_{x_m} = EA \left[\frac{\partial u}{\partial x} + \frac{1}{2} \left(\frac{\partial w}{\partial x} \right)^2 - \frac{1}{2} \left(\frac{dw_0}{dx} \right)^2 \right].$$

Upon integration over the entire length of the arch,

$$PL = EA \left[u|_0^L + \frac{1}{2} \int_0^L (w_{,x}^2 - w_{0,x}^2) dx \right]$$

where

$$w_{,x} = \frac{\partial w}{\partial x}.$$

With use of the boundary conditions $u(L) = u(0) = 0$, which hold for both the pinned and the clamped arch, one obtains

$$P = \frac{EA}{2L} \int_0^L (w_{,x}^2 - w_{0,x}^2) dx. \quad (15)$$

Thus, the total potential may be expressed solely in terms of the displacement w and its derivatives with respect to the space coordinate x :

$$U_T^* = \int_0^L \left[\frac{EA}{8L^2} \left\{ \int_0^L (w_{,x}^2 - w_{0,x}^2) dx \right\}^2 + \frac{EI}{2} (w_{,xx} - w_{0,xx})^2 - Q^*(w - w_0) \right] dx. \quad (16)$$

Nondimensionalization

Before proceeding with the actual solution of the different arch problems, it is convenient to express all of the parameters to be dealt with in a nondimensional form as follows:

$$x = \frac{L}{\pi}\xi, \quad w(x, t) = \rho\eta(\xi, \tau) \quad \text{where } \rho^2 = \frac{I}{A},$$

$$t = \tau \frac{L/\pi}{\sqrt{E\varepsilon_E/\sigma}}, \quad \text{where } \varepsilon_E = (\pi\rho/L)^2,$$

and

$$q(\xi, \tau) = \frac{\rho}{AE\varepsilon_E^2} Q^*(x, t). \quad (17)$$

Denoting the first Euler load ($\pi^2 EI/L^2$) by P_E and the two partial derivatives by a prime (with respect to ξ) and by a dot (with respect to τ), one may write

$$P = \frac{P_E}{2\pi} \int_0^\pi (\eta'^2 - \eta'_0)^2 d\xi, \quad (18)$$

$$M = -P_E\rho(\eta'' - \eta''), \quad (19)$$

$$U_T^* = \frac{P_E\varepsilon_E L}{4\pi} \int_0^\pi \left[\frac{1}{2\pi^2} \left\{ \int_0^\pi (\eta'^2 - \eta'_0)^2 d\xi \right\}^2 + 2(\eta'' - \eta''_0)^2 - 4q(\eta - \eta_0) \right] d\xi. \quad (20)$$

Using $\frac{1}{4}(P_E\varepsilon_E L)$ as a nondimensionalizing parameter, and denoting the different energy terms by the same symbols but without the asterisk, one may write

$$U_{bT} = \frac{2}{\pi} \int_0^\pi (\eta'' - \eta''_0)^2 d\xi, \quad (21)$$

$$U_{mT} = \frac{1}{2\pi^2} \left[\int_0^\pi (\eta'^2 - \eta'_0)^2 d\xi \right], \quad (22)$$

$$U_{pT} = -\frac{4}{\pi} \int_0^\pi q(\eta - \eta_0) d\xi, \quad (23)$$

$$U_T = U_{bT} + U_{mT} + U_{pT} \quad (23a)$$

and finally the kinetic energy becomes

$$T = \frac{2}{\pi} \int_0^\pi \dot{\eta}^2 d\xi. \quad (24)$$

7.2.2 The Pinned Arch

The problem to be considered in this section is the following: A low arch for which $w_0(x)$, and consequently $\eta_0(\xi)$, is a half-sine wave is loaded laterally by a half-sine-wave distributed load with the following timewise distributions:

1. Quasi-static application of the load (dead weight)
2. Load of constant magnitude, infinite duration
3. Ideal impulsive load (Dirac delta function)
4. Load of constant magnitude, finite duration

Note that only the static case is considered in this section, but expressions needed for the dynamic cases are obtained for convenience herein.

Thus the initial shape is given by

$$\eta_0(\xi) = e \sin \xi, \quad 0 < \xi < \pi \quad (25a)$$

where e is the initial rise parameter. Since $(w_0)_{\max} = \rho e$, then $e = (w_0)_{\max}/\rho$, and if the cross section is rectangular of width b and thickness h then $\rho = h/2\sqrt{3}$ and $e = 2\sqrt{3}(w_0)_{\max}/h$, which clearly shows that e is a measure of the ratio of the initial maximum rise to the thickness of the arch.

The expression for the loading is given by

$$q(\xi, \tau) = q_1(\tau) \sin \xi. \quad (25b)$$

The deflected shape may be represented by an infinite series, each term of which satisfies the boundary conditions and is multiplied by an undetermined coefficient; these undetermined coefficients are constant in the case of quasi-static application of the load and are time dependent for the dynamic cases. The boundary conditions are

$$\eta(0, \tau) = \eta(\pi, \tau) = 0,$$

$$\eta''(0, \tau) = \eta''(\pi, \tau) = 0.$$

Since both the vibration eigenfunctions for a beam pinned at both ends and the buckling modes of a pinned column consist only of sine harmonics, it is decided to represent the deflected shape by

$$\eta(\xi, \tau) = \eta_0(\xi) + \sum_{n=1}^{\infty} a_n(\tau) \sin n\xi, \quad 0 < \xi < \pi, \tau > 0. \quad (26)$$

Thus the different energies and consequently the total potential and the kinetic energy may be expressed in terms of the initial rise parameter e , the

magnitude of the applied load, and the coefficients a_n (and their time rates of change). From eqs. (21)–(24):

$$\left. \begin{aligned} U_{b_T} &= \sum_{n=1}^{\infty} n^4 a_n^2, \\ U_{m_T} &= \frac{1}{8} \left[\sum_{n=1}^{\infty} n^2 a_n^2 + 2ea_1 \right]^2, \\ U_{p_T} &= -2q_1 a_1, \\ T &= \sum_{n=1}^{\infty} \dot{a}_n^2. \end{aligned} \right\} \quad (27)$$

The expression for the total potential becomes

$$U_T = \frac{1}{8} \left(\sum_{n=1}^{\infty} n^2 a_n^2 + 2ea_1 \right)^2 + \sum_{n=1}^{\infty} n^4 a_n^2 - 2q_1 a_1, \quad (28)$$

and by employing the principle of the stationary value of the total potential ($\partial U_T / \partial a_n = 0, n = 1, 2, \dots$) the following relations must hold for equilibrium:

$$\left. \begin{aligned} \frac{1}{4} \left(\sum_{n=1}^{\infty} n^2 a_n^2 + 2ea_1 \right) (a_1 + e) + a_1 - q_1 &= 0 \\ \frac{1}{4} \left(\sum_{n=1}^{\infty} n^2 a_n^2 + 2ea_1 \right) k^2 a_k + k^4 a_k &= 0 \end{aligned} \right\} \quad (29)$$

for $k = 2, 3, 4, \dots$, etc. These represent an infinite set of equations, but it is seen that only one harmonic, say a_k , may enter the solution other than a_1 ; therefore equilibrium is mathematically denoted by the following set of two equations:

$$\left. \begin{aligned} \frac{1}{4}(a_1^2 + 2ea_1 + k^2 a_k^2)(a_1 + e) + a_1 &= q_1 \\ [\frac{1}{4}(a_1^2 + 2ea_1 + k^2 a_k^2) + k^2]a_k &= 0 \end{aligned} \right\} \quad (30a)$$

where k is a positive integer from the set $[2, 3, 4, \dots]$.

A more convenient set of equations may be obtained by introducing the following new parameters [1]:

$$r_1 = a_1 + e \quad \text{and} \quad Q = q_1 + e. \quad (31)$$

Substituting these new parameters into eqs. (30a) one obtains the following new set of equations:

$$\left. \begin{aligned} \frac{1}{4}(r_1^2 - e^2 + k^2 a_k^2)r_1 + r_1 &= Q \\ [\frac{1}{4}(r_1^2 - e^2 + k^2 a_k^2) + k^2]a_k &= 0. \end{aligned} \right\} \quad (30b)$$

There are two possible solutions to the above system: (1) $a_1 \neq 0$ and $a_k = 0$ for all k and (2) both $a_1 \neq 0$ and $a_k \neq 0$ for all k .

1. If $a_k = 0$ then the equation

$$r_1^3 - (e^2 - 4)r_1 = 4Q \quad (32a)$$

represents effectively the load-displacement relation. It is seen from eq. (32a) that for $e \leq 2$ there is a one-to-one Q -to- r_1 dependence and there is no possibility of a snap-through phenomenon. For $e > 2$, since there is a range of Q values for which there are three equilibrium positions for the same Q value, the possibility of a snap-through phenomenon exists (see Figure 7.2a).

2. If $e > 4k^2$ then it is possible for $a_k \neq 0$, and the load-displacement relation

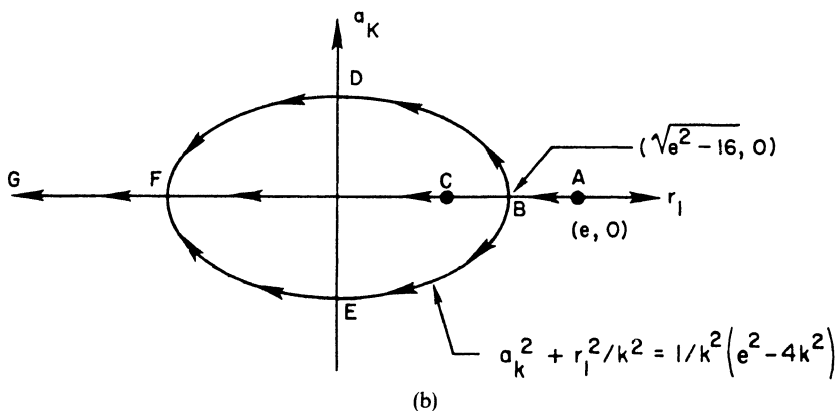
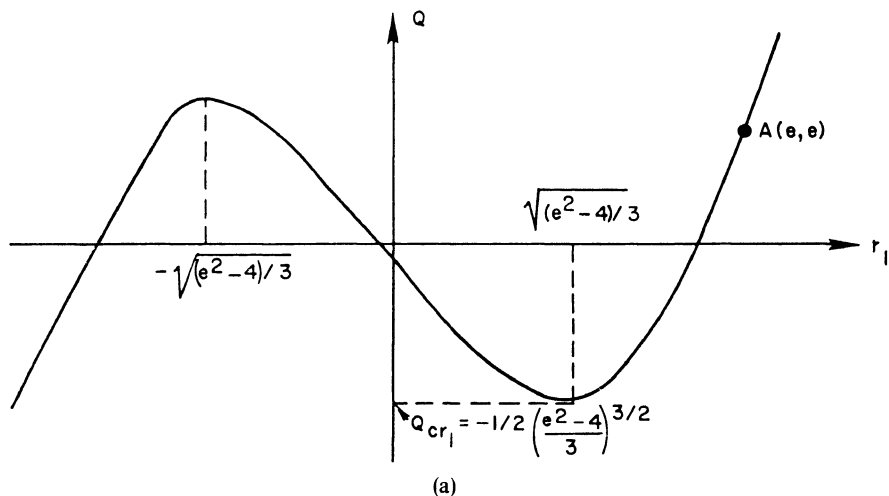


FIGURE 7.2. (a) Load-deflection graph for symmetric buckling of the pinned arch (quasi-static). (b) Positions of equilibrium in the (r_1, a_k) space for the pinned arch (quasi-static).

is given by the following set of equations:

$$\left. \begin{aligned} r_1 &= -\frac{Q}{k^2 - 1} \\ a_k^2 &= \frac{1}{k^2} \left[e^2 - \frac{Q^2}{(k^2 - 1)^2} - 4k^2 \right] \end{aligned} \right\} \quad (32b)$$

Thus it is seen from eq. (32a) and eqs. (32b) that the load-displacement relation for the entire range of initial rise parameter values may be represented by the four graphs of Figure 7.3 and the corresponding paths are given in Figure 7.2b.

Since critical load in this case means the smallest load for which the equilibrium positions [eqs. (32)] of the load-displacement curve become unstable (in the small) it is imperative to examine the stability of these equilibrium positions for infinitesimal disturbances.

The necessary and sufficient condition for stability (in the small) of the

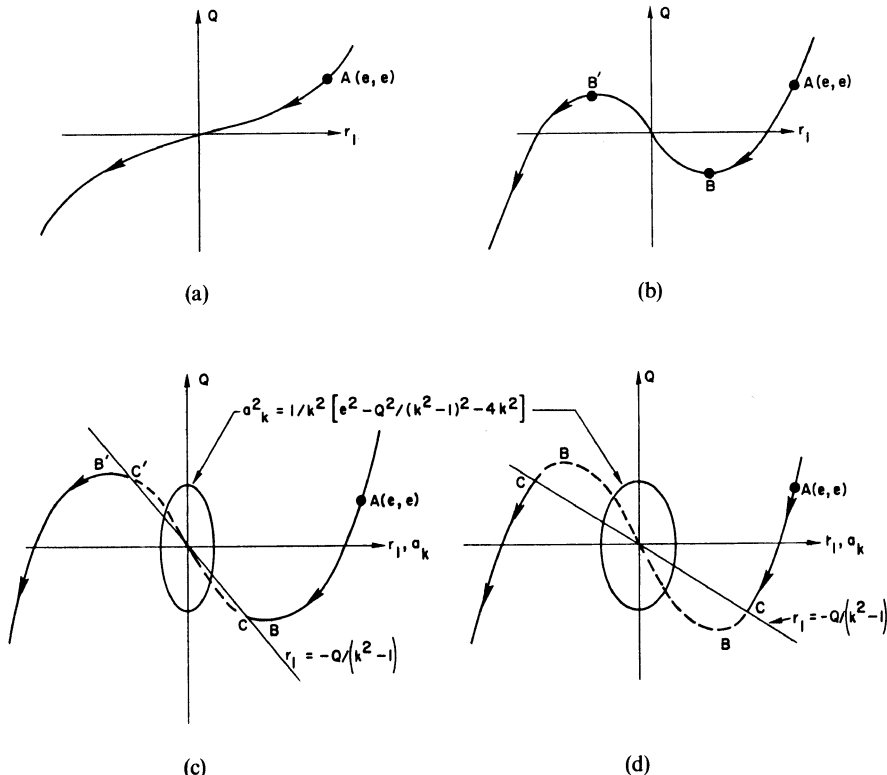


FIGURE 7.3. Typical load-deflection curves for the pinned arch (quasi-static). (a) $e \leq 2$. (b) $2 < e \leq 2k$. (c) $2k \leq e < [2(3k^2 - 1)]^{1/2}$. (d) $e > [2(3k^2 - 1)]^{1/2}$.

static equilibrium points given by the roots of eqs. (32) is that

$$\begin{aligned} \frac{\partial^2 U_T}{\partial r_1^2} &> 0, \\ \left(\frac{\partial^2 U_T}{\partial r^2} \right) \left(\frac{\partial^2 U_T}{\partial a_k^2} \right) &> \left(\frac{\partial^2 U_T}{\partial r_1 \partial a_k} \right)^2. \end{aligned} \quad (33)$$

The expression for U_T obtained by substitution from eq. (31) into eq. (28) is given by

$$U_T = \frac{1}{8}(r_1^2 - e^2 + k^2 a_k^2)^2 + r_1^2 - e^2 + k^4 a_k^2 + 2Qe - 2Qr_1. \quad (34)$$

From eq. (34) one obtains the following expressions for the second derivatives:

$$\left. \begin{aligned} \frac{\partial^2 U_T}{\partial r_1^2} &= \frac{1}{2}[3r_1^2 - e^2 + 4 + k^2 a_k^2], \\ \frac{\partial^2 U_T}{\partial a_k^2} &= \frac{k^2}{2}[r_1^2 - e^2 + 4k^2 + 3k^2 a_k^2], \\ \frac{\partial^2 U_T}{\partial r_1 \partial a_k} &= k^2 r_1 a_k. \end{aligned} \right\} \quad (35)$$

The equilibrium positions corresponding to eqs. (32b) (CC' portion of the graph on Figure 7.3c and d) are proved to be unstable because conditions (33) do not hold, or since

$$\begin{aligned} \frac{\partial^2 U_T}{\partial r_1^2} &= \frac{1}{2}[3r_1^2 - e^2 + 4 + e^2 - r_1^2 - 4k^2] = (r_1^2 + 2 - 2k^2) \\ &= [r_1^2 - 2(k^2 - 1)] \end{aligned}$$

and

$$\frac{\partial^2 U_T}{\partial a_k^2} = \frac{k^2}{2}[-a_k^2 k^2 + 3k^2 a_k^2] = k^4 a_k^2,$$

then the conditions become

$$r_1^2 > 2(k^2 - 1) \quad \text{and} \quad [r_1^2 - 2(k^2 - 1)]k^4 a_k^2 > k^4 r_1^2 a_k^2$$

or

$$-2(k^2 - 1)k^4 a_k^2 > 0.$$

It is clear that this last condition cannot be satisfied as long as a_k is nonzero. Only at points C and C' of the graph (see Figure 7.3), this last inequality becomes an equality and the test fails.

Next, for the equilibrium points corresponding to eq. (32a), the conditions denoted by eqs. (33) become

$$\frac{1}{2}(3r_1^2 - e^2 + 4) > 0 \quad \text{and} \quad \frac{k^2}{4}(3r_1^2 - e^2 + 4)(r_1^2 - e^2 + 4k^2) > 0.$$

The inequalities are equivalent to

$$\left(r_1 - \sqrt{\frac{e^2 - 4}{3}}\right)\left(r_1 + \sqrt{\frac{e^2 - 4}{3}}\right) > 0 \quad (36a)$$

and

$$\left(r_1 - \sqrt{\frac{e^2 - 4}{3}}\right)\left(r_1 + \sqrt{\frac{e^2 - 4}{3}}\right)(r_1 - \sqrt{e^2 - 4k^2})(r_1 + \sqrt{e^2 - 4k^2}) < 0. \quad (36b)$$

For $2 < e \leq 2k$, $r_1^2 - e^2 + 4k^2$ is always nonnegative and the unstable equilibrium points lie between $-\sqrt{(e^2 - 4)/3}$ and $+\sqrt{(e^2 - 4)/3}$ (see Figure 7.2a).

For $e > 2k$, there are two possibilities, which shall be denoted by (i) and (ii). For some value of e the two radicals $\sqrt{(e^2 - 4)/3}$ and $\sqrt{e^2 - 4k^2}$ have the same value; this corresponds to

$$e = \sqrt{2(3k^2 - 1)}.$$

It is observed from inequalities (36) that

(i) for $e \leq \sqrt{2(3k^2 - 1)}$, the unstable equilibrium points lie between $-\sqrt{(e^2 - 4)/3}$ and $+\sqrt{(e^2 - 4)/3}$, which includes the CC' range of Figure 7.3c, and

(ii) for $e \geq \sqrt{2(3k^2 - 1)}$ the unstable points lie between $-\sqrt{e^2 - 4k^2}$ and $+\sqrt{e^2 - 4k^2}$, which corresponds to the curved (cubic) portion of the graph between points C and C' on Figure 7.3d.

Since snap-through buckling is associated with the stability (in the small) of the near equilibrium positions, in examining the equilibrium paths of Figure 7.2b one concludes that there are two possibilities. First, if the near equilibrium point becomes unstable between A and B (see Figure 7.2b), snapping will initially be symmetric; but if the near equilibrium position becomes unstable at B , snapping will occur through an asymmetric path (from B toward either D or E ; Figure 7.2b).

Finally, associating critical loads with the instability (in the small) of the near equilibrium point, one concludes that

1. For $e \leq 2$ there is no snap-through critical load (see Figure 7.3a).
2. For $2 < e \leq 2k$ the critical load is given by

$$Q_{cr1} = -\frac{1}{2}\left(\frac{e^2 - 4}{3}\right)^{3/2} \quad (\text{see Figure 7.3b}).$$

3. For $2k \leq e \leq \sqrt{2(3k^2 - 1)}$, although asymmetric modes are possible (after

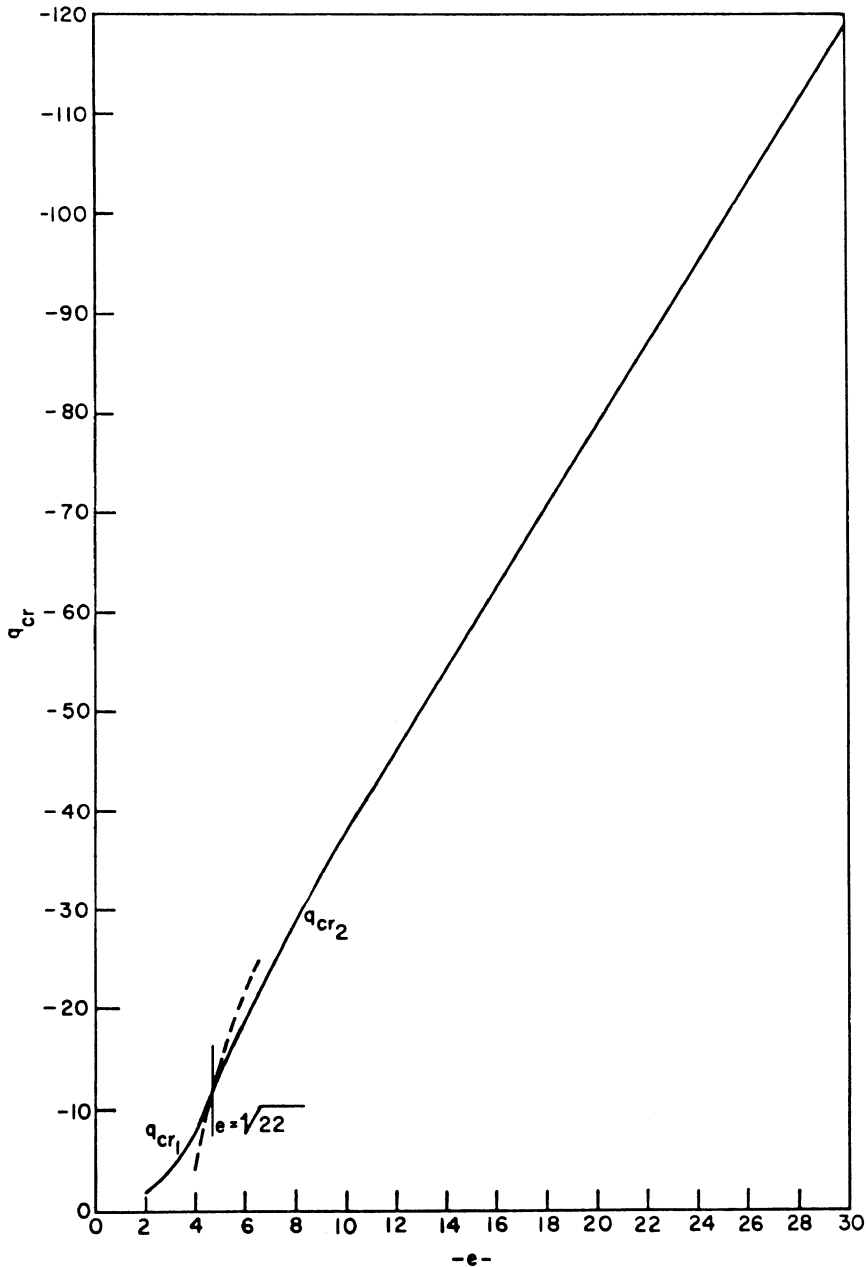


FIGURE 7.4. Nondimensional critical load q versus initial rise parameter e (the pinned arch; quasi-static).

buckling), the critical load is still given by

$$Q_{\text{cr}_1} = -\frac{1}{2} \left(\frac{e^2 - 4}{3} \right)^{3/2}$$

because equilibrium points between A and B (see Figure 7.3c) are stable.

4. Lastly, for $e > \sqrt{2(3k^2 - 1)}$ the critical load is given by

$$Q_{\text{cr}_2} = -(k^2 - 1)\sqrt{e^2 - 4k^2}$$

and corresponds to point C on Figure 7.3d.

Since

$$|Q_{\text{cr}_2}| = (k^2 - 1)(e^2 - 4k^2)^{1/2} \quad \text{for } e^2 > 4k^2,$$

then

$$\frac{d|Q_{\text{cr}_2}|}{dk} = 2k \frac{e^2 - 2k^2 - 2}{(e^2 - 4k^2)^{1/2}} > 0,$$

and this critical load increases with k . Thus the smallest load corresponds to $k = 2$, and for $e > \sqrt{22}$ the critical load is given by

$$Q_{\text{cr}_2} = -3\sqrt{e^2 - 16}.$$

In summary, for quasi-static application of the load the expressions for the critical load are

$$\begin{aligned} \text{for } 2 < e \leq \sqrt{22}, \quad Q_{\text{cr}_1} &= -\frac{1}{2} \left(\frac{e^2 - 4}{3} \right)^{3/2}, \\ \text{for } e > \sqrt{22}, \quad Q_{\text{cr}_2} &= -3\sqrt{e^2 - 16}, \end{aligned} \tag{37a}$$

from which

$$\begin{aligned} q_{\text{cr}_1} &= -e - \frac{1}{2} \left(\frac{e^2 - 4}{3} \right)^{3/2}, \\ q_{\text{cr}_2} &= -e - 3\sqrt{e^2 - 16}. \end{aligned} \tag{37b}$$

These results are presented graphically on curves of q_{cr} versus the rise parameter e on Figure 7.4.

7.3 Dynamic Analysis of the Pinned Arch

Critical conditions and estimates for critical loads are obtained by employing the total potential energy approach, described in Section 1.2.

7.3.1 Load of Constant Magnitude, Infinite Duration

For this case also the total potential is given by expression (34). The equilibrium points in the configuration space are obtained by setting the

generalized velocities equal to zero, which implies

$$\frac{\partial U_T}{\partial r_1} = \frac{\partial U_T}{\partial a_2} = 0. \quad (38)$$

These conditions lead to eqs. (30b) and the possible static equilibrium points are given by eqs. (32a) and eqs. (32b).

The roots of eqs. (32a) define three static equilibrium points, which are denoted by $(r_{11}, 0)$, $(r_{12}, 0)$, and $(r_{13}, 0)$; the roots of eqs. (32b) define two more static equilibrium points which are symmetric with respect to the r_1 axis. The last two points represent saddle points. Note that U_T is also symmetric with respect to the r_1 axis.

The existence of three or five equilibrium points depends on the value of the initial rise parameter: (1) for $2 < e \leq 2k$ there are three equilibrium points given by the solution of eq. (32a) and (2) for $e > 2k$ there are five equilibrium points given by the solution of eq. (32a) and eqs. (32b).

In the first case (1) the total potential is a function of r_1 , e , and Q_D , and the static equilibrium point $(r_{12}, 0)$ is unstable in the small. Since $T + U_T = 0$, $T_i = 0$, and for small values of Q_D , $U_T(r_{12}, 0)$ is positive, then the motion is unbuckled, and the system oscillates about the near equilibrium point $(r_{11}, 0)$. As Q_D is increased the value of $U_T(r_{12}, 0)$ decreases until it reaches the value zero (see Figure 1.4, P_3 -case) and the motion could possibly be a buckled one. Further increase in Q_D will result in a negative value for $U_T(r_{12}, 0)$ and the motion will definitely be a buckled one. Thus the load for which $U_T(r_{12}, 0) = 0$ is for this case both the minimum possible critical load and the minimum guaranteed critical load, and it is denoted by $Q_{D_{cr}}$.

Setting the total potential at $(r_{12}, 0)$ equal to zero,

$$U_T(r_{12}, 0) = 0 = \frac{1}{8}(r_{12}^2 + 4 - e^2)^2 - 2 - 2Q_{D_{cr}}(r_{12} - e),$$

and solving for $Q_{D_{cr}}$ one obtains

$$Q_{D_{cr}} = \frac{1}{16}(r_{12}^2 + 8 - e^2)(r_{12} + e).$$

Also, since $(r_{12}, 0)$ is a static equilibrium point,

$$r_{12}(r_{12}^2 - e^2 + 4) = 4Q_{D_{cr}}.$$

The simultaneous slution of these two equations yields both $Q_{D_{cr}}$ and r_{12} .

The following is an equivalent system of equations:

$$\left. \begin{aligned} 3r_{12}^2 - er_{12}^2 - (3e^2 - 8)r_{12} + e(e^2 - 8) &= 0, \\ Q_{D_{cr}} &= \frac{r_{12}}{4}(r_{12}^2 - e^2 - 4). \end{aligned} \right\} \quad (39)$$

In the second case where $e > 2k$ the total potential depends on r_1 , a_k , e , and Q_D , the saddle points as well as the static equilibrium point $(r_{12}, 0)$ are unstable in the small. Since for fixed values of e and low values of Q_D the value of U_T at the unstable points is positive, there is no possibility of buckled motion

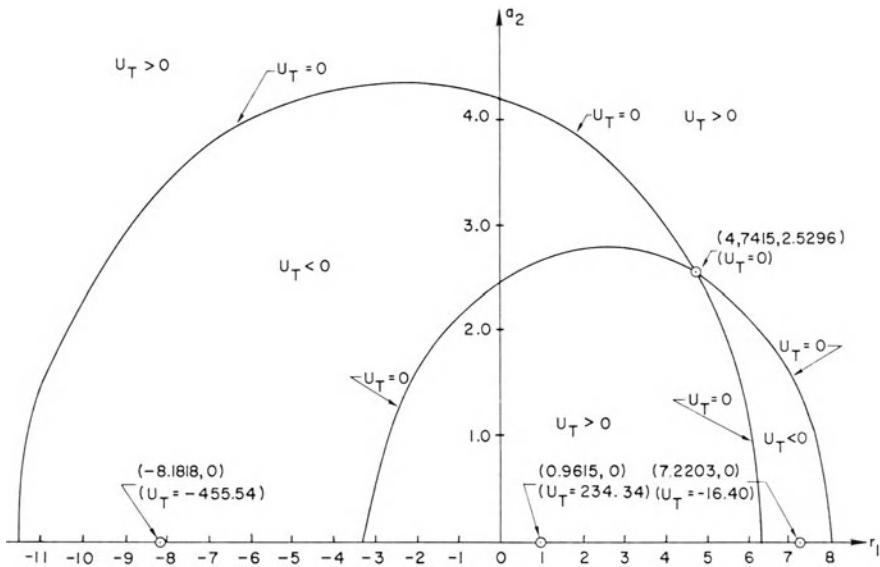


FIGURE 7.5. Total potential contour lines in the configuration space of the generalized coordinates r_1 and a_2 for the pinned arch ($e = 8$, $q = \text{MPCL}$).

(see Figure 1.5a); but as Q_D increases the value of U_T at the saddle points becomes zero, and at this load it is possible for the motion to be buckled (see Figure 1.5b and also Figure 7.5 for numerical values calculated for $e = 8$). This critical load defined as minimum possible critical load will be denoted by $Q_{D_{\text{MP}}}$; its magnitude is obtained by setting the expression, eq. (34), for U_T at the saddle point equal to zero. The result of this substitution is a quadratic equation in $Q_{D_{\text{MP}}}$, the solution of which yields

$$Q_{D_{\text{MP}}} = -[(k^2 - 1)e - k^2 \sqrt{2(k^2 - 1)}]. \quad (40a)$$

By rewriting eq. (40a) as

$$Q_{D_{\text{MP}}} = -(k^2 - 1)2k \left[\frac{e}{2k} - \frac{1}{\sqrt{2(1 - 1/k^2)}} \right]$$

and noting that $e/2k > 1$, one concludes that $|Q_{D_{\text{MP}}}|$ increases with k , and the smallest value corresponds to $k = 2$. Therefore

$$\begin{aligned} Q_{D_{\text{MP}}} &= -3e + 4\sqrt{6} & (\text{a}) \\ (\text{MPCL}) &= -4e + 4\sqrt{6} & (\text{b}) \end{aligned} \quad (40)$$

and only the first asymmetric mode governs snap-through buckling as in the case of quasi-static application of the load.

As the load increases further the value of U_T at the saddle points becomes negative but still larger than $U_T(r_1, 0)$. If $U_T(r_1, 0) > 0$, there are possible

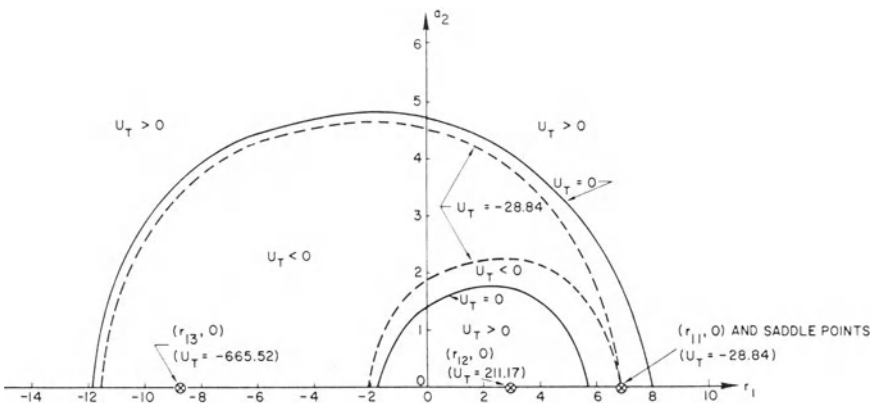


FIGURE 7.6. Total potential contour lines in the configuration space of the generalized coordinates r_1 and a_2 for the pinned arch ($e = 8$, $q = \text{MGCL}$).

loci corresponding to unbuckled motion. Further increase of the load forces the saddle points to move toward position $(r_{11}, 0)$, until at $Q_D = -3e^2 - 16$ the saddle points and $(r_{11}, 0)$ coincide. At this value of the load there is no possibility of unbuckled motion (the motion is buckled; see Figure 7.6 for numerical values calculated for $e = 8$). The load is defined as the minimum guaranteed critical load:

$$\begin{aligned} Q_{D_{\text{MG}}} &= -3\sqrt{e^2 - 16} & (\text{a}) \\ (\text{MGCL}) &= -e - 3\sqrt{e^2 - 16} & (\text{b}). \end{aligned} \quad \left. \right\} \quad (41)$$

Note that the expression for this load is identical to the expression for the critical load under quasi-static application of the load.

The critical loads for the dynamic case (b) are plotted versus the initial rise parameter e in Figure 7.7.

7.3.2 Ideal Impulse

In this case, every point in the middle line of the system is assumed to be instantaneously accelerated to a known finite velocity before any displacement occurs, and for all $t > 0$ there is no further external load. Thus the ideal impulsive loading is imparted into the system as initial kinetic energy. Furthermore, since the system is conservative and stationary the Hamiltonian is constant, or

$$H = T + U_T = \text{constant} = T_i + U_{T_i}$$

where T_i and U_{T_i} are in nondimensional form and evaluated at $r_1 = e$ and $a_2 = 0$. Therefore, by defining U_T in such a manner that $U_T(e, 0) = 0$ one may

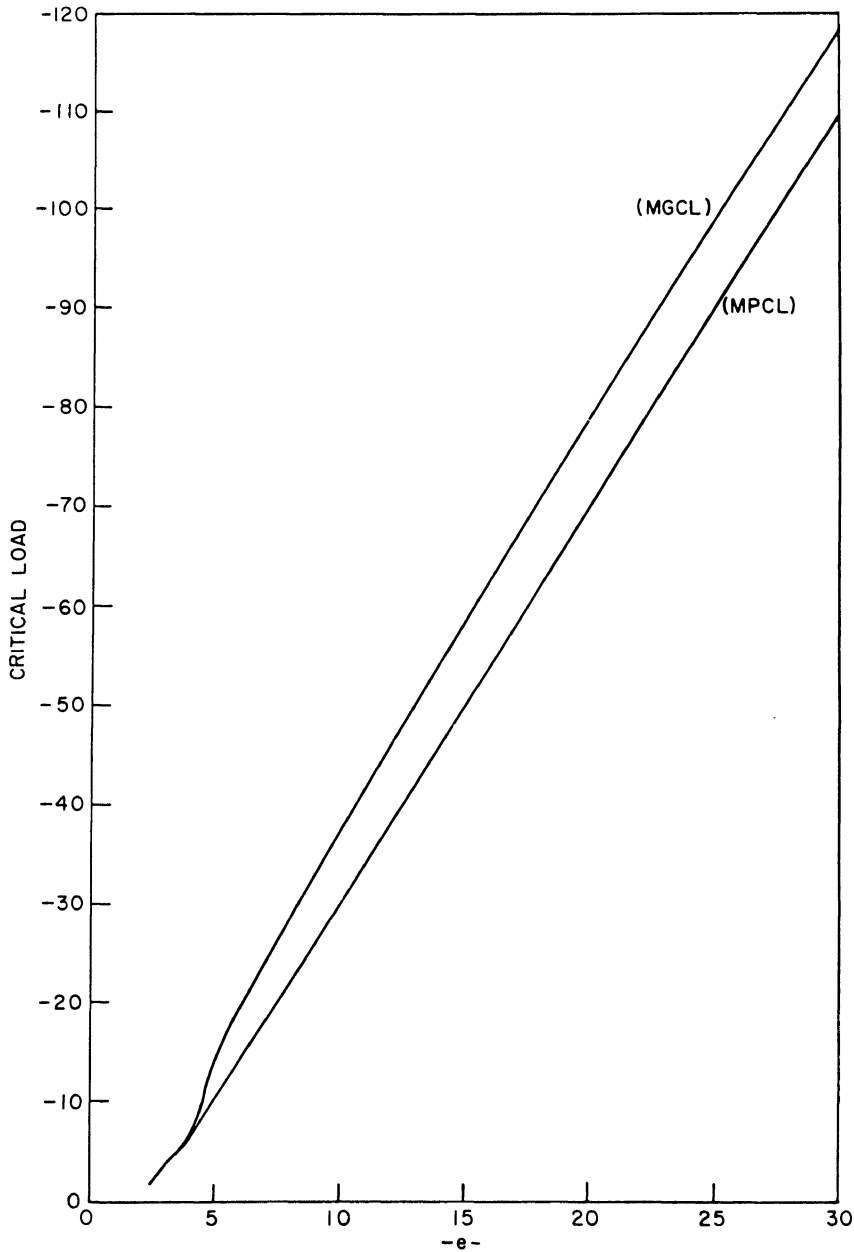


FIGURE 7.7. Nondimensional critical load versus initial rise parameter e (the pinned arch; constant load, infinite duration).

write

$$T + U_T = T_i, \quad (42)$$

and critical impulses, in this case also, may be associated with characteristics of the zero-load potential surface.

In order to find expressions for the critical impulse, one should express the impulse in terms of the initial kinetic energy and study the zero-load potential surface in the configuration space.

Denoting by Imp^* the impulse per unit mass imparted to the arc by the loading,

$$\text{Imp}^* dm = \left(\frac{\partial w}{\partial t} \right)_{\text{initial}} dm$$

or

$$\text{Imp}^* = \left(\frac{\partial w}{\partial t} \right)_{\text{initial}},$$

and substituting into the expression for the kinetic energy, eq. (10), one obtains

$$T_i^* = \frac{\sigma A}{2} \int_0^L (\text{Imp}^*)^2 dx = \frac{\sigma A (\text{Imp}^*)^2 L}{2}.$$

On dividing both sides by the nondimensionalizing parameter $(P_E \varepsilon_E L)/4$, the equation becomes

$$T_i = \frac{2\sigma A}{P_E \varepsilon_E} (\text{Imp}^*)^2,$$

and letting

$$\text{Imp} = \sqrt{\frac{2\sigma A}{P_E \varepsilon_E}} \text{Imp}^*, \quad (43)$$

then $T_i = \text{Imp}^2$, from which one obtains

$$\text{Imp} = -T_i^{1/2}. \quad (44)$$

Note that the negative sign is used because the impulse is associated with a negative loading according to the adopted sign convention

$$\text{Imp} = \lim_{T_0 \rightarrow 0} (q \cdot T_0).$$

The expression for the total potential is obtained from eq. (34) by letting $q = 0$ ($Q = e$) and $k = 2$, which by rearranging terms becomes

$$U_T = \frac{(r_1 - e)^2}{8} (r_1^2 + 2er_1 + e^2 + 8) + a_2^2 (2a_2^2 + r_1^2 + 16 - e^2). \quad (45)$$

Making use of eq. (45), the static equilibrium points are given as follows.

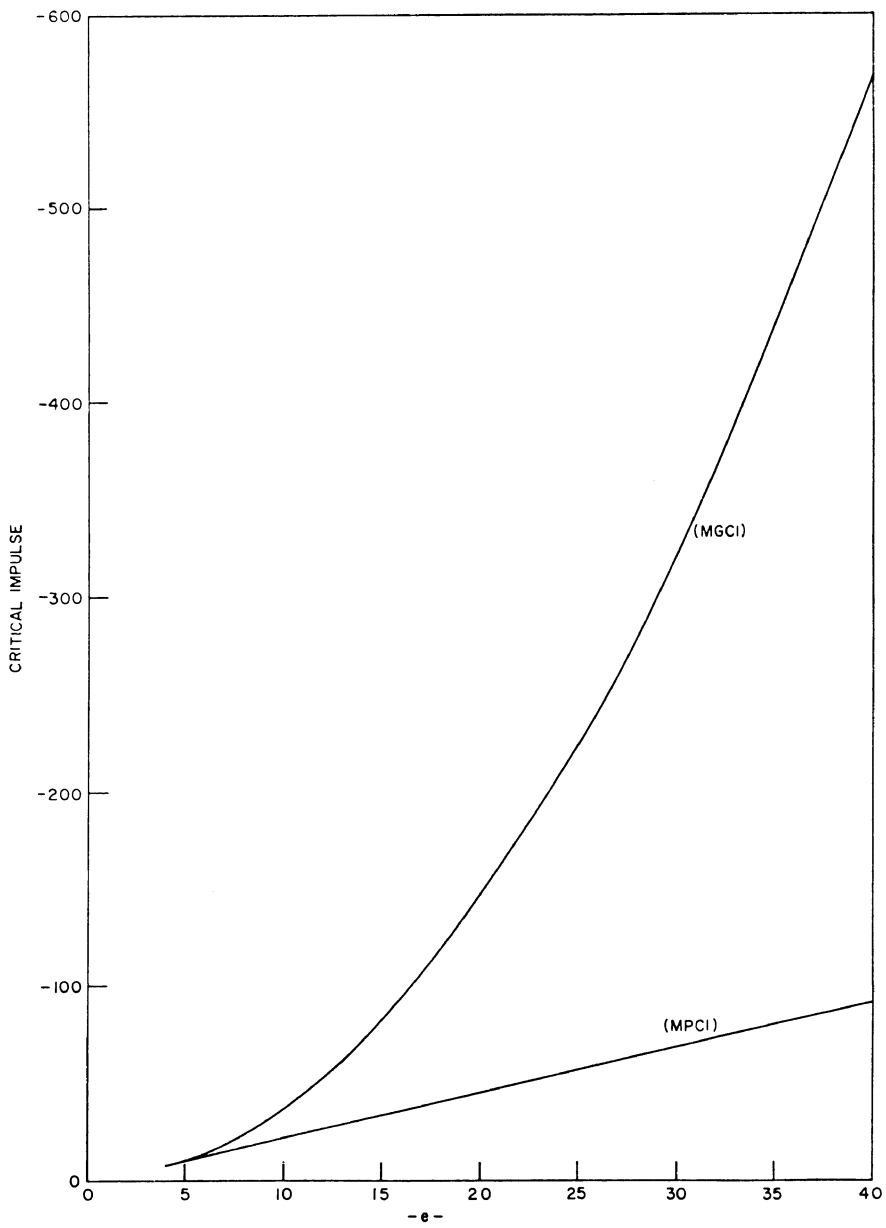


FIGURE 7.8. Nondimensional critical impulse versus initial rise parameter e (the pinned arch).

For $e < 4$

$$r_1 = 0 \quad \text{and} \quad a_2 = 0 \quad (46)$$

in which case no snap-through buckling can take place, and the system can only oscillate about this static equilibrium point ($r_1 = e$, $a_2 = 0$).

For $e \geq 4$ there are five static equilibrium points given by

$$\left. \begin{array}{lll} r_1 = e & a_2 = 0 & \text{(i)} \\ r_1 = \frac{1}{2}(-e + \sqrt{e^2 - 16}) & a_2 = 0 & \text{(ii)} \\ r_1 = -\frac{1}{2}(e + \sqrt{e^2 - 16}) & a_2 = 0 & \text{(iii)} \\ r_1 = -\frac{e}{3} & a_2 = +\sqrt{\frac{2e^2}{9} - 4} & \text{(iv)} \\ r_1 = -\frac{e}{3} & a_2 = -\sqrt{\frac{2e^2}{9} - 4} & \text{(v),} \end{array} \right\} \quad (47)$$

and the corresponding expressions for the total potential are

$$\left. \begin{array}{lll} U_T = 0 & \text{(i)} \\ U_T = \frac{1}{64}(3e - \sqrt{e^2 - 16})^2(e^2 + 8 + e\sqrt{e^2 - 16}) & \text{(ii)} \\ U_T = \frac{1}{64}(3e + \sqrt{e^2 - 16})^2(e^2 + 8 - e\sqrt{e^2 - 16}) & \text{(iii)} \\ U_T = 166\left(\frac{e^2}{3} - 2\right) & \text{(iv) and (v).} \end{array} \right\} \quad (48)$$

Note that U_T for (ii)–(v) is positive for all $e > 4$, and equilibrium point (iii) is stable (in the small) for all $e > 4$, while equilibrium points (ii), (iv), and (v) are unstable for all $e > 4$. Thus snap-through buckling is possible for all $e > 4$.

For this case also (of an ideal impulsive loading), critical impulses can only be bracketed between upper and lower bounds in accordance with the definition of (MGCI) and (MPCI). By using eqs. (44) and (48) one can write the following expressions for critical impulses:

$$(\text{MPCI}) = -4\sqrt{\frac{e^2}{3} - 2} \quad (49)$$

and

$$(\text{MGCI}) = -\frac{1}{8}(3e - \sqrt{e^2 - 16})\sqrt{e^2 + 8 + e\sqrt{e^2 - 16}}. \quad (50)$$

In Figure 7.8, the critical impulses are plotted versus the initial rise parameter e .

7.3.3 Load of Constant Magnitude, Finite Duration

Dynamic Stability under constant load of finite duration has been discussed in Chapter 3 and, through simple mechanical models, criteria and estimates

for critical conditions were presented. The same problem is posed here but applied to a pinned low arch.

The expression for the zero-load total potential is given by

$$U_T^0 = \frac{(r_1 - e)^2}{8} (r_1^2 + 2er + e^2 + 8) + a_2^2(2a_2^2 + r_1^2 + 16 - e^2). \quad (45)$$

Furthermore, neglecting the rotatory and in-plane kinetic energies, the following expression for the nondimensionalized kinetic energy (T is the kinetic energy) is given by eq. (24):

$$T = \frac{2}{\pi} \int_0^\pi \dot{\eta}^2 d\xi. \quad (24)$$

Use of eq. (26) in eq. (24) yields the following expression for T :

$$T = \dot{r}_1^2 + \dot{a}_2^2 = (1 + a_2'^2)\dot{r}_1^2 \quad (51)$$

where $(') = \partial/\partial r$ and $(\cdot) = d/dt$.

Through a static stability analysis, the stationary points on the zero-load total potential, U_T^0 , surface are obtained and given by eqs. (47). Note that points (i) and (iii) are stable (relative minima in the space of r_1 and a_2), point (ii) is unstable (relative maximum), and points (iv) and (v) are also unstable (saddle points). It was already shown that saddle points exist for $e > 4$. For this range of e values, the zero-load total potential value at the saddle points, points (iv) and (v), is smaller than the corresponding value at the relative maximum, point (ii) [see eqs. (48)]. On the basis of this observation, the motion can possibly become buckled by passing through the saddle points, points (iv) and (v). The corresponding condition for this case is a possible critical condition. On the other hand, if the energy imparted by the applied force at the release time is sufficient to reach the relative maximum (unstable) static equilibrium point, point (ii), buckled motion is guaranteed and the corresponding critical condition is a minimum guaranteed one. The former is termed a sufficient condition for dynamic stability and the latter is termed a sufficient condition for dynamic instability by Hsu (see Chapter 1).

Next, the computational procedure for finding the possible critical condition is outlined. This procedure is identical to the one used for model C in Chapter 3.

The stability criterion for this case is expressed by eq. (5) of Chapter 3, or

$$U_T^0(\tau_0) - U_T^P(\tau_0) \leq U_T^0(L_u^0) = 16 \left(\frac{e^2}{3} - 2 \right) \quad (52)$$

where L_u^0 is the unstable static equilibrium point under zero load and τ_0 the release time. The equality sign refers to a critical condition, while the inequality sign refers to a dynamically stable condition.

From eq. (34), with $k = 2$, one can write

$$\begin{aligned} U_T^0 &= \frac{1}{8}(r_1^2 - e^2 + 4a_2^2)^2 + r_1^2 - e^2 + 16a_2^2 \\ \text{and} \quad U_T^P &= \frac{1}{8}(r_1^2 - e^2 + 4a_2^2)^2 + r_1^2 - e^2 + 16a_2^2 + 2Q(e - r_1). \end{aligned} \quad (53)$$

Use of eqs. (53) in eq. (52) with the equality sign yields

$$r_{1_{cr}} = r_1|_{\tau=\tau_{0_{cr}}} = e + \frac{8}{Q} \left(\frac{e^2}{3} - 2 \right) \quad (54)$$

where $\tau_{0_{cr}}$ is the critical release time.

Moreover, for $0 < \tau < \tau_0$ conservation of energy yields (during this time the system is loaded)

$$U_T^P + T^P = 0. \quad (55)$$

For a given path of motion, integration of eq. (55) yields a relation between the time of release and the position at that instant. Note that the problem has been cast in the following terms: for a given load Q find the smallest release time $\tau_{0_{cr}}$ such that the system may reach an unstable point (saddle point for the minimum possible critical condition) with zero velocity, eq. (54). Since one is interested in obtaining the smallest release time $\tau_{0_{cr}}$, and since the

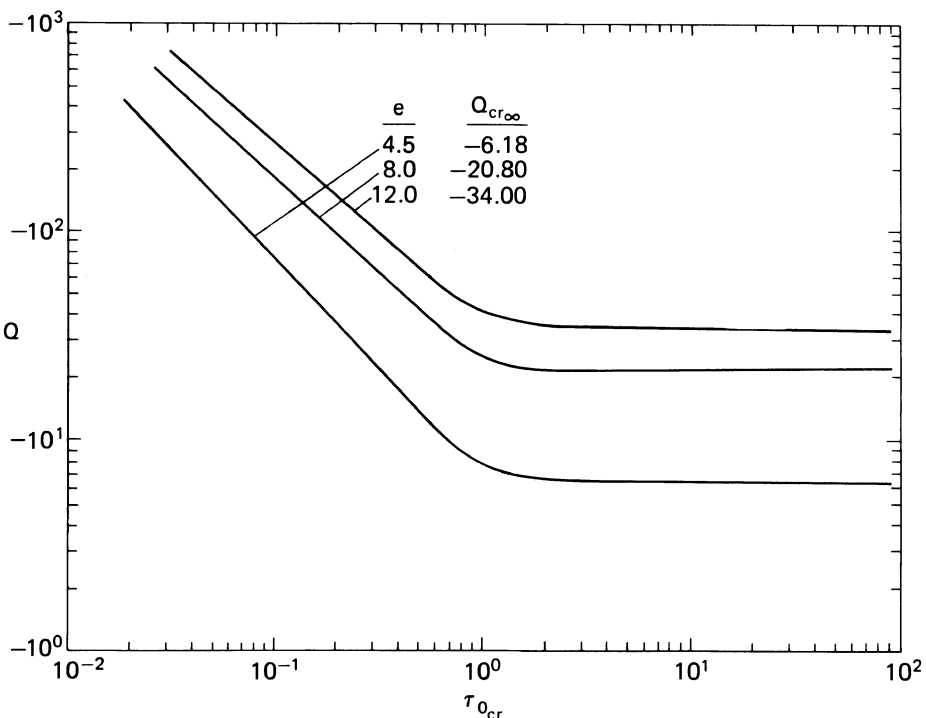


FIGURE 7.9. Constant load Q versus critical duration time $\tau_{0_{cr}}$, pinned arch.

position at the time of release is path dependent, one can solve the problem by considering the associated brachistochrone problem. The brachistochrone problem makes use of Eq. (55) for this system, and through its solution one obtains the relation between the smallest release time $\tau_{0,\text{cr}}$ and the position at the instant of release r_1 , as well as the path that yields $\tau_{0,\text{cr}}$. The details of the solution to this brachistochrone problem are similar to the ones presented in Appendix B for the two-degree-of-freedom model, model C. The solution to the brachistochrone problem yields that the minimizing path is characterized by $a_2 \equiv 0$ (symmetric path) and the relation between $\tau_{0,\text{cr}}$ and the position of the system $r_{1,\text{cr}}$ at $\tau_{0,\text{cr}}$ is

$$\tau_{0,\text{cr}} = - \int_e^{r_{1,\text{cr}}} \frac{dr_1}{\sqrt{2Q(r_1 - e) + e^2 - r_1^2 - \frac{1}{8}(r_1^2 - e^2)^2}}. \quad (56)$$

Computationally, it is simpler to assign values of $r_{1,\text{cr}}$ (starting with values close to the initial position, $r_1 = e$ and $a_2 = 0$), solve for Q through eq. (54), and then solve for $\tau_{0,\text{cr}}$ through eq. (56).

Note that for the case of the minimum guaranteed critical condition eq. (54) is replaced by a comparable equation that employs the value of the zero-load total potential at the relative maximum unstable static point.

Numerical results are presented graphically on Figures 7.9 and 7.10 for

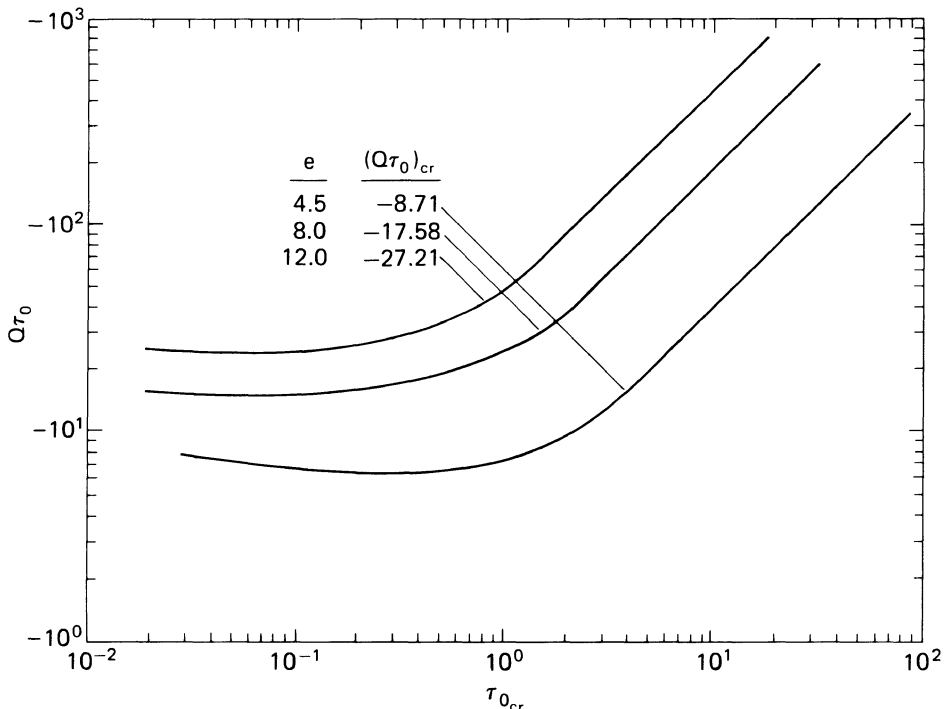


FIGURE 7.10 Impulse ($p\tau_0$) versus critical duration time $\tau_{0,\text{cr}}$, pinned arch.

the minimum possible critical condition only and various values of e . The curves of Figure 7.9 depict critical conditions in terms of applied load Q versus critical release time $\tau_{0,\text{cr}}$. One may observe that as $\tau_{0,\text{cr}}$ increases, the corresponding load approaches asymptotically the value of Q_{cr} for the infinite duration time. Figure 7.10 presents the same results as Figure 7.9, but in terms of $(Q\tau_0)_{\text{cr}}$ versus critical release time $\tau_{0,\text{cr}}$. Note that as $\tau_{0,\text{cr}}$ approaches zero, the value of $(Q\tau_0)_{\text{cr}}$ approaches that of the critical ideal impulse (see Section 7.3.2).

7.3.4 Effect of Static Preloading

In evaluating the effect of static preloading for the low simply supported arch, the concepts and methodologies discussed in Chapter 4 are employed.

Three values for the rise parameter e are used ($e = 5.0, 6.0, 8.0$), and for each e value the system is initially loaded quasi-statistically with load Q_0 smaller in magnitude than the static critical load Q_{cr} . Then the system is loaded suddenly. Only the extreme cases of ideal impulse ($\tau_0 \rightarrow 0$) and of constant magnitude with infinite duration ($\tau_0 \rightarrow \infty$) are treated here. The case of finite duration can easily be obtained and it can be assigned as a homework problem. In the dynamic analysis presented here the following values for e and Q_0 are employed, while the values for $Q_{\text{st,cr}}$ can be obtained by using eq. (37a). The static critical load in eq. (37a) is denoted by Q_{cr2} since the e values are greater than 4.0.

$$e = 4.5; \quad Q_0 = -1.0, -3.0, -5.0; \quad Q_{\text{st,cr}} = -6.18,$$

$$e = 5.0; \quad Q_0 = -2.0, -4.0, -6.0; \quad Q_{\text{st,cr}} = -9.00,$$

$$e = 6.0; \quad Q_0 = -3.0, -4.0, -6.0; \quad Q_{\text{st,cr}} = -13.41.$$

First we deal with the case of the ideal impulse ($\tau_0 \rightarrow 0$). As explained in Chapter 4, the impulse is related to an initial kinetic energy, $T_i^{P_0}$ (the impulse is imparted to the system as initial velocity) and from conservation of energy (for the preloaded system)

$$\bar{U}_T^{P_0} + \bar{T}_T^{P_0} = \bar{U}_T^{P_0}(L_s^{P_0}) + \bar{T}_i^{P_0} \quad (57)$$

where $L_s^{P_0}$ is the near static (stable) equilibrium position under P_0 (static preloading). Then, $\bar{T}_i^{P_0}$ is critical (and the corresponding ideal impulse) if the system can reach the unstable static equilibrium point L_u^P with zero kinetic energy, or

$$\bar{T}_{i,\text{cr}}^{P_0} = \bar{U}_T^{P_0}(L_u^{P_0}) - \bar{U}_T^{P_0}(L_s^{P_0}). \quad (58)$$

The ideal impulse ($p\tau_0$) may be related to the initial kinetic energy $\bar{T}_i^{P_0}$ (in the nondimensionalized form) by the expression

$$(p\tau_0) = -[\bar{T}_i^{P_0}(r_s^{P_0})]^{1/2} \quad (59)$$

where $r_s^{P_0}$ is the near static (stable) equilibrium position under load P_0 .

The critical ideal impulse, through eqs. (59) and (58), is obtained by

$$(p\tau_0)_{cr} = -[\bar{U}_T^{P_0}(r_u^{P_0}) - \bar{U}_T^{P_0}(r_s^{P_0})]^{1/2}. \quad (60)$$

Note that the negative sign on the right-hand side of eqs. (59) and (60) is present because of the sign convention on the load p (Q on Figure 7.1). The expression for the total potential is given by the second of eqs. (52). Note that the bar has been removed and by replacing P by P_0 and Q by Q_0 , eq. (52) becomes

$$U_T^{P_0} = \frac{1}{8}(r_1^2 - e^2 + 4a_2^2)^2 + r_1^2 - e^2 + 16a_2^2 + 2Q_0(e - r_1). \quad (53)$$

Use of eq. (53) in eq. (60) yields critical values for the ideal impulse, provided that the static problem has been solved for, for each value of Q_0 . This means that one has solved for the values of $r_u^{P_0}$ and $r_s^{P_0}$ needed in eq. (60).

The numerical results are presented on Table 7.1. The values for the first row, corresponding to $Q_0 = 0$, are those characterized by eq. (49). Note that these values correspond to minimum possible critical impulses (MPCIs). Further note that by definition

$$\text{Imp} = \lim_{\tau_0 \rightarrow 0} (q_1 \tau_0) = \lim_{\tau_0 \rightarrow 0} (Q \tau_0) - \lim_{\tau_0 \rightarrow 0} (e \tau_0) = \lim_{\tau_0 \rightarrow 0} (Q \tau_0). \quad (61)$$

Note also that, as the value of Q_0 approaches the value of the static critical load, the additionally imposed critical impulse tends to zero. This is reflected by the results of the last row of Table 7.1.

For the second extreme case ($\tau_0 \rightarrow \infty$), Q_{cr} may also be obtained from energy considerations and the criteria developed in Chapter 4. The characteristic equation for this case is obtained from

$$\bar{U}_T^{P_0+P}(L_u^{P_0+P}) = \bar{U}_T^{P_0+P}(L_s^{P_0}), \quad (62)$$

which is eq. (12) of Chapter 4.

The critical load for the case of infinite duration $Q_{cr,\infty}$ is obtain by the following steps, for a given (e, Q_0) combination.

1. Solve the symmetric response equilibrium equation, eq. (32a), given below, for $r_s^{P_0}$ (near stable position):

$$(r_s^{P_0})^3 - (e^2 - 4)r_s^{P_0} = 4P_0. \quad (63)$$

TABLE 7.1. Critical ideal impulse $(p\tau_0)_{cr}$.

$e = 4.5$		$e = 5.0$		$e = 6.0$	
Q_0	$(Q\tau_0)_{cr}$	Q_0	$(Q\tau_0)_{cr}$	Q_0	$(Q\tau_0)_{cr}$
0	-8.72	0	-10.07	0	-12.65
-1.0	-5.11	-2.0	-4.95	-3.0	-7.95
-3.0	-3.53	-4.0	-3.64	-4.0	-6.80
-5.0	-1.93	-6.0	-2.28	-6.0	-5.31
-6.18	0	-9.00	0	-13.41	0

TABLE 7.2. Critical dynamic loads $Q_{cr,\infty}$ (infinite duration).

$e = 4.5$			$e = 5.0$			$e = 6.0$		
Q_0	$Q_{cr,\infty}$	$Q_0 + Q_{cr,\infty}$	Q_0	$Q_{cr,\infty}$	$Q_0 + Q_{cr,\infty}$	Q_0	$Q_{cr,\infty}$	$Q_0 + Q_{cr,\infty}$
0	-3.7	-3.7	0	-5.20	-5.20	0	-8.8	-8.8
-1.0	-4.05	-5.05	-2.0	-5.54	-7.54	-3.0	-8.61	-11.61
-3.0	-2.54	-5.54	-4.0	-3.90	-7.90	-4.0	-8.2	-12.02
-5.0	-0.99	-5.99	-6.0	-2.24	-8.24	-6.0	-6.77	-12.77
-6.18	0	-6.18	-9.0	0	-9.00	-13.41	0	-13.41

2. The static unstable (saddle) equilibrium positions are characterized by [see eqs. (32b) with $k = 2$]

$$r_u^{P_0+P} = -\frac{Q_0 + Q}{3}$$

and

$$a_2^2 = \frac{1}{4} \left[e^2 - \frac{Q + Q_0}{9} - 16 \right]. \quad (64)$$

3. Equation (61) for this system becomes

$$\begin{aligned} & \frac{1}{8}(r_1^2 + 4a_2^2 - e^2)^2 + r_1^2 - e^2 + 16a_2^2 + 2(Q_0 + Q)(e - r_1) \\ &= \frac{1}{8}(r_s^{P_0} - e^2)^2 + (r_s^{P_0})^2 - e^2 + 2(Q_0 + Q)(e - r_s^{P_0}) \end{aligned} \quad (65)$$

where r_1 stands for $r_u^{P_0+P}$. The simultaneous solution of eqs. (63) and (64) yields $r_u^{P_0+P}$, $a_2^{P_0+P}$, and $Q_{cr,\infty}$. Note that we have three equations in three unknowns.

The numerical results for all e, Q_0 combinations are presented in tabular form on Table 7.2.

Note that the first-row results of Table 7.2 correspond to those of eq. (40) for QDMP (minimum possible critical load). The results of the last row reflect the fact that if the system is loaded quasi-statically up to the limit point, then the additional suddenly applied load that the system can withstand tends to zero.

7.3.5 Summary of Results for the Pinned Arch

The results obtained for the problem of a pinned low arch are summarized for the different cases of timewise distribution of the load.

In the case of quasi-static application of the load, the critical load, for any given structural geometry (cross section, material, and distance between the end points), depends entirely on the initial rise parameter. For small values of the initial rise parameter, $e \leq 2$, there is no possibility of snap-through buckling. For $1 < e \leq \sqrt{22}$ the critical load is given by

$$q_{st,cr} = - \left[e + \frac{1}{2} \left(\frac{e^2 - 4}{3} \right)^{3/2} \right],$$

and at this load the governing deformation mode is a symmetric one, except at $e = \sqrt{22}$, in which case an asymmetric path may be followed.

For $e \geq \sqrt{22}$ the critical load is given by

$$q_{st_{cr}} = -e + 3\sqrt{e^2 - 16},$$

and at this load the governing deformation mode is an asymmetric one. For this case it was proved that the asymmetric mode is the first harmonic antisymmetric buckling mode of a straight simply supported column, compressed by an axial force P (it is the same as the first antisymmetric vibration mode of a pinned straight beam). It can easily be shown that for this case the stretching energy of the low arch is equal to the stretching energy of the corresponding column when the axial force is the one associated with the first-harmonic antisymmetric mode (second Euler load).

In the case of a load of constant magnitude and infinite duration, it is concluded that the critical load can only be bracketed between an upper bound (MGCL) and a lower bound (MPCL). In this case also, the critical load depends on the initial rise parameter for a fixed structural geometry. For small values of the initial rise parameter, $e < 2.47$, there is no possibility of snap-through buckling, and for any given load the system can only oscillate nonlinearly about the near equilibrium point. For $2.47 < e < 4$ the upper and lower bounds are coincident, the governing deformation mode is symmetric, and the magnitude of the critical load is found by solving the following system of equations:

$$\begin{aligned} 3r_{12}^3 - er_{12}^2 - (3e^2 - 8)r_{12} + e(e^2 - 8) &= 0, \\ Q_{D_{cr_1}} &= \frac{r_{12}}{4}(r_{12}^2 - e^2 - 4), \\ (\text{MPCL}) &= (\text{MGCL}) = Q_{D_{cr_1}} - e. \end{aligned} \quad (39)$$

For $e > 4$ the lower bound is given by the expression

$$(\text{MPCL}) = -3e + 4\sqrt{6}, \quad (40b)$$

and the possible locus of buckled motion consists of both symmetric and asymmetric deformation modes. If the initial conditions are zero, then the path initially is symmetric. For $4 < e < 5.4$ the upper bound (MGCL) is obtained by solving the system of eqs. (39) and the locus is a symmetric one. For $e > 5.4$ the upper bound is given by

$$(\text{MGCL}) = -(e + 3\sqrt{e^2 - 16}), \quad (41b)$$

and the locus, in the absence of initial conditions, is a symmetric one until $r_1 = \sqrt{e^2 - 16}$; for smaller values of r_1 , it could possibly be asymmetric (see Figure 7.6). Values of critical loads are plotted versus the initial rise parameter e on Figure 7.7.

In the case of an ideal impulsive load, the critical impulse can be bracketed

between an upper bound (MGCI) and a lower bound (MPCI). These critical impulses depend only on the initial rise parameter for a fixed structural geometry, and they are given by the following expressions:

$$(MPCI) = -4\sqrt{(e^2/3) - 2}, \quad (49)$$

$$(MGCI) = -\frac{1}{8}(3e - \sqrt{e^2 - 16})\sqrt{e^2 + 8 + e\sqrt{e^2 - 16}} \quad (50)$$

for $e > 4$.

For values of e smaller than four, there is no possibility of snap-through buckling under an ideal impulsive load. The numerical results are shown graphically on Figure 7.8.

The results obtained for the case of constant load, finite duration, are plotted in Figure 7.9 and 7.10. In Figure 7.10 the critical impulse is plotted versus the duration time τ_0 . It is seen from this figure that for a considerable range of duration times (lower end of values for $\tau_{0,c}$) there is no significant change in the corresponding critical impulse. It is the same as (MPCI). For larger values of the duration time the critical impulse increases considerably. Furthermore, it is seen from Figure 7.9 that for small duration times τ_0 , the system can withstand extremely large loads. As the duration time increases, the corresponding critical load approaches asymptotically the value of (MPCL) for the case of a load of constant magnitude, infinite duration.

Finally, the effect of static preloading is shown on Tables 7.1 and 7.2. From Table 7.1 one sees that the magnitude of the critical impulse decreases as the magnitude of static preloading increases. Similarly, from Table 7.2 one observes that the total load (sum of static preload and critical dynamic load) increases with increasing values of static preloading. Both of these observations are very significant in the design of dynamically loaded systems. This is so because the analyses corresponding to zero-magnitude static preloading are much simpler in execution, but yet they provide a limiting behavior under finite-magnitude static preloading. For example, from Table 7.2 and $e = 6.0$ the total load that the arch can carry is between -8.8 and -13.41 . The value of -8.8 corresponds to the sudden application with zero preload and the value of -13.41 to static critical load. Both values can be obtained without using "static preloading" analyses.

7.4 The Clamped Arch

The problem of the arch is reexamined under the assumption of clamped edges. The initial shape of the arch is again assumed to be a half-sine wave, and the lateral load is taken to be a concentrated load at the midpoint of the arch. The concentrated load is chosen for investigation in order to compare the results for quasi-static applications of the load with the results of [18]. Theoretical analysis and experimental data are reported in [18] for

the case of a concentrated lateral load (quasi-static) applied at the midpoint of a low circular arch.

The following timewise distributions are considered in the present analysis: (1) quasi-static; (2) load of constant magnitude, infinite duration; and (3) ideal impulsive load.

The initial shape of the arch is given by the same expression as for the pinned arch, eq. (25):

$$\eta_0 = e \sin \xi.$$

The concentrated load at the center is specified by setting

$$Q^*(X, t) = 0 \quad \text{for } x \neq \frac{L}{2} \text{ and } t \geq 0 \quad (66)$$

and

$$\int_0^L Q^*(x, t) dx = F(t) = \frac{AE\varepsilon_E^2}{\rho} L q(\tau) \quad \text{for } t, \tau > 0.$$

It was concluded in [18] that the deflected shape could be represented accurately by two symmetric modes and the first antisymmetric mode for values of e less than 30. It can easily be shown that static equilibrium points exist if the deflected shape is represented by a series of symmetric modes and one antisymmetric mode. Furthermore, it can be shown that the smallest value of the critical load for both quasi-static and dynamic loads corresponds to the first antisymmetric mode. Thus the problem is reduced to representing the symmetric deformations with sufficient accuracy. On the basis of this and the conclusions of [18] it is ascertained that the deflected shape of the clamped arch can be represented with sufficient accuracy by a three-mode approximation, two symmetric and one antisymmetric.

Since the boundary conditions are

$$\begin{aligned} \eta(0, \tau) &= \eta(\pi, \tau) = 0, \\ \eta'(0, \tau) &= \eta'_0(0), \\ \eta'(\pi, \tau) &= \eta'_0(\pi), \end{aligned}$$

then each term, $n = 0, 1, 2, \dots$, of the following infinite series representation of η satisfies these conditions:

$$\begin{aligned} \eta(\xi, \tau) &= \eta_0(\xi) + \sum_{n=0}^{\infty} b_n(\tau) (1 - \cos 2\xi) \cos n\xi, \\ 0 < \xi < \pi, \quad \tau > 0. \end{aligned} \quad (67a)$$

With the definitions $a_0 = b_0$, $a_1 = b_1/2$, and $a_2 = b_2/2$, the three-mode approximation for η can be written

$$\eta = e \sin \xi + (a_0 - a_2)(1 - \cos 2\xi) + a_1(\cos \xi - \cos 3\xi) + a_2(\cos 2\xi - \cos 4\xi). \quad (67b)$$

By use of eq. (67b), eq. (21), and eq. (22) the expressions for the different energies become

$$U_{b_T} = 16(a_0 - 2a_2) + 82a_1^2 + 256a_2^2,$$

$$U_{m_T} = \frac{1}{8} \left[4(a_0 - 2a_2)^2 + 10a_1^2 + 16a_2^2 + \frac{32}{3\pi} e(a_0 - 2a_2) + \frac{128}{15\pi} ea_2 \right]^2$$

and

$$U_{p_T} = -8q(a_0 - 2a_2).$$

Therefore the expression for the total potential can now be obtained from eq. (23a):

$$U_T = \frac{1}{8} \left[4(a_0 - 2a_2)^2 + 10a_1^2 + 16a_2^2 + \frac{32}{3\pi} e(a_0 - 2a_2) + \frac{128}{15\pi} ea_2 \right]^2$$

$$+ 16(a_0 - 2a_2)^2 + 82a_1^2 + 256a_2^2 - 8q(a_0 - 2a_2). \quad (68a)$$

By introducing the following new variables:

$$r_1 = a_0 - 2a_2 + \frac{4e}{3\pi},$$

$$r_2 = a_2 + \frac{4e}{15\pi},$$

$$Q = q + \frac{16e}{3\pi},$$

the expression for the total potential, eq. (68a), assumes the simplified form

$$U_T = \frac{1}{8} \left[4r_1^2 + 10a_1^2 + 16r_2^2 - \frac{1856e^2}{225\pi^2} \right]^2 + 16 \left(r_1 - \frac{4e}{3\pi} \right)^2$$

$$+ 82a_1^2 + 256 \left(r_2 - \frac{4e}{15\pi} \right)^2 - 8 \left(Q - \frac{16e}{3\pi} \right) \left(r_1 - \frac{4e}{3\pi} \right).$$

7.4.1 Static Analysis

Employing the principles of the stationary value of the total potential, the following relations must hold for equilibrium:

$$4r_1 + \left(r_1^2 + 2.5a_1^2 + 4r_2^2 - \frac{464e^2}{225\pi^2} \right) r_1 = Q,$$

$$\left[8.2 + \left(r_1^2 + 2.5a_1^2 + 4r_2^2 - \frac{464e^2}{225\pi^2} \right) \right] a_1 = 0, \quad (69)$$

$$16r_2 + \left(r_1^2 + 2.5a_1^2 + 4r_2^2 - \frac{464e^2}{225\pi^2} \right) r_2 = \frac{64e}{15\pi}.$$

Critical loads are associated with the stability in the small of the near equilibrium position. One possible solution of eqs. (69) is

$$a_1 \equiv 0$$

and

$$4r_1 + \left(r_1^2 + 4r_2^2 - \frac{464e^2}{225\pi^2} \right) r_1 = Q,$$

$$16r_2 + \left(r_1^2 + 4r_2^2 - \frac{464e^2}{225\pi^2} \right) r_2 = \frac{64e}{15\pi}. \quad (70)$$

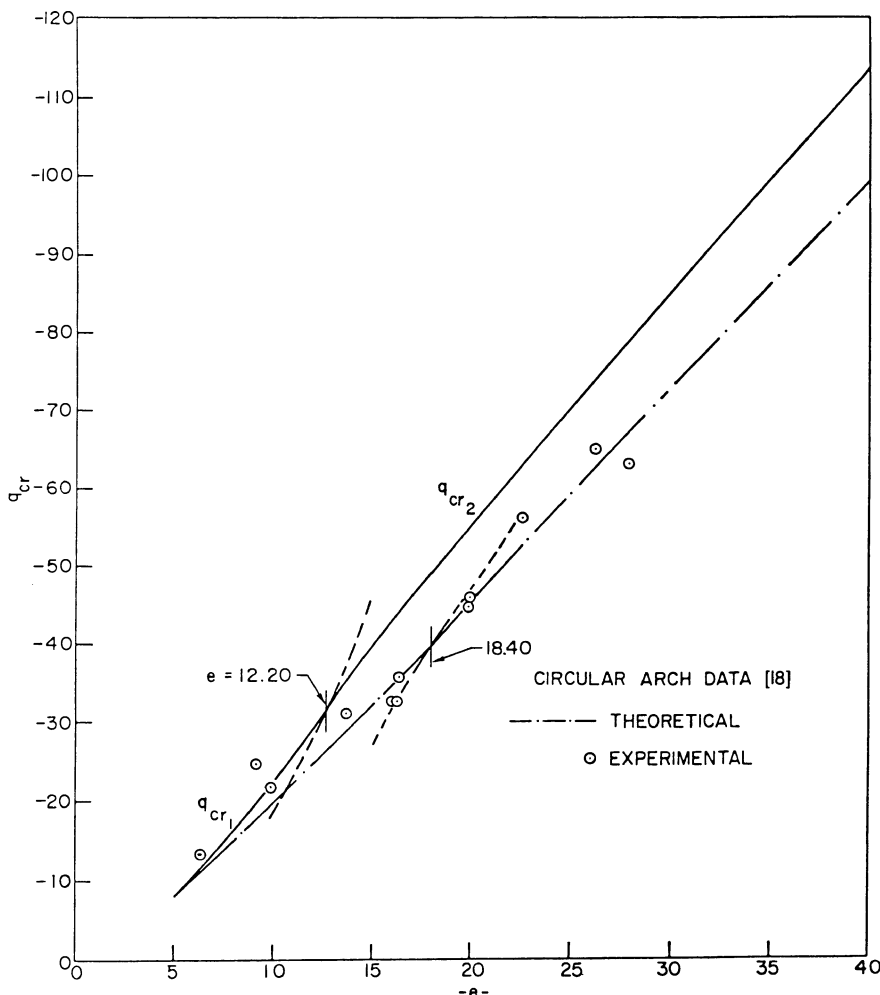


FIGURE 7.11. Nondimensional critical load q versus initial rise parameter e (the clamped arch; quasi-static).

In this case the governing deflectional mode is symmetric and the critical load, denoted by q_{cr_1} , corresponds to the relative maximum (in absolute value) of Q for the load-displacement relation given by eqs. (70).

The second possible solution of eqs. (69) is $a_1 \neq 0$, in which case

$$\begin{aligned} r_1 &= -\frac{Q}{4.2}, \\ r_2 &= \frac{64e}{117\pi}, \\ 2.5a_1^2 &= \frac{194.704e^2}{225\pi^2} - \left(\frac{Q}{4.2}\right)^2 - 8.2. \end{aligned} \quad (71)$$

In this case the near equilibrium point can become unstable through the appearance of the antisymmetric deflectional mode (a_1) as long as

$$\frac{194.704e^2}{225\pi^2} - 8.2 > 0 \quad \text{or} \quad e > 9.73.$$

The value of Q for which the asymmetric equilibrium point (saddle point) disappears corresponds to q_{cr_2} ; this value is found from the last of eqs. (71) by setting $a_1 = 0$ in this equation, which then can be written as

$$q_{\text{cr}_2} = -\frac{16e}{3\pi} - 4.2\sqrt{0.0835e^2 - 8.2}. \quad (72)$$

Although asymmetric modes can appear for $e > 9.73$, q_{cr_1} represents the critical load for $e < 12.2$ and q_{cr_2} represents the critical load for $e > 12.2$. For values of $e < 12.2$ the governing deflectional mode is symmetric, and for $e > 12.2$ the governing deflectional mode is antisymmetric. The results are plotted in Figure 7.11 as q_{cr} versus the initial rise parameter e . In the same figure the theoretical results and experimental data of [18] are shown for comparison.

7.4.2 Load of Constant Magnitude, Infinite Duration

For this load case, the critical load is bracketed between an upper bound (MGPL) and a lower bound (MPCL). When there is a possible locus of buckled motion, the corresponding critical load ($Q_{\text{D}_{\text{MP}}}$) is given by

$$Q_{\text{D}_{\text{MP}}} = -\frac{32.8}{3\pi}e + 4.2\sqrt{0.05616e^2 + 8.005}, \quad (73)$$

and this expression is applicable for $e > 9.73$.

Equation (73) is obtained by substituting the coordinates of the saddle point, eq. (71), into the expression for the total potential, eq. (68b), and setting the total potential equal to zero. The solution of this equation yields the critical value of Q_{D} and consequently q_{u} (MPCL), through the following

expression:

$$(MPCL) = Q_D - \frac{16e}{3\pi}. \quad (74)$$

For values of $e < 9.73$, since antisymmetric buckling is not possible, (MPCL) and (MGCL) are coincident and their magnitudes are obtained through the simultaneous solution of the following system of equations:

$$\begin{aligned} 16\left(r_1 - \frac{4e}{3\pi}\right)^2 + 256\left(r_2 - \frac{4e}{15\pi}\right)^2 + \frac{1}{8}\left[4r_1^2 + 16r_2^2 - \frac{1856e^2}{225\pi^2}\right]^2 \\ - 8\left(Q_D - \frac{16e}{3\pi}\right)\left(r_1 - \frac{4e}{3\pi}\right) = 0 \end{aligned} \quad (75)$$

and

$$\begin{aligned} 4r_1 + \left(r_1^2 + 4r_2^2 - \frac{464e^2}{225\pi^2}\right)r_1 = Q_D, \\ 16r_2 + \left(r_1^2 + 4r_2^2 - \frac{464e^2}{225\pi^2}\right)r_2 = \frac{64e}{15\pi}. \end{aligned} \quad (76)$$

Equation (75) is the total potential evaluated at the symmetric equilibrium points and set equal to zero, and eqs. (76) denote the symmetric static equilibrium points for any value of the load Q_D . With use of eq. (74) the values of (MPCL) are obtained for $e < 9.73$.

As far as the upper bound (MGCL) is concerned, it is coincident with the lower bound (MPCL) for values of $e < 9.73$. For values $9.73 < e < 14.5$, the upper bound (MGCL) is obtained by the simultaneous solution of eq. (75) and eqs. (76) and the following relation:

$$(MGCL) = Q_D - \frac{16e}{3\pi}. \quad (74)$$

Finally, for values of $e > 14.5$ the (MGCL) corresponds to the condition for which the near equilibrium point becomes unstable in the small through the appearance of an antisymmetric path and there is no possibility of unbuckled motion. In this case the expression for the (MGCL) is given by

$$(MGCL) = -\frac{16e}{3\pi} - 4.2\sqrt{0.0835e^2 - 8.2}. \quad (77)$$

Values of (MGCL) and (MPCL) are plotted versus the initial rise parameter e in Figure 7.12.

7.4.3 Ideal Impulsive Load

In this case also, upper and lower bounds are given for the critical impulse. Snap-through buckling is possible for $e > 9.73$. When the motion can possibly be a buckled one toward the far zero-load equilibrium point, the corres-

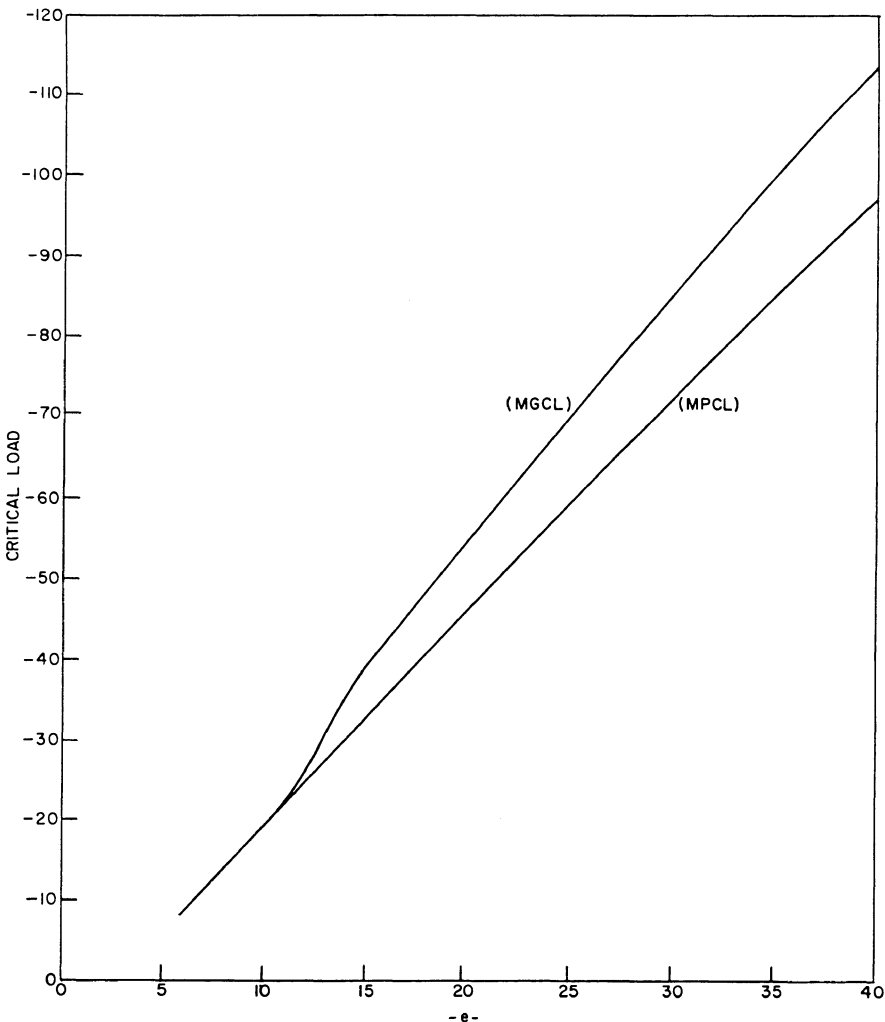


FIGURE 7.12. Nondimensional critical load versus initial rise parameter e (the clamped arch; constant load, infinite duration).

ponding critical impulse is defined as a minimum possible critical impulse and is given by

$$(MPCI) = -\sqrt{10.5407e^2 - 134.48}. \quad (78)$$

The right-hand side of eq. (78) is obtained by evaluating the total potential at the zero-load saddle points and taking the square root of it. The negative sign is in accordance with the sign convention used.

When there is no possibility of unbuckled motion the corresponding critical impulse is obtained as follows. The expression for the zero-load total potential

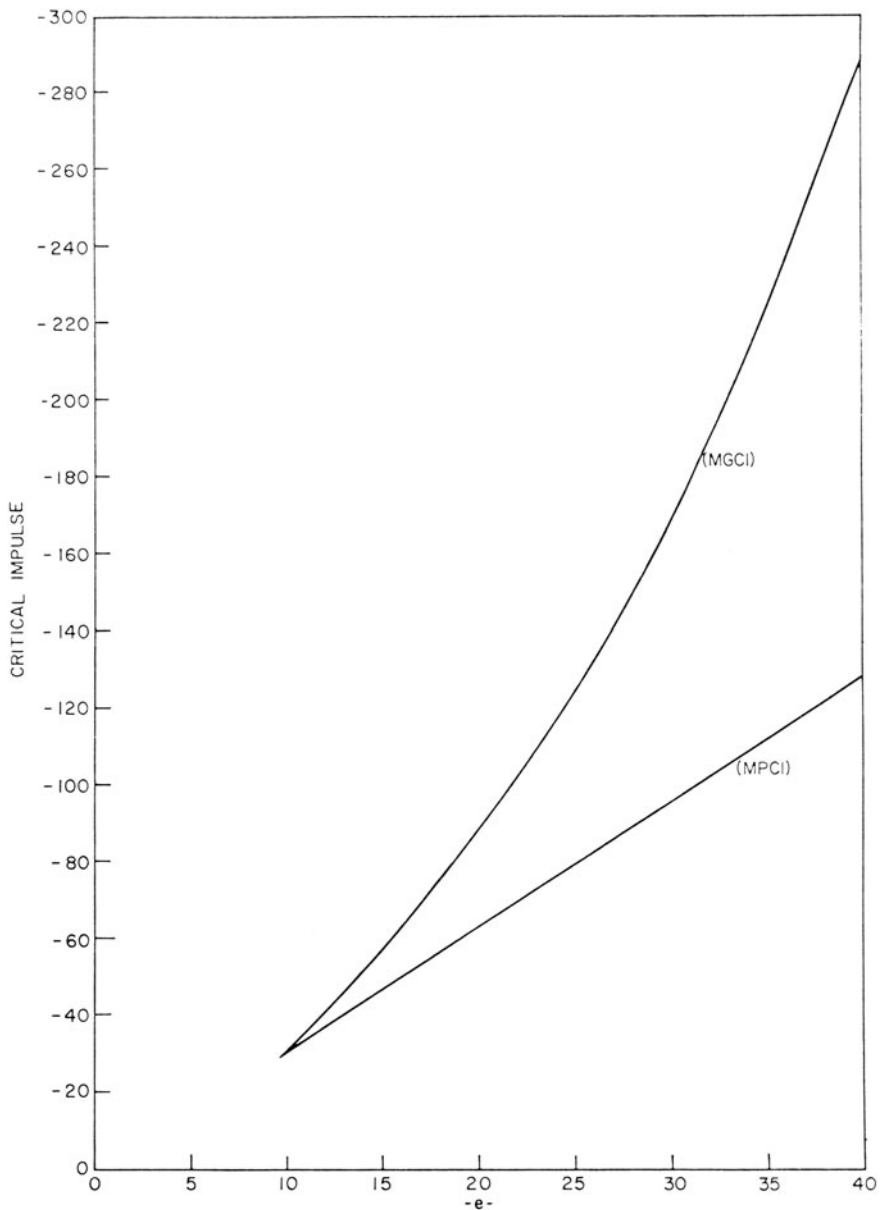


FIGURE 7.13. Nondimensional critical impulse versus initial rise parameter e (the clamped arch).

is first written for $a_1 = 0$:

$$U_T = 16 \left(r_1 - \frac{4e}{3\pi} \right)^2 + 256 \left(r_1 - \frac{4e}{15\pi} \right)^2 + \frac{1}{8} \left(4r_1^2 + 16r_2^2 - \frac{1856e^2}{225\pi^2} \right)^2. \quad (79)$$

The value of U_T is obtained at the symmetric unstable equilibrium position through computations for various values of e . Denoting these values of U_T by U_{T_2} , one can write

$$(MGCI) = (U_{T_2})^{1/2}. \quad (80)$$

Values of (MPCI) and (MGCI) are plotted versus the initial rise parameter in Figure 7.13.

7.4.4 Summary of Results for the Clamped Arch

The overall results for this problem are very similar to the results of the pinned arch problem.

For quasi-static application of the load there is no possibility of a snap-through phenomenon for $e < 5.0$. For $5 < e < 12.2$ snap-through occurs, and the governing initial deformation mode is symmetric. It should be noted, however, that for $9.73 < e < 12.2$ the initial deformation mode at the critical load is symmetric but the asymmetric mode can be followed at some later time. For values of $e > 12.2$ the governing initial deformation mode is asymmetric (a bifurcation point on the load-displacement curve has been reached), and the critical load is given by eq. (72).

Values of the critical load are plotted versus the initial rise parameter e in Figure 7.11. In this figure, the theoretical and experimental results obtained by Gjelsvik and Bodner [18] for a clamped, circular low arch are also shown for comparison. The agreement between theory [18] and experiment is obviously good. The theoretical two-term solution of Gjelsvik and Bodner predicts lower critical loads than the present two-term solution by as much as 20% for larger values of e . Two-term solution refers to two symmetric modes and one antisymmetric mode, which is equivalent to the two-term solution of Gjelsvik and Bodner. This difference in results is due to the difference in the initial shape of the arch. However, because of the close agreement between theoretical and experimental results of [18], it is postulated that the present two-term solution yields sufficient approximations for arches with a half-sine-wave initial shape and clamped edges.

In the case of load of constant magnitude, infinite duration, there is no possibility of a snap-through phenomenon for $e < 5.86$. For $5.86 < e < 9.73$ snap-through can occur, and the corresponding critical load is uniquely determined. For $e > 9.73$ the critical load is bracketed between a lower bound (MPCL) and an upper bound (MGCL). The expression for the lower bound is given by eq. (73). The upper bound for $9.73 < e < 14.50$ is found numerically by solving eq. (75) and eqs. (76), while for $e > 14.50$ the upper bound is given by eq. (77). The results are plotted versus the initial rise parameter e in Figure 7.12.

Finally, in the case of an ideal impulsive load snap-through is possible for $e > 9.73$ and the critical impulse is bracketed between an upper bound (MGCI) and a lower bound (MPCI). The two bounds are plotted versus the initial rise parameter e in Figure 7.13. The (MPCI) is given by eq. (78), while the determination of the upper bound required machine computations.

References

1. Hoff, N.J., and Bruce, V.G. Dynamic analysis of the buckling of laterally loaded flat arches. *J. Math. Phys.*, 32, C, 1954, 276–288.
2. Lock, M.H. The snapping of a shallow sinusoidal arch under a step pressure load. *AIAA J.*, 4, 7, 1966, 1249–1256.
3. Hsu, C.S. On dynamic stability of elastic bodies with prescribed initial conditions. *Int. J. Eng. Sci.*, 4, 1966, 1–21.
4. Hsu, C.S. The effect of various parameters on the dynamic stability of a shallow arch. *J. Appl. Mech.*, 34, 2, 1967, 349–358.
5. Hsu, C.S. Stability of shallow arches against snap-through under timewise step loads. *J. Appl. Mech.*, 35, 1, 1968, 31–39.
6. Hsu, C.S., Kuo, C.T., and Lee, S.S. On the final states of shallow arches on elastic foundations subjected to dynamic loads. *J. Appl. Mech.*, 35, 4, 1968, 713–723.
7. Simitses, G.J. Dynamic Snap-Through Buckling of Flow Arches and Shallow Spherical Caps. Ph.D. Dissertation, Department of Aeronautics and Astronautics, Stanford University, June 1965.
8. Budiansky, B., and Roth, R.S. Axisymmetric dynamic buckling of clamped shallow spherical shells. Collected Papers on Instability of Shell Structures. NASA TN D-1510, 1962, 597–606.
9. Fulton, R.E., and Barton, F.W. Dynamic buckling of shallow arches. *J. Eng. Mech. Div., ASCE*, 97, EM3, 1971, 865–877.
10. Lo, D.L.C., and Masur, E.F. Dynamic buckling of shallow arches. *J. Eng. Mech. Div., ASCE*, 102, EM3, 1976, 901–917.
11. Huang, N.C., and Nachbar, W. Dynamic snap-through of imperfect viscoelastic shallow arches. *J. Appl. Mech.*, 35, 2, 1968, 289–296.
12. Gregory, W.E., Jr., and Plaut, R.H. Dynamic stability boundaries for shallow arches. *J. Eng. Mech. Div., ASCE*, 108, EM6, 1982, 1036–1050.
13. Donaldson, M.T., and Plaut, R.H. Dynamic stability boundaries for a sinusoidal shallow arch under pulse loads. *AIAA J.*, 21, 3, 1983, 469–471.
14. Johnson, E.R. The effect of damping on dynamic snap-through. *J. Appl. Mech.*, 47, 3, 1980, 601–606.
15. Ariaratnam, S.T., and Sankar, T.S. Dynamic snap-through of shallow arches under stochastic loads. *AIAA J.*, 6, 5, 1968, 798–802.
16. Sundararajan, V., and Kumani, D.S. Dynamic snap-buckling of shallow arches under inclined loads. *AIAA J.*, 10, 8, 1972, 1090–1091.
17. Huang, K.Y., and Plaut, R.H. Snap-through of a shallow arch under pulsating load. *Stability in the Mechanics of Continua* (edited by F.H. Schroeder), pp. 215–223. Springer-Verlag, Berlin, 1982.
18. Gjelsvik, A., and Bodner, S.R. The energy criterion and snap buckling of arches. *J. Eng. Mech. Div., ASCE*, 88, EMS, 1962, 87–104.

8

The Shallow Spherical Cap

8.1 Introduction

Shallow spherical configurations, such as domes with small height-to-span ratios, can be subjected to sudden loads of various spatial distributions. Because of this, the designer of such systems is interested in their response and in particular in the level of the load under which snap-through can take place. This, of course, is a primary consideration in the design of these configurations.

Most of the analyses found in the literature and reported here assume that the loads are applied uniformly or at the minimum are axisymmetric. They also are either applied impulsively (ideal impulse that is instantaneously imparted into the system as initial velocity) or are of constant magnitude and infinite duration. Some studies consider step loads of constant magnitude and finite duration.

First, a historical perspective of the problem is presented. The emphasis here is on what has been reported in relation to the dynamic buckling of spherical caps.

The first reported study, by Suhara [1] in 1960, dealt with the response of a shallow cap subjected to a suddenly applied uniform pressure of infinite duration. A buckling configuration, geometrically similar to that found in the static analyses, was employed and an axisymmetric solution to the dynamic equations was obtained by a variational method, with an analog computer used to integrate the equations of motion. The study was of a rather qualitative nature since the author concluded that a more accurate deflection function should have been employed. In 1962, Budiansky and Roth [2] treated the case of a cap under a constant uniform pressure applied suddenly for a finite time. The initial cap geometry was taken to be a paraboloid of revolution and the response was assumed to be axisymmetric. The frequently used Budiansky–Roth criterion (see Chapter 1) was suggested and successfully used in this work [2] to determine critical pressures as a function of duration time. Details of their reported results appear in two reports that are cited as references 2 and 3 in their paper. Critical pressures are presented versus duration time for one value of the spherical cap rise parameter ($\lambda = 5$). Moreover, they present critical impulse values for several rise parameter values λ . They also compared

these results with results reported for this load case (ideal impulse) by Humphreys and Bodner [3]. They concluded that their results and those of [3] must not be taken seriously for λ values larger than five or six. The most important reason given is that the assumption of axisymmetric response is not a good one for deeper caps. For these caps the deformation is expected to be nonaxisymmetric.

In 1965 the present author treated the same problem in his Ph.D. thesis [4] and presented criteria and results for a wide range of cap rise parameter values λ . This work is presented in detail in later sections. The developed criterion has already been presented and discussed in Chapter 1. According to this criterion, the critical conditions may be bracketed between a lower bound (minimum possible critical load, MPCL) and an upper bound (minimum guaranteed critical load, MGCL).

Humphreys, Roth, and Zatlers [5] performed a series of experiments in a large shock tube on the dynamic buckling threshold of shallow spherical caps. The purpose of these experiments was to test the analytical method and buckling criterion proposed in [2]. They reported that the theoretical predictions of critical pressures are 10 to 20% higher than the experimentally observed values. The reason for the discrepancy and the applicability of the analysis are discussed by the authors.

Experiments were also performed and reported by Lock, Okubo, and Whittier [6]. Some of their findings are reported in a later section in this chapter, in which a comparison of various analytical and experimental results is presented.

Several studies followed these initial works and most of them employed the Budiansky–Roth criterion. In order to apply this criterion, a quantitative measure of the response is needed (see Chapters 1 and 2). Some of the studies use the change in cap volume per unit of initial volume, while others consider the displacement of the crown point.

In applying the Budiansky–Roth criterion, certain difficulties were encountered and discussed by some investigators. For example, plots of maximum response versus load magnitude did not always exhibit a clear and distinct sudden jump in the maximum response and therefore a critical load could not clearly be identified by this criterion. Other difficulties were observed and “fixes” have been proposed by some of the investigators. The studies that employed the Budiansky–Roth criterion or some modification of it include those of Archer and Lange [7], Huang [8], Stephens and Fulton [9], and Stricklin and Martinez [10].

Another criterion has been discussed in connection with primarily spherical caps, when acted on by symmetric (axisymmetric) loads [11–14]. Snap-through buckling often involves asymmetric components of the response [15]. This new criterion is based on an initial growth or a significant growth of the asymmetric component. However, since it is possible to have substantial asymmetric response without snapping, this criterion has not gained in popularity.

Fairly extensive reviews on the subject have been presented by Ball [16] and by Holzer [17].

Several extensions have appeared in the literature with regard to dynamic buckling of spherical caps. These extensions include the effect of initial geometric imperfections [18, 19], of applying two or more independent loads on shallow caps [20] as well as on a lattice dome [21], and of polar and circumferential stiffening [22]. Attention was also given to the effect of orthotropy [23], of inelastic material behavior [19], and of the presence of holes [23]. In addition, the effect of damping has been discussed by Mescall and Tsui [24].

Finally, dynamic buckling studies of shallow space trusses [21, 25] and shallow space frames [26] have also been reported. In these geometries snapping can be either local or global, and critical conditions are identified with both modes of failure.

Results of these investigations will be discussed further in later sections. The emphasis, though, is placed on results obtained by the author and his collaborators.

8.2 General Formulation

A shallow spherical cap of perfect geometry and clamped boundaries is loaded under uniform lateral pressure q^* for the following timewise distributions of the load:

- $\alpha)$ Quasi-static application of the load.
- $\beta)$ Load of constant magnitude, infinite duration.
- $\gamma)$ Ideal impulsive load.

Critical loads and impulses are found for the above timewise distribution load cases under the following simplifying assumptions:

- i. The deformation is taken to be rotationally symmetric.
- ii. Rotatory and in-plane kinetic energies are considered small compared to the normal kinetic energy.¹
- iii. The effect of shear forces on deformations is neglected.

The approach used here is similar to the one used in the arch problems. The basic geometry and notation for a perfect shallow spherical cap are shown in Figure 8.1. The nonlinear strain-displacement and curvature-displacement relations known as the shallow shell or Marguerre equations are taken from [29]. The sign convention is the same as the one used by Vlasov [30, p. 309]. Under the assumption of rotationally symmetric deformations, the following

¹This assumption is justified in [27] and [28].

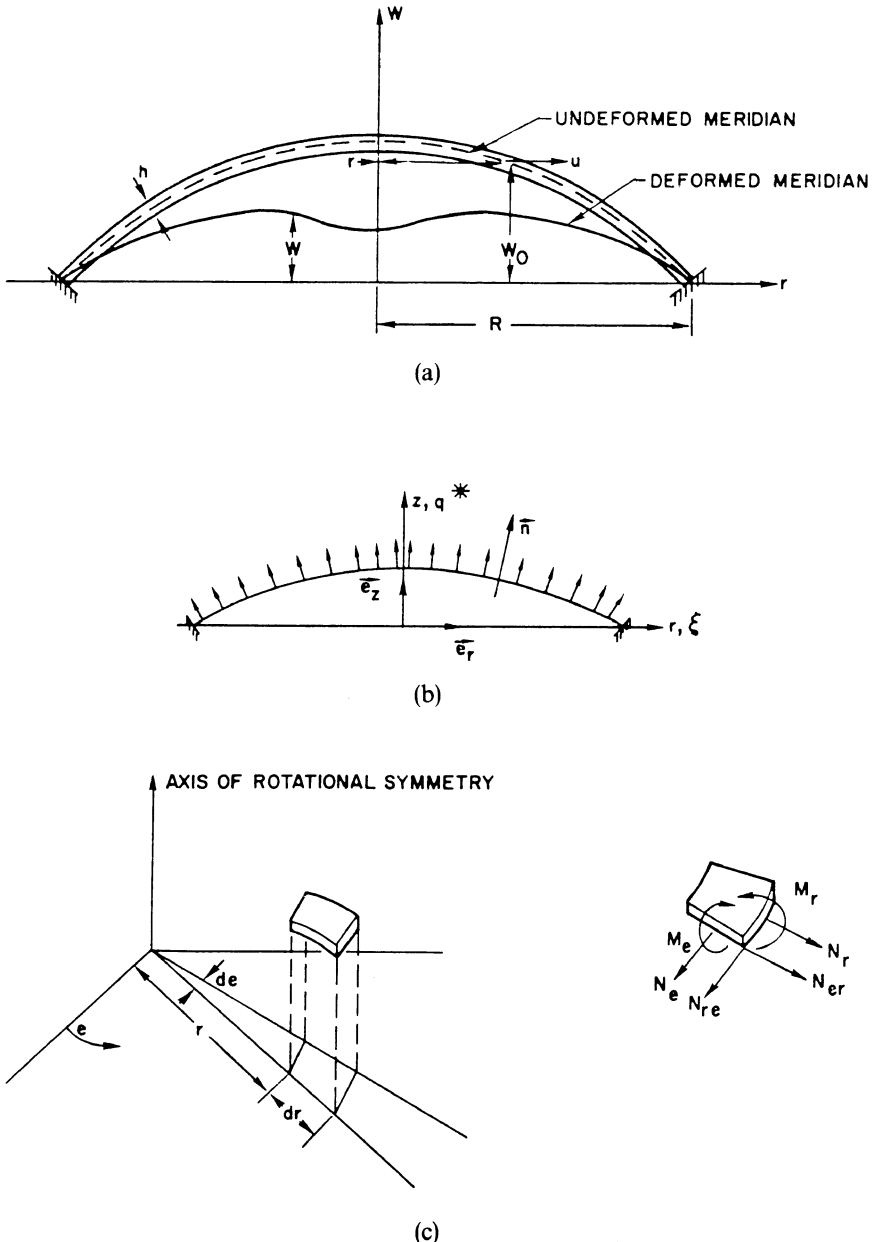


FIGURE 8.1. The spherical cap: Geometry and sign convention. (a) Geometry: $w_0 = (w_0)_{\max} [1 - (r/R)^2]$. (b) Loading: $\bar{q}^* = q^* \bar{n}$. (c) Internal force and moment sign convention.

basic relations can be written:

$$\left. \begin{aligned} \varepsilon_{r_m} &= u_{,r} + \frac{1}{2}(w_{,r}^2 - w_{0,r}^2), \\ \varepsilon_{\theta_m} &= \frac{u}{r}, \\ \gamma_{r\theta_m} &= 0; \end{aligned} \right\} \quad (1)$$

$$\left. \begin{aligned} \kappa_r &= -(w_{,rr} - w_{0,rr}), \\ \kappa_\theta &= -\frac{1}{r}(w_{,r} - w_{0,r}), \\ \kappa_{r\theta} &= 0; \end{aligned} \right\} \quad (2)$$

$$\left. \begin{aligned} N_r &= \frac{Eh}{1-\nu^2}(\varepsilon_{r_m} + \nu\varepsilon_{\theta_m}), \\ N_\theta &= \frac{Eh}{1-\nu^2}(\varepsilon_{\theta_m} + \nu\varepsilon_{r_m}), \end{aligned} \right\} \quad (3)$$

$$\left. \begin{aligned} N_{r\theta} &= \frac{Eh}{2(1+\nu)}\gamma_{r\theta_m}; \\ M_r &= -D(\kappa_r + \nu\kappa_\theta), \\ M_\theta &= -D(\kappa_\theta + \nu\kappa_r), \\ M_{r\theta} &= D(1-\nu)\kappa_{r\theta}; \end{aligned} \right\} \quad (4)$$

where

$$D = \frac{Eh^3}{12(1-\nu^2)}.$$

On the basis of the assumptions made, the following expressions may be written for the different types of energies:

$$\left. \begin{aligned} T^* &= \pi\sigma h \int_0^R w_{,r}^2 r dr, \\ U_{m_T}^* &= \frac{\pi}{Eh} \int_0^R [(N_r + N_\theta)^2 - 2(1+\nu)N_r N_\theta] r dr, \\ U_{b_T}^* &= \pi D \int_0^R [(\kappa_r + \kappa_\theta)^2 - 2(1-\nu)\kappa_r \kappa_\theta] r dr, \\ U_{p_T}^* &= -2\pi q^*(t) \int_0^R (w - w_0) r dr, \\ U_T^* &= U_{m_T}^* + U_{b_T}^* + U_{p_T}^*. \end{aligned} \right\} \quad (5)$$

Since only $U_{m_T}^*$ depends on the displacement u , the equation of motion in the r direction (in-plane equilibrium) is obtained by extremizing $U_{m_T}^*$ with

respect to $u(r, t)$. The result is the following ordinary differential equation:

$$N_\theta - (rN_r)_{,r} = 0. \quad (6)$$

Furthermore, from eqs. (1) and eqs. (3) one may write

$$\begin{aligned} N_r - N_\theta &= \frac{Eh}{1+v} \left[r \frac{d}{dr} \left(\frac{u}{r} \right) + \frac{1}{2} (w_{,r}^2 - w_{0,r}^2) \right] \\ &= \frac{Eh}{1+v} \left[r \frac{1}{Eh} \frac{d}{dr} (N_\theta - vN_r) + \frac{1}{2} (w_{,r}^2 - w_{0,r}^2) \right], \end{aligned}$$

and the following compatibility equation is derived:

$$\frac{d}{dr} (N_r + N_\theta) + \frac{Eh}{2r} (w_{,r}^2 - w_{0,r}^2) = 0. \quad (7)$$

Next, the in-plane equilibrium equation, eq. (6), in its force or displacement version; the compatibility relation, eq. (7); and the boundary conditions in u are used to express U_{mT}^* and consequently U_T^* entirely in terms of the displacement w and its space-dependent derivatives. By multiplying eq. (6) by rN_r and integrating from 0 to R one obtains

$$\int_0^R rN_r N_\theta dr = \frac{R^2}{2} (N_r)_R^2. \quad (8)$$

Integration of the compatibility equation from r to R yields

$$(N_r + N_\theta) = (N_r + N_\theta)_R + \frac{Eh}{2} \int_r^R \frac{1}{r} (w_{,r}^2 - w_{0,r}^2) dr. \quad (9)$$

The boundary conditions on u are

$$\begin{aligned} u &= \text{finite} & \text{at } r = 0, \\ u &= 0 & \text{at } r = R. \end{aligned}$$

The last one implies that

$$\left. \begin{aligned} \varepsilon_\theta &= 0 & \text{at } r = R \\ \text{and consequently} \\ N_\theta &= vN_r & \text{at } r = R. \end{aligned} \right\} \quad (10)$$

For the boundary condition, eq. (10), the following important relation is obtained:

$$(N_r)_R = \frac{1}{1+v} (N_r + N_\theta)_R \quad (11)$$

where $(\)_R$ is the value of the parameter at $r = R$.

From the displacement version of the equilibrium equation, eq. (6), one may write

$$\frac{d}{dr} \left(u_r + \frac{u}{r} \right) + \frac{1-v}{2} (w_{,r}^2 - w_{0,r}^2) + \frac{r}{2} \frac{d}{dr} (w_{,r}^2 - w_{0,r}^2) = 0,$$

and on dividing by r the above equation becomes

$$\frac{d}{dr} \left[\frac{1}{r} \frac{d}{dr} (ru) \right] + \frac{1-v}{2r} (w_{,r}^2 - w_{0,r}^2) + \frac{1}{2} \frac{d}{dr} (w_{,r}^2 - w_{0,r}^2) = 0.$$

Integration from r to R and use of the boundary condition $(u)_R = 0$ yields

$$(u_{,r})_R - \frac{1}{r} \frac{d}{dr} (ru) + \frac{1-v}{2} \int_r^R \frac{1}{r} (w_{,r}^2 - w_{0,r}^2) dr - \frac{1}{2} (w_{,r}^2 - w_{0,r}^2)_R \\ + \frac{1}{2} (w_{,r}^2 - w_{0,r}^2)_R = 0.$$

Next, multiplying this equation by r , integrating from 0 to R , and using the boundary conditions on u , the following equation is obtained:

$$\frac{R^2}{2} (u_{,r})_R - \frac{1}{2} \int_0^R r (w_{,r}^2 - w_{0,r}^2) dr + \frac{1-v}{2} \int_0^R r \left[\int_r^R \frac{1}{r} (w_{,r}^2 - w_{0,r}^2) dr \right] dr \\ + \frac{1}{2} \int_0^R r (w_{,r}^2 - w_{0,r}^2)_R dr = 0.$$

Solving the above equations for $(u_{,r})_R$,

$$(u_{,r})_R = \frac{1}{R^2} \int_0^R \left[(w_{,r}^2 - w_{0,r}^2) - (w_{,r}^2 - w_{0,r}^2)_R - (1-v) \int_r^R \frac{1}{r} (w_{,r}^2 - w_{0,r}^2) dr \right] r dr. \quad (12)$$

Since

$$(N_r + N_\theta)_R = \frac{Eh}{1-v} [u_{,r} + \frac{1}{2} (w_{,r}^2 - w_{0,r}^2)]_R,$$

by using eq. (12)

$$(N_r + N_\theta)_R = \frac{Eh}{(1-v)R^2} \int_0^R \left[(w_{,r}^2 - w_{0,r}^2) - (w_{,r}^2 - w_{0,r}^2)_R - (1-v) \int_0^r \frac{1}{r} (w_{,r}^2 - w_{0,r}^2) dr \right. \\ \left. - (w_{0,r}^2)_R dr + \int_0^r \frac{1}{r} (w_{,r}^2 - w_{0,r}^2) dr \right] r dr + \frac{Eh}{2(1-v)} (w_{,r}^2 - w_{0,r}^2)_R. \quad (13)$$

Substitution of eq. (13) into eq. (9) gives the following result:

$$(N_r + N_\theta) = \frac{Eh}{(1-v)R^2} \int_0^R \left[(w_{,r}^2 - w_{0,r}^2) - (w_{,r}^2 - w_{0,r}^2)_R \right. \\ \left. - (1-v) \int_0^r \frac{1}{r} (w_{,r}^2 - w_{0,r}^2) dr + \int_0^r \frac{1}{r} (w_{,r}^2 - w_{0,r}^2) dr \right] r dr \\ + \frac{Eh}{2(1-v)} (w_{,r}^2 - w_{0,r}^2)_R + \frac{Eh}{2} \int_0^R \frac{1}{r} (w_{,r}^2 - w_{0,r}^2) dr \\ - \frac{Eh}{2} \int_0^r \frac{1}{r} (w_{,r}^2 - w_{0,r}^2) dr. \quad (14a)$$

Note that the above expression is independent of the boundary conditions in w . For the case of clamped boundary conditions

$$\left. \begin{array}{ll} w = 0 & \text{at } r = R, \\ w_{,r} = w_{0,r} & \text{at } r = R. \end{array} \right\} \quad (15)$$

Use of these boundary conditions simplifies the expression for $(N_r + N_\theta)$:

$$\begin{aligned} (N_r + N_\theta) = & \frac{Eh}{(1-v)R^2} \int_0^R \left[(w_{,r}^2 - w_{0,r}^2) - (1-v) \int_0^R \frac{1}{r} (w_{,r}^2 - w_{0,r}^2) dr \right. \\ & \left. + (1-v) \int_0^r \frac{1}{r} (w_{,r}^2 - w_{0,r}^2) dr \right] r dr + \frac{Eh}{2} \int_0^R \frac{1}{r} (w_{,r}^2 - w_{0,r}^2) dr \\ & - \frac{Eh}{2} \int_0^r \frac{1}{r} (w_{,r}^2 - w_{0,r}^2) dr. \end{aligned} \quad (14b)$$

Finally, using eq. (14b), eq. (11), and eq. (8), the stretching energy can be expressed solely in terms of w and its space-dependent derivatives:

$$\begin{aligned} U_{\text{mT}}^* = & \pi Eh \int_0^R \left\{ \frac{1}{(1-v)R^2} \int_0^R \left[(w_{,r}^2 - w_{0,r}^2) - (1-v) \int_0^R \frac{1}{r} (w_{,r}^2 - w_{0,r}^2) dr \right. \right. \\ & \left. + (1-v) \int_0^R \frac{1}{r} (w_{,r}^2 - w_{0,r}^2) dr \right] r dr + \frac{1}{2} \int_0^R \frac{1}{r} (w_{,r}^2 - w_{0,r}^2) dr \\ & \left. - \frac{1}{2} \int_0^r \frac{1}{r} (w_{,r}^2 - w^{20,r}) dr \right\}^2 r dr \\ & - \frac{\pi Eh}{(1+v)(1-v)^2 R^2} \left\{ \int_0^R \left[(w_{,r}^2 - w_{0,r}^2) - (1-v) \int_0^R \frac{1}{r} (w_{,r}^2 - w_{0,rr}^2) dr \right. \right. \\ & \left. + (1-v) \int_0^r \frac{1}{r} (w_{,r}^2 - w_{0,r}^2) dr \right] r dr \left. \right\}^2. \end{aligned} \quad (16)$$

Note that in deriving eq. (16), the boundary conditions on w , eq. (15), were used.

The bending energy may be expressed in terms of the normal displacement w and its space-dependent derivatives. From eq. (12) one may write

$$\begin{aligned} \kappa_r + \kappa_\theta &= -w_{,rr} - \frac{1}{r} w_{,r} + w_{0,rr} + \frac{1}{r} w_{0,r} \\ &= -(w - w_0)_{,rr} - \frac{1}{r} (w - w_0)_{,r} \\ &= -\nabla_*^2(w - w_0) \end{aligned}$$

where the operator ∇_*^2 is the Laplacean operator in polar coordinates for the rotationally symmetric case

$$\nabla_*^2 = \frac{d^2}{dr^2} + \frac{1}{r} \frac{d}{dr}.$$

Furthermore

$$\begin{aligned}\kappa_r \kappa_\theta &= (w - w_0)_{,rr} \left(\frac{1}{r} \right) (w - w_0)_{,r} \\ &= \frac{1}{2r} \frac{d}{dr} [(w - w_0)_{,r}^2].\end{aligned}$$

Substitution of these expressions into the expression for the bending energy, eq. (5), yields

$$U_{b_T}^* = \pi D \left[\int_0^R \{\nabla_*^2(w - w_0)\}^2 r dr - (1 - v)(w - w_0)_{,r} \Big|_0^R \right].$$

Using the boundary conditions on w and recognizing that for rotationally symmetric displacements

$$w_{,r} = w_{0,r} \quad \text{at } r = 0,$$

the expression for the bending energy assumes the simple form

$$U_{b_T}^* = \pi D \int_0^R [\nabla_*^2(w - w_0)]^2 r dr. \quad (17)$$

8.2.1 Nondimensionalization

It is convenient to nondimensionalize all the dimensional quantities. The different types of energy and consequently the total potential are nondimensionalized by using the following relations:

$$\begin{aligned}\xi &= \frac{r}{R}, \quad \eta = \frac{w}{h}, \quad \eta_0 = \frac{w_0}{h}; \\ (\)' &= \frac{d}{d\xi}, \quad \nabla^2 = \frac{d^2}{d\xi^2} + \frac{1}{\xi} \frac{d}{d\xi}, \quad \tau = t \left[\frac{\pi Eh^2}{(1 - v)^2 \sigma R^4} \right]^{1/2}; \\ Q(\xi, \tau) &= \frac{(1 - v)^2 R^4}{Eh^4} q^*(r, t), \quad \text{Imp} = (1 - v) \sqrt{\frac{\sigma}{2E}} \left(\frac{R}{h} \right)^2 \text{Imp}^*;\end{aligned}$$

where Imp^* represents the impulse per unit of mass imparted to the shell by the loading.

$$U = \frac{(1 - v)^2 R^2}{\pi Eh^5} U^*$$

where U stands for all the types of energy and the total potential. Using the quantities defined above, the nondimensionalized total potential becomes

$$\begin{aligned}U_T &= \int_0^1 \left\{ (\eta'^2 - \eta_0'^2) - (1 - v) \int_0^1 \frac{1}{\xi} (\eta'^2 - \eta_0'^2) d\xi + (1 - v) \int_0^\xi \frac{1}{\xi} (\eta'^2 - \eta_0'^2) d\xi \right\} \xi d\xi \\ &+ \frac{1 - v}{2} \int_{\eta_0}^1 \frac{1}{\xi} (\eta'^2 - \eta_0'^2) d\xi - \frac{1 - v}{2} \int_0^\xi \frac{1}{\xi} (\eta'^2 - \eta_0'^2) d\xi \Big\}^2 \xi d\xi\end{aligned}$$

$$\begin{aligned}
& -\frac{1}{1+v} \left\{ \int_0^1 \left[(\eta'^2 - \eta'_0)^2 - (1-v) \int_0^1 \frac{1}{\xi} (\eta'^2 - \eta'_0)^2 d\xi \right. \right. \\
& + (1-v) \int_0^1 \frac{1}{\xi} (\eta'^2 - \eta'_0)^2 d\xi \left. \right] \xi d\xi \right\}^2 \\
& + \frac{1-v}{12(1+v)} \int_0^1 [\nabla^2(\eta - \eta_0)]^2 \xi d\xi - 2Q \int_0^1 (\eta - \eta_0) \xi d\xi. \tag{18}
\end{aligned}$$

8.2.2 General Procedures

The initial shape of the midsurface is taken to be spherical, and the meridional curve is approximated by the following parabola:

$$\eta_0(\xi) = e(1 - \xi^2).$$

The spherical cap is assumed to be clamped along its circular boundary. Thus the boundary conditions in nondimensional form become

$$\left. \begin{array}{l} \eta(1, \tau) = 0, \\ \eta'(1, \tau) = \eta'_0(1). \end{array} \right\} \tag{19}$$

The nondimensional vertical displacement, $\eta - \eta_0$, is expressed in terms of the following series:

$$\eta - \eta_0 = \sum_{n=1}^{\infty} a_n(\tau) [J_0(k_n^{(1)} \xi) - J_0(k_n^{(1)})] \tag{20}$$

where $k_n^{(1)}$ are the zeros of $J_1(x) = 0$, and the time-dependent coefficients $a_n(\tau)$ become undetermined constants for the quasi-static load case. Each term of the series in eq. (20) satisfies the boundary conditions in w , eqs. (19). The time-dependent coefficients for the dynamic cases may be thought of as generalized coordinates, and the time history of the displacements is completely defined in terms of these generalized coordinates. In the mathematical work that follows, these coefficients will simply be denoted by a_n , and it will be understood that they are time dependent for the dynamic load cases to be considered.

The functions $[J_0(k_n^{(1)} \xi) - J_0(k_n^{(1)})]$ represent the buckling modes (rotationally symmetric) of a flat circular plate uniformly compressed around its circumstances (see [31]).

Before substituting the displacement functions, eq. (20), into the expression for the total potential, eq. (18), it is necessary to define certain definite and indefinite integrals. All the definite integrals are evaluated by use of the properties of Bessel functions and/or machine computations.

From eq. (20), by first differentiating it with respect to ξ , one obtains

$$\eta'^2 - \eta'_0^2 = \sum_{n=1}^{\infty} \sum_{m=1}^{\infty} a_n a_m (k_n^{(1)})(k_m^{(1)}) J_1(k_n^{(1)} \xi) J_1(k_m^{(1)} \xi) - 4e \sum_{n=1}^{\infty} a_n k_n^{(1)} j_0(k_n^{(1)} \xi)$$

where (\cdot) denote differentiation with respect to the argument $(k_n^{(1)}\xi)$. Dividing both sides by ξ and integrating from zero to ξ ,

$$\int_0^\xi \frac{1}{\xi} (\eta'^2 - \eta_0'^2) d\xi = \sum_{n=1}^{\infty} \sum_{m=1}^{\infty} a_n a_m \phi_{nm}(\xi) + 4e \sum_{n=1}^{\infty} a_n [1 - J_0(k_n^{(1)}\xi)] \quad \left. \right\} (21)$$

where

$$\phi_{nm}(\xi) = \phi_{mn}(\xi) = \int_0^\xi \frac{(k_n^{(1)}) (k_m^{(1)})}{\xi} J_1(k_n^{(1)}\xi) J_1(k_m^{(1)}\xi) d\xi.$$

Use of the following properties of Bessel functions (see [32])

$$\begin{aligned} \int_0^x x^{n+1} J_n(x) dx &= x^{n+1} J_{n+1}(x), \\ [J_1'(k_n^{(1)})]^2 &= [-J_0(k_n^{(1)})]^2 = [J_2(k_n^{(1)})]^2 \end{aligned}$$

yields

$$\int_0^1 \xi (\eta'^2 - \eta_0'^2) d\xi = \sum_{n=1}^{\infty} a_n J_0(k_n^{(1)}) [\frac{1}{2} a_n (k_n^{(1)})^2 J_0(k_n^{(1)}) - 4e]. \quad (22)$$

Similarly, since

$$\nabla^2(\eta - \eta_0) = - \sum_{n=1}^{\infty} a_n (k_n^{(1)})^2 J_0(k_n^{(1)}\xi)$$

use of eq. (24) of [32, p. 70] yields

$$\int_0^1 \xi [\nabla^2(\eta - \eta_0)]^2 d\xi = \frac{1}{2} \sum_{n=1}^{\infty} a_n^2 (k_n^{(1)})^4 [J_0(k_n^{(1)})]^2. \quad (23)$$

Finally,

$$\int_0^1 \xi (\eta - \eta_0) d\xi = \sum_{n=1}^{\infty} a_n \psi_n \quad \left. \right\} (24)$$

where

$$\psi_n = \int_0^1 [J_0(k_n^{(1)}\xi) - J_0(k_n^{(1)})] \xi d\xi.$$

Substitution of eqs. (21) through (24) into the expression for the total potential, eq. (18), yields

$$\begin{aligned} U_T &= \int_0^1 \left[\sum_{n=1}^{\infty} a_n J_0(k_n^{(1)}) \{ \frac{1}{2} a_n J_0(k_n^{(1)}) - 4e \} \right. \\ &\quad \left. + (1-v) \int_0^1 \left\{ \sum_{n=1}^{\infty} \sum_{m=1}^{\infty} a_n a_m \phi_{nm}(\xi) + 4e \sum_{n=1}^{\infty} a_n [1 - J_0(k_n^{(1)}\xi)] \right\} \xi d\xi \right. \\ &\quad \left. - \frac{1-v}{2} \left(\sum_{n=1}^{\infty} \sum_{m=1}^{\infty} a_n a_m \phi_{nm}(\xi) + 4e \sum_{n=1}^{\infty} a_n [1 - J_0(k_n^{(1)}\xi)] \right) \right]^2 \xi d\xi \end{aligned}$$

$$\begin{aligned}
& -\frac{1}{1+v} \left[\sum_{n=1}^{\infty} a_n J_0(k_n^{(1)}) \left\{ \frac{1}{2} a_n (k_n^{(1)})^2 J_0(k_n^{(1)}) - 4e \right\} \right. \\
& - \frac{1-v}{2} \left\{ \sum_{n=1}^{\infty} \sum_{m=1}^{\infty} a_n a_m \phi_{nm}(1) + 4e \sum_{n=1}^{\infty} a_n [1 - J_0(k_n^{(1)})] \right\} \\
& + (1-v) \int_0^1 \left\{ \sum_{n=1}^{\infty} \sum_{m=1}^{\infty} a_n a_m \phi_{nm}(\xi) + 4e \sum_{n=1}^{\infty} a_n [1 - J_0(k_n^{(1)} \xi)] \right\} \xi d\xi \Big]^2 \\
& \left. + \frac{1-v}{24(1-v)} \sum_{n=1}^{\infty} a_n^2 (k_n^{(1)})^4 [J_0(k_n^{(1)})]^2 - 2Q \sum_{n=1}^{\infty} a_n \psi_n \right]. \quad (25)
\end{aligned}$$

By performing the indicated operations and by defining certain integrals involving Bessel functions, the total potential may be expressed as a polynomial of the fourth degree in the generalized coordinates a_i :

$$\left. \begin{aligned}
\alpha_{nm} &= \int_0^1 \xi \phi_{nm}(\xi) d\xi, \\
\gamma_{nmpq} &= \int_0^1 \xi \phi_{nm}(\xi) \phi_{pq}(\xi) d\xi, \\
\zeta_{nm} &= \int_0^1 [1 - J_0(k_n^{(1)} \xi)] [1 - J_0(k_m^{(1)} \xi)] \xi d\xi, \\
\tau_{nmp} &= \int_0^1 \xi \phi_{nm}(\xi) [1 - J_0(k_p^{(1)} \xi)] d\xi,
\end{aligned} \right\} \quad (26)$$

and

$$\begin{aligned}
U_T = & \frac{1}{2} \left[\frac{1}{2} \sum_{n=1}^{\infty} a_n^2 (k_n^{(1)})^2 J_0^2(k_n^{(1)}) + 4e \sum_{n=1}^{\infty} a_n \left\{ \frac{1-v}{2} - J_0(k_n^{(1)}) \right\} \right. \\
& + (1-v) \sum_{n=1}^{\infty} \sum_{m=1}^{\infty} a_n a_m \alpha_{nm} \Big]^2 + \left(\frac{1-v}{2} \right)^2 \sum_{n=1}^{\infty} \sum_{m=1}^{\infty} \sum_{p=1}^{\infty} \sum_{q=1}^{\infty} a_n a_m a_p a_q \gamma_{nmpq} \\
& + 4(1-v)^2 e^2 \sum_{n=1}^{\infty} \sum_{m=1}^{\infty} a_n a_m \zeta_{nm} - (1-v) \left[\frac{1}{2} \sum_{n=1}^{\infty} a_n^2 (k_n^{(1)})^2 J_0^2(k_n^{(1)}) \right. \\
& + 4e \sum_{n=1}^{\infty} a_n \left\{ \frac{1-v}{2} - J_0(k_n^{(1)}) \right\} + (1-v) \sum_{n=1}^{\infty} \sum_{m=1}^{\infty} a_n a_m \alpha_{nm} \Big] \\
& \times \left[2e \sum_{p=1}^{\infty} a_p + \sum_{p=1}^{\infty} \sum_{q=1}^{\infty} a_p a_q \alpha_{pq} \right] + 2e(1-v) \sum_{n=1}^{\infty} \sum_{m=1}^{\infty} \sum_{p=1}^{\infty} a_n a_m a_p \tau_{nmp} \\
& - \frac{1}{1+v} \left[\frac{1}{2} \sum_{n=1}^{\infty} a_n^2 (k_n^{(1)})^2 J_0^2(k_n^{(1)}) - 2(1-v)e \sum_{n=1}^{\infty} a_n J_0(k_n^{(1)}) \right. \\
& + (1-v) \sum_{n=1}^{\infty} \sum_{m=1}^{\infty} a_n a_m \left\{ \alpha_{nm} - \frac{1}{2} \phi_{nm}(1) \right\} \Big]^2 \\
& \left. + \frac{1-v}{24(1+v)} \sum_{n=1}^{\infty} a_n^2 (k_n^{(1)})^4 J_0^2(k_n^{(1)}) - 2Q \sum_{n=1}^{\infty} a_n \psi_n \right]. \quad (27)
\end{aligned}$$

8.3 Numerical Procedures and Results

8.3.1 Procedure for Static Analysis

By the principle of the stationary value of the total potential, the following relations must hold for static equilibrium.

$$\begin{aligned}
 & \left[\frac{1}{2} \sum_{m=1}^{\infty} a_m^2 (k_m^{(1)})^2 J_0^2(k_m^{(1)}) + 4e \sum_{m=1}^{\infty} a_m \left\{ \frac{1-v}{2} - J_0(k_m^{(1)}) \right\} \right. \\
 & \quad \left. + (1-v) \sum_{m=1}^{\infty} \sum_{p=1}^{\infty} a_m a_p \alpha_{mp} \right] \times [a_n(k_n^{(1)})^2 J_0^2(k_n^{(1)}) - 4e J_0(k_n^{(1)})] \\
 & + (1-v)^2 \sum_{m=1}^{\infty} \sum_{p=1}^{\infty} \sum_{q=1}^{\infty} a_m a_p a_q \gamma_{nmpq} + 8(1-v)^2 e^2 \sum_{m=1}^{\infty} a_m \zeta_{nm} \\
 & - (1-v) \left[2e \sum_{m=1}^{\infty} a_m + \sum_{m=1}^{\infty} \sum_{p=1}^{\infty} a_m a_p \alpha_{mp} \right] \\
 & \times \left[a_n(k_n^{(1)})^2 J_0^2(k_n^{(1)}) + 4e \left\{ \frac{1-v}{2} - J_0(k_n^{(1)}) \right\} + 2(1-v) \sum_{q=1}^{\infty} a_q \alpha_{nq} \right] \\
 & + 6e(1-v) \sum_{m=1}^{\infty} \sum_{p=1}^{\infty} a_m a_p \tau_{nmp} + \frac{2}{1+v} \left[\frac{1}{2} \sum_{m=1}^{\infty} a_m^2 (k_m^{(1)})^2 J_0^2(k_m^{(1)}) \right. \\
 & \quad \left. - 2e(1+v) \sum_{m=1}^{\infty} a_m J_0(k_m^{(1)}) + (1-v) \sum_{m=1}^{\infty} \sum_{p=1}^{\infty} a_m a_p \{ \alpha_{mp} - \frac{1}{2} \phi_{mp}(1) \} \right] \\
 & \times \left[a_n(k_n^{(1)})^2 J_0^2(k_n^{(1)}) - 2e(1+v) J_0(k_n^{(1)}) + 2(1-v) \sum_{q=1}^{\infty} a_q \{ \alpha_{nq} - \frac{1}{2} \phi_{nq}(1) \} \right] \\
 & + \frac{1-v}{12(1+v)} a_n(k_n^{(1)})^4 J_0^2(k_n^{(1)}) - 2Q\psi_n = 0
 \end{aligned} \tag{28}$$

where $n = 1, 2, 3, \dots$.

The infinite system of these equations, eqs. (28), in a_n and Q represents effectively the load-deflection relation, or the relation between the load Q and a nondimensional volume $\Delta V/V_0$, displaced during deformation.

$$\begin{aligned}
 \Delta V &= - \int_0^R \int_0^{2\pi} (w - w_0)r dr d\theta = - 2\pi R^2 h \sum_{n=1}^{\infty} a_n \psi_n, \\
 V_0 &= \int_0^R \int_0^{2\pi} w_0 r dr d\theta = \frac{\pi R^2 h e}{2},
 \end{aligned}$$

and finally

$$\frac{\Delta V}{V_0} = - \frac{4}{e} \sum_{n=1}^{\infty} a_n \psi_n. \tag{29}$$

Since the load Q becomes critical when the equilibrium becomes unstable

(in the small), at Q_{cr} the following relation must hold:

$$\begin{vmatrix} \frac{\partial^2 U_T}{\partial a_1^2} & \frac{\partial^2 U_T}{\partial a_1 \partial a_2} & \dots & \frac{\partial^2 U_T}{\partial a_1 \partial a_n} \\ \frac{\partial^2 U_T}{\partial a_2 \partial a_1} & \frac{\partial^2 U_T}{\partial a_2^2} & \dots & \frac{\partial^2 U_T}{\partial a_2 \partial a_n} \\ \vdots & \vdots & & \vdots \\ \frac{\partial^2 U_T}{\partial a_n \partial a_1} & \frac{\partial^2 U_T}{\partial a_n \partial a_2} & \dots & \frac{\partial^2 U_T}{\partial a_n^2} \end{vmatrix} = 0. \quad (30)$$

The simultaneous solution of eqs. (28) and eq. (30) yields Q_{cr} (the largest in magnitude) and the corresponding values of a_n or, by using eq. (29), the corresponding value of $\Delta V/V_0$.

The numerical procedure that was actually used in generating results is explained in a later section.

8.3.2 Procedure for Sudden Loads of Infinite Duration

In this load case the load Q_D is considered to be critical when the unstable equilibrium point is reached with zero kinetic energy ($U_T + T = 0$); therefore $U_T = 0$, and thus buckled motion is possible. The critical load $Q_{D_{cr}}$ is found by solving simultaneously eqs. (28) and $U_T = 0$ [see eq. (27)]. Note that at this particular equilibrium point (saddle point) the value of the determinant in eq. (30) must be negative.

8.3.3 Procedure for Ideal Impulse

For this load case it is assumed that the ideal impulsive loading is imparted uniformly into the shell as initial kinetic energy before any displacement takes places. If Imp^* represents the impulse per unit mass imparted to the shell by the loading, then

$$\text{Imp}^* d_m = \left(\frac{\partial w}{\partial t} \right)_i d_m \quad \text{or} \quad \text{Imp}^* = \left(\frac{\partial w}{\partial t} \right)_i.$$

Since

$$T_i^* = \int_0^R \int_0^{2\pi} \frac{\sigma h}{2} \left(\frac{\partial w}{\partial t} \right)_i r dr d\theta,$$

then

$$T_i^* = \frac{\sigma h \pi R^2}{2} (\text{Imp}^*)^2.$$

Nondimensionalizing T_i^* and Imp^* , one may write

$$\text{Imp}_n = T_i^{1/2} \quad (31)$$

where

$$\text{Imp} = (1 - \nu) \sqrt{\frac{\sigma}{2E}} \left(\frac{R}{h} \right)^2 \text{Imp}^*.$$

Furthermore, since the system is conservative so that

$$T + U_T = \text{const.} = T_i + U_{T_i} = T_i$$

the impulse (or the initial kinetic energy) is considered critical if the zero-load unstable static equilibrium point is reached with zero kinetic energy. Thus, buckled motion is possible, and

$$(\text{Imp})_{\text{cr}} = (U_T)_{\text{cr}}^{1/2} \quad (32)$$

where $(U_T)_{\text{cr}}$ is the value of the total potential at the zero-load unstable static equilibrium point. The unstable static equilibrium point is found by solving eqs. (28) setting $Q_D = 0$, subject to the condition that the value of the determinant in eq. (30) is negative.

8.3.4 Approximate Numerical Solution and Results

Before proceeding with the different approximate solutions by taking a finite number of terms in the series representation of the displacement w , it is convenient to introduce some new parameters. These new parameters will facilitate comparison with existing theoretical as well as experimental results.

Since the classical critical buckling pressure for the complete sphere is given by

$$q_{\text{cl}}^* = \frac{2Eh^2}{\sqrt{3(1 - \nu^2)a^2}},$$

it is convenient to define the ratio

$$\rho_{\text{cr}} = \frac{q_{\text{cr}}^*}{q_{\text{cl}}^*}.$$

Using the expression for q_{cr}^* ,

$$q_{\text{cr}}^* = -\frac{Eh^4}{(1 - \nu)^2 R^4} Q_{\text{cr}},$$

one finally obtains

$$\rho_{\text{cr}} = -\frac{\sqrt{3(1 - \nu^2)} Q_{\text{cr}}}{8(1 - \nu)^2 e_2}. \quad (33)$$

Furthermore, a new initial rise parameter λ is introduced, which is mathematically defined by

$$\lambda = 2[3(1 - \nu^2)]^{1/4} \left(\frac{w_{0,\text{max}}}{h} \right)^{1/2},$$

and since $w_{0\max} = eh$, then

$$\lambda = 2[3(1 - \nu^2)]^{1/4}e^{1/2}. \quad (34)$$

One- and two-term approximations are used to represent the deflected shapes, and the desired results are obtained by examining the total potential surface in the configuration space of the generalized coordinates a_1 and a_2 . Instead of solving systems of nonlinear algebraic equations as indicated in Section 8.3.1, a computer program is written that gives values of the total potential at closely spaced points in the configuration space for different values of the load and initial rise parameter. At every value of the initial rise parameter λ , the calculations are carried out for different values of the load parameter Q by using small increments in Q to ensure accuracy in predicting critical loads. Thus, a family of potential surfaces is obtained. At $Q = 0$ the square root of the value of the total potential at the unstable equilibrium position represents the nondimensional critical impulse for the case of the ideal impulsive load. As the load is increased in absolute value, the near stable and the unstable static equilibrium points approach each other, and the value of the total potential at the unstable point decreases. At some value of the load Q , the value of the total potential at the unstable static equilibrium point becomes zero and buckled motion is possible. This value of the load represents the magnitude of the critical load for the case of constant load, infinite duration. As the absolute value of the load is further increased, the

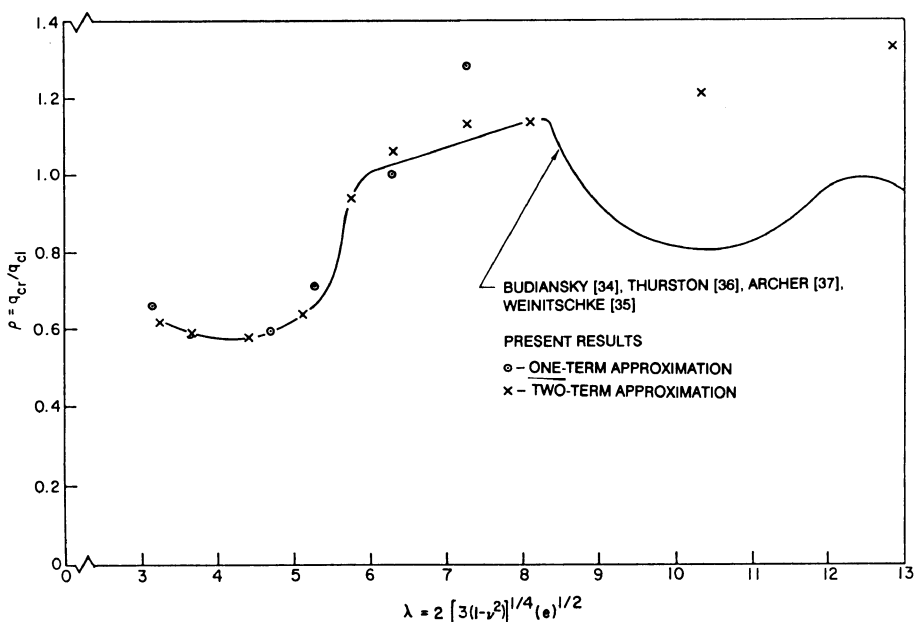


FIGURE 8.2. Critical pressure ratio ρ versus initial rise parameter λ (the spherical cap; quasi-static).

near static equilibrium point becomes unstable and the corresponding load represents the critical load for the case of quasi-static application of the load.

The results are shown in Figures 8.2, 8.3, and 8.4. In Figure 8.2, the pressure ratio parameter ρ for quasi-static loads is plotted versus the initial rise parameter λ , and the one- and two-term solutions are compared to the well-known solution of Budiansky [34], Weinitzschke [35], Thurston [36], and Archer [37]. The present solution shows that snap-through buckling is possible for $\lambda > 3.15$. The two-term solution is a good approximation for values of λ up to 8.3.

In Figure 8.3 the pressure parameter ρ is plotted versus the initial rise parameter λ for the case of constant load, infinite duration. The value calculated by Budiansky and Roth [2] is in excellent agreement with the two-term solution. The two-term solution is a good approximation as long as the deflection shape at the unstable equilibrium point can be well approximated when the total potential vanishes at this point (critical dynamic load). This deformation shape, which corresponds to a postbuckled equilibrium shape under quasi-static loading, can be well represented by two terms in the series for values of λ up to 10. Because of this, the two-term solution is believed to be a good approximation for values of λ up to 10.

In Figure 8.4, critical impulses are plotted versus the initial rise parameter λ . The present solution is compared with those of Humphreys and Bodner [3] and Budiansky and Roth [2]. For the same reasons as in the case of

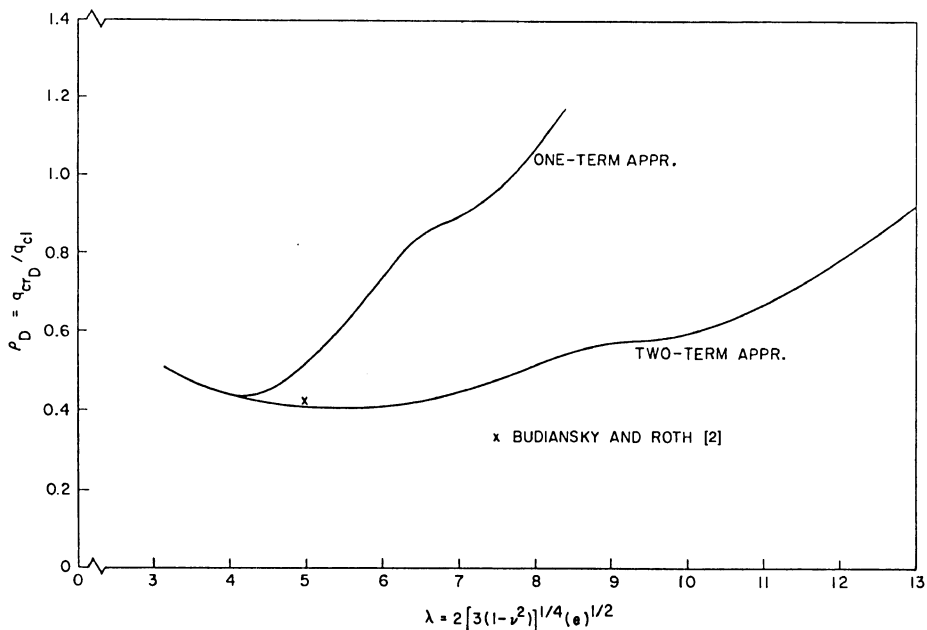


FIGURE 8.3. Critical pressure ratio ρ_D versus initial rise parameter λ (the spherical cap; constant load, infinite duration).

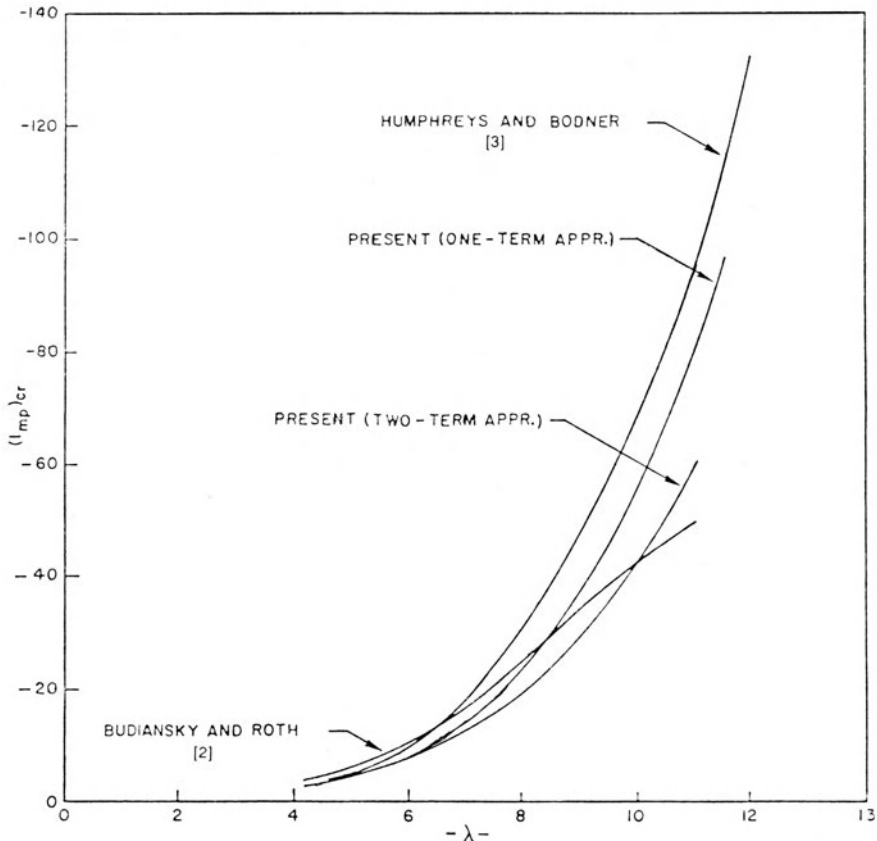


FIGURE 8.4. Nondimensional critical impulse versus initial rise parameter λ (the spherical cap).

constant load, infinite duration, the two-term solution is believed to be a good approximation for values of λ up to 10.

If a solution to all three cases of timewise distribution of the load is desired for higher values of λ , more terms must be taken in the series representation of the deflected shape. For λ values greater than six, it is more important to consider the effect of asymmetric modes than to improve the approximation obtained under the assumption of axisymmetric deformations.

8.3.5 Observations

Snap-through buckling of shallow spherical shells is possible under dynamic loads. For the ideal impulsive load case, buckling is possible if a far stable static equilibrium point exists. Such equilibrium points exist when $\lambda \geq 4.2$.

The two-term approximate solution is good up to $\lambda = 8.3$ for quasi-static loads. For dynamic loads, the solution is believed to be good up to $\lambda = 10$.

It is seen from the results obtained that when the load is suddenly applied, the critical load is less than that for quasi-static loads. The reduction is anywhere from 22 to 65%, depending on the value of the initial rise parameter λ for $\lambda \leq 10$.

Using Reissner's criterion of shallowness for spherical caps [33],

$$\frac{(w_0)_{\max}}{R} < \frac{1}{6},$$

the following limitation is deduced for the initial rise parameter λ :

$$72\lambda^2 \leq [3(1 - v^2)]^{1/2} \left(\frac{a}{h} \right).$$

On this basis, the results of the present analysis are applicable to shallow spherical caps with ratios of radius of curvature to thickness between 400 and 4,000 (approximately).

If buckling loads are to be used as a design criterion, the stresses must be of such magnitude and direction that no plasticity effects have appeared in the prebuckling states.

8.4 Comparison with Other Solutions

On Figures 8.3 and 8.4 a limited comparison of the approximate results obtained by the method discussed in this chapter and those reported by Budiansky and Roth [2] is presented. Moreover, on Figure 8.4 the analytical results obtained by Humphreys and Bodner [2] are shown. All of the results shown on Figure 8.4 are obtained by assuming axisymmetric response. Because of this assumption, it is doubtful that these results are applicable for λ values greater than six or seven. In this range the response is expected to be asymmetric.

As already mentioned in the introduction, several solutions to the spherical cap problem appeared in the literature in the 1960s and later, following the initial attempt by Suhara [1].

A comparison of the results reported for the case of constant load of infinite duration is presented here in both tabular and graphical forms.

Table 8.1 presents critical pressure ratios for different rise parameters as reported by the various investigators. The first column refers to rise parameters, while the next two give upper and lower bounds as obtained by the two-term approximation presented in this chapter. The next six columns refer to the analytical results of Huang [8], Stricklin and Martinez [10], and Ball and Burt [11]. Finally, the experimental results of Lock, Okubo, and Whittier [6] appear in the last column.

All the analytical results assume axisymmetric response except those of Stricklin and Martinez [10] and those of Ball and Burt [11]. Their results suggest that asymmetric modes have some influence on the critical load.

TABLE 8.1. Critical pressure ratios for different rise parameters.

λ	ρ_{cr}			Stricklin and Martinez [10]		Budiansky and Roth [2]		Ball and Burt [11]		Experimental [6]
		MGCL	MGCL	Huang [8]	Stephens and Fulton [9]	Axisym.	Asym.	Axisym.	Asym.	
3.3	0.47	0.62								
3.75		0.58								
4.0	0.42	0.57	0.45	0.44	0.43					
4.5	0.41	0.58								
5.0	0.40	0.62	0.49	0.48	0.45	0.424	0.48	0.48		
5.5	0.39	0.76								
5.75	0.38	0.98								
6.0	0.38	1.03								
6.5	0.38	1.08								
7.0	0.40	1.11	0.56	0.56	0.51					
7.5	0.42	1.13	0.50	0.50	0.44	0.62	0.54	0.51	0.39	-0.43
8.0	0.45	1.15	0.44	0.47	0.40	0.48	0.48	0.48		

Because of the approximate nature of all the reported results, it is difficult to say at what λ values this influence is significant.

It should be noted that the energy method employed here provides a true lower bound only for the mechanical system for which the energy is actually formulated. Thus, if a continuous system is approximated by an n -degree-of-freedom discrete system, the resulting lower bounds are true only for the discrete system. The extent of applicability of the discrete system bounds to the continuous system depends on the accuracy of the approximation. The two-term solution should provide an accurate lower bound (MPCL) for $\lambda \leq 7.0$, a range for which the behavior is expected to be axisymmetric. The comparison with the solutions obtained from other criteria reinforces this conjecture.

References

1. Suhara, J., Snapping of shallow spherical shells under static and dynamic loadings. ASRL TR 76-4, Aeroelastic and Structures Research Laboratory, Cambridge, Mass., June 1960.
2. Budiansky, B., and Roth, R.S. Axisymmetric dynamic buckling of clamped shallow spherical caps. *Collected Papers on Instability of Shells Structures*. NASA TN D-1510, Washington, D.C., 1962, 597–606.
3. Humphreys, J.S., and Bodner, S.R. Dynamic buckling of shells under impulsive loading. *J. Eng. Mech. Div., ASCE*, 88, EML, 1962, 17–36.
4. Simitses, G.J. (a) Dynamic snap-through buckling of low arches and shallow spherical caps. Ph.D. Dissertation, Stanford University, 1965; (b) Dynamic snap-through buckling of shallow spherical caps. *Proc. Seventh AIAA/ASME Structures and Materials Conference*, Cocoa Beach, Fla., April 1966, 112–124; (c) Axisymmetric dynamic snap-through buckling of shallow spherical caps. *AIAA J.*, 5, 5, 1967, 1019–1021.
5. Humphreys, J.S., Roth, R.S., and Zatlers, J. Experiments on dynamic buckling of shallow spherical shells under shock loading. *AIAA J.*, 3, 1, 1965, 33–39.
6. Lock, M.H., Okubo, S., and Whittier, J.S. Experiments on the snapping of a shallow dome under a step pressure load. *AIAA J.*, 6, 7, 1968, 1320–1326.
7. Archer, R.R., and Lange, C.G. Nonlinear dynamic behavior of shallow spherical shells. *AIAA J.*, 3, 2, 1965, 2313–2317.
8. Huang, N.C. Axisymmetric dynamic snap-through of elastic clamped shallow spherical shells. *AIAA J.*, 7, 2, 1969, 215–220.
9. Stephens, W.B., and Fulton, R.E. Axisymmetric static and dynamic buckling of spherical caps due to centrally distributed pressures. *AIAA J.*, 7, 11, 1969, 2120–2126.
10. Stricklin, J.A., and Martinez, J.E. Dynamic buckling of clamped spherical shells under step pressure loadings. *AIAA J.*, 7, 6, 1969, 1212–1213.
11. Ball, R.E., and Burt, J.A. Dynamic buckling of shallow spherical shells. *J. Appl. Mech.*, 40, 2, 1973, 411–416.
12. Akkas, N. Bifurcation and snap-through phenomena in asymmetric dynamic analysis of shallow spherical shells. *Comput. Struct.*, 6, 1976, 241–251.
13. Svalbonas, V., and Kalnins, A. Dynamic buckling of shells: Evaluation of various methods. *Nucl. Eng. Des.*, 44, 1977, 331–356.

14. Ball, R.E., and Shutt, M.D. Buckling of shallow spherical shells—the significance of the pole conditions. *J. Appl. Mech.*, 46, 3, 1979, 710–711.
15. Huang, N.C. Unsymmetrical buckling of shallow spherical shells. *J. Appl. Mech.*, 31, 3, 1964, 447–457.
16. Ball, R.E. Dynamic buckling of structures. *Shock and Vibration Computer Programs: Reviews and Summaries* (edited by W. Pilkey and B. Pilkey), pp. 299–321. Shock and Vibration Information Center, Washington, D.C., 1975.
17. Holzer, S.M. Dynamic snap-through of shallow arches and spherical caps. *Shock Vibration Digest*, 11, 3, 1979, 3–6.
18. Kao, R., and Perrone, N. Dynamic buckling of axisymmetric spherical caps with initial imperfections. *Comput. Struct.*, 9, 1978, 463–473.
19. Kao, R. Nonlinear dynamic buckling of spherical caps with initial imperfections. *Comput. Struct.*, 12, 1, 1980, 49–63.
20. Kato, S., and Matsuoka, O. A new method for dynamic buckling analysis of rotational shells by combined use of finite element and mode superposition methods. *Application of Computer Methods in Engineering*, vol. 1 (edited by L.C. Wellford), pp. 97–106. University of Southern California, 1977.
21. Coan, C.H., and Plaut, R.H. Dynamic stability of a lattice dome. *J. Earthquake Eng. Struct. Dyn.*, 11, 2, 1983, 269–274.
22. Blackmon, C.M., and Simitses, G.J. Snap-through buckling of eccentrically stiffened shallow spherical caps. *Int. J. Solids Struct.*, 11, 9, 1975, 1035–1049.
23. Alwar, R.S., and Reddy, B.S. Dynamic buckling of isotropic and orthotropic shallow spherical caps with circular hole. *Int. J. Mech Sci.*, 21, 1979, 681–688.
24. Mescall, J., and Tsui, T. Influence of damping on the dynamic stability of spherical caps under step pressure loading. *AIAA J.*, 9, 7, 1971, 1244–1248.
25. Holzer, S.M. Static and dynamic stability of reticulated shells. *Stability of Structures Under Static and Dynamic Loads*, Proceedings of an International Colloquium, Washington, D.C., May 1977, ASCE Publications, pp. 27–39.
26. Belytschko, T., Schwer, L., and Klein, M.J. Large displacement, transient analysis of space frames. *Int. J. Numer. Methods Eng.*, 11, 1977, 65–84.
27. Reissner, E. On transverse vibrations of thin shallow elastic shells. *Q. Appl. Math.*, 13, 1955, 169–176.
28. Reissner, E. On axisymmetric vibrations of shallow spherical shells. *Q. Appl. Math.*, 13, 1955, 279–290.
29. Sanders, J.L., Jr. Nonlinear theories for thin shells. *Q. Appl. Math.*, 21, 1963, 21–36.
30. Vlasov, V.Z. General Theory of Shells and Its Applications in Engineering. NASA TT F-9, Washington, D.C., April 1964.
31. Bryan, G.H. Buckling of plates. *Proc. London Math Soc.*, 22, 1891, 54–96.
32. Gray, A., et al. *A Treatise of Bessel Functions*. Macmillan, London, 1931.
33. Reissner, E. Symmetric shallow shells of revolution. *J. Math. Mech.*, 7, 2, 1958, 121–140.
34. Budiansky, B. Buckling of clamped shallow spherical shells. *The Theory of Thin Elastic Shells*. North-Holland, Amsterdam, 1959.
35. Weinitzschke, H.J. On the stability problem for shallow spherical shells. *J. Math. Phys.*, 38, 1960, 209–231.
36. Thurston, G.A. A numerical solution of the nonlinear equations for axisymmetric bending of shallow spherical shells. *J. Appl. Mech.*, 28, 1961, 557–562.
37. Archer, R.R. On the numerical solution of the nonlinear equations for shells of revolution. *J. Math. Phys.*, 40, 3, 1962, 165–180.

9

Thin Cylindrical Shells

9.1 Introduction

Thin cylindrical shells of various constructions have been extensively used as structures or primary components in complex structural configurations. These systems are subjected to destabilizing loads in service, and since these loads are often dynamic in nature, it is not surprising that a great deal of interest was generated in the dynamic stability of cylindrical shells. Most of the analyses make use of monocoque metallic construction, but in this chapter applications to stiffened metallic and laminated composite configurations will also be presented.

Since the late 1950s several studies have been reported on the subject. Most of these studies concentrated on impulsive or step loads and other simple transient loading histories, wherein some inertial forces must be considered.

The initial studies [1–5] concentrated on impulsive and step loads and tried to establish criteria and estimates of critical conditions by carefully analyzing the effect of the sudden loads on the deflectional response of the cylindrical shell. Budiansky and Hutchinson [6–8] provided general results for these configurations by using a modified version of the already discussed Budiansky–Roth criterion. In addition, Budiansky [7] addressed dynamic instability as related to parametric resonance. Special studies of this phenomenon were reported by Goodier and McIvor [5], and Danielson [9].

Dynamic buckling under high-velocity impact was investigated experimentally by Lindberg and Herbert [10]. Through ultrahigh-speed movies, they observed buckles with very short wavelengths. They showed that buckling modes can be predicted with classical buckling theory. Finally, they showed that these modes are random, with statistics determined by the amplification of “white noise” imperfections.

Similar studies were reported by Maymon and Libai [11] and by Zimcik and Tennsyon [12]. Finally, other investigations that provided experiments and experimental results are those of Sunakawa and Kibe [13], Abramowicz and Jones [14, 15], Lindberg et al. [16], and Kirkpatrick and Holmes [17].

The theoretical studies that deal exclusively with impulsive loads are those of Hubka [18] and Lovell and McIvor [19].

Studies that deal with step loads of finite or infinite duration include those of Almroth et al. [20], Tamura and Babcock [21], Lockhart and Amazigo [22], Lockhart [23, 24], and Simitses et al. [25–28].

Before closing this section, mention of a few additional studies is in order. Svalbonas and Kalnins [29] in 1977 presented a review and critique of the various methods of analysis for dynamic buckling of shells. Simitses [30] in 1987 presented a more general review that included all structural problems and phenomena that come under the general heading of dynamic instability. Finally, dynamic instability of a cylindrical shell caused by sudden heating of the shell material is discussed by Ray and Lovell [31].

In this chapter the total potential energy approach is used to arrive at critical conditions for cylindrical shells of isotropic, stiffened isotropic, and laminated composite construction when acted by sudden loads of infinite duration. First, the needed equations are presented, and then static and dynamic critical loads are derived and discussed. Results are presented primarily for the case of uniform axial compression. Some limited results are presented for uniform external pressure.

9.2 Mathematical Formulation

9.2.1 Preliminary Remarks

The governing equations are derived in this section for the following geometry and loading. The thin, circular, cylindrical shell is assumed to be geometrically imperfect. The construction is laminated (each lamina is orthotropic), and the shell is orthogonally and eccentrically stiffened. The stiffeners are uniform and with uniform close spacing, which allows one to employ the “smeared” technique. The boundary conditions can be of any transverse and in-plane variety. This includes free, simply supported, and clamped with all possible in-plane combinations. The loading consists of transverse (lateral pressure) and eccentric in-plane loads, such as uniform axial compression and shear. Eccentric means that the line of action of these loads (applied stress resultants) is not necessarily in the plane of the reference surface. In the derivation of the governing equations, the usual lamination theory is employed. Moreover, thin-shell theory (Kirchhoff–Love hypotheses) and linearly elastic material behavior are assumed. The primary assumptions are listed below:

1. The shell is thin (total smeared thickness is much smaller than the initial average radius of curvature—cylinder radius).
2. Normals remain normal and inextensional.
3. The strains are small, the rotations about the normal are small, and the rotations about in-plane axes are moderate.
4. The imperfection shape is such that the initial curvature is small ($R/w_{ii}^0 \ll 1$);

$i = x, y, w^0$ is the initial geometric imperfection, and R is the cylinder radius).

5. The stiffeners are along principal directions.
6. The stiffener-laminate connections are monolithic.
7. The stiffeners do not carry shear; shear is transmitted entirely by the laminate.
8. The stiffeners are torsionally weak and thus they do not contribute to the shell twisting stiffness (the equations and related programs can easily be changed to accommodate the case of torsionally strong stiffeners).

On the basis of these general assumptions, the field equations are derived, based on Donnell-type kinematic relations. The governing equations consist of the transverse equilibrium equation and the in-plane compatibility equation. These two equations and the proper boundary conditions are

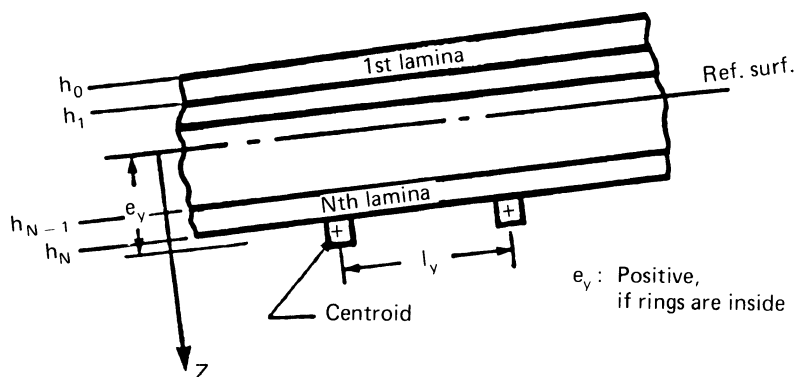
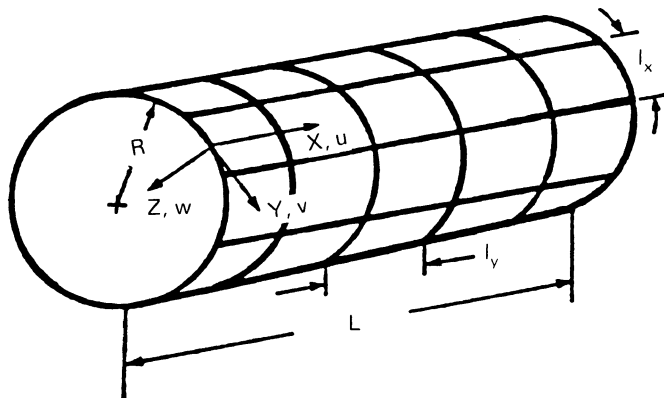


FIGURE 9.1. Geometry.

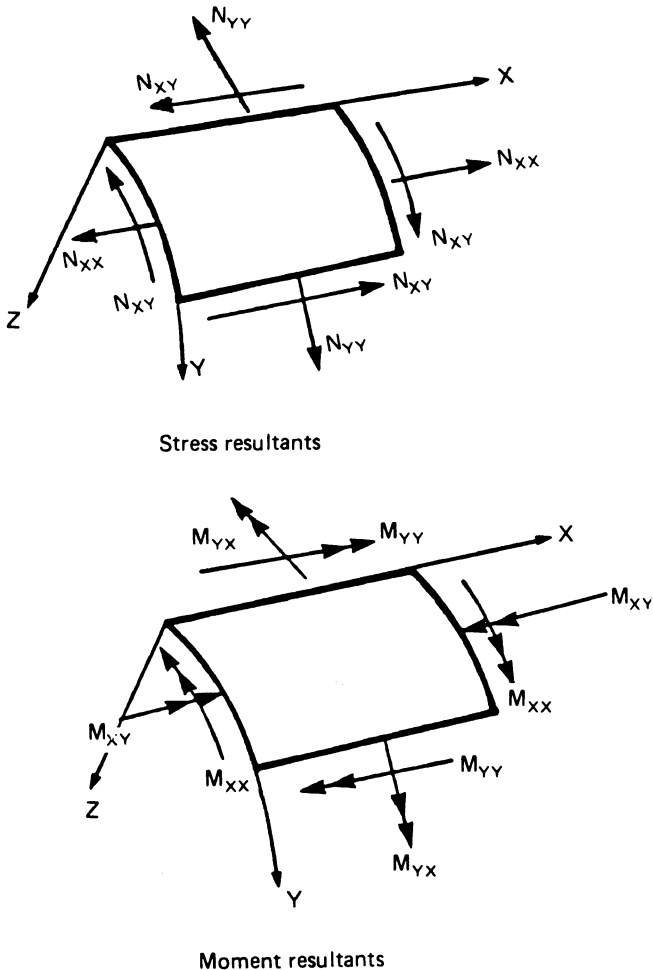


FIGURE 9.2. Sign convention.

expressed in terms of the transverse displacement component w and an Airy stress resultant function F .

The geometry and sign convention for this formulation are shown on Figures 9.1 and 9.2.

The topics of kinematic relations, stress and moment resultants, governing equations, boundary conditions, and solution procedure are treated separately.

9.2.2 Kinematic Relations

Let w^0 be measured from the perfectly cylindrical surface to the reference surface of the laminated shell. Let w denote the transverse displacement

component of reference surface material points and be measured from the undeformed surface. Let u and v denote the usual in-plane displacement components along the x and y directions, respectively.

The Donnell-type [32] kinematic relations are given by

$$\begin{aligned}\varepsilon_{xx}^0 &= \varepsilon_{xx}^0 - z\kappa_{xx}, \\ \varepsilon_{yy}^0 &= \varepsilon_{yy}^0 - z\kappa_{yy}, \\ \gamma_{xy}^0 &= \gamma_{xy}^0 - 2z\kappa_{xy},\end{aligned}\quad (1)$$

where the superscript 0 denotes reference surface strains and the κ 's denote the reference surface changes in curvature and torsion. Note that the positive z -direction is inward (see Figure 9.1). According to Donnell, the ε^0 's and κ 's are related to the displacement components by

$$\begin{aligned}\varepsilon_{xx}^0 &= u_{,x} + \frac{1}{2}w_{,x}^2 + w_{,x}w_{,x}^0, \\ \varepsilon_{yy}^0 &= v_{,y} - \frac{w}{R} + \frac{1}{2}w_{,y}^2 + w_{,y}w_{,y}^0, \\ \gamma_{xy}^0 &= u_{,y} + v_{,x} + w_{,x}w_{,y} + w_{,x}w_{,y}^0 + w_{,x}^0w_{,y},\end{aligned}\quad (2)$$

$$\begin{aligned}\kappa_{xx} &= \phi_{x,x} = (w_{,x})_{,x} = w_{,xx}, \\ \kappa_{yy} &= \phi_{y,y} = (w_{,y})_{,y} = w_{,yy}, \\ \kappa_{xy} &= \phi_{x,y} = \phi_{y,x} = w_{,xy}.\end{aligned}\quad (3)$$

9.2.3 Stress–Strain Relations

Each lamina is assumed to be orthotropic and the directions of orthotropy (1, 2) make an angle θ with the in-plane structural axes (x, y).

The orthotropic constitutive (it is assumed that the generalized Hooke's law holds) relations for the k th lamina are given below. Note that for an n -ply laminate k varies from one to n , and the first ply (or lamina) is on the outside, while the n th ply is on the inside (see Figure 9.1).

$$\left\{ \begin{array}{c} \sigma_{11} \\ \sigma_{22} \\ \sigma_{12} \end{array} \right\}^{(k)} = \left[\begin{array}{ccc} Q_{11} & Q_{12} & 0 \\ Q_{12} & Q_{22} & 0 \\ 0 & 0 & Q_{33} \end{array} \right]^{(k)} \left\{ \begin{array}{c} \varepsilon_{11} \\ \varepsilon_{22} \\ 2\varepsilon_{12} \end{array} \right\} \quad (4)$$

where $2\varepsilon_{12} = \gamma_{12}$ and 1, 2 are the orthotropic directions.

Since one is interested in relating the stresses to the strains in the xy frame of axes, the usual transformation relations for second-order tensors are employed (see [33] for details) and the transformed constitutive equations (for the k th ply) become

$$\left\{ \begin{array}{c} \sigma_{xx} \\ \sigma_{yy} \\ \sigma_{xy} \end{array} \right\}^{(k)} = \left[\begin{array}{ccc} \bar{Q}_{11} & \bar{Q}_{12} & 2\bar{Q}_{13} \\ \bar{Q}_{12} & \bar{Q}_{22} & 2\bar{Q}_{23} \\ \bar{Q}_{13} & \bar{Q}_{23} & 2\bar{Q}_{33} \end{array} \right]^{(k)} \left\{ \begin{array}{c} \varepsilon_{xx} \\ \varepsilon_{yy} \\ \varepsilon_{xy} \end{array} \right\} \quad (5)$$

where

$$[\bar{Q}] = [T]^{-1} [Q] [T] \quad (6)$$

and

$$[T] = \begin{bmatrix} \cos^2 \theta & \sin^2 \theta & \sin 2\theta \\ \sin^2 \theta & \cos^2 \theta & -\sin 2\theta \\ -\frac{1}{2} \sin 2\theta & \frac{1}{2} \sin 2\theta & \cos 2\theta \end{bmatrix}. \quad (7)$$

Next, the stress-strain relations for the stiffness are

$$\begin{aligned} \sigma_{xx_{st}} &= E_{st} \epsilon_{xx}, \\ \sigma_{yy_{st}} &= E_r \epsilon_{yy}, \end{aligned} \quad (8)$$

where E_{st} and E_r denote the Young's moduli for stringer and ring material, respectively. Note that according to the smeared-technique assumptions, stiffeners do not transmit shear.

9.2.4 Stress and Moment Resultants

Instead of dealing with stresses, it is more convenient in thin-shell and plate theory to deal with integrated stresses. This leads to the introduction and definition of stress (N_{ij}) and moment (M_{ij}) resultants. For a stiffened laminate these are

$$\begin{Bmatrix} N_{xx} \\ N_{yy} \\ N_{xy} \end{Bmatrix} = \int_{h_0}^{h_n} \begin{Bmatrix} \sigma_{xx} \\ \sigma_{yy} \\ \sigma_{xy} \end{Bmatrix} dz + \int_{A_i} \begin{Bmatrix} \frac{\sigma_{xx_{st}}}{l_x} dA_x \\ \frac{\sigma_{yy_r}}{l_y} dA_y \\ 0 \end{Bmatrix} \quad (9)$$

and

$$\begin{Bmatrix} M_{xx} \\ M_{yy} \\ M_{xy} \end{Bmatrix} = \int_{h_0}^{h_n} z \begin{Bmatrix} \sigma_{xx} \\ \sigma_{yy} \\ \sigma_{xy} \end{Bmatrix} dz + \int_{A_i} \begin{Bmatrix} z \frac{\sigma_{xx_{st}}}{l_x} dA_x \\ z \frac{\sigma_{yy_r}}{l_y} dA_y \\ 0 \end{Bmatrix} \quad (10)$$

where l_x and l_y are the stringer and ring spacings (respectively), A_i denotes the proper stiffener cross-sectional area with A_x denoting stringer area and A_y ring area, and h_0 and h_n denote the outer surface and inner surface coordinates of the laminate (see Figure 9.1). Note also that the above definitions lead to the sign convention shown on Figure 9.2.

Substitution of eqs. (5) and (8) for the stresses in eqs. (9) and (10) [first substitution of eqs. (1) for the strains in eqs. (5) and (8) is needed] and some

minor mathematical operations lead to

$$\begin{aligned} \begin{Bmatrix} N_{xx} \\ N_{yy} \\ N_{xy} \end{Bmatrix} &= \sum_{k=1}^N [\bar{Q}]^{(k)} \int_{h_{k-1}}^{h_k} \left\{ \begin{Bmatrix} \varepsilon_{xx}^0 \\ \varepsilon_{yy}^0 \\ \gamma_{xy}^0 \end{Bmatrix} - z \begin{Bmatrix} \kappa_{xx} \\ \kappa_{yy} \\ 2\kappa_{xy} \end{Bmatrix} \right\} dz \\ &+ \begin{Bmatrix} \frac{E_{st}A_x}{l_x} \varepsilon_{xx}^0 \\ \frac{E_r A_y}{l_y} \varepsilon_{yy}^0 \\ 0 \end{Bmatrix} - \begin{Bmatrix} \frac{E_{st}A_x}{l_x} e_x \kappa_{xx} \\ \frac{E_r A_y}{l_y} e_y \kappa_{yy} \\ 0 \end{Bmatrix}, \end{aligned} \quad (11)$$

$$\begin{aligned} \begin{Bmatrix} M_{xx} \\ M_{yy} \\ M_{xy} \end{Bmatrix} &= \sum_{k=1}^N [\bar{Q}]^{(k)} \int_{h_{k-1}}^{h_k} \left\{ z \begin{Bmatrix} \varepsilon_{xx}^0 \\ \varepsilon_{yy}^0 \\ \gamma_{xy}^0 \end{Bmatrix} - z \begin{Bmatrix} \kappa_{xx} \\ \kappa_{yy} \\ 2\kappa_{xy} \end{Bmatrix} \right\} dz \\ &+ \begin{Bmatrix} \frac{E_{st}A_x}{l_x} e_x \varepsilon_{xx}^0 \\ \frac{E_r A_y}{l_y} e_y \varepsilon_{yy}^0 \\ 0 \end{Bmatrix} - \begin{Bmatrix} \frac{E_{st}}{l_x} (I_{xc} + A_x e_x^2) \\ \frac{E_r}{l_y} (I_{yc} + A_y e_y^2) \\ 0 \end{Bmatrix} \end{aligned} \quad (12)$$

where e_x and e_y are the stiffener eccentricities (positive if on the side of positive z), A_x and A_y the stringer and ring cross-sectional areas, E_{st} and E_r the Young's moduli for the stringer and ring materials, and I_{xc} and I_{yc} the stiffener second moment of areas about centroidal axes.

After performing the indicated operations [eqs.(11) and (12)], one may write

$$\begin{Bmatrix} N_{xx} \\ N_{yy} \\ N_{xy} \\ M_{xx} \\ M_{yy} \\ M_{xy} \end{Bmatrix} = \begin{bmatrix} \bar{A}_{11} & \bar{A}_{12} & \bar{A}_{13} & -\bar{B}_{11} & -\bar{B}_{12} & -\bar{B}_{13} \\ \bar{A}_{12} & \bar{A}_{22} & \bar{A}_{23} & -\bar{B}_{12} & -\bar{B}_{22} & -\bar{B}_{23} \\ \bar{A}_{13} & \bar{A}_{23} & \bar{A}_{33} & -\bar{B}_{13} & -\bar{B}_{23} & -\bar{B}_{33} \\ \bar{B}_{11} & \bar{B}_{12} & \bar{B}_{13} & -\bar{D}_{11} & -\bar{D}_{12} & -\bar{D}_{13} \\ \bar{B}_{12} & \bar{B}_{22} & \bar{B}_{23} & -\bar{D}_{12} & -\bar{D}_{22} & -\bar{D}_{23} \\ \bar{B}_{13} & \bar{B}_{23} & \bar{B}_{33} & -\bar{D}_{13} & -\bar{D}_{23} & -\bar{D}_{33} \end{bmatrix} \begin{Bmatrix} \varepsilon_{xx}^0 \\ \varepsilon_{yy}^0 \\ \gamma_{xy}^0 \\ \kappa_{xx} \\ \kappa_{yy} \\ 2\kappa_{xy} \end{Bmatrix} \quad (13)$$

where

$$[\bar{A}_{ij}] = [A_{ij}] + \begin{bmatrix} \frac{E_{st}A_x}{l_x} & 0 & 0 \\ 0 & \frac{E_r A_y}{l_y} & 0 \\ 0 & 0 & 0 \end{bmatrix}, \quad (14a)$$

$$[\bar{B}_{ij}] = [B_{ij}] + \begin{bmatrix} \frac{E_{st}A_x}{l_x} e_x & 0 & 0 \\ 0 & \frac{E_r A_y}{l_y} e_y & 0 \\ 0 & 0 & 0 \end{bmatrix}, \quad (14b)$$

and

$$[\bar{D}_{ij}] = [D_{ij}] + \begin{bmatrix} \frac{E_{st}}{l_x} (I_{xc} + e_x^2 A_x) & 0 & 0 \\ 0 & \frac{E_r}{l_y} (I_{yc} + e_y^2 A_y) & 0 \\ 0 & 0 & 0 \end{bmatrix} \quad (14c)$$

with

$$\begin{aligned} A_{ij} &= \sum_{k=1}^N \bar{Q}_{ij}^{(k)} (h_k - h_{k-1}) \\ B_{ij} &= \sum_{k=1}^N \bar{Q}_{ij}^{(k)} (h_k^2 - h_{k-1}^2) \\ D_{ij} &= \sum_{k=1}^N \bar{Q}_{ij}^{(k)} (h_k^3 - h_{k-1}^3). \end{aligned} \quad (15)$$

Since in the derivation of the field equations the dependent variables are w and a stress function F (through which the stress resultants are derived), it is convenient to express the moment resultants in terms of the N_{ij} 's and the κ 's.

Starting with eqs. (13), one may write

$$\begin{Bmatrix} N_{xx} \\ N_{yy} \\ N_{xy} \end{Bmatrix} = [\bar{A}_{ij}] \begin{Bmatrix} \varepsilon_{xx}^0 \\ \varepsilon_{yy}^0 \\ \gamma_{xy}^0 \end{Bmatrix} - [\bar{B}_{ij}] \begin{Bmatrix} \kappa_{xx} \\ \kappa_{yy} \\ 2\kappa_{xy} \end{Bmatrix}. \quad (16)$$

From this, one can solve for the strain vector, or

$$\begin{Bmatrix} \varepsilon_{xx}^0 \\ \varepsilon_{yy}^0 \\ \gamma_{xy}^0 \end{Bmatrix} = [\bar{A}_{ij}]^{-1} \begin{Bmatrix} N_{xx} \\ N_{yy} \\ N_{xy} \end{Bmatrix} + [\bar{A}_{ij}]^{-1} [\bar{B}_{ij}] \begin{Bmatrix} \kappa_{xx} \\ \kappa_{yy} \\ 2\kappa_{xy} \end{Bmatrix}. \quad (17)$$

Another form for eq. (17) is the following:

$$\begin{Bmatrix} \varepsilon_{xx}^0 \\ \varepsilon_{yy}^0 \\ \gamma_{xy}^0 \end{Bmatrix} = [a_{ij}] \begin{Bmatrix} N_{xx} \\ N_{yy} \\ N_{xy} \end{Bmatrix} + [b_{ij}] \begin{Bmatrix} \kappa_{xx} \\ \kappa_{yy} \\ 2\kappa_{xy} \end{Bmatrix} \quad (18)$$

where

$$[a_{ij}] = [\bar{A}_{ij}]^{-1}, \quad [b_{ij}] = [\bar{A}_{ij}]^{-1} [\bar{B}_{ij}]. \quad (19)$$

Next, substitution of eqs. (18) into the expression for the moment resultants, eqs. (13), yields

$$\begin{aligned} \begin{Bmatrix} M_{xx} \\ M_{yy} \\ M_{xy} \end{Bmatrix} &= [\bar{B}_{ij}] \begin{Bmatrix} \varepsilon_{xx}^0 \\ \varepsilon_{yy}^0 \\ \gamma_{xy}^0 \end{Bmatrix} - [\bar{D}_{ij}] \begin{Bmatrix} \kappa_{xx} \\ \kappa_{yy} \\ 2\kappa_{xy} \end{Bmatrix} \\ &= [\bar{B}_{ij}] [a_{ij}] \begin{Bmatrix} N_{xx} \\ N_{yy} \\ N_{xy} \end{Bmatrix} + [[\bar{B}_{ij}] [b_{ij}] - [\bar{D}_{ij}]] \begin{Bmatrix} \kappa_{xx} \\ \kappa_{yy} \\ 2\kappa_{xy} \end{Bmatrix} \\ &= [b_{ij}]^T \begin{Bmatrix} N_{xx} \\ N_{yy} \\ N_{xy} \end{Bmatrix} + [d_{ij}] \begin{Bmatrix} \kappa_{xx} \\ \kappa_{yy} \\ 2\kappa_{xy} \end{Bmatrix} \end{aligned} \quad (20)$$

where

$$[d_{ij}] = [\bar{B}_{ij}] [b_{ij}] - [\bar{D}_{ij}]. \quad (21)$$

Note that $[a_{ij}]$ and $[d_{ij}]$ are asymmetric 3×3 matrices, while $[b_{ij}]$ is a nonsymmetric 3×3 matrix.

9.2.5 Equilibrium Equations

The equilibrium equations are derived by employing the principle of the stationary value of the total potential.

According to the principle, for equilibrium

$$\delta U_T = 0 \quad (22)$$

where

$$U_T = U_i + U_p \quad (23)$$

is the sum of the strain energy and the potential of the external forces. From eq. (22) one may write

$$\begin{aligned} \delta U_T &= \delta U_i + \delta U_p = 0 \\ &= \int_0^{2\pi R} \int_0^L (N_{xx} \delta \varepsilon_{xx}^0 + N_{yy} \delta \varepsilon_{yy}^0 + N_{xy} \delta \gamma_{xy}^0 \\ &\quad - M_{xx} \delta \kappa_{xx} - M_{yy} \delta \kappa_{yy} - 2M_{xy} \delta \kappa_{xy}) dx dy \\ &\quad - \int_0^{2\pi R} \int_0^L q \delta w dx dy - \int_0^{2\pi R} (-\bar{N}_{xx} \delta u + \bar{N}_{xy} \delta v \\ &\quad + \bar{Q}_x \delta w - \bar{M}_{xx} \delta w_{,x} - \bar{M}_{xy} \delta w_{,y}) |_0^L dy \end{aligned} \quad (24)$$

where q denotes the external pressure (positive in the positive z direction) and the bar quantities denote external loads applied at the boundaries (\bar{N}_{xx} and \bar{N}_{xy} are in-plane loads, while \bar{Q}_x is transverse shear load and \bar{M}_{xx} and \bar{M}_{xy} are moments). Note that \bar{M}_{xx} and \bar{M}_{xy} could represent moments arising from eccentrically applied \bar{N}_{xx} and \bar{N}_{xy} .

Use of eqs. (2) and (3) to express the variations in the reference surface strains and changes of curvature and torsion in terms of variations in displacement components yields

$$\begin{aligned} \delta U_T = & \int_0^{2\pi R} \int_0^L \left\{ N_{xx} [\delta u_{,x} + w_{,x} \delta w_{,x} + w_{,x}^0 \delta w_{,x}] \right. \\ & + N_{yy} \left[\delta v_{,y} - \frac{1}{R} \delta w + w_{,y} \delta w_{,y} + w_{,y}^0 \delta w_{,y} \right] \\ & + N_{xy} [\delta u_{,y} + \delta v_{,x} + w_{,x} \delta w_{,y} + w_{,y} \delta w_{,x} \\ & + w_{,x}^0 \delta w_{,y} + w_{,y}^0 \delta w_{,x}] - M_{xx} \delta w_{,xx} - M_{yy} \delta w_{,yy} \\ & - 2M_{xy} \delta w_{,xy} \} dx dy - \int_0^{2\pi R} \int_0^L q \delta w dx dy \\ & - \int_0^{2\pi R} \int_0^L [-\bar{N}_{xx} \delta u + \bar{N}_{xy} \delta v + \bar{Q}_x \delta w - \bar{M}_{xx} \delta \phi_x \\ & \left. - \bar{M}_{xy} \delta \phi_y] |_0^L dy. \right\} \end{aligned} \quad (25)$$

Rewriting the above in a convenient form in order to use Green's theorem, one may write

$$\begin{aligned} \delta U_T = & \int_0^{2\pi R} \int_0^L \left\{ [N_{xx} \delta u + N_{xx} (w_{,x} + w_{,x}^0) \delta w \right. \\ & + N_{xy} (w_{,y} + w_{,y}^0) \delta w - M_{xx} \delta w_{,x}]_{,x} \\ & + [N_{yy} \delta v + N_{yy} (w_{,y} + w_{,y}^0) \delta w + N_{xy} \delta u \\ & + N_{xy} (w_{,x} + w_{,x}^0) \delta w - M_{yy} \delta w_{,y}]_{,y} \\ & - [N_{xx,x} \delta u + [N_{xx} (w_{,x} + w_{,x}^0)]_{,x} \delta w + N_{xy,x} \delta v \\ & + [N_{xy} (w_{,y} + w_{,y}^0)]_{,x} \delta w - M_{xx,x} \delta w + N_{yy,y} \delta v \\ & + [N_{yy} (w_{,y} + w_{,y}^0)]_{,y} \delta w + N_{xy,y} \delta u \\ & + [N_{xy} (w_{,x} + w_{,x}^0)]_{,y} \delta w - M_{yy,y} \delta w_{,y}] \\ & \left. - \frac{N_{yy}}{R} \delta w - 2M_{xy} \delta w_{,xy} \right\} dx dy \\ & - \int_0^{2\pi R} \int_0^L q \delta w dx dy - \int_0^{2\pi R} [-\bar{N}_{xx} \delta u + \bar{N}_{xy} \delta v \\ & + \bar{Q}_x \delta w - \bar{M}_{xx} \delta \phi_x - \bar{M}_{xy} \delta \phi_y] |_0^L dy \\ = & \int_0^{2\pi R} \int_0^L \left\{ [N_{xx} \delta u + N_{xx} (w_{,x} + w_{,x}^0) \delta w + N_{xy} \delta v \right. \\ & + N_{xy} (w_{,y} + w_{,y}^0) \delta w - M_{xx} \delta w_{,x} + M_{xx,x} \delta w + 2M_{xx,y} \delta w]_{,x} \\ & + [N_{yy} \delta v + N_{yy} (w_{,y} + w_{,y}^0) \delta w + N_{xy} \delta u \\ & + N_{xy} (w_{,x} + w_{,x}^0) \delta w - M_{yy} \delta w_{,y} + M_{yy,y} \delta w + 2M_{xy,x} \delta w]_{,y} \\ & - [N_{xx,x} \delta u + [N_{xx} (w_{,x} + w_{,x}^0)]_{,x} \delta w + N_{xy,x} \delta v \\ & \left. + [N_{xy} (w_{,y} + w_{,y}^0)]_{,x} \delta u + M_{xx,x} \delta w + N_{yy,y} \delta v \right\} \end{aligned}$$

$$\begin{aligned}
 & + [N_{yy}(w_{,y} + w_{,yy}^0)]_{,y} \delta w + N_{xy,y} \delta u + [N_{xy}(w_{,x} + w_{,xx}^0)]_{,y} \delta w + M_{yy,yy} \delta w \\
 & - \frac{N_{yy}}{R} \delta w - 2M_{xy,xy} \delta w \Big\} dx dy - \int_0^{2\pi R} \int_0^L q \delta w \, dx \, dy \\
 & - \int_0^{2\pi R} [-\bar{N}_{xx} \delta u + \bar{N}_{xy} \delta v + \bar{Q}_x \delta w - \bar{M}_{xx} \delta \phi_x - \bar{M}_{xy} \delta \phi_y] |_0^L dy. \quad (26)
 \end{aligned}$$

By Green's theorem, one obtains the following equilibrium equations and associated boundary terms.

Equilibrium equations:

$$\begin{aligned}
 N_{xx,x} + N_{xy,y} &= 0, \\
 N_{xy,x} + N_{yy,y} &= 0, \\
 M_{xx,xx} + 2M_{xy,xy} + M_{yy,yy} + \frac{N_{yy}}{R} + N_{xx}(w_{,xx} + w_{,xx}^0) \\
 &+ 2N_{xy}(w_{,xy} + w_{,xy}^0) + N_{yy}(w_{,yy} + w_{,yy}^0) + q = 0. \quad (27)
 \end{aligned}$$

Boundary terms:

$$\begin{array}{ll}
 \text{either} & \text{or} \\
 N_{xx} = -\bar{N}_{xx}, & \delta u = 0, \\
 N_{xy} = \bar{N}_{xy}, & \delta v = 0, \\
 N_{xx}(w_{,x} + w_{,xx}^0) + N_{xy}(w_{,y} + w_{,yy}^0) & \\
 + M_{xx,x} + 2M_{xy,y} = \bar{Q}_x + \bar{M}_{xy,y}, & \delta w = 0, \\
 M_{xx} = \bar{M}_{xx}, & \delta w_{,x} = 0. \quad (28)
 \end{array}$$

The first two equilibrium equations, eqs. (27), can be identically satisfied through the introduction of the following stress function:

$$\begin{aligned}
 N_{xx} &= F_{,yy} - \bar{N}_{xx}, \\
 N_{yy} &= F_{,xx}, \\
 N_{xy} &= -F_{,xy} + \bar{N}_{xy}. \quad (29)
 \end{aligned}$$

With the introduction of the stress function F , the third equilibrium equation becomes

$$\begin{aligned}
 M_{xx,xx} + 2M_{xy,xy} + M_{yy,yy} + \frac{1}{R} F_{,xx} + F_{,yy}(w_{,xx} + w_{,xx}^0) \\
 + F_{,xx}(w_{,yy} + w_{,yy}^0) - 2F_{,xy}(w_{,xy} + w_{,xy}^0) - \bar{N}_{xx}(w_{,xy} + w_{,xy}^0) \\
 + 2\bar{N}_{xy}(w_{,xy} + w_{,xy}^0) + q = 0. \quad (30)
 \end{aligned}$$

9.2.6 Compatibility Equation

Since the in-plane equilibrium equations are identically satisfied with the introduction of the Airy stress function F , the governing equations consist of the transverse equilibrium equation, eq. (30), and one more. This one more results from requiring compatibility of the in-plane displacement components

u and v . From eqs. (2) one obtains

$$\begin{aligned}\varepsilon_{xy,yy}^0 &= u_{,xyy} + \frac{1}{2}w_{,xyy}(w_{,x} + 2w_{,x}^0) + \frac{1}{2}w_{,x}(w_{,xyy} + 2w_{,xyy}^0) \\ \varepsilon_{yy,xx}^0 &= v_{,yx} - \frac{w_{,xx}}{R} + \frac{1}{2}(2w_{,y}w_{,yxx} + 2w_{,yxx}w_{,y}^0 + 2w_{,y}w_{,yxx}^0) \\ \gamma_{xy,xy}^0 &= u_{,xyx} + u_{,xxy} + w_{,xxy}w_{,y} + w_{,x}w_{,xyy} + w_{,xyy}w_{,x}^0 \\ &\quad + w_{,y}w_{,xxy}^0 + w_{,xxy}w_{,y}^0 + w_{,x}w_{,xyy}^0.\end{aligned}\tag{31}$$

Elimination of u and v leads to the following equation:

$$\begin{aligned}\varepsilon_{xx,yy}^0 + \varepsilon_{yy,xx}^0 - \gamma_{xy,xy}^0 &= -\frac{w_{,xx}}{R} + w_{,xy}(w_{,xy} + 2w_{,xy}^0) - \frac{1}{2}w_{,xx}(w_{,yy} + 2w_{,yy}^0) \\ &\quad - \frac{1}{2}w_{,yy}(w_{,xx} + 2w_{,xx}^0).\end{aligned}\tag{32}$$

Substitution of Eqs. (18) [eqs. (29) for the N 's and eqs. (3) for the κ 's] into the compatibility equation, eq. (32), yields

$$\begin{aligned}a_{11}F_{,yyyy} + a_{12}F_{,xxyy} + a_{13}F_{,xyyy} + b_{11}w_{,xxyy} + b_{12}w_{,yyyy} + 2b_{13}w_{,xyyy} \\ + a_{12}F_{,xxyy} + a_{22}F_{,xxxx} - a_{23}F_{,xxx} + b_{21}w_{,xxxx} + b_{22}w_{,xxyy} + 2b_{23}w_{,xxx} \\ - a_{13}F_{,xyyy} - a_{23}F_{,xxxy} + a_{33}F_{,xxyy} - b_{31}w_{,xxxy} - b_{32}w_{,xyyy} - 2b_{33}w_{,xxyy} \\ = -\frac{w_{,xx}}{R} + w_{,xy}(w_{,xy} + 2w_{,xy}^0) - \frac{1}{2}w_{,xx}(w_{,yy} + 2w_{,yy}^0) - \frac{1}{2}w_{,yy}(w_{,xx} + 2w_{,xx}^0).\end{aligned}\tag{33}$$

Similarly, substitution of eqs. (19) into the transverse equilibrium equation, eq. (30), yields

$$\begin{aligned}b_{11}F_{,xxxy} + b_{21}F_{,xxxx} + b_{12}F_{,yyyy} + b_{22}F_{,xxyy} - b_{31}F_{,xxxy} - b_{32}F_{,xyyy} \\ + 2b_{13}F_{,xyyy} + 2b_{23}F_{,xxx} - 2b_{33}F_{,xxxy} + d_{11}w_{,xxxx} + d_{12}w_{,xxyy} \\ + 2d_{13}w_{,xxxy} + 2d_{31}w_{,xxxy} + 2d_{32}w_{,xyyy} + d_{21}w_{,xxyy} + 4d_{33}w_{,xxyy} \\ + 2d_{23}w_{,xyyy} + d_{22}w_{,yyyy} + F_{,xx}/R + F_{,yy}(w_{,xx} + w_{,xx}^0) + F_{,xx}(w_{,yy} + w_{,yy}^0) \\ - 2F_{,xy}(w_{,xy} + w_{,xy}^0) - \bar{N}_{xx}(w_{,xx} + w_{,xx}^0) + 2\bar{N}_{xy}(w_{,xy} + w_{,xy}^0) + q = 0.\end{aligned}\tag{34}$$

9.2.7 Boundary Conditions

The boundary conditions, eqs. (28), can be designated as transverse ones (simply supported, clamped, free) and in-plane ones. Since all of the applications to be considered deal with supported boundaries, only simply supported (SS- i ; $i = 1, 2, 3, 4$) and clamped (CC- i) boundary conditions are listed. These are (at $x = 0, L$)

$$\begin{aligned}\text{SS-1: } w &= 0, & M_{xx} &= \bar{M}_{xx}, & N_{xx} &= -\bar{N}_{xx}, & N_{xy} &= \bar{N}_{xy}, \\ \text{SS-2: } w &= 0, & M_{xx} &= \bar{M}_{xx}, & u &= \text{const}, & N_{xy} &= \bar{N}_{xy}, \\ \text{SS-3: } w &= 0, & M_{xx} &= \bar{M}_{xx}, & N_{xx} &= -\bar{N}_{xx}, & v &= \text{const}, \\ \text{SS-4: } w &= 0, & M_{xx} &= \bar{M}_{xx}, & u &= \text{const}, & v &= \text{const},\end{aligned}\tag{35}$$

and

- | | | | | |
|-------|-----------|----------------|----------------------------|---------------------------|
| CC-1: | $w = 0$, | $w_{,x} = 0$, | $N_{xx} = -\bar{N}_{xx}$, | $N_{xy} = \bar{N}_{xy}$, |
| CC-2: | $w = 0$, | $w_{,x} = 0$, | $u = \text{const}$, | $N_{xy} = \bar{N}_{xy}$, |
| CC-3: | $w = 0$, | $w_{,x} = 0$, | $N_{xx} = -\bar{N}_{xx}$, | $v = \text{const}$, |
| CC-4: | $w = 0$, | $w_{,x} = 0$, | $u = \text{const}$, | $v = \text{const}$. (36) |

The above boundary conditions may be written in terms of the dependent variables F and w . The kinematic conditions $u = \text{const}$ and $v = \text{const}$ are first expressed in terms of equivalent conditions. This is shown below for each of the relevant conditions separately (see [32] for proper credit).

Note first that the expressions for the M_{ij} 's and N_{ij} 's are given by eqs. (20) and (29).

$$\text{SS-1: } w = 0$$

$$\begin{aligned} b_{21}F_{,xx} + d_{11}w_{,xx} + 2d_{13}w_{,xy} &= \bar{M}_{xx} + b_{11}\bar{N}_{xx} - b_{31}\bar{N}_{xy} \\ F_{,yy} = 0 \quad \text{and} \quad F_{,xy} = 0. \end{aligned} \quad (37)$$

$$\text{SS-2: } w = 0$$

$$\begin{aligned} b_{11}F_{,yy} + b_{21}F_{,xx} + d_{11}w_{,xx} + 2d_{13}w_{,xy} &= \bar{M}_{xx} + b_{11}\bar{N}_{xx} - b_{31}\bar{N}_{xy} \\ u = \text{const} \quad \text{and} \quad F_{,xy} = 0. \end{aligned} \quad (38)$$

The $u = \text{const}$ condition is expressed in terms of an equivalent condition by employing the following steps.

The expressions for γ_{xy}^0 from the kinematic relations, eq. (2), and from the constitutive equations, eqs. (18), are first equated to each other, or

$$\begin{aligned} \gamma_{xy}^0 &= u_{,y} + v_{,x} + w_{,x}w_{,y} + w_{,x}w_{,y}^0 + w_{,x}^0w_{,y} \\ &= a_{13}(F_{,yy} - \bar{N}_{xx}) + a_{23}F_{,xx} + a_{33}(\bar{N}_{xy} - F_{,xy}) \\ &\quad + b_{31}w_{,xx} + b_{32}w_{,yy} + 2b_{33}w_{,xy}. \end{aligned} \quad (38a)$$

One differentiation with respect to y and use of the conditions $w = 0$ and $F_{,xy} = 0$ yields at $x = 0$, L

$$v_{,xy} + w_{,xy}w_{,y}^0 + w_{,x}w_{,yy}^0 = a_{13}F_{,yyy} + a_{23}F_{,xxy} + b_{31}w_{,xxy} + 2b_{33}w_{,xyy}. \quad (38b)$$

Similarly,

$$\begin{aligned} \varepsilon_{yy}^0 &= v_{,y} - \frac{w}{R} + \frac{1}{2}w_{,y}^2 + w_{,y}w_{,y}^0 \\ &= a_{12}(F_{,yy} - \bar{N}_{xx}) + a_{22}F_{,xx} + a_{23}(\bar{N}_{xy} - F_{,xy}) \\ &\quad + b_{21}w_{,xx} + b_{22}w_{,yy} + 2b_{23}w_{,xy} \end{aligned} \quad (39a)$$

from which one differentiation with respect to x yields

$$\begin{aligned} v_{,yx} - \frac{w_{,x}}{R} + w_{,xy}w_{,y}^0 &= a_{22}F_{,xxx} - a_{23}F_{,xxy} + b_{21}w_{,xxx} \\ &\quad - 2b_{23}w_{,xyy} + b_{12}w_{,xxy}. \end{aligned} \quad (39b)$$

Elimination of $v_{,xy}$ and $v_{,yx}$ from eqs. (38) and (39) yields the equivalent (to $u = \text{const}$) boundary term, which is

$$\begin{aligned} a_{13}F_{,yyy} + 2a_{23}F_{,xxy} - a_{22}F_{,xxx} - w_{,x}/R - w_{,x}w_{,yy}^0 - b_{21}w_{,xxx} \\ + (b_{31} - 2b_{23})w_{,xxy} - (b_{22} - 2b_{33})w_{,xyy} = 0. \end{aligned}$$

Note that because $F_{,xy} = 0$ for this boundary condition, the term containing $F_{,xy}$ has been dropped.

Thus, for SS-2 the final form of the boundary terms becomes

$$\begin{aligned} w = 0, \quad F_{,xy} = 0; \\ b_{11}F_{,yy} + b_{21}F_{,xx} + d_{11}w_{,xx} + 2d_{13}w_{,xy} = \bar{M}_{xx} + b_{11}\bar{N}_{xx} - b_{31}\bar{N}_{xy}; \\ a_{13}F_{,yyy} + 2a_{23}F_{,xxy} - a_{22}F_{,xxx} - w_{,x}/R - w_{,x}w_{,yy}^0 - b_{21}w_{,xxx} \\ + (b_{31} - 2b_{23})w_{,xxy} - (b_{22} - 2b_{33})w_{,xyy} = 0. \end{aligned} \quad (40)$$

For SS-3,

$$\begin{aligned} w = 0, \quad F_{,yy} = 0, \quad v = \text{const.}, \\ b_{11}F_{,yy} + b_{21}F_{,xx} + d_{11}w_{,xx} + 2d_{13}w_{,xy} - b_{31}F_{,xy} = \bar{M}_{xx} + b_{11}\bar{N}_{xx} - b_{31}\bar{N}_{xy}. \end{aligned}$$

Similarly, as in the case of SS-2 ($u = \text{const}$), an equivalent condition is obtained for $v = \text{const}$. From eq. (39a), since $w = 0$ and $v_{,y} = 0$, the equivalent condition becomes $\varepsilon_{yy}^0 = 0$ or

$$a_{12}\bar{N}_{xx} + a_{22}F_{,xx} + a_{23}(\bar{N}_{xy} - F_{,xy}) + b_{21}w_{,xx} + 2b_{23}w_{,xy} = 0.$$

Thus, for SS-3 the final form of the boundary terms becomes

$$\begin{aligned} w = 0, \quad F_{,yy} = 0, \\ b_{21}F_{,xx} - b_{31}F_{,xy} + d_{11}w_{,xx} + 2d_{13}w_{,xy} = \bar{M}_{xx} + b_{11}\bar{N}_{xx} - b_{31}\bar{N}_{xy}, \\ a_{22}F_{,xx} - a_{23}F_{,xy} + b_{21}w_{,xx} + 2b_{23}w_{,xy} = a_{12}\bar{N}_{xx} - a_{23}\bar{N}_{xy}. \end{aligned} \quad (41)$$

For SS-4 the equivalent set of the boundary terms becomes

$$\begin{aligned} w = 0, \\ b_{11}F_{,yy} + b_{21}F_{,xx} - b_{31}F_{,xy} + d_{11}w_{,xx} + 2d_{13}w_{,xy} = \bar{M}_{xx} + b_{11}\bar{N}_{xx} - b_{31}\bar{N}_{xy}, \\ a_{22}F_{,xx} + a_{12}F_{,yy} - a_{23}F_{,xy} + b_{21}w_{,xx} + 2b_{23}w_{,xy} = a_{12}\bar{N}_{xx} - a_{23}\bar{N}_{xy}, \\ a_{13}F_{,yyy} + 2a_{23}F_{,xxy} - (a_{12} + a_{33})F_{,xyy} - a_{22}F_{,xxx} - w_{,x}/R - w_{,x}w_{,yy}^0 \\ + (2b_{33} - b_{22})w_{,xyy} + (b_{31} - 2b_{23})w_{,xxy} - b_{21}w_{,xxx} = 0. \end{aligned} \quad (42)$$

Following similar steps, boundary conditions CC- i , $i = 1, 2, 3$ and 4, are also expressed in terms of w and F only, or

$$\text{CC-1: } w = w_{,x} = F_{,yy} = F_{,xy} = 0. \quad (43)$$

$$\begin{aligned} \text{CC-2: } w = w_{,x} = F_{,xy} = 0, \\ a_{13}F_{,yyy} + 2a_{23}F_{,xxy} - a_{22}F_{,xxx} - b_{21}w_{,xxx} + (b_{31} - 2b_{23})w_{,xxy} = 0. \end{aligned} \quad (44)$$

$$\begin{aligned} \text{CC-3: } w = w_{,x} = F_{,yy} = 0, \\ a_{21}F_{,xx} - a_{23}F_{,xy} + b_{21}w_{,xx} = a_{12}\bar{N}_{xx} - a_{23}\bar{N}_{xy}. \end{aligned} \quad (45)$$

$$\begin{aligned} \text{CC-4: } w &= w_{,x} = 0, \\ a_{12}F_{,yy} + a_{22}F_{,xx} - a_{23}F_{,xy} + b_{21}w_{,xx} &= a_{12}\bar{N}_{xx} - a_{23}\bar{N}_{xy}, \\ a_{13}F_{,yyy} + 2a_{23}F_{,xxy} - (a_{12} + a_{33})F_{,xyy} - a_{22}F_{,xxx} - b_{21}w_{,xxx} \\ &+ (b_{31} - 2b_{23})w_{,xxy} = 0. \end{aligned} \quad (46)$$

9.3 Solution Methodology—Static

9.3.1 Basic Equations

The solution methodology is an improvement and modification of the one employed and outlined in [32] and [34].

The separated form, shown below, is used for the two dependent variables $w(x, y)$ and $F(x, y)$:

$$\begin{aligned} F(x, y) &= C_0(x) + \sum_{i=1}^{2k} \left[C_i(x) \cos \frac{iny}{R} + D_i(x) \sin \frac{iny}{R} \right], \\ w(x, y) &= A_0(x) + \sum_{i=1}^k \left[A_i(x) \cos \frac{iny}{R} + B_i(x) \sin \frac{iny}{R} \right] \end{aligned} \quad (47)$$

where n denotes the circumferential wave number.

In addition, a similar expression can be employed for the imperfection parameter $w^0(x, y)$ and the external pressure $q(x, y)$. Note that in most applications the pressure is assumed uniform (q_0 only).

$$\begin{aligned} w^0(x, y) &= A_0^0(x) + \sum_{i=1}^k \left[A_i^0(x) \cos \frac{iny}{R} + \beta_i^0(x) \sin \frac{iny}{R} \right], \\ q(x, y) &= q_0^1(x) + \sum_{i=1}^k \left[q_i^1(x) \cos \frac{iny}{R} + q_i^2(x) \sin \frac{iny}{R} \right]. \end{aligned} \quad (48)$$

Because of the nonlinearity of the field equations, eqs. (33) and (34), substitution of eqs. (47) and (48) into them yields double summations for the trigonometric functions. These double summations involve products of the sine and cosine of iny/R in all four possible combinations (cosine-cosine, sine-cosine, cosine-sine, and sine-sine). Furthermore, these products have different origins. Some of them come from products of $w_{,xy}w_{,xy}$, others from products of $F_{,xx}w_{,yy}$ [see eqs. (33) and (34)]. In order to simplify the final expressions (and use single sums instead of double sums), and in order to cover all possible combinations of double sums, the following simplifying equations are presented. These are based on trigonometric identities involving products.

$$\sum_{i=0}^K \sum_{j=0}^L [jb_j \cos j\theta] a_i i \cos i\theta = \sum_{i=0}^{K+L} A_{IJ1(K)}^i(b, a) \cos i\theta,$$

$$\begin{aligned}
\sum_{i=0}^K \sum_{j=0}^L [jb_j \cos j\theta] a_i i \sin i\theta &= \sum_{i=0}^{K+L} A_{IJ1(K)}^i(b, a) \sin i\theta, \\
\sum_{i=0}^K \sum_{j=0}^L [jb_j \sin j\theta] a_i i \cos i\theta &= \sum_{i=0}^{K+L} A_{IJ3(K)}^i(b, a) \sin i\theta, \\
\sum_{i=0}^K \sum_{j=0}^L [jb_j \sin j\theta] a_i i \sin i\theta &= \sum_{i=0}^{K+L} A_{IJ4(K)}^i(b, a) \cos i\theta;
\end{aligned} \tag{49}$$

$$\begin{aligned}
\sum_{i=0}^K \sum_{j=0}^L [b_j \cos j\theta] a_i i^2 \cos i\theta &= \sum_{i=0}^{K+L} A_{I21(K)}^i(b, a) \cos i\theta, \\
\sum_{i=0}^K \sum_{j=0}^L [b_j \cos j\theta] a_i i^2 \sin i\theta &= \sum_{i=0}^{K+L} A_{I22(K)}^i(b, a) \sin i\theta, \\
\sum_{i=0}^K \sum_{j=0}^L [b_j \sin j\theta] a_i i^2 \cos i\theta &= \sum_{i=0}^{K+L} A_{I23(K)}^i(b, a) \sin i\theta, \\
\sum_{i=0}^K \sum_{j=0}^L [b_j \sin j\theta] a_i i^2 \sin i\theta &= \sum_{i=0}^{K+L} A_{I24(K)}^i(b, a) \cos i\theta;
\end{aligned} \tag{50}$$

$$\begin{aligned}
\sum_{i=0}^K \sum_{j=0}^L [j^2 b_j \cos j\theta] a_i \cos i\theta &= \sum_{i=0}^{K+L} A_{J21(K)}^i(b, a) \cos i\theta, \\
\sum_{i=0}^K \sum_{j=0}^L [j^2 b_j \cos j\theta] a_i \cos i\theta &= \sum_{i=0}^{K+L} A_{J22(K)}^i(b, a) \sin i\theta, \\
\sum_{i=0}^K \sum_{j=0}^L [j^2 b_j \sin j\theta] a_i \cos i\theta &= \sum_{i=0}^{K+L} A_{J23(K)}^i(b, a) \sin i\theta, \\
\sum_{i=0}^K \sum_{j=0}^L [j^2 b_j \sin j\theta] a_i \sin i\theta &= \sum_{i=0}^{K+L} A_{J24(K)}^i(b, a) \cos i\theta;
\end{aligned} \tag{51}$$

where

$$\begin{aligned}
A_{IJ1(K)}^i(b, a) &= \frac{1}{2} \sum_{j=0}^K [(i+j)b_{i+j} + (1 - \eta_{j-i}^2 + \eta_i)|i-j|b_{|i-j|}] ja_j, \\
A_{IJ2(K)}^i(b, a) &= \frac{1}{2} \sum_{j=0}^K [-(i+j)b_{i+j} + (1 - \eta_{j-i}^2 + \eta_i)|i-j|b_{|i-j|}] ja_j, \\
A_{IJ3(K)}^i(b, a) &= \frac{1}{2} \sum_{j=0}^K [(i+j)b_{i+j} + (-1 + \eta_{i-j} + \eta_i)|i-j|b_{|i-j|}] ja_j, \\
A_{IJ4(K)}^i(b, a) &= \frac{1}{2} \sum_{j=0}^K [(i+j)b_{i+j} + (-1 - \eta_{i-j} + \eta_i)|i-j|b_{|i-j|}] ja_j;
\end{aligned} \tag{52}$$

$$\begin{aligned}
A_{I22(K)}^i(b, a) &= \frac{1}{2} \sum_{j=0}^K [-b_{i+j} + (1 - \eta_{j-i}^2 + \eta_i)b_{|i-j|}] j^2 a_j, \\
A_{I23(K)}^i(b, a) &= \frac{1}{2} \sum_{j=0}^K [b_{i+j} + (-1 + \eta_{i-j} + \eta_i)b_{|i-j|}] j^2 a_j, \\
A_{I24(K)}^i(b, a) &= \frac{1}{2} \sum_{j=0}^K [b_{i+j} + (-1 - \eta_{i-j} + \eta_i)b_{|i-j|}] j^2 a_j; \quad (53) \\
A_{J21(K)}^i(b, a) &= \frac{1}{2} \sum_{j=0}^K [(i+j)^2 b_{i+j} + (1 - \eta_{j-i}^2 + \eta_i)(i-j)^2 b_{|i-j|}] a_j, \\
A_{J22(K)}^i(b, a) &= \frac{1}{2} \sum_{j=0}^K [-(i+j)^2 b_{i+j} + (1 - \eta_{j-i}^2 + \eta_i)(i-j)^2 b_{|i-j|}] a_j, \\
A_{J23(K)}^i(b, a) &= \frac{1}{2} \sum_{j=0}^K [(i+j)^2 b_{i+j} + (-1 + \eta_{i-j} + \eta_i)(i+j)^2 b_{|i-j|}] a_j, \\
A_{J24(K)}^i(b, a) &= \frac{1}{2} \sum_{j=0}^K [(i+j)^2 b_{i+j} + (-1 - \eta_{i-j} + \eta_i)(i+j)^2 b_{|i-j|}] a_j; \quad (54)
\end{aligned}$$

and

$$K \geq L, \quad \eta_l = \begin{cases} 1 & \text{if } l > 0, \\ 0 & \text{if } l = 0, \\ -1 & \text{if } l < 0. \end{cases}$$

Next, returning to the solution procedure, the expressions for F , w , w^0 , and q , eqs. (47) and (48), are substituted into the equilibrium and compatibility equations, eqs. (33) and (34). This substitution yields the following nonlinear differential equations.

Equilibrium Equation

$$\begin{aligned}
&\sum_{i=0}^k \left[h_{40} \left(A_{i,xxxx} \cos \frac{iny}{R} + B_{i,xxxx} \sin \frac{iny}{R} \right) + h_{31} \left(\frac{in}{R} \right) \right. \\
&\times \left(-A_{i,xxx} \sin \frac{iny}{R} + B_{i,xxx} \cos \frac{iny}{R} \right) - h_{22} \left(\frac{in}{R} \right)^2 \\
&\times \left(A_{i,xx} \cos \frac{iny}{R} + B_{i,xx} \sin \frac{iny}{R} \right) + h_{13} \left(\frac{in}{R} \right)^3 \left(A_{i,x} \sin \frac{iny}{R} - B_{i,x} \cos \frac{iny}{R} \right) \\
&+ h_{04} \left(\frac{in}{R} \right)^4 \left(A_i \cos \frac{iny}{R} + B_i \sin \frac{iny}{R} \right) \Big] \\
&+ \sum_{i=0}^k \left[g_{40} \left(C_{i,xxxx} \cos \frac{iny}{R} + D_{i,xxxx} \sin \frac{iny}{R} \right) + g_{31} \left(\frac{in}{R} \right) \right. \\
&\left. + g_{22} \left(\frac{in}{R} \right)^2 \right. \\
&\left. + g_{13} \left(\frac{in}{R} \right)^3 \right. \\
&\left. + g_{04} \left(\frac{in}{R} \right)^4 \right]
\end{aligned}$$

$$\begin{aligned}
& \times \left(-C_{i,xxx} \sin \frac{iny}{R} + D_{i,xxx} \cos \frac{iny}{R} \right) - g_{22} \left(\frac{in}{R} \right)^2 \\
& \times \left(C_{i,xx} \cos \frac{iny}{R} + D_{i,xx} \sin \frac{iny}{R} \right) + g_{13} \left(\frac{in}{R} \right)^3 \left(C_{i,x} \sin \frac{iny}{R} - D_{i,x} \cos \frac{iny}{R} \right) \\
& + g_{04} \left(\frac{in}{R} \right)^4 \left(C_i \cos \frac{iny}{R} + D_i \sin \frac{iny}{R} \right) \Big] + \frac{1}{R} \sum_{i=0}^{2k} \left(C_{i,xx} \cos \frac{iny}{R} + D_{i,xx} \sin \frac{iny}{R} \right) \\
& + L(F, w + w^0) - \bar{N}_{xx} \sum_{i=0}^k \left[(A_{i,xx} + A_{i,xx}^0) \cos \frac{iny}{R} + (B_{i,xx} + B_{i,xx}^0) \sin \frac{iny}{R} \right] \\
& + 2\bar{N}_{xy} \sum_{i=0}^k \left(\frac{in}{R} \right) \left[-(A_{i,x} + A_{i,x}^0) \sin \frac{iny}{R} + (B_{i,x} + B_{i,x}^0) \cos \frac{iny}{R} \right] \\
& + \sum_{i=0}^k \left[q_i^1 \cos \frac{iny}{R} + q_i^2 \sin \frac{iny}{R} \right] = 0 \tag{55}
\end{aligned}$$

where

$$\begin{aligned}
L(F, w + w^0) &= \left[\sum_{i=0}^{2k} C_{i,xx} \cos \frac{iny}{R} + D_{i,xx} \sin \frac{iny}{R} \right] \left[\sum_{i=0}^k \left(\frac{in}{R} \right)^2 \right. \\
&\quad \times \left. \left\{ -(A_i + A_i^0) \cos \frac{iny}{R} - (B_i + B_i^0) \sin \frac{iny}{R} \right\} \right] - 2 \left[\sum_{i=0}^{2k} \left(\frac{in}{R} \right) \right. \\
&\quad \times \left. \left(-C_{i,x} \sin \frac{iny}{R} + D_{i,x} \cos \frac{iny}{R} \right) \right] \left[\sum_{i=0}^k \left(\frac{in}{R} \right) \left\{ -(A_{i,x} + A_{i,x}^0) \sin \frac{iny}{R} \right. \right. \\
&\quad \left. \left. + (B_{i,x} + B_{i,x}^0) \cos \frac{iny}{R} \right\} \right] + \left[- \sum_{i=0}^{2k} \left(\frac{in}{R} \right)^2 \left(C_i \cos \frac{iny}{R} + D_i \sin \frac{iny}{R} \right) \right] \\
&\quad \times \left[\sum_{i=0}^k \left\{ (A_{i,xx} + A_{i,xx}^0) \cos \frac{iny}{R} + (B_{i,xx} + B_{i,xx}^0) \sin \frac{iny}{R} \right\} \right] = 0 \tag{56a}
\end{aligned}$$

or

$$\begin{aligned}
L(F, w + w^0) &= \left(\frac{n}{R} \right)^2 \sum_{i=0}^{2k} \sum_{j=0}^k \left[-j^2 (A_j + A_j^0) \cos \frac{jny}{R} \right] C_{i,xx} \cos \frac{iny}{R} \\
&\quad + \left(\frac{n}{R} \right)^2 \sum_{i=0}^{2k} \sum_{j=0}^k \left[-j^2 (A_j + A_j^0) \cos \frac{jny}{R} \right] D_{i,xx} \sin \frac{iny}{R} \\
&\quad + \left(\frac{n}{R} \right)^2 \sum_{i=0}^{2k} \sum_{j=0}^k \left[-j^2 (B_j + B_j^0) \sin \frac{jny}{R} \right] C_{i,xx} \cos \frac{iny}{R} \\
&\quad + \left(\frac{n}{R} \right)^2 \sum_{i=0}^{2k} \sum_{j=0}^k \left[-j^2 (B_j + B_j^0) \sin \frac{jny}{R} \right] D_{i,xx} \sin \frac{iny}{R} \\
&\quad + \left(\frac{n}{R} \right)^2 \sum_{i=0}^{2k} \sum_{j=0}^k \left[(A_{j,xx} + A_{j,xx}^0) \cos \frac{jny}{R} \right] C_{i,xx}^2 \cos \frac{iny}{R}
\end{aligned}$$

$$\begin{aligned}
& - \left(\frac{n}{R} \right)^2 \sum_{i=0}^{2k} \sum_{j=0}^k \left[(A_{j,xx} + A_{j,xx}^0) \cos \frac{jny}{R} \right] D_i i^2 \sin \frac{iny}{R} \\
& - \left(\frac{n}{R} \right)^2 \sum_{i=0}^{2k} \sum_{j=0}^k \left[(B_{j,xx} + B_{j,xx}^0) \sin \frac{jny}{R} \right] C_i i^2 \cos \frac{iny}{R} \\
& - \left(\frac{n}{R} \right)^2 \sum_{i=0}^{2k} \sum_{j=0}^k \left[(B_{j,xx} + B_{j,xx}^0) \sin \frac{jny}{R} \right] D_i i^2 \sin \frac{iny}{R} \\
& + 2 \left(\frac{n}{R} \right)^2 \sum_{i=0}^{2k} \sum_{j=0}^k \left[-j(A_{j,x} + A_{j,x}^0) \sin \frac{jny}{R} \right] C_{i,x} i \sin \frac{iny}{R} \\
& + 2 \left(\frac{n}{R} \right)^2 \sum_{i=0}^{2k} \sum_{j=0}^k \left[j(A_{j,x} + A_{j,x}^0) \sin \frac{jny}{R} \right] D_{i,x} i \cos \frac{iny}{R} \\
& + 2 \left(\frac{n}{R} \right)^2 \sum_{i=0}^{2k} \sum_{j=0}^k \left[j(B_{j,x} + B_{j,x}^0) \cos \frac{jny}{R} \right] C_{i,x} i \sin \frac{iny}{R} \\
& + 2 \left(\frac{n}{R} \right)^2 \sum_{i=0}^{2k} \sum_{j=0}^k \left[-j(B_{j,x} + B_{j,x}^0) \cos \frac{jny}{R} \right] D_{i,x} i \cos \frac{iny}{R}
\end{aligned} \tag{56b}$$

and

$$\begin{aligned}
h_{40} &= d_{11}, & g_{40} &= b_{21}, \\
h_{31} &= 2(d_{13} + d_{31}), & g_{31} &= -b_{31} + 2b_{23}, \\
h_{22} &= d_{12} + 4d_{33} + d_{21}, & g_{22} &= b_{11} - 2b_{33} + b_{22}, \\
h_{13} &= 2(d_{23} + d_{32}), & g_{13} &= 2b_{13} - b_{32}, \\
h_{04} &= d_{22}, & g_{04} &= b_{12}.
\end{aligned}$$

Note that the operator $L(F, w + w^0)$, eqs. (56), can be written in terms of a single series, which is the most appropriate form for use in eq. (55). This is accomplished through the use of eqs. (49)–(54).

$$\begin{aligned}
L(F, w + w^0) = & - \left(\frac{n}{R} \right)^2 \sum_{i=0}^{3k} [A_{J21(2k)}^i (A + A^0, C_{,xx}) + A_{J24(2k)}^i (B + B^0, D_{,xx}) \\
& + A_{I21(2k)}^i (A_{,xx} + A_{,xx}^0, C) + A_{I24(2k)}^i (B_{,xx} + B_{,xx}^0, D) \\
& + 2A_{IJ4(2k)}^i (A_{,x} + A_{,x}^0, C_{,x}) + 2A_{IJ1(2k)}^i (B_{,x} + B_{,x}^0, D_{,x})] \cos \frac{iny}{R} \\
& - \left(\frac{n}{R} \right)^2 \sum_{i=0}^{3k} [A_{J22(2k)}^i (A + A^0, D_{,xx}) + A_{J23(2k)}^i (B + B^0, C_{,xx}) \\
& + A_{I22(2k)}^i (A_{,xx} + A_{,xx}^0, D) + A_{I23(2k)}^i (B_{,xx} + B_{,xx}^0, C) \\
& - 2A_{IJ3(2k)}^i (A_{,x} + A_{,x}^0, D_{,x}) - 2A_{IJ2(2k)}^i (B_{,x} + B_{,x}^0, C_{,x})] \sin \frac{iny}{R}.
\end{aligned} \tag{57}$$

Compatibility Equation

$$\begin{aligned}
& \sum_{i=0}^k \left[g_{40} \left(A_{i,xxxx} \cos \frac{iny}{R} + B_{i,xxxx} \sin \frac{iny}{R} \right) + g_{31} \frac{in}{R} \left(-A_{i,xxx} \sin \frac{iny}{R} \right. \right. \\
& \quad \left. \left. + B_{i,xxx} \cos \frac{iny}{R} \right) + g_{22} \left(\frac{in}{R} \right)^2 \left(-A_{i,xx} \cos \frac{iny}{R} - B_{i,xx} \sin \frac{iny}{R} \right) + g_{13} \left(\frac{in}{R} \right)^3 \right. \\
& \quad \times \left(A_{i,x} \sin \frac{iny}{R} - B_{i,x} \cos \frac{iny}{R} \right) + g_{04} \left(\frac{in}{R} \right)^4 \left(A_i \cos \frac{iny}{R} + B_i \sin \frac{iny}{R} \right) \left. \right] \\
& \quad + \sum_{i=0}^k \left[a_{22} \left(C_{i,xxxx} \cos \frac{iny}{R} + D_{i,xxxx} \sin \frac{iny}{R} \right) + 2a_{23} \left(\frac{in}{R} \right) \left(C_{i,xxx} \sin \frac{iny}{R} \right. \right. \\
& \quad \left. \left. - D_{i,xxx} \cos \frac{iny}{R} \right) + (2a_{12} + a_{33}) \left(\frac{in}{R} \right)^2 \left(-C_{i,xx} \cos \frac{iny}{R} - D_{i,xx} \sin \frac{iny}{R} \right) \right. \\
& \quad \left. + 2a_{13} \left(\frac{in}{R} \right)^3 \left(-C_{i,x} \sin \frac{iny}{R} + D_{i,x} \cos \frac{iny}{R} \right) + a_{11} \left(\frac{in}{R} \right)^4 \right. \\
& \quad \times \left(C_i \cos \frac{iny}{R} + D_i \sin \frac{iny}{R} \right) \left. \right] + \sum_{i=0}^k \left(\frac{A_{i,xx}}{R} \cos \frac{iny}{R} + \frac{B_{i,xx}}{R} \sin \frac{iny}{R} \right) \\
& \quad - \frac{1}{2} \left(\frac{n}{R} \right)^2 \sum_{i=0}^{2k} [A_{J21(k)}^i (A + 2A^0, A_{,xx}) + A_{J24(k)}^i (B + 2B^0, B_{,xx}) + A_{I21(k)}^i \\
& \quad \times (A_{,xx} + 2A_{,xx}^0, A) + A_{I24(k)}^i (B_{,xx} + 2B_{,xx}^0, B) + 2A_{IJ4(k)}^i (A_{,x} + 2A_{,x}^0, A_{,x}) \\
& \quad + 2A_{IJ1(k)}^i (B_{,x} + 2B_{,x}^0, B_{,x})] \cos \frac{iny}{R} - \frac{1}{2} \left(\frac{n}{R} \right)^2 \sum_{i=0}^{2k} [A_{J22(k)}^i (A + 2A^0, B_{,xx}) \\
& \quad + A_{J23(k)}^i (B + 2B^0, A_{,xx}) + A_{I22(k)}^i (A_{,xx} + 2A_{,xx}^0, B) + A_{I23(k)}^i (B_{,xx} + 2B_{,xx}^0, A) \\
& \quad - 2A_{IJ3(k)}^i (A_{,x} + 2A_{,x}^0, B_{,x}) - 2A_{IJ(k)}^i (B_{,x} + 2B_{,x}^0, A_{,x})] \sin \frac{iny}{R} = 0. \quad (58)
\end{aligned}$$

Parenthesis. As far as the equilibrium equation is concerned, the summation starts from zero and goes up to $3k$ [see eqs. (55) and (57)] because of the nonlinearity. The Galerkin procedure will be employed for this equation in the circumferential direction. This will yield $2k + 1$ nonlinear ordinary differential equation (from the vanishing of $2k + 1$ Galerkin integrals).

On the other hand, the compatibility equation, eq. (58), is written in series form, from zero to $2k$. Because of the orthogonality of the trigonometric functions, $4k + 1$ nonlinear differential equations result, which relate the C 's and D 's to the A 's and B 's [see eqs. (47)]. This set of ordinary differential equations is shown in complete form in the pages that follow. Before showing them, though, some simplifications can be made.

For the case of $i=0$, one obtains the following equation from the

compatibility equation, eq. (58):

$$\begin{aligned} g_{40}A_{0,xxxx} + \frac{1}{R}A_{0,xx} + a_{22}C_{0,xxxx} - \frac{1}{2}\left(\frac{n}{R}\right)^2 [A_{J21(k)}^i(A + 2A^0, A_{,xx}) \\ + A_{J24(k)}^i(B + 2B^0, B_{,xx}) + A_{I21(k)}^0(A_{,xx} + 2A_{,xx}^0, A) + A_{I24(k)}^i(B_{,xx} + 2B_{,xx}^0, B) \\ + 2A_{IJ4(k)}^0(A_{,x} + 2A_{,x}^0, A_{,x}) + 2A_{IJ1(k)}^0(B_{,x} + 2B_{,x}^0, B_{,x})] = 0 \end{aligned}$$

or

$$\begin{aligned} C_{0,xxxx} = \frac{1}{a_{22}} \left\{ -g_{40}A_{0,xxxx} - \frac{1}{R}A_{0,xx} + \frac{1}{4}\left(\frac{n}{R}\right)^2 \sum_{j=1}^k [j^2(A_j + 2A_j^0)A_{j,xx} \right. \\ \left. + j^2(B_j + 2B_j^0)B_{j,xx} + j^2(A_{j,xx} + 2A_{j,xx}^0)A_j + j(B_{j,xx} + 2B_{j,xx}^0)B_j \right. \\ \left. + 2j^2(A_{j,x} + 2A_{j,x}^0)A_{j,x} + 2j^2(B_{j,x} + 2B_{j,x}^0)B_{j,x}] \right\}. \quad (59) \end{aligned}$$

Moreover, the displacement component $v(x, y)$ is a continuous and single-valued function of y (and x); therefore

$$\int_0^{2\pi R} v_{,y} dy = v(x, 2\pi R) - v(x, 0) = 0. \quad (60)$$

From the second of eqs. (2) one may write

$$v_{,y} = \varepsilon_{yy}^0 + w/R - w_{,y}(w_{,y} + 2w_{,y}^0)/2. \quad (61)$$

Furthermore, use of eqs. (18) (relation between ε_{yy}^0 and N_{ij}, κ_{ij}), eqs. (29) (definition of stress resultant function), and eqs. (47) and (48) (assumed form for w, F , and w^0) yields the following relation:

$$\begin{aligned} \int_0^{2\pi R} v_{,y} dy = \int_0^{2\pi R} (-a_{12}\bar{N}_{xx} + a_{23}\bar{N}_{xy}) dy \\ + \int_0^{2\pi R} \left[a_{12}F_{,yy} + a_{22}F_{,xx} - a_{23}F_{,xy} + b_{23}w_{,xx} \right. \\ \left. + b_{22}w_{,yy} + 2b_{23}w_{,xy} + \frac{w}{R} - \frac{1}{2}w_{,y}(w_{,y} + 2w_{,y}^0) \right] dy = 0 \quad (62) \end{aligned}$$

or

$$\begin{aligned} \int_0^{2\pi R} (-a_{12}\bar{N}_{xx} + a_{23}\bar{N}_{xy}) dy + \int_0^{2\pi R} \left\{ a_{12} \sum_{i=0}^{2k} \left(\frac{in}{R}\right)^2 \left(-C_i \cos \frac{iny}{R} \right. \right. \\ \left. \left. - D_i \sin \frac{iny}{R} \right) + a_{22} \sum_{i=0}^{2k} \left[C_{i,xx} \cos \frac{iny}{R} + D_{i,xx} \sin \frac{iny}{R} \right] \right. \\ \left. - a_{23} \sum_{i=0}^{2k} \left(\frac{in}{R}\right) \left[-C_{i,xy} \sin \frac{iny}{R} + D_{i,xy} \cos \frac{iny}{R} \right] \right\} dy = 0 \end{aligned}$$

$$\begin{aligned}
& + b_{21} \sum_{i=0}^k \left[A_{i,xx} \cos \frac{iny}{R} + B_{i,xx} \sin \frac{iny}{R} \right] + b_{22} \sum_{i=0}^k \left(\frac{in}{R} \right)^2 \left[-A_i \cos \frac{iny}{R} \right. \\
& \left. - B_i \sin \frac{iny}{R} \right] + 2b_{23} \sum_{i=0}^k \left(\frac{in}{R} \right) \left[-A_{i,x} \sin \frac{iny}{R} + B_{i,x} \cos \frac{iny}{R} \right] \\
& + \frac{1}{R} \sum_{i=0}^k \left(A_i \cos \frac{iny}{R} + B_i \sin \frac{iny}{R} \right) - \frac{1}{2} \sum_{i=0}^k \left(\frac{in}{R} \right) \left[-A_i \sin \frac{iny}{R} + B_i \cos \frac{iny}{R} \right] \\
& \times \sum_{j=0}^k \left(\frac{jn}{R} \right) \left[-(A_j + 2A_j^0) \sin \frac{jny}{R} + (B_j + 2B_j^0) \cos \frac{jny}{R} \right] \Big\} dy = 0. \quad (63)
\end{aligned}$$

This equation, after the indicated operations (integrations), becomes

$$\begin{aligned}
& \int_0^{2\pi R} \left\{ -a_{12} \bar{N}_{xx} + a_{23} \bar{N}_{xy} + a_{22} C_{0,xx} + b_{21} A_{0,xx} + \frac{A_0}{R} \right. \\
& \left. - \frac{n^2}{4R^2} \sum_{j=0}^k j^2 [(A_j + 2A_j^0) A_j + (B_j + 2B_j^0) B_j] \right\} dy = 0 \quad (64)
\end{aligned}$$

from which one may write

$$\begin{aligned}
C_{0,xx} = & \frac{1}{a_{22}} \left\{ -b_{21} A_{0,xx} - \frac{A_0}{R} + \frac{n^2}{4R^2} \sum_{j=0}^k j^2 [(A_j + 2A_j^0) A_j \right. \\
& \left. + (B_j + 2B_j^0) B_j] + a_{12} \bar{N}_{xx} - a_{23} \bar{N}_{xy} \right\}. \quad (65)
\end{aligned}$$

The remaining *compatibility* (nonlinear, ordinary differential) equations are as follows. For $i = 1, 2, \dots, 2k$ and cosine terms:

$$\begin{aligned}
& a_{22} C_{i,xxxx} - 2a_{23} \left(\frac{in}{R} \right) D_{i,xxx} - (2a_{12} + a_{33}) \left(\frac{in}{R} \right)^2 C_{i,xx} + 2a_{13} \left(\frac{in}{R} \right)^3 D_{i,x} \\
& + a_{11} \left(\frac{in}{R} \right)^4 C_i + \delta_i \left[g_{40} A_{i,xxxx} + g_{31} \left(\frac{in}{R} \right) B_{i,xxx} - g_{22} \left(\frac{in}{R} \right)^2 A_{i,xx} \right. \\
& \left. - g_{13} \left(\frac{in}{R} \right)^3 B_{i,x} + g_{04} \left(\frac{in}{R} \right)^4 A_i + \frac{A_{i,xx}}{R} - \frac{1}{2} \left(\frac{n}{R} \right)^2 i^2 (A_i + 2A_i^0) A_{0,xx} \right] \\
& - \left(\frac{n}{2R} \right)^2 \sum_{j=0}^k \left\{ [(i+j)^2 (A_{i+j} + 2A_{i+j}^0)] \right. \\
& \left. + (2 - \eta_{j-1}^2)(i-j)^2 (A_{|i-j|} + 2A_{|i-j|}^0)] A_{j,xx} \right. \\
& \left. + [(i+j)^2 (B_{i+j} + 2B_{i+j}^0) - \eta_{i-j}(i-j)^2 (B_{|i-j|} + 2B_{|i-j|}^0)] B_{j,xx} \right. \\
& \left. + [A_{i+j,xx} + 2A_{i+j,xx}^0 + (2 - \eta_{j-1}^2)(A_{|i-j|,xx} + 2A_{|i-j|,xx}^0)] j^2 A_j \right. \\
& \left. + [B_{i+j,xx} + 2B_{i+j,xx}^0 - \eta_{i-j}(B_{|i-j|,xx} + 2B_{|i-j|,xx}^0)] j^2 B_j \right. \\
& \left. + 2[(i+j)(A_{i+j,x} + 2A_{i+j,x}^0) - \eta_{i-j}(i-j)(A_{|i-j|,x} + 2A_{|i-j|,x}^0)] j A_{j,x} \right\}
\end{aligned}$$

$$+ 2[(i+j)(B_{i+j,x} + 2B_{i+j,x}^0) + (2 - \eta_{j-i}^2)|i-j|(B_{|i-j|,x} \\ + 2B_{|i-j|,x}^0)]jB_{j,x} \Big\} = 0. \quad (66)$$

For $i = 1, 2, \dots, 2k$ and sine terms:

$$a_{22}D_{i,xxxx} + 2a_{23}\left(\frac{in}{R}\right)C_{i,xxx} - (2a_{12} + a_{33})\left(\frac{in}{R}\right)^2 D_{i,xx} - 2a_{13}\left(\frac{in}{R}\right)^3 C_{i,x} \\ + a_{11}\left(\frac{in}{R}\right)^4 D_i + \delta_i \left[g_{40}B_{i,xxxx} - g_{31}\left(\frac{in}{R}\right)A_{i,xxx} - g_{22}\left(\frac{in}{R}\right)^2 B_{i,xx} \right. \\ \left. + g_{13}\left(\frac{in}{R}\right)^3 A_{i,x} + g_{04}\left(\frac{in}{R}\right)^4 B_i + \frac{B_{i,xx}}{R} - \frac{1}{2}\left(\frac{n}{R}\right)^2 i^2(B_i + B_i^0)A_{0,xx} \right] \\ - \frac{1}{4}\left(\frac{n}{R}\right)^2 \sum_{j=1}^k \left\{ [-(i+j)^2(A_{i+j} + 2A_{i+j}^0) \right. \\ \left. + (2 - \eta_{j-i}^2)(i-j)^2(A_{|i-j|} + 2A_{|i-j|}^0)]B_{j,xx} + [(i+j)^2(B_{j+i} + 2B_{i+j}^0) \right. \\ \left. + \eta_{i-j}(i-j)^2(B_{|i-j|} + 2B_{|i-j|}^0)]A_{j,xx} + [-(A_{i+j,xx} + 2A_{i+j,xx}^0) \right. \\ \left. + (2 - \eta_{j-i}^2)(A_{|i-j|,xx} + 2A_{|i-j|,xx}^0)]j^2B_j + [(B_{i+j,xx} + 2B_{i+j,xx}^0) \right. \\ \left. + \eta_{i-j}(B_{|i-j|,xx} + 2B_{|i-j|,xx}^0)]j^2A_j - 2[(i+j)(A_{i+j,x} + 2A_{i+j,x}^0) + \eta_{i-j}|i-j| \right. \\ \times (A_{|i-j|,x} + 2A_{|i-j|,x}^0)]jB_{j,x} - 2[-(i+j)(B_{i+j,x} + 2B_{i+j,x}^0) \right. \\ \left. + (2 - \eta_{j-i}^2)|i-j|(B_{|i-j|,x} + 2B_{|i-j|,x}^0)]jA_{j,x} \right\} = 0 \quad (67)$$

where

$$\delta_i = \begin{cases} 0, & i > k, \\ 1, & i \leq k, \end{cases}$$

$$\eta_l = \begin{cases} -1, & l < 0, \\ 0, & l = 0, \\ 1, & l > 0. \end{cases}$$

As already mentioned, the Galerkin procedure is employed in connection with the equilibrium equation, eq. (54), in the circumferential direction. The vanishing of the $2k + 1$ Galerkin integrals yields the following set of nonlinear ordinary differential equations.

For $i = 0$:

$$h_{40}A_{0,xxxx} + g_{40}C_{0,xxxx} + \frac{1}{R}C_{0,xx} - (A_{0,xx} + A_{0,xx}^0)\bar{N}_{xx} \\ - \left(\frac{n}{R}\right)^2 \frac{1}{2} \sum_{j=0}^{2k} [j^2(A_j + A_j^0)C_{j,xx} + j^2(B_j + B_j^0)D_{j,xx} + j^2(A_{j,xx} + A_{j,xx}^0)C_j$$

$$\begin{aligned}
& + j^2(B_{j,xx} + B_{j,xx}^0)D_j + 2j^2(A_{j,x} + A_{j,x}^0)C_{j,x} \\
& + 2j^2(B_{j,x} + B_{j,x}^0)D_{j,x}] + q_0^1 = 0. \tag{68}
\end{aligned}$$

Employing eqs. (59) and (65), one obtains

$$\begin{aligned}
& A_{0,xxxx}\left(d_{11} - \frac{b_{21}^2}{a_{22}}\right) - A_{0,xx}\left(2\frac{b_{21}}{Ra_{22}}\right) - \bar{N}_{xx}(A_{0,xx} + A_{0,xx}^0) - \frac{A_0}{a_{22}R^2} \\
& + \left(\frac{n}{2R}\right)^2 \sum_{j=1}^k j^2 \left\{ \frac{b_{21}}{a_{22}} [(A_j + 2A_j^0)A_{j,xx} + (A_{j,xx} + 2A_{j,xx}^0)A_j] \right. \\
& + 2(A_{j,x} + 2A_{j,x}^0)A_{j,x} + (B_j + 2B_j^0)B_{j,xx} + (B_{j,xx} + 2B_{j,xx}^0)B_j \\
& + 2(B_{j,x} + 2B_{j,x}^0)B_{j,x}] + \frac{1}{a_{22}R} [(A_j + 2A_j^0)A_j + (B_j + 2B_j^0)B_j] \\
& - 2[(A_j + A_j^0)C_{j,xx} + (B_j + B_j^0)D_{j,xx} + 2(A_{j,x} + A_{j,x}^0)C_{j,x} \\
& \left. + 2(B_{j,x} + B_{j,x}^0)D_{j,x} + (A_{j,xx} + A_{j,xx}^0)C_j + (B_{j,xx} + B_{j,xx}^0)D_j] \right\} \\
& + \frac{a_{12}}{a_{22}R} \bar{N}_{xx} - \frac{a_{23}}{a_{22}R} \bar{N}_{xy} + q_0^1 = 0. \tag{69}
\end{aligned}$$

For $i = 1, 2, \dots, k$ [when the weighting function is $\cos(iny/R)$]:

$$\begin{aligned}
& d_{11}A_{i,xxxx} + 4d_{13}\left(\frac{in}{R}\right)B_{i,xxx} - (2d_{12} + 4d_{33})\left(\frac{in}{R}\right)^2 A_{i,xx} \\
& - 4d_{23}\left(\frac{in}{R}\right)^3 B_{i,x} + d_{22}\left(\frac{in}{R}\right)^4 A_i + b_{21}C_{i,xxxx} + (2b_{23} - b_{31})\left(\frac{in}{R}\right)D_{i,xxx} \\
& - (b_{11} - 2b_{33} + b_{22})\left(\frac{in}{R}\right)^2 C_{i,xx} - (2b_{13} - b_{32})\left(\frac{in}{R}\right)^3 D_{i,x} \\
& + b_{12}\left(\frac{in}{R}\right)^4 C_i + \frac{1}{R}C_{i,xx} - \left(\frac{in}{R}\right)^2 \left(\frac{A_i + A_i^0}{d_{22}}\right) \left\{ -b_{21}A_{0,xx} - \frac{A_0}{R} \right. \\
& \left. + \left(\frac{n}{2R}\right)^2 \sum_{j=1}^k j^2 [(A_j + 2A_j^0)A_j + (B_j + 2B_j^0)B_j] \right\} \\
& - \left(\frac{in}{R}\right)^2 \left(\frac{A_i + A_i^0}{a_{22}}\right) (a_{12}\bar{N}_{xx} - a_{23}\bar{N}_{xy}) - (A_{i,xx} + A_{i,xx}^0)\bar{N}_{xx} \\
& + 2\bar{N}_{xy}\left(\frac{in}{R}\right)(B_{i,x} + B_{i,x}^0) - \frac{1}{2}\left(\frac{n}{R}\right)^2 \sum_{j=1}^{2k} \{ [(i+j)^2 \delta_{i+j}(A_{i+j} + A_{i+j}^0) \\
& + (2 - \eta_{j-i}^2)(i-j)^2 \delta_{|i-j|}(A_{|i-j|} + A_{|i-j|}^0)] C_{j,xx} \\
& + [(i+j)^2 \delta_{i+j}(B_{i+j} + B_{i+j}^0) - \eta_{i-j}(i-j)^2 \delta_{|i-j|}(B_{|i-j|} + B_{|i-j|}^0)] D_{j,xx}
\end{aligned}$$

$$\begin{aligned}
& + 2[(i+j)\delta_{i+j}(A_{i+j,x} + A_{i+j,x}^0) - \eta_{i-j}|i-j|\delta_{|i-j|}(A_{|i-j|,x} \\
& + A_{|i-j|,x}^0)]jC_{j,x} + 2[(i+j)\delta_{i+j}(B_{i+j,x} + B_{i+j,x}^0) \\
& + (2 - \eta_{j-i}^2)|i-j|\delta_{|i-j|}(B_{|i-j|,x} + B_{|i-j|,x}^0)]jD_{j,x} + [\delta_{i+j}(A_{i+j,xx} + A_{i+j,xx}^0) \\
& + (2 - \eta_{j-i}^2)\delta_{|i-j|}(A_{|i-j|,xx} + A_{|i-j|,xx}^0)]j^2C_j + [\delta_{i+j}(B_{i+j,xx} + B_{i+j,xx}^0) \\
& - \eta_{i-j}\delta_{|i-j|}(B_{|i-j|,xx} + B_{|i-j|,xx}^0)]j^2D_j\} + q_i^1 = 0. \tag{70}
\end{aligned}$$

For $i = 1, 2, \dots, k$ [when the weighting function is $\sin(iny/R)$]

$$\begin{aligned}
& d_{11}B_{i,xxxx} - 4d_{13}\left(\frac{in}{R}\right)A_{i,xxx} - (2d_{12} + 4d_{33})\left(\frac{in}{R}\right)^2B_{i,xx} + 4d_{23}\left(\frac{in}{R}\right)^3A_{i,x} \\
& + d_{22}\left(\frac{in}{R}\right)^4B_i + b_{21}D_{i,xxxx} - (2b_{23} - b_{31})\left(\frac{in}{R}\right)C_{i,xxx} \\
& - (b_{11} - 2b_{33} + b_{22})\left(\frac{in}{R}\right)^2D_{i,xx} + (2b_{13} - b_{32})\left(\frac{in}{R}\right)^3C_{i,x} + b_{12}\left(\frac{in}{R}\right)^4D_i \\
& + \frac{D_{i,xx}}{R} - \left(\frac{in}{R}\right)^2\left(\frac{B_i + B_i^0}{a_{22}}\right)\left\{ -b_{21}A_{0,xx} - \frac{A_0}{R} \right. \\
& \left. + \left(\frac{n}{2R}\right)^2\sum_{j=1}^k j^2[(A_j + 2A_j^0)A_j + (B_j + 2B_j^0)B_j]\right\} \\
& - \left(\frac{in}{R}\right)^2\left(\frac{B_i + B_i^0}{a_{22}}\right)(a_{12}\bar{N}_{xx} - a_{23}\bar{N}_{xy}) - (B_{i,xx} + B_{i,xx}^0)\bar{N}_{xx} \\
& - 2\bar{N}_{xy}\left(\frac{in}{R}\right)(A_{i,x} + A_{i,x}^0) - \frac{1}{2}\left(\frac{n}{R}\right)^2\sum_{j=1}^{2k}\{[(i+j)^2\delta_{i+j}(B_{i+j} + B_{i+j}^0) \\
& + \eta_{i-j}(i-j)^2\delta_{|i-j|}(B_{|i-j|} + B_{|i-j|}^0)]C_{i,xx} + [-(i+j)^2\delta_{i+j}(A_{i+j} + A_{i+j}^0) \\
& + (2 - \eta_{j-i}^2)(i-j)^2\delta_{|i-j|}(A_{|i-j|} + A_{|i-j|}^0)]D_{j,xx} \\
& - 2[-(i+j)\delta_{i+j}(B_{i+j,x} + B_{i+j,x}^0) \\
& + (2 - \eta_{j-i}^2)|i-j|\delta_{|i-j|}(B_{|i-j|,x} + B_{|i-j|,x}^0)]jC_{j,x} \\
& - 2[(i+j)\delta_{i+j}(A_{i+j,x} + A_{i+j,x}^0) + \eta_{i-j}|i-j|\delta_{|i-j|}(A_{|i-j|,x} + A_{|i-j|,x}^0)]jD_{j,x} \\
& + (\delta_{i+j}(B_{i+j,xx} + B_{i+j,xx}^0) + \eta_{i-j}\delta_{|i-j|}(B_{|i-j|,xx} + B_{|i-j|,xx}^0)]j^2C_j \\
& + [-\delta_{i+j}(A_{i+j,xx} + A_{i+j,xx}^0) + (2 - \eta_{j-i}^2)\delta_{|i-j|}(A_{|i-j|,xx} + A_{|i-j|,xx}^0)]j^2D_j\} \\
& + q_i^2 = 0. \tag{71}
\end{aligned}$$

Clearly, the response of the configuration is known, provided one can solve the nonlinear ordinary differential equations. Their number is $6k + 2$ and the number of unknown dependent variables (functions of x) is also $6k + 2$. These are $(k + 1)A$'s, $(k)B$'s, $(2k + 1)C$'s, and $(2k)S$'s. Note that C_0 can and has

been eliminated, through eqs. (59) and (65), and therefore both the number of equations and number of unknowns are reduced by one to $6k + 1$. In these equations there is one more underdetermined parameter, the wave number n . This number is determined by requiring the total potential to be a minimum at a given level of the load. In other words, the response is obtained for various n values and, through comparison, the true response (n value and corresponding values for the dependent variables) is established.

So far, the partial differential equations have been reduced to a set of $6k + 1$ nonlinear ordinary differential equations. Next, the generalized Newton's method [35] applicable to differential equations is used to reduce the nonlinear field equations and boundary conditions to a sequence of linear systems. Iteration equations are derived by assuming that the solution to the nonlinear set can be achieved by small corrections to an approximate solution. The small corrections or the values of the variables at the $(m + 1)$ step in terms of the closely spaced state m can be obtained by solving the linearized differential equations. Note through eq. (72) the way that a typical nonlinear term (product of X and Y) in the differential equation is linearized.

$$\begin{aligned}
 X^{m+1} Y^{m+1} &= (X^m + dX^m)(Y^m + dY^m) \\
 &= X^m Y^m + X^m dY^m + Y^m dX^m + dX dY^m \\
 &= X^m Y^m + Y^m dX^m + X^m Y^m + X^m dY^m - X^m Y^m \\
 &= X^m(Y^m + dY^m) + Y^m(X^m + dX^m) - X^m Y^m \\
 &= X^m Y^{m+1} + Y^{m+1} - X^m Y^m
 \end{aligned} \tag{72}$$

where X and Y can be A_i, B_i, C_i , or D_i .

By making use of eq. (72), the linearized set of governing equations (iteration equation) is obtained from eqs. (66), (67), (69), and (71). These are as follows:

Compatibility

1. Cosine terms, eqs. (67). For $i = 2, \dots, k$:

$$\begin{aligned}
 a_{22} C_{i,xxx}^{m+1} - 2a_{23} \left(\frac{in}{R} \right) D_{i,xxx}^{m+1} - (2a_{12} + a_{33}) \left(\frac{in}{R} \right)^2 C_{i,xx}^{m+1} \\
 + 2a_{13} \left(\frac{in}{R} \right)^3 D_{i,x}^{m+1} + a_{11} \left(\frac{in}{R} \right)^4 C_i^{m+1} + \delta_i \left\{ b_{21} A_{i,xxxx}^{m+1} \right. \\
 \left. + (2b_{23} - b_{31}) \left(\frac{in}{R} \right) B_{i,xxx}^{m+1} - (b_{11} - 2b_{33} + b_{22}) \left(\frac{in}{R} \right)^2 A_{i,xx}^{m+1} \right. \\
 \left. - (2b_{13} - b_{32}) \left(\frac{in}{R} \right)^3 B_{i,x}^{m+1} + b_{12} \left(\frac{in}{R} \right)^4 A_i^{m+1} + \frac{1}{R} A_{i,xx}^{m+1} \right. \\
 \left. - \frac{1}{2} \left(\frac{in}{R} \right)^2 [A_i^{m+1} A_{0,xx}^m + (A_i^m + 2A_i^0) A_{0,xx}^{m+1} - A_i^m A_{0,xx}^m] \right\}
 \end{aligned}$$

$$\begin{aligned}
& - \left(\frac{n}{2R} \right)^2 \sum_{j=1}^k \{ J_{ij}^{m+1} (A + 2A^0) A_{j,xx}^m + J_{ij}^m (A + 2A^0) A_{j,xx}^{m+1} - J_{ij}^m (A + 2A^0) A_{j,xx}^m \\
& + K_{ij}^{m+1} (B + 2B^0) B_{j,xx}^m + K_{ij}^m (B + 2B^0) B_{j,xx}^{m+1} - K_{ij}^m (B + 2B^0) B_{j,xx}^m \\
& + 2 [L_{ij}^{m+1} (A + 2A^0) A_{j,x}^m + L_{ij}^m (A + 2A^0) A_{j,x}^{m+1} - L_{ij}^m (A + 2A^0) A_{j,x}^m] \\
& + 2 [M_{ij}^{m+1} (B + 2B^0) B_{j,x}^m + M_{ij}^m (B + 2B^0) B_{j,x}^{m+1} - M_{ij}^m (B + 2B^0) B_{j,x}^m] \\
& + N_{ij}^{m+1} (A + 2A^0) A_j^m + N_{ij}^m (A + 2A^0) A_j^{m+1} - N_{ij}^m (A + 2A^0) A_j^m \\
& + O_{ij}^{m+1} (B + 2B^0) B_j^m + O_{ij}^m (B + 2B^0) B_j^{m+1} - O_{ij}^m (B + 2B^0) B_j^m \} = 0 \quad (73)
\end{aligned}$$

where

$$\begin{aligned}
J_{ij}^m(Y) &= (i+j)\delta_{i+j} Y_{i+j}^m + (2-\eta_{j-i}^2)(i-j)^2 \delta_{|i-j|} Y_{|i-j|}^m \\
K_{ij}^m(Y) &= (i+j)^2 \delta_{i+j} Y_{i+j}^m - \eta_{i-j}(i-j)^2 \delta_{|i-j|} Y_{|i-j|}^m \\
L_{ij}^m(Y) &= [(i+j)\delta_{i+j} Y_{i+j,x}^m - \eta_{i-j}|i-j|\delta_{|i-j|} Y_{|i-j|,x}^m]j \\
M_{ij}^m(Y) &= [(i+j)\delta_{i+j} Y_{i+j,x}^m + (2-\eta_{j-i}^2)|i-j|\delta_{|i-j|} Y_{|i-j|,x}^m]j \\
N_{ij}^m(Y) &= [\delta_{i+j} Y_{i+j,x}^m + (2-\eta_{j-i}^2)\delta_{|i-j|} Y_{|i-j|,xx}^m]j^2 \\
O_{ij}^m(Y) &= [\delta_{i+j} Y_{i+j,xx}^m - \eta_{i-j}\delta_{|i-j|} Y_{|i-j|,xx}^m]j^2.
\end{aligned}$$

2. Sine terms, eq. (68). For $i = 1, 2, \dots, k$:

$$\begin{aligned}
& a_{22} D_{i,xxxx}^{m+1} + 2a_{33} \left(\frac{in}{R} \right) C_{i,xxx}^{m+1} - (2a_{12} + a_{33}) \left(\frac{in}{R} \right)^2 D_{i,xx}^{m+1} \\
& - 2a_{13} \left(\frac{in}{R} \right)^3 C_{i,x}^{m+1} + a_{11} \left(\frac{in}{R} \right)^4 D_i^{m+1} + \delta_i \left[b_{21} B_{i,xxxx}^{m+1} - (2b_{23} - b_{31}) \right. \\
& \times \left(\frac{in}{R} \right) A_{i,xxx}^{m+1} - (b_{11} - 2b_{33} + b_{22}) \left(\frac{in}{R} \right)^2 B_{i,xx}^{m+1} + (2b_{13} - b_{32}) \left(\frac{in}{R} \right)^3 A_{i,x}^{m+1} \\
& + b_{12} \left(\frac{in}{R} \right)^4 B_i^{m+1} + \frac{B_{i,xx}^{m+1}}{R} - \frac{1}{2} \left(\frac{in}{R} \right)^2 [B_i^{m+1} A_{0,xx}^m + (B_i^m + 2B_i^0) A_{0,xx}^{m+1} \\
& - B_i^m A_{0,xx}^m] - \left(\frac{n}{2R} \right)^2 \sum_{i=0}^k \{ Q_{ij}^{m+1} (B + 2B^0) A_{j,xx}^m + Q_{ij}^m (B + 2B^0) A_{j,xx}^{m+1} \\
& - Q_{ij}^m (B + 2B^0) A_{j,xx}^m + R_{ij}^{m+1} (A + 2A^0) B_{j,xx}^m + R_{ij}^m (A + 2A^0) B_{j,xx}^{m+1} \\
& - R_{ij}^m (A + 2A^0) B_{j,xx}^{m+1} - 2[S_{ij}^{m+1} (B + 2B^0) A_{j,x}^m + S_{ij}^m (B + 2B^0) A_{j,x}^{m+1} \\
& - S_{ij}^m (B + 2B^0) A_{j,x}^m] - 2[T_{ij}^{m+1} (A + 2A^0) B_{j,x}^m + T_{ij}^m (A + 2A^0) B_{j,x}^{m+1} \\
& - T_{ij}^m (A + 2A^0) B_{j,x}^m] + U_{ij}^{m+1} (B + 2B^0) A_j^m + U_{ij}^m (B + 2B^0) A_j^{m+1} \\
& - U_{ij}^m (B + 2B^0) A_j^m + V_{ij}^{m+1} (A + 2A^0) B_j^m + V_{ij}^m (A + 2A^0) B_j^{m+1} \\
& - V_{ij}^m (A + 2A^0) B_j^m \} = 0 \quad (74)
\end{aligned}$$

where

$$\begin{aligned}
 Q_{ij}^m(Y) &= (i+j)^2 \delta_{i+j} Y_{i+j}^m + \eta_{i-j}(i-j)^2 \delta_{|i-j|} Y_{|i-j|}^m \\
 R_{ij}^m(Y) &= -(i+j)^2 \delta_{i+j} Y_{i+j}^m + (2 - \eta_{j-i}^2)(i-j)^2 \delta_{|i-j|} Y_{|i-j|}^m \\
 S_{ij}^m(Y) &= [-(i+j)\delta_{i+j} Y_{i+j,x}^m + (2 - \eta_{j-i}^2)|i-j|\delta_{|i-j|} Y_{|i-j|,x}^m]j \\
 T_{ij}^m(Y) &= [(i+j)\delta_{i+j} Y_{i+j,x}^m + \eta_{i-j}|i-j|\delta_{|i-j|} Y_{|i-j|,x}^m]j \\
 U_{ij}^n(Y) &= [\delta_{i+j} Y_{i+j,xx}^m + \eta_{i-j}\delta_{|i-j|} Y_{|i-j|,xx}^m]j^2 \\
 V_{ij}^n(Y) &= [-\delta_{i+j} Y_{i+j,xx}^m + (2 - \eta_{j-i}^2)\delta_{|i-j|} Y_{|i-j|,xx}^m]j^2.
 \end{aligned}$$

Equilibrium

1. $i = 0$, eq. (69):

$$\begin{aligned}
 A_{0,xxxx}^{m+1} &\left(d_{11} - \frac{b_{21}^2}{a_{22}} \right) - A_{0,xx}^{m+1} \left(\frac{2b_{21}}{Ra_{22}} \right) - A_0^{m+1} \left(\frac{1}{R^2 a_{22}} \right) - \bar{N}_{xx} (A_{0,xx}^{m+1} + A_{0,xx}^0) \\
 &+ \left(\frac{n}{2R} \right)^2 \sum_{j=1}^k j^2 \left\{ \frac{b_{21}}{a_{22}} [A_j^{m+1} A_{j,xx}^m + (A_j^m + 2A_j^0) A_{j,xx}^{m+1} \right. \\
 &- A_j^m A_{j,xx}^m + A_{j,xx}^{m+1} A_j^m + (A_{j,xx}^m + 2A_{j,xx}^0) A_j^{m+1} - A_{j,xx}^m A_j^m + 2A_{j,x}^{m+1} A_{j,x}^m \\
 &+ 2(A_{j,x}^m + 2A_{j,x}^0) A_{j,x}^{m+1} - 2A_{j,x}^m A_{j,x}^m + B_j^{m+1} B_{j,xx}^m \\
 &+ (B_j^m + 2B_j^0) B_{j,xx}^{m+1} - B_j^m B_{j,xx}^m + (B_{j,xx}^{m+1} + 2B_{j,xx}^0) B_j^m \\
 &+ (B_{j,xx}^m + 2B_{j,xx}^0) B_j^{m+1} - (B_{j,xx}^m + 2B_{j,xx}^0) B_j^m \\
 &+ 2B_{j,x}^{m+1} B_{j,x}^m + 2(B_{j,x}^m + 2B_{j,x}^0) B_{j,x}^{m+1} - 2B_{j,x}^m B_{j,x}^m] \\
 &+ \frac{1}{a_{22}R} [A_j^{m+1} A_j^m + (A_j^m + 2A_j^0) A_j^{m+1} - A_j^m A_j^m \\
 &+ B_j^{m+1} B_j^m + (B_j^m + 2B_j^0) B_j^{m+1} - B_j^m B_j^m] \Big\} \\
 &- \frac{1}{2} \left(\frac{n}{R} \right)^2 \sum_{j=1}^k \{ j^2 [A_j^{m+1} C_{j,xx}^m + (A_j^m + A_j^0) C_{j,xx}^{m+1} - A_j^m C_{j,xx}^m \right. \\
 &+ B_j^{m+1} D_{j,xx}^m + (B_j^m + B_j^0) D_{j,xx}^{m+1} - B_j^m D_{j,xx}^m] \\
 &+ 2A_{j,x}^{m+1} C_{j,x}^m + 2(A_{j,x}^m + A_{j,x}^0) C_{j,x}^{m+1} - 2A_{j,x}^m C_{j,x}^m \\
 &+ 2B_{j,x}^{m+1} D_{j,x}^m + (B_{j,x}^m + B_{j,x}^0) D_{j,x}^{m+1} - 2B_{j,x}^m D_{j,x}^m \\
 &+ A_{j,xx}^{m+1} C_j^m + (A_{j,xx}^m + A_{j,xx}^0) C_j^{m+1} - A_{j,xx}^m C_j^m + B_{j,xx}^{m+1} D_j^m \\
 &+ (B_{j,xx}^m + B_{j,xx}^0) D_j^{m+1} - B_{j,xx}^m D_j^m \} + \frac{a_{12}}{a_{22}R} \bar{N}_{xx} - \frac{a_{23}}{a_{22}R} \bar{N}_{xy} + q_0^1 = 0. \quad (75)
 \end{aligned}$$

2. $i = 1, 2, \dots, k$; weighting function is $\cos(iny/R)$:

$$d_{11} A_{i,xxxx}^{m+1} + 4d_{13} \left(\frac{in}{R} \right) B_{i,xxx}^{m+1} - (2d_{12} + 4d_{33}) \left(\frac{in}{R} \right)^2 A_{i,xx}^{m+1}$$

$$\begin{aligned}
& -4d_{23}\left(\frac{in}{R}\right)^3 B_{i,x}^{m+1} + d_{22}\left(\frac{in}{R}\right)^4 A_i^{m+1} + b_{21} C_{i,xxx}^{m+1} \\
& + (2b_{23} - b_{31})\left(\frac{in}{R}\right) D_{i,xxx}^{m+1} - (b_{11} - 2b_{33} + b_{22})\left(\frac{in}{R}\right)^2 C_{i,xx}^{m+1} \\
& - (2b_{13} - b_{32})\left(\frac{in}{R}\right)^3 D_{i,x}^{m+1} + b_{12}\left(\frac{in}{R}\right)^4 C_i^{m+1} + \frac{1}{R} C_{i,xx}^{m+1} \\
& - \left(\frac{in}{R}\right)\frac{1}{a_{22}} \left\{ -b_{21} A_i^{m+1} A_{0,xx}^m - b_{21}(A_i^m + A_i^0) A_{0,xx}^{m+1} + b_{21} A_i^m A_{0,xx}^m \right. \\
& - \frac{1}{R} A_i^{m+1} A_0^m - \frac{1}{R} (A_i^m + A_i^0) A_0^{m+1} + \frac{1}{R} (A_i^m + A_i^0) A_0^{m+1} + \frac{1}{R} A_i^m A_0^m \\
& + \left(\frac{n}{2R}\right)^2 \sum_{j=1}^k j^2 [(A_i^{m+1} + A_i^0)(A_j^m + 2A_j^0) A_j^m + (A_i^m + A_i^0)(A_j^{m+1} + 2A_j^0) A_j^m \\
& + (A_i^m + A_i^0)(A_j^m + 2A_j^0) A_j^{m+1} - 2(A_i^m + A_i^0)(A_j^m + 2A_j^0) A_j^m \\
& + (A_i^m + A_i^0)(B_j^m + 2B_j^0) B_j^m + (A_i^m + A_i^0)(B_j^{m+1} + 2B_j^0) B_j^m \\
& + (A_i^m + A_i^0)(B_j^m + 2B_j^0) B_j^{m+1} - 2(A_i^m + A_i^0)(B_j^m + 2B_j^0) B_j^m] \Big\} \\
& - \left(\frac{in}{R}\right)^2 \left(\frac{A_i^{m+1} + A_i^0}{a_{22}}\right) (a_{12} \bar{N}_{xx} - a_{23} \bar{N}_{xy}) - (A_{i,xx}^{m+1} + A_{i,xx}^0) \bar{N}_{xx} + 2\bar{N}_{xy} \\
& \times \left(\frac{in}{R}\right) (B_{i,x}^{m+1} + B_{i,x}^0) - \frac{1}{2} \left(\frac{n}{R}\right)^2 \sum_{j=1}^{2k} j^2 \{ [J_{ij}^{m+1}(A) C_{j,xx}^m + J_{ij}^m(A + A^0) C_{j,xx}^{m+1} \\
& - J_{ij}^m(A) C_{j,xx}^m] + [K_{ij}^{m+1}(B) D_{j,xx}^m + K_{ij}^m(B + B^0) D_{j,xx}^{m+1} \\
& - K_{ij}^m(B) D_{j,xx}^m] + 2[L_{ij}^{m+1}(A) C_{j,x}^m + L_{ij}^m(A + A^0) C_{j,x}^{m+1} - L_{ij}^m(A) C_{j,x}^m] \\
& + 2[M_{ij}^{m+1}(B) D_{j,x}^m + M_{ij}^m(B + B^0) D_{j,x}^{m+1} - M_{ij}^m(B) D_{j,x}^m] \\
& + N_{ij}^{m+1}(A) C_j^m + N_{ij}^m(A + A^0) C_j^{m+1} - N_{ij}^m(A) C_j^m \\
& \left. + O_{ij}^{m+1}(B) D_j^m + O_{ij}^m(B + B^0) D_j^{m+1} - O_{ij}^m(B) D_j^m \right\} + q_i^1 = 0. \quad (76)
\end{aligned}$$

3. $i = 1, 2, \dots, k$; weighting function is $\sin(iny/R)$, eq. (71):

$$\begin{aligned}
& d_{11} B_{i,xxxx}^{m+1} - 4d_{13}\left(\frac{in}{R}\right) A_{i,xxx}^{m+1} - (2d_{12} + 4d_{33})\left(\frac{in}{R}\right)^2 B_{i,xx}^{m+1} + 4d_{23}\left(\frac{in}{R}\right)^3 A_{i,x}^{m+1} \\
& + d_{22}\left(\frac{in}{R}\right)^4 B_i^{m+1} + b_{21} D_{i,xxx}^{m+1} - (2b_{23} - b_{31})\left(\frac{in}{R}\right) C_{i,xxx}^{m+1} \\
& - (b_{11} - 2b_{33} + b_{22})\left(\frac{in}{R}\right)^2 D_{i,xx}^{m+1} + (2b_{13} - b_{32})\left(\frac{in}{R}\right)^3 C_{i,x}^{m+1}
\end{aligned}$$

$$\begin{aligned}
& + b_{12} \left(\frac{in}{R} \right)^4 D_i^{m+1} + \frac{D_{i,xx}^{m+1}}{R} - \left(\frac{in}{R} \right)^2 \frac{1}{a_{22}} \left\{ -b_{21} B_i^{m+1} A_{0,xx}^m - b_{21} (B_i^m + B_i^0) \right. \\
& \times A_{0,xx}^{m+1} + b_{21} B_i^m A_{0,xx}^m - \frac{1}{R} B_i^{m+1} A_0^m - \frac{1}{R} (B_i^m + B_i^0) A_0^{m+1} + \frac{1}{R} B_i^m A_0^m \\
& + \left(\frac{n}{2R} \right)^2 \sum_{j=1}^k j^2 [(B_i^{m+1} + B_i^0)(A_j^m + 2A_j^0) A_j^m + (B_i^m + B_i^0)(A_j^{m+1} + 2A_j^0) A_j^m \\
& + (B_i^m + B_i^0)(A_j^m + 2A_j^0) A_j^{m+1} - 2(B_i^m + B_i^0)(A_j^m + 2A_j^0) A_j^m \\
& + (B_i^{m+1} + B_i^0)(B_j^m + 2B_j^0) B_j^m + (B_i^m + B_i^0)(B_j^{m+1} + 2B_j^0) B_j^m \\
& + (B_i^m + B_i^0)(B_j^m + 2B_j^0) B_j^{m+1} - 2(B_i^m + B_i^0)(B_j^m + 2B_j^0) B_j^m] \Big\} \\
& - \left(\frac{in}{R} \right)^2 \left(\frac{B_i^{m+1} + B_i^0}{a_{22}} \right) (a_{12} \bar{N}_{xx} - a_{23} \bar{N}_{xy}) - (B_{i,xx}^{m+1} + B_{i,xx}^0) \bar{N}_{xx} \\
& - 2 \bar{N}_{xy} \left(\frac{in}{R} \right) (A_{i,x}^{m+1} + A_{i,x}^0) - \frac{1}{2} \left(\frac{n}{R} \right)^2 \sum_{j=1}^{2k} \{ Q_{ij}^{m+1}(B) C_{j,xx}^m \\
& + Q_{ij}^m(B + B^0) C_{j,xx}^{m+1} - Q_{ij}^m(B) C_j^m + R_{ij}^{m+1}(A) D_{j,xx}^m + R_{ij}^m(A + A^0) D_{j,xx}^{m+1} \\
& - R_{ij}^m(A) D_{j,xx}^m - 2[S_{ij}^{m+1}(B) C_{j,x}^m + S_{ij}^m(B + B^0) C_{j,x}^{m+1} - S_{ij}^m(A) C_{j,x}^m] \\
& - 2[T_{ij}^{m+1}(A) D_{j,x}^m + T_{ij}^m(A + A^0) D_{j,x}^{m+1} - T_{ij}^m(A) D_{j,x}^m] + U_{ij}^{m+1}(B) C_j^m \\
& + U_{ij}^m(B + B^0) C_j^{m+1} - U_{ij}^m(B) C_j^m + V_{ij}^{m+1}(A) D_j^m \\
& + V_{ij}^m(A + A^0) D_j^m - V_{ij}^m(A) D_j^m \} + q_i^2 = 0. \tag{77}
\end{aligned}$$

Finally, the boundary conditions [SS-*i*, CC-*i*, eqs. (37) and (40)–(46)] are also expressed in terms of the dependent variables, through the use of eqs. (47).

SS-1: $A_0 = 0$,

$$\begin{aligned}
A_{0,xx} \left(d_{11} - \frac{b_{21}^2}{a_{22}} \right) &= \frac{b_{21}}{a_{22}} (-a_{12} \bar{N}_{xx} + a_{23} \bar{N}_{xy}) \\
& + \bar{M}_{xx} + b_{11} \bar{N}_{xx} - b_{31} \bar{N}_{xy}, \\
A_i = B_i &= 0 \\
d_{11} A_{i,xx} + b_{21} C_{i,xx} + 2d_{13} \left(\frac{in}{R} \right) B_{i,x} &= 0 \\
d_{11} B_{i,xx} + b_{21} D_{i,xx} - 2d_{13} \left(\frac{in}{R} \right) A_{i,x} &= 0 \\
C_i = D_{i,x} = D_i = C_{i,x} &= 0, \quad i = 1, 2, \dots, 2k. \tag{78}
\end{aligned}$$

SS-2: $A_0 = 0,$

$$\left. \begin{aligned} A_{0,xx} \left(d_{11} - \frac{b_{21}^2}{a_{22}} \right) &= \frac{b_{21}}{a_{22}} (-a_{12} \bar{N}_{xx} + a_{23} \bar{N}_{xy}) \\ &\quad + \bar{M}_{xx} + b_{11} \bar{N}_{xx} - b_{31} \bar{N}_{xy}, \\ A_i = B_i = 0 \\ d_{11} A_{i,xx} + b_{21} C_{i,xx} - b_{11} \left(\frac{in}{R} \right)^2 C_i + 2d_{13} \left(\frac{in}{R} \right) B_{i,x} &= 0 \\ d_{11} B_{i,xx} + b_{21} D_{i,xx} - b_{11} \left(\frac{in}{R} \right)^2 D_i - 2d_{13} \left(\frac{in}{R} \right) A_{i,x} &= 0 \end{aligned} \right\} \\ i = 1, 2, \dots, k, \end{math>$$

$$D_{i,x} = C_{i,x} = 0, \quad i = 1, 2, \dots, 2k,$$

$$\begin{aligned} a_{22} C_{i,xxx} - 2a_{23} \left(\frac{in}{R} \right) D_{i,xx} + a_{13} \left(\frac{in}{R} \right)^3 D_i + b_{21} A_{i,xxx} \\ + (2b_{23} - b_{31}) \frac{in}{R} B_{i,xx} + (2b_{33} - b_{22}) \left(\frac{in}{R} \right)^2 A_i + \frac{A_{i,x}}{R} \\ - \frac{n^2}{2R^2} \sum_{j=0}^k \{ [(i+j)^2 A_{i+j}^0 + (1 - \eta_{j-i}^2 + \eta_i)(i-j)^2 A_{|i-j|}^0] A_{j,x} \\ + [(i+j)^2 B_{i+j}^0 + (-1 - \eta_{i-j} + \eta_i)(i-j)^2 B_{|i-j|}^0] B_{j,x} \} &= 0, \\ i = 1, 2, \dots, 2k, \end{aligned}$$

(79)

$$\begin{aligned} a_{22} D_{i,xxx} + 2a_{23} \left(\frac{in}{R} \right) C_{i,xx} - a_{13} \left(\frac{in}{R} \right)^3 + b_{21} B_{i,xxx} \\ - (2b_{23} - b_{31}) \left(\frac{in}{R} \right) A_{i,xx} + (2b_{33} - b_{22}) \left(\frac{in}{R} \right)^2 B_{i,x} \\ + \frac{B_{i,x}}{R} - \frac{n^2}{2R^2} \sum_{j=0}^k \{ [-(i+j)^2 A_{i+j}^0 \\ + (1 - \eta_{j-i}^2 + \eta_i)(i-j)^2 A_{|i-j|}^0] B_{i,xx} + [(i+j)^2 B_{i+j}^0 \\ + (-1 + \eta_{i-j} + \eta_i)(i-j)^2 B_{|i-j|}^0] A_{j,x} \} &= 0, \\ i = 1, 2, \dots, 2k. \end{aligned}$$

SS-3: $A_0 = 0,$

$$\begin{aligned} A_{0,xx} \left(d_{11} - \frac{b_{21}^2}{a_{22}} \right) &= \frac{b_{21}}{a_{22}} [-a_{12} \bar{N}_{xx} + a_{23} \bar{N}_{xy}] \\ &\quad + \bar{M}_{xx} + b_{11} \bar{N}_{xx} - b_{31} \bar{N}_{xy}, \end{aligned}$$

$$\left. \begin{array}{l} A_i = B_i = 0 \\ d_{11}B_{i,xx} + b_{21}D_{i,xx} + b_{31}\left(\frac{in}{R}\right)C_{i,x} - 2d_{13}\left(\frac{in}{R}\right)B_{i,x} = 0 \\ d_{11}B_{i,xx} + b_{21}D_{i,xx} + b_{31}\left(\frac{in}{R}\right)C_{i,x} - 2d_{13}\left(\frac{in}{R}\right)A_{i,x} = 0 \end{array} \right\} \\ i = 1, 2, \dots, k, \quad (80)$$

$$\left. \begin{array}{l} C_i = D_i = 0 \\ a_{22}C_{i,xx} - a_{23}\left(\frac{in}{R}\right)D_{i,x} + b_{21}A_{i,xx} + 2b_{23}\left(\frac{in}{R}\right)B_{i,x} = 0 \\ a_{22}D_{i,xx} + a_{23}\left(\frac{in}{R}\right)C_{i,x} + b_{21}B_{i,xx} - 2b_{23}A_{i,x} = 0 \end{array} \right\} \\ i = 1, 2, \dots, 2k.$$

SS-4: $A_0 = 0,$

$$\begin{aligned} A_{0,xx}\left(d_{11} - \frac{b_{21}^2}{a_{22}}\right) &= \frac{b_{21}}{a_{22}}[-a_{12}\bar{N}_{xx} + a_{23}\bar{N}_{xy}] \\ &\quad + \bar{M}_{xx} + b_{11}\bar{N}_{xx} - b_{31}\bar{N}_{xy}, \end{aligned}$$

$$\left. \begin{array}{l} A_i = B_i = 0 \\ b_{21}C_{i,xx} - b_{11}\left(\frac{in}{R}\right)^2C_i - b_{31}\left(\frac{in}{R}\right)D_{i,x} + d_{11}A_{i,xx} + 2d_{13}\left(\frac{in}{R}\right)B_{i,x} = 0 \\ b_{21}D_{i,xx} - b_{11}\left(\frac{in}{R}\right)^2D_i + b_{31}\left(\frac{in}{R}\right)D_{i,x} + d_{11}B_{i,xx} - 2d_{13}\left(\frac{in}{R}\right)B_{i,x} = 0 \end{array} \right\} \\ i = 1, 2, \dots, k,$$

$$\left. \begin{aligned} &-a_{12}\left(\frac{in}{R}\right)^2C_i + a_{22}C_{i,xx} - a_{23}\left(\frac{in}{R}\right)D_{i,x} \\ &\quad + b_{21}A_{i,xx} + 2b_{23}\left(\frac{in}{R}\right)B_{i,x} = 0 \\ &-a_{13}\left(\frac{in}{R}\right)^3D_i + 2a_{23}\left(\frac{in}{R}\right)D_{i,xx} + (a_{33} + a_{12})C_{i,x}\left(\frac{in}{R}\right)^2 - a_{22}C_{i,xxx} \\ &\quad + (b_{31} - 2b_{23})\left(\frac{in}{R}\right)B_{i,xx} - (2b_{33} - b_{22})\left(\frac{in}{R}\right)^2A_{i,x} - b_{21}A_{i,xxx} \\ &\quad - \frac{A_{i,x}}{R} + \frac{n^2}{2R^2} \sum_{j=0}^k \{[(i+j)^2A_{i+j}^0 + (1-\eta_{j-i}^2 + \eta_i)(i-j)^2A_{|i-j|}^0]A_{j,x} \\ &\quad + [(i+j)^2B_{i+j} + (-1 - \eta_{i-j} + \eta_i)(i-j)^2B_{|i-j|}^0]B_{j,x}\} = 0 \end{aligned} \right\}$$

$$\left. \begin{aligned}
& -a_{12} \left(\frac{in}{R} \right)^2 D_i + a_{22} D_{i,xx} + a_{23} \left(\frac{in}{R} \right) C_{i,x} \\
& + b_{21} B_{i,xx} - 2b_{23} \left(\frac{in}{R} \right) A_{i,x} = 0 \\
& a_{13} \left(\frac{in}{R} \right)^3 C_i - 2a_{23} \left(\frac{in}{R} \right) C_{i,xx} + (a_{33} + a_{12}) D_{i,x} \left(\frac{in}{R} \right)^2 - a_{22} D_{i,xxx} \\
& - (b_{31} - 2b_{33}) \left(\frac{in}{R} \right) A_{i,xx} - (2b_{33} - b_{22}) \left(\frac{in}{R} \right)^2 B_{i,x} - b_{21} B_{i,xxx} \\
& - \frac{B_{i,x}}{R} + \frac{n^2}{2R^2} \sum_{j=0}^k \{ [-(i+j)^2 A_{i+j}^0 + (1 - \eta_{j-i}^2 + \eta_i)(i-j)^2 A_{|i-j|}^0] \\
& \times B_{j,x} + [(i+j)^2 B_{i+j}^0 + (-1 + \eta_{i-j} + \eta_i)(i-j)^2 B_{|i-j|}^0] A_{j,x} \} = 0 \\
& i = 1, 2, \dots, 2k.
\end{aligned} \right\} \quad (81)$$

$$\begin{aligned}
\text{CC-1: } & A_0 = A_{0,x} = 0, \\
& A_i = A_{i,x} = B_i = B_{i,x} = 0, \quad i = 1, 2, \dots, k, \\
& C_i = D_{i,x} = D_i = C_{i,x} = 0, \quad i = 1, 2, \dots, 2k.
\end{aligned} \quad (82)$$

$$\left. \begin{aligned}
& A_0 = A_{0,x} = 0, \\
& A_i = A_{i,x} = B_i = B_{i,x} = 0, \quad i = 1, 2, \dots, k, \\
& D_{i,x} = C_{i,x} = 0 \\
& -a_{13} \left(\frac{in}{R} \right)^3 D_i + 2a_{23} \left(\frac{in}{R} \right) D_{i,xx} - a_{22} C_{i,xxx} - b_{21} A_{i,xxx} \\
& + (b_{31} - 2b_{23}) \left(\frac{in}{R} \right) B_{i,xx} = 0 \\
& a_{13} \left(\frac{in}{R} \right)^3 C_i - 2a_{23} \left(\frac{in}{R} \right) C_{i,xx} - a_{22} D_{i,xxx} - b_{21} B_{i,xxx} \\
& - (b_{31} - 2b_{23}) \left(\frac{in}{R} \right) A_{i,xx} = 0
\end{aligned} \right\} \quad i = 1, 2, \dots, 2k. \quad (83)$$

$$\left. \begin{aligned}
& A_0 = A_{0,x} = 0, \\
& A_i = A_{i,x} = B_i = B_{i,x} = 0, \quad i = 1, 2, \dots, k, \\
& C_i = D_i = a_{22} C_{i,xx} - a_{23} \left(\frac{in}{R} \right) D_{i,x} + b_{21} A_{i,xx} = 0 \\
& a_{22} D_{i,xx} + a_{23} \left(\frac{in}{R} \right) C_{i,x} + b_{21} B_{i,xx} = 0
\end{aligned} \right\} \quad i = 1, 2, \dots, 2k. \quad (84)$$

$$\left. \begin{aligned}
 \text{CC-4: } & A_0 = A_{0,x} = 0, \\
 & A_i = A_{i,x} = B_i = B_{i,x}, \quad i = 1, 2, \dots, k, \\
 & -a_{12}\left(\frac{in}{R}\right)^2 C_i + a_{22}C_{i,xx} - a_{23}\left(\frac{in}{R}\right)D_{i,x} + b_{21}A_{i,xx} = 0 \\
 & -a_{13}\left(\frac{in}{R}\right)^2 D_i + 2a_{23}\left(\frac{in}{R}\right)D_{i,xx} + (a_{33} + a_{12})\left(\frac{in}{R}\right)^2 C_{i,x} \\
 & -a_{22}C_{i,xxx} - b_{21}A_{i,xxx} + (b_{31} - 2b_{23})\left(\frac{in}{R}\right)B_{i,xx} = 0 \\
 & -a_{12}\left(\frac{in}{R}\right)^2 D_i + a_{22}D_{i,xx} + a_{23}\left(\frac{in}{R}\right)C_{i,x} + b_{21}B_{i,xx} = 0 \\
 & a_{13}\left(\frac{in}{R}\right)^3 C_i - 2a_{23}\left(\frac{in}{R}\right)C_{i,xx} + (a_{33} + a_{12})\left(\frac{in}{R}\right)^2 D_{i,x} \\
 & -a_{22}D_{i,xxx} - b_{21}B_{i,xxx} - (b_{31} - 2b_{23})\left(\frac{in}{R}\right)A_{i,xx} = 0
 \end{aligned} \right\} \quad i = 1, 2, \dots, 2k. \quad (85)$$

9.3.2 Finite-Difference Equations

Before casting the field equations into finite-difference form, the linearized ordinary differential equations of compatibility and equilibrium, eqs. (73)–(77), can be written in matrix form.

$$\begin{aligned}
 [M_1]\{X_{,xxxx}\} + [M_2]\{X_{,xxx}\} + [M_3]\{X_{,xx}\} \\
 + [M_4]\{X_{,x}\} + [M_5]\{X\} + \{M_6\} = 0
 \end{aligned} \quad (86)$$

where

$$\{X\} = \{A_0^{m+1}, \dots, A_k^{m+1}, B_1^{m+1}, \dots, B_k^{m+1}, C_1^{m+1}, \dots, C_{2k}^{m+1}, D_1^{m+1}, \dots, D_{2k}^{m+1}\}^T$$

is the column matrix of the unknown function of position x , and $[M_j]$, $j = 1, 2, \dots, 5$, are square matrices [($6k + 1$) by ($6k + 1$); see eqs. (73)–(77)] with elements composed of known parameters (applied loads, geometry, and values of the unknowns evaluated at the previous step m and therefore known). $\{M_6\}$ is a column matrix of known elements.

Next, transformation equations are introduced to reduce the order of the linearized differential equations. This step increases (doubles) the number of equations, but it is introduced for convenience, because it is easier to deal with low-order equations when employing the finite-difference scheme. These transformation equations are

$$\{\eta\} = \{X_{,xx}\}, \quad (87)$$

and they are used only in connection with the third and fourth derivatives.

By the transformation in eq. (87), eq. (86) becomes

$$[R] \begin{Bmatrix} \{X_{,xx}\} \\ \{\eta_{,xx}\} \end{Bmatrix} + [S] \begin{Bmatrix} \{X_{,x}\} \\ \{\eta_{,x}\} \end{Bmatrix} + [T] \begin{Bmatrix} \{X\} \\ \{\eta\} \end{Bmatrix} = \{G\} \quad (88)$$

where

$$\begin{aligned} [R] &= \begin{bmatrix} [0] & [M_1] \\ [I] & [0] \end{bmatrix}, & [S] &= \begin{bmatrix} [M_4] & [M_2] \\ [0] & [0] \end{bmatrix}, \\ [T] &= \begin{bmatrix} [M_5] & [M_3] \\ [0] & -[I] \end{bmatrix}, & \{G\} &= \begin{Bmatrix} -[M_6] \\ \{0\} \end{Bmatrix}, \end{aligned} \quad (89)$$

and $[0]$ and $[I]$ are the zero and identity matrices, respectively.

The governing equations (linearized ordinary differential equations) are shown in matrix form, and eqs. (88) are next cast into finite-difference form. The usual central difference formula is employed and the equation becomes

$$\begin{aligned} \left(\frac{1}{h^2} [R]^{(j)} + \frac{1}{2h} [S]^{(j)} \right) \begin{Bmatrix} \{X\} \\ \{\eta\} \end{Bmatrix}^{(j+1)} &+ \left(-\frac{1}{2h} [R]^{(j)} + [T]^{(j)} \right) \begin{Bmatrix} \{X\} \\ \{\eta\} \end{Bmatrix}^{(j)} \\ &+ \left(\frac{1}{h^2} [R]^{(j)} - \frac{1}{2h} [S]^{(j)} \right) \begin{Bmatrix} \{X\} \\ \{\eta\} \end{Bmatrix}^{(j-1)} = \{G\}^j \end{aligned} \quad (90)$$

where j denotes the j th node of the finite-difference grid. At each end ($x = 0$ and L) one more fictitious point is used. This requires $12k + 2$ additional equations at each end (the total number is $24k + 4$). These needed additional equations are the boundary conditions at each end, eqs. (78)–(85) (whichever set applies from SS- i or CC- i), and their number is $12k + 2$. The boundary conditions may also be first expressed in matrix form and then cast into finite-difference form.

At either $x = 0$ or $x = L$

$$[N_1] \{X_{,xxx}\} + [N_2] \{X_{,xx}\} + [N_3] \{X_{,x}\} + [N_4] \{X\} + \{N_5\} = 0 \quad (91)$$

where $[N_j]$, $j = 1, 2, 3, 4$, are matrices $[(12k + 2) \text{ by } (6k + 1)]$ with known elements, and $\{N_5\}$ is a column matrix $[(12k + 2) \text{ by one}]$, also with known elements.

Use of the transformation equations, eq. (87) yields

$$[BS] \begin{Bmatrix} \{X_{,x}\} \\ \{\eta_{,x}\} \end{Bmatrix} + [BT] \begin{Bmatrix} \{X\} \\ \{\eta\} \end{Bmatrix} = [BG] \quad (92)$$

where

$$\begin{aligned} [BS] &= [[N_3][N_1]], \\ [BT] &= [[N_4][N_2]], \end{aligned} \quad (93)$$

and

Note that $[BS]$ and $[BT]$ are square matrices [($12k + 2$) by ($12k + 2$)]. In finite-difference form, eq. (92) becomes

$$\frac{1}{2h} [BS]^j \left\{ \begin{matrix} \{X\} \\ \{\eta\} \end{matrix} \right\}^{j+1} + [BT]^j \left\{ \begin{matrix} \{X\} \\ \{\eta\} \end{matrix} \right\}^j - \frac{1}{2h} [BS]^j \left\{ \begin{matrix} \{X\} \\ \{\eta\} \end{matrix} \right\}^{j-1} = \{BG\}^j \quad (94)$$

where j is the node number at $x = 0$ and $x = L$ (1 or N).

9.3.3 Expressions for Total Potential and Average Strains

Before outlining in detail the numerical scheme of the solution methodology, it is necessary to write the expressions for the average end shortening, average shear strain, and the total potential in terms of the dependent variables, A_i , B_i , C_i , and D_i .

The average end shortening and shear strain are defined by

$$e_{av} = -\frac{1}{2\pi RL} \int_0^{2\pi R} \int_0^L \frac{\partial u}{\partial x} dx dy,$$

$$\gamma_{av} = \frac{1}{2\pi RL} \int_0^{2\pi R} \int_0^L \left(\frac{\partial u}{\partial y} + \frac{\partial v}{\partial x} \right) dx dy. \quad (95)$$

In terms of the variables $w(x, y)$ and $F(x, y)$, the above expressions become

$$e_{av} = a_{11}\bar{N}_{xx} - a_{13}\bar{N}_{xy} - \frac{1}{2\pi RL} \int_0^{2\pi R} \int_0^L [a_{11}F_{yy} + a_{12}F_{xx} - a_{13}F_{xx} + b_{11}w_{xx} + b_{12}w_{yy} + 2b_{23}w_{xy} - \frac{1}{2}w_{x}(w_{,x} + 2w_{,x}^0)] dx dy, \quad (96)$$

$$\gamma_{av} = -a_{13}\bar{N}_{xx} + a_{33}\bar{N}_{xy} + \frac{1}{2\pi RL} \int_0^{2\pi R} \int_0^L [a_{13}F_{yy} + a_{23}F_{xx} - a_{33}F_{xy} + b_{31}w_{xx} + b_{32}w_{yy} + 2b_{33}w_{xy} - \frac{1}{2}w_{x}(w_{,y} + 2w_{,y}^0) - \frac{1}{2}w_{y}(w_{,x} + 2w_{,x}^0)] dx dy. \quad (97)$$

Finally, if the expressions for w and F are substituted into eqs. (96) and (97), these equations become

$$e_{av} = a_{11}\bar{N}_{xx} - a_{13}\bar{N}_{xy} - \frac{1}{2} \int_0^L \left\{ \frac{a_{12}}{a_{22}} \left\{ -b_{21}A''_0 - A_0/R + a_{12}\bar{N}_{xx} - a_{23}\bar{N}_{xy} + \left(\frac{n}{2R} \right)^2 \sum_{j=1}^k j^2 [(A_j + 2A_j^0)A_j + (B_j + 2B_j^0)B_j] \right\} + b_{11}A''_0 - \frac{1}{2}(A'_0 + 2A_0^0)A'_0 - \frac{1}{4}[A'_j(A'_j + 2A_j^0) + B'_j(B'_j + 2B_j^0)] \right\} dx, \quad (98)$$

$$\begin{aligned} \gamma_{av} = & -a_{13}\bar{N}_{xx} + a_{33}\bar{N}_{xy} + \frac{1}{2} \int_0^L \left\{ \frac{a_{23}}{a_{22}} \left\{ -b_{21}A''_0 - A_0/R \right. \right. \\ & + a_{12}\bar{N}_{xx} - a_{23}\bar{N}_{xy} + \left(\frac{n}{2R} \right)^2 \sum_{j=1}^k j^2 [(A_j + 2A_j^0)A_j \right. \\ & \left. \left. + (B_j + 2B_j^0)B_j] \right\} + b_{31}A''_0 - \sum_{j=1}^k \left(\frac{jn}{2R} \right)^2 [A'_j(B_j + B_j^0) \right. \\ & \left. \left. - B'_j(A_j + A_j^0) + A_j^{0'}B_j - B_j^{0'}A_j] \right\} dx. \right. \end{aligned} \quad (99)$$

Similarly, the expression for the total potential is

$$\begin{aligned} U_T = & \frac{1}{2} \int_0^{2\pi R} \int_0^L (N_{xx}\varepsilon_{xx}^0 + N_{yy}\varepsilon_{yy}^0 + N_{xy}\gamma_{xy}^0 - M_{xx}\kappa_{xx} - M_{yy}\kappa_{yy} - 2M_{xy}\kappa_{xy}) dx dy \\ & - \int_0^{2\pi R} \int_0^L qw dx dy - \int_0^{2\pi R} [-\bar{N}_{xx}u + \bar{N}_{xy}v] \Big|_0^L dy + \int_0^{2\pi R} (\bar{M}_{xx}w_{,x}) \Big|_0^L dy \end{aligned} \quad (100)$$

where $\bar{M}_{xx} = -\bar{E}\bar{N}_{xx}$, \bar{E} is the load eccentricity measured positive in the positive z -direction, and

$$u|_0^L = \int_0^L \frac{\partial u}{\partial x} dx, \quad v|_0^L = \int_0^L \frac{\partial v}{\partial x} dx.$$

Thus, the contribution of the in-plane loads to the total potential becomes

$$-\int_0^{2\pi R} [-\bar{N}_{xx}u + \bar{N}_{xy}v] \Big|_0^L dy = -\int_0^{2\pi R} \left[-\bar{N}_{xx} \int_0^L \frac{\partial u}{\partial x} dx + \bar{N}_{xy} \int_0^L \frac{\partial v}{\partial x} dx \right] dy.$$

In terms of w and F , the expression for U_T becomes

$$\begin{aligned} U_T = & \frac{1}{2} \int_0^{2\pi R} \int_0^L [a_{11}F_{,yy}^2 + a_{22}F_{,xx}^2 + a_{33}F_{,xy}^2 + 2a_{12}F_{,xx}F_{,yy} \\ & - 2a_{13}F_{,yy}F_{,xy} - 2a_{23}F_{,xx}F_{,xy}] dx dy - \frac{1}{2} \int_0^{2\pi R} \int_0^L (d_{11}w_{,xx}^2 + d_{22}w_{,yy}^2 \\ & + 4d_{33}w_{,xy}^2 + 2d_{12}w_{,xx}w_{,yy} + 4d_{13}w_{,xx}w_{,xy} + 4d_{23}w_{,yy}w_{,xy}) dx dy \\ & - \bar{N}_{xx} \int_0^{2\pi R} \int_0^L (a_{11}F_{,yy} + a_{12}F_{,xx} - a_{13}F_{,xy}) dx dy \\ & + \bar{N}_{xy} \int_0^{2\pi R} \int_0^L (a_{23}F_{,xx} - a_{33}F_{,xy} + a_{13}F_{,yy}) dx dy \\ & - \int_0^{2\pi R} \int_0^L qw dx dy + \pi RL(a_{11}\bar{N}_{xx}^2 + a_{33}\bar{N}_{xy}^2) - 2\pi RL(e_{av}\bar{N}_{xx} + \gamma_{av}\bar{N}_{xy}) \\ & - 2\pi RL(a_{13}\bar{N}_{xx}\bar{N}_{xy} - \int_0^{2\pi R} (\bar{E}\bar{N}_{xx}w_{,x}) \Big|_0^L dy). \end{aligned} \quad (101)$$

Finally, the expression for the total potential in terms of A_i , B_i , C_i , and D_i becomes

$$\begin{aligned}
 U_T = \pi R \int_0^L & \left\{ \frac{1}{a_{22}} \left\{ -b_{21} A''_0 - A_0/R + \left(\frac{n}{2R} \right)^2 \sum_{j=1}^k j^2 [(A_j + 2A_j^0) A_j \right. \right. \\
 & + (B_j + 2B_j^0) B_j] + a_{12} \bar{N}_{xx} - a_{23} \bar{N}_{xy} \left. \right\}^2 + 2(a_{23} \bar{N}_{xy} - a_{12} \bar{N}_{xx}) \\
 & \times \frac{1}{a_{22}} \left\{ -b_{21} A''_0 - A_0/R + \left(\frac{n}{2R} \right)^2 \sum_{j=1}^k j^2 [(A_j + 2A_j^0) A_j \right. \\
 & + (B_j + 2B_j^0) B_j] + a_{12} \bar{N}_{xx} - a_{23} \bar{N}_{xy} \left. \right\} - d_{11} (A''_0)^2 \\
 & + \frac{1}{2} \sum_{i=1}^{2k} \left\{ a_{11} \left(\frac{in}{R} \right)^4 (C_i^2 + D_i^2) + a_{22} [(C_i'')^2 + (D_i'')^2] \right. \\
 & + a_{33} \left(\frac{in}{R} \right)^2 [(C_i')^2 + (D_i')^2] - 2a_{12} \left(\frac{in}{R} \right)^2 (C_i'' C_i + D_i'' D_i) \\
 & - 2a_{13} \left(\frac{in}{R} \right)^3 (-C_i D_i' + D_i C_i) - 2a_{23} \left(\frac{in}{R} \right) (C_i'' D_i - D_i'' C_i) \left. \right\} \\
 & - \frac{1}{2} \sum_{i=1}^k \left\{ d_{11} [(A_i'')^2 + (B_i'')^2] + d_{22} \left(\frac{in}{R} \right)^4 (A_i^2 + B_i^2) \right. \\
 & + 4d_{33} \left(\frac{in}{R} \right)^2 [(A_i')^2 + (B_i')^2] - 2d_{12} \left(\frac{in}{R} \right)^2 (A_i'' A_i + B_i'' B_i) \\
 & - 4d_{13} \left(\frac{in}{R} \right) (-A_i'' B_i' + B_i'' A_i) - 4d_{23} \left(\frac{in}{R} \right)^3 (A_i B_i' - B_i A_i') \left. \right\} dx \\
 & - \pi R \int_0^L \left\{ 2q_0^1 A_0 + \sum_{j=1}^k [q_j^1 A_j + q_j^2 B_j] \right\} dx \\
 & - 2\pi RL(e_{av} \bar{N}_{xx} + \gamma_{av} \bar{N}_{xy}) + \pi RL(a_{11} \bar{N}_{xx}^2 - 2a_{13} \bar{N}_{xx} \bar{N}_{xy} + a_{33} \bar{N}_{xy}) \\
 & - 4\pi \bar{E} \bar{N}_{xx} R A'_0. \tag{102}
 \end{aligned}$$

9.3.4 Numerical Procedure

The linearized finite-difference equations can be solved by an algorithm which is a modification of the one described in [36]. The modification, which consists of a generalization of the algorithm of [36], is fully described in [37]. The solution procedure steps are as follows.

The field equation, eq. (90), can be written as

$$\left[\tilde{C}_k \right] \{\tilde{Z}_j\} + \left[\tilde{D}_k \right] \{\tilde{Z}_j\} + \left[\tilde{A}_k \right] \{\tilde{Z}_j\} = \{\tilde{G}_k\}. \tag{103}$$

where $k = 1, 2, \dots, N$ and

$$\begin{aligned} [\bar{C}_k] &= \frac{1}{h^2}[R]^k - \frac{1}{2h}[S]^k, & [\bar{B}_k] &= -\frac{1}{2h^2}[\bar{R}]^k + [T]^k, \\ [\bar{A}_k] &= \frac{1}{h^2}[R]^k + \frac{1}{2h}[S]^k, & \{\bar{Z}_k\} &= \left\{ \begin{array}{l} \{X\} \\ \{\eta\} \end{array} \right\}^k. \end{aligned} \quad (104)$$

Note that there are $12k + 2$ elements in the $\{\bar{Z}_k\}$ vector.

In addition, the boundary conditions, eqs. (94), can be written in a form similar to that of eqs. (103). At $x = 0$ ($k = 1$),

$$-\bar{C}_1\{\bar{Z}_0\} + \bar{B}_1\{\bar{Z}_1\} + \bar{A}_1\{\bar{Z}_2\} = \{BG_1\}, \quad (105)$$

and at $x = L$ ($k = N$),

$$-\bar{C}_N\{\bar{Z}_{N-1}\} + \bar{B}_N\{\bar{Z}_N\} + \bar{A}_N\{\bar{Z}_{N+1}\} = \{BG_N\} \quad (106)$$

where

$$[\bar{C}_i] = \frac{1}{2h}[BS]^i; [\bar{B}_i] = [BT]^i; [\bar{A}_i] = \frac{1}{2h}[BS]^i, \quad i = 1, N. \quad (107)$$

Note that $\{\bar{Z}_0\}$ and $\{\bar{Z}_{N+1}\}$ denote the vectors of the unknowns at the fictitious points ($k = 0$ and $k = N + 1$).

By properly arranging eqs. (103), (105), and (106) for the entire cylinder, the matrix representation on page 215 is obtained.

Equation (108) can be put in the form of eq. (109) on page 217 and is a special case of this form, through the following changes: First, there is no common unknown vector Z_i and thus all the $\{d_i\}$ vectors are zero (tridiagonal matrix). Next,

$$[B_1] = \begin{bmatrix} [\bar{C}_1] & [\bar{B}_1] \\ [\bar{C}_1] & [\bar{B}_1] \end{bmatrix}, \quad (24k + 4) \text{ by } (24k + 4);$$

$$\{Z_1\} = \left\{ \begin{array}{l} \{\bar{Z}_0\} \\ \{\bar{Z}_1\} \end{array} \right\}, \quad (24k + 4) \text{ by one};$$

$$[A_1] = \begin{bmatrix} [\bar{A}_1] \\ [\bar{A}_1] \end{bmatrix}, \quad (24k + 4) \text{ by } (12k + 2);$$

$$[g_1] = \left\{ \begin{array}{l} \{BG_1\} \\ \{G_1\} \end{array} \right\}, \quad (24k + 4) \text{ by one};$$

$$[C_2] = [[0]], [\bar{C}_2]], \quad (12k + 2) \text{ by } (24k + 4);$$

$$[C_j] = [\bar{C}_j], \quad j = 3, 4, \dots, N - 1;$$

$$[B_j] = [\bar{B}_j], \quad j = 2, 3, \dots, N - 1;$$

$$[A_j] = [\bar{A}_j], \quad j = 2, 3, \dots, N - 2;$$

$$\{Z_j\} = \{\bar{Z}_j\}, \quad \{g_j\} = \{\bar{g}_j\}, \quad j = 2, 3, \dots, N - 1.$$

$$\left[\begin{array}{c|c|c}
 \bar{C}_1 & \bar{\bar{B}}_1 & \bar{\bar{A}}_1 \\
 \bar{C}_1 & \bar{B}_1 & \bar{A}_1 \\
 \hline
 \bar{C}_2 & \bar{B}_2 & \bar{A}_2 \\
 \hline
 \bar{C}_3 & \bar{B}_3 & \bar{A}_3
 \end{array} \right] \left[\begin{array}{c|c|c}
 \bar{Z}_0 & & \\
 \bar{Z}_1 & & \\
 \bar{Z}_2 & & \\
 \bar{Z}_3 & & \\
 \vdots & & \\
 \bar{Z}_{i-1} & & \\
 \hline
 \bar{Z}_i & & \\
 \bar{Z}_{i+1} & & \\
 \vdots & & \\
 \bar{Z}_{N-2} & & \\
 \bar{Z}_{N-1} & & \\
 \bar{Z}_N & & \\
 \bar{C}_N & & \\
 \bar{\bar{C}}_N & & \\
 \hline
 \bar{B}_N & & \\
 \bar{\bar{B}}_N & & \\
 \hline
 \bar{A}_N & & \\
 \bar{\bar{A}}_N & &
 \end{array} \right] = \left\{ \begin{array}{c}
 BG_1 \\
 G_1 \\
 G_2 \\
 G_3 \\
 \vdots \\
 G_{i-1} \\
 \hline
 G_i \\
 G_{i+1} \\
 \vdots \\
 G_{N-2} \\
 G_{N-1} \\
 G_N \\
 GB_N
 \end{array} \right\}. \quad (108)$$

$$[A_{N-1}] = [[\bar{A}_{N-1}], [0]], \quad (12k + 2) \text{ by } (24k + 4);$$

$$[C_N] = \begin{bmatrix} [\bar{C}_N] \\ [\bar{\bar{C}}_N] \end{bmatrix}, \quad (24k + 4) \text{ by } (12k + 2);$$

$$[B_N] = \begin{bmatrix} [\bar{B}_N] & [\bar{A}_N] \\ [\bar{\bar{B}}_N] & [\bar{\bar{A}}_N] \end{bmatrix}, \quad (24k + 4) \text{ by } (24k + 4);$$

$$\{Z_N\} = \left\{ \begin{array}{l} \{\bar{Z}_N\} \\ \{\bar{\bar{Z}}_{N+1}\} \end{array} \right\}, \quad (24k + 4) \text{ by one};$$

$$\{g_N\} = \left\{ \begin{array}{l} \{G_N\} \\ \{BG_N\} \end{array} \right\}, \quad (24k + 4) \text{ by one}.$$

Note that $m_1 = m_N = 24k + 4$, while $m_i = 12k + 2$ for $i = 2, 3, 4, \dots, N - 1$ (see p. 217).

Note also that eq. (108) represents equilibrium and compatibility equations in which displacement components (A_i, B_i) and stress resultant components (C_i, D_i) are the unknown functions, while the geometry and the loading (taken in increments) are taken as known parameters (assigned every time the equations are solved). Thus, this special case of the algorithm, eq. (108), is employed to find the pre-limit point response. When approaching the critical load, the increment in the applied load parameter is kept small and the sign of the determinant of the coefficients (see [37]) must be checked. If convergence fails, the load level is over the limit point. But if convergence does not fail and the sign of the determinant changes from what it was at the previous load level, then the load level is also over the limit point. Desired accuracy can be achieved by taking smaller and smaller increments in the load parameter. It is also observed that by employing this procedure (special case of the algorithm in which the load parameter is known), no solution can be obtained past the limit point. Because of this, the more general algorithm, described in [37], is employed at this point of the solution procedure. The new and more general algorithm simply exchanges the role of one of the displacement terms with that of the applied load parameter. By so doing, the form of the equations changes and the matrix of the coefficients of the unknown ceases to be tridiagonal. Depending on the position of the particular term that replaces the load parameter [which one of the $6k + 2$ terms, and at which node (x position)], column matrices appear all along the column corresponding to the vector $\{Z_L\}$ and the new equations assume exactly the form shown in eq. (109). Thus, at some level before the limit point, the procedure is switched to the more general algorithm, in which one of the displacement parameters (A_i or B_i) at some specified node is taken as known (specified increments) and the load parameter is the unknown. This solution procedure is continued until the desired portion of the post-limit point response is obtained.

Finally, in generating data, numerical integration is used to find the values

$$\begin{array}{c}
 \left[\begin{array}{ccccccccc} m_{N-2} & m_{N-1} & m_N \\ \vdots & \vdots & \vdots \\ g_1 & g_2 & g_3 & \cdots & \cdots & \cdots & g_{L-2} \\ \end{array} \right] = \left[\begin{array}{ccccccccc} Z_1 & & & & & & & & \\ Z_2 & & & & & & & & \\ Z_3 & & & & & & & & \\ \vdots & & & & & & & & \\ Z_{L-2} & & & & & & & & \\ \end{array} \right] \\
 \\
 \left[\begin{array}{ccccccccc} m_L & & & & & & & & \\ \vdots & & & & & & & & \\ \text{---} & \\ j & \nearrow [d_1] & & & & & & & \\ j & \nearrow [d_2] & & & & & & & \\ j & \nearrow [d_3] & & & & & & & \\ \text{---} & & & & & & & & \\ C_L & B_L & A_L & & & & & & \\ C_{L-1} & B_{L-1} & A_{L-1} & & & & & & \\ C_{L-2} & B_{L-2} & A_{L-2} & & & & & & \\ C_{L-1} & B_{L-1} & A_{L-1} & & & & & & \\ C_{L+1} & B_{L+1} & A_{L+1} & & & & & & \\ C_{L+2} & B_{L+2} & A_{L+2} & & & & & & \\ C_{L+1} & B_{L+1} & A_{L+1} & & & & & & \\ C_{L+2} & B_{L+2} & A_{L+2} & & & & & & \\ \vdots & & & & & & & & \\ Z_L & & & & & & & & \\ Z_{L-1} & & & & & & & & \\ g_L & & & & & & & & \\ g_{L-1} & & & & & & & & \\ \vdots & & & & & & & & \\ g_{N-2} & & & & & & & & \\ g_{N-1} & & & & & & & & \\ g_N & & & & & & & & \\ \end{array} \right] = \left[\begin{array}{cc|cc} C_{N-2} & B_{N-2} & A_{N-2} & \\ \hline C_{N-1} & B_{N-1} & A_{N-1} & \\ \end{array} \right] \left[\begin{array}{cc|cc} C_N & B_N & Z_N & \\ \hline \end{array} \right]
 \end{array}$$

(109)

of the total potential, the average end shortening, and the average shear [eqs. (102), (98), and (99)].

9.4 Solution Methodology—Dynamic

For the case of loads applied suddenly with infinite duration, the criterion is given in Section 5.2. The equation that is used to arrive at critical conditions is given by eq. (2) of Chapter 5. In applying this equation to the cylindrical shell problem, the functional U_T must be modified by introducing a constant C . This C is such that it eliminates all trajectories that are represented in U_T but that do not lead to a buckling mode.

$$U_{T_{\text{mod.}}} = U_T - C. \quad (110)$$

In order to make this point clear, consider the case of a thin circular cylindrical shell under uniform external pressure and with ends which are free to expand and/or contract. For this particular case the primary path is the breathing mode and buckling is associated with the existence of nonbreathing modes. Therefore, the breathing mode, which is represented in the functional U_T , does not belong to the family of admissible buckling trajectories. Then C in eq. (111) accounts for the potential of the external forces in connection with inadmissible “primary path” modes.

Specifically, the value of C is obtained in the following manner for the case of a suddenly applied pressure. At each level of the applied load, the static problem is solved, up to the critical static pressure (limit point). In so doing, the corresponding axisymmetric displacement (breathing mode) is known. Note that this mode, since the ends are not allowed to move in the radial direction (expand or contract), is a bending mode. Then at each level of the pressure the corresponding total potential is calculated, and this value for the total potential denotes the value of C in eq. (110) for this level of the pressure.

For the case of in-plane loads \bar{N}_{xx} and \bar{N}_{xy} the modified potential is also associated with the deflectional response of the system. When an axial load is applied statically, an in-plane displacement will result in addition to the transverse one. Then, for the case of sudden loads, an escaping motion type of instability (buckled motion) is possible only through trajectories that do not contain the in-plane mode. The expression for C in this case contains the terms related to $F(x, y)$ [$C_{0,xx}$, eq. (65)], which correspond to in-plane displacement (motion), and the strictly load terms (terms containing only the load parameter).

The expression for the modified potential, for in-plane loads, is given below:

$$\begin{aligned} U_{T_{\text{mod.}}} = U_T &+ \pi RL[\bar{N}_{xx}(a_{11} - a_{12}^2/a_{22}) + \bar{N}_{xy}(a_{33} - a_{23}^2/a_{22}) \\ &+ 2\bar{N}_{xx}\bar{N}_{xy}(a_{12}a_{23}/a_{22} - a_{13})]. \end{aligned} \quad (111)$$

Note that the expression for U_T given by eq. (102) contains e_{av} and γ_{av}

terms. The expressions for e_{av} and γ_{av} are given by eqs. (98) and (99), respectively.

9.5 Numerical Results

Numerical results are presented for three distinctly different construction groups. The first one consists of an isotropic monocoque cylindrical shell, the second of a stiffened isotropic cylindrical shell, and the third of a laminated cylindrical shell. The geometry, structural properties, and all pertinent information are given below for each group.

Unstiffened Shell (Aluminum)

$$E = 10.5 \times 10^6 \text{ psi}, \quad v = 0.3, \quad R = 4 \text{ in.}$$

$$0.004 \text{ in.} < h = h_N - h_0 \leq 0.050 \text{ in.}, \quad 4 \text{ in.} \leq L \leq 40 \text{ in.}$$

Boundary conditions: SS-3, eqs. (80)

$$w^0(x, y) = \xi h \left(-\cos \frac{2\pi x}{L} + 0.1 \sin \frac{\pi x}{L} \cos \frac{ny}{R} \right).$$

Note that ξ is the imperfection amplitude parameter. Moreover, the imperfection shape used for this group is virtually axisymmetric.

Ring and Stringer Stiffened Shell (Aluminum)

$$E_{st} = E_r = E = 10.5 \times 10^6 \text{ psi}, \quad v = 0.3, \quad R = 4 \text{ in.},$$

$$h = 0.04 \text{ in.}, \quad L = 4 \text{ in.},$$

$$e_x = \pm 0.24 \text{ in.}, \quad e_y = \pm 0.12 \text{ in. (+ for internal stiffeners)},$$

$$\lambda_{xx} = \frac{E_{st} A_x (1 - v^2)}{E h l_x} = 0.910, \quad \lambda_{yy} = \frac{E_r A_y (1 - v^2)}{E h l_y} = 0.455,$$

$$\rho_{xx} = \frac{E_{st} I_{xc}}{D l_x} = 100, \quad \rho_{yy} = \frac{E_r I_{yc}}{D l_y} = 20$$

where $D = Eh^3/12(1 - v^2)$.

Boundary conditions: SS-3, eqs. (80),

$$w^0(x, y) = \xi h \sin \frac{\pi x}{L} \cos \frac{ny}{R}.$$

Note that the imperfection shape for this group is symmetric.

Laminated Shell

This group consists of a four-ply laminate with five different stacking combinations. Each ply is orthotropic (boron/epoxy; AVCO 5505) with the

following properties:

$$\begin{aligned} E_{11} &= 30 \times 10^6 \text{ psi}, & E_{22} &= 2.7 \times 10^6 \text{ psi}, & v_{12} &= 0.21; \\ G_{12} &= 0.65 \times 10^6 \text{ psi}, & L &= 15 \text{ in.}, & R &= 7.5 \text{ in.}, & h_{\text{ply}} &= 0.0053 \text{ in.}; \\ h_{\text{ply}} &= h_k - h_{k-1}, & k &= 1, 2, 3, 4. \end{aligned}$$

The five different stacking sequences are denoted by I-*i* (*i* = 1, 2, 3, 4, 5) and correspond to

$$\begin{aligned} \text{I-1: } & 45^\circ / -45^\circ / -45^\circ / 45^\circ, \\ \text{I-2: } & 45^\circ / -45^\circ / 45^\circ / -45^\circ, \\ \text{I-3: } & -\text{I-2}, \\ \text{I-4: } & 90^\circ / 60^\circ / 30^\circ / 0^\circ, \\ \text{I-5: } & 0^\circ / 30^\circ / 60^\circ / 90^\circ, \end{aligned}$$

where the first number denotes the orientation of the fibers of the outmost ply (strong orthotropic axis) with respect to the *x* axis (longitudinal structural axis) and the last member has the corresponding meaning for the innermost ply. Geometry I-1 is a symmetric one and it corresponds to the one for which test (static) results are reported in [38]. Geometries I-4 and I-5 are completely asymmetric.

Boundary conditions: SS-3, eqs. (80).

$$w^0(xy) = \xi h \sin \frac{\pi x}{L} \cos \frac{\pi y}{R}.$$

The imperfection shape for this group is also symmetric.

Note that for the symmetric imperfection $\xi = w_{\max}^0/h$, while for the virtually axisymmetric shape, employed for the unstiffened configurations, $\xi = w_{\max}^0/1.1h$. For all construction groups the load is uniform axial compression.

The numerical results are presented and discussed separately for each of the three geometries. First the static and then the dynamic results are discussed. For the dynamic case, results are presented for suddenly applied loads with infinite duration.

9.5.1 Unstiffened Shell Geometries—Static

Before discussing the results, a few more clarifying remarks about this group are needed. The unstiffened geometry is taken from [34]. Note that in this reference only the critical load is given, not the complete behavior. This geometry employs virtually an axisymmetric imperfection. Note that the nonaxisymmetric amplitude is 10% of the axisymmetric amplitude. A smaller value was tried (1% for the nonaxisymmetric amplitude) and the response (see Figure 9.3; $R/t = 500$) is, for all purposes, identical to that of the unstiffened shell geometry. The only difference is the value for $\bar{N}_{xx,cr}$ (limit-point load). This difference reflects the effect of imperfection amplitude;

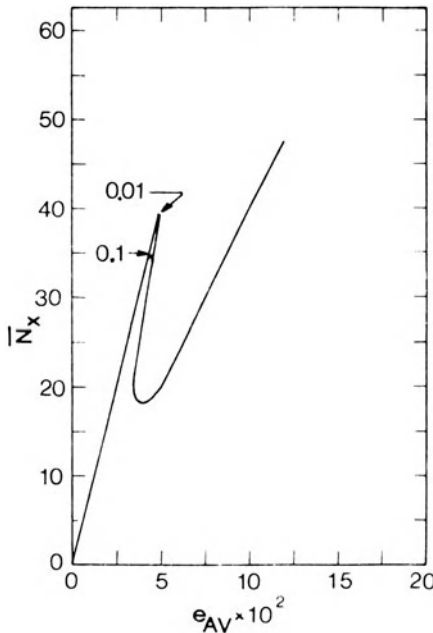


FIGURE 9.3. Effect of the asymmetric imperfection amplitude ($R/h = 500$, $L/R = 1$, $n = 10$).

that is, for $\xi = 1$, $N_{xx,cr} = 38.87$ lb/in. for 1% nonaxisymmetric amplitude, while $N_{xx,cr} = 35.00$ lb/in. for 10% nonaxisymmetric amplitude. Note that in the former case the maximum imperfection amplitude is $1.01h$, while in the latter it is $1.10h$. The classical load for this case is 101.81 lb/in. The 11% amplitude is used for the numerical results, because the higher the nonaxisymmetric amplitude, the faster the solution. Moreover, in this geometry, ξ is varied from zero to four in order to study the effect of imperfection amplitude. Note that for the chosen imperfection,

$$w_{\max}^0/h = 1.1\xi. \quad (112)$$

Finally, results are generated for several values of n (number of circumferential full waves). This must be done in order to obtain a clear picture of the complete response. Note that in [34] only limit point loads are reported. In the present work, SS-3 boundary conditions are employed. The most important results are presented in graphical and tabular forms.

Tables 9.1 and 9.2 describe the various unstiffened shell geometries for which results are presented (axial compression). Table 9.1 also gives values of critical static and dynamic loads, as well as minimum post-limit point loads and the linear theory (classical) static critical loads. Finally, for each example, it gives the number of mesh points used in the finite-difference

TABLE 9.1. Axially loaded unstiffened cylindrical shells.

Number	L (in.)	h (in.)	L/R	R/h	ξ	Classical			N_{xx}^d (lb/in.)	N_{xx}^m (lb/in.)	N_{xx}^d (lb/in.)	n	Number mesh points	λ^1	λ^m	λ^d
						N_{xx}^l (lb/in.)	N_{xx}^l (lb/in.)	N_{xx}^m (lb/in.)								
1	4.0	0.044	1.0	1,000	0.5	25.42	24.44	1.174	20.420	8	55	0.961	0.046	0.083		
2						24.13	0.524	17.740	9	55	0.949	0.021	0.698			
3						23.46	1.027	14.920	10	55	0.922	0.040	0.587			
4						20.71	2.050	13.199	11	35	0.815	0.081	0.519			
5						17.55	3.456	11.059	12	35	0.690	0.136	0.435			
6						16.61	4.804	10.199	13	35	0.653	0.189	0.401			
7						17.17	6.025	10.142	14	35	0.675	0.237	0.399			
8		0.004			1.0	24.21	0.977	19.460	8	55	0.952	0.038	0.766			
9						23.44	0.565	16.139	9	55	0.922	0.022	0.635			
10						19.22	1.310	12.550	10	35	0.756	0.052	0.494			
11						14.16	2.521	9.538	11	35	0.557	0.099	0.375			
12						11.86	3.860	8.110	12	35	0.467	0.152	0.319			
13						11.34	5.169	7.789	13	35	0.446	0.203	0.306			
14						20.98	2.083	15.770	7	35	0.825	0.082	0.620			
15						8.47	1.780	6.944	8	35	0.333	0.070	0.273			
16						3.30	2.000	2.874	9	35	0.130	0.078	0.113			
17						2.10*	—	—	10	35	0.083	—	—			
18						2.30*	—	—	11	35	0.091	—	—			
19						3.40*	—	—	12	35	0.134	—	—			
20						4.50*	—	—	13	35	0.177	—	—			
21						5.85*	—	—	14	35	0.230	—	—			
22						98.75	19.01	89.46	6	65	0.970	0.187	0.879			
23						91.84	10.90	68.95	7	65	0.902	0.107	0.677			
24						65.33	7.80	46.09	8	35	0.642	0.077	0.453			
25						43.24	12.29	31.17	9	35	0.425	0.121	0.306			
26						35.00	17.98	26.09	10	35	0.344	0.177	0.256			
27						35.17	24.10	26.46	11	35	0.345	0.237	0.260			
28						39.18	29.97	—	12	35	0.385	0.295	—			
29						45.30	34.89	—	13	35	0.445	0.343	—			

30	407.23	406.00	—	—	4	35	0.997	—	—	—	—	—
31	—	362.50	—	291.21	5	35	0.890	—	—	0.715	—	—
32	—	257.90	42.89	187.42	6	35	0.633	0.105	0.460	0.261	—	—
33	—	138.30	51.55	106.41	7	35	0.340	0.127	0.177	0.198	—	—
34	—	101.10	72.15	80.61	8	35	0.248	0.177	0.240	—	—	—
35	—	104.90	97.79	—	9	35	0.258	0.240	—	—	—	—
36	—	129.00	126.30	—	10	35	0.313	0.310	—	—	—	—
37	—	3500.00	2509.00	2894.00	3	35	0.880	0.631	0.728	—	—	—
38	—	1356.00	683.80	1103.20	4	35	0.341	0.172	0.277	—	—	—
39	—	623.80	599.70	—	5	35	0.157	0.151	—	—	—	—
40	—	675.00*	—	—	6	35	0.169	—	—	—	—	—
41	—	621.40	108.40	382.04	3	35	1.526	0.266	0.938	—	—	—
42	—	292.80	47.79	174.16	4	35	0.719	0.117	0.428	—	—	—
43	—	353.20	137.00	188.48	5	35	0.867	0.336	0.463	—	—	—
44	—	355.80	132.90	190.00	3	65	0.873	0.326	0.466	—	—	—
45	—	408.60	178.90	212.12	4	65	1.003	0.439	0.521	—	—	—
46	—	910.20	—	545.18	2	65	2.235	—	1.339	—	—	—
47	—	356.30	159.60	193.21	3	65	0.875	0.392	0.474	—	—	—
48	—	537.80	175.30	214.39	4	65	1.321	0.430	0.526	—	—	—
49	—	402.30	—	—	5	65	0.988	—	—	—	—	—
50	—	80	0.08	3977.00	—	5	35	0.826	—	—	—	—
51	—	500	1.0	101.81	39.38	18.08	27.42	10	35	0.387	0.178	0.269
52	—	80	0.32	3977.00	2234.00	766.70	1595.43	5	35	0.562	0.193	0.401
53	—	250	1.0	407.23	416.20	46.00	—	4	35	1.020	0.113	—
54	—	3.0	—	—	242.40	53.05	162.05	5	35	0.595	0.130	0.398
55	—	12.0	0.016	—	265.00	—	—	6	35	0.651	—	—
56	—	—	—	315.00	—	—	—	7	35	0.774	—	—
57	—	—	—	361.10	—	—	—	8	35	0.887	—	—

*Change of slope (not a critical load); see Figure 9.6.

TABLE 9.2. Summary of results for axially loaded unstiffened shells.

R/h	L/R	ξ	Classical \bar{N}_{xx} (lb/in.)	\bar{N}_{xx}^1 (lb/in.)	\bar{N}_{xx}^m (lb/in.)	\bar{N}_{xx}^d (lb/in.)	n	λ^1	λ^m	λ^d	n^1	n^m
1,000	1	0.5	25.42	16.61	0.5244	10.1996	8-13	0.653	0.0206	0.401	13	9
1,000	1	1.0	25.42	11.34	0.5649	7.7890	8-13	0.446	0.0222	0.306	13	9
1,000	1	4	25.42	2.10*	1.7800	2.8740	7-10	0.096	0.0700	0.113	10	8
250	1	1	407.23	101.10	42.89	80.61	6-8	0.248	0.1053	0.198	8	6
250	3	1	407.23	242.40	46.00	162.05	4-5	0.595	0.1130	0.398	5	5
250	5	1	407.23	292.80	47.79	174.16	3-5	0.719	0.1174	0.428	4	4
250	8	1	407.23	355.80	132.90	190.00	3-4	0.873	0.326	0.466	3	3
250	10	1	407.23	356.30	159.60	193.21	3-5	0.875	0.3919	0.474	3	3
1,000	1	1	25.42	11.34	0.5649	7.7890	8-13	0.446	0.0222	0.306	13	9
500	1	1	101.81	35.00	7.80	26.09	7-11	0.344	0.0766	0.256	10	8
250	1	1	407.23	101.10	42.890	80.61	6-8	0.248	0.105	0.198	8	6
80	1	1	3977.00	623.08	599.700	—	4-6	0.157	0.151	—	5	5
80	1	0.08	3977.00	3287.00	—	—	5	0.826	—	—	5	5
80	1	0.32	3977.00	2234.00	766.70	1595.43	5	0.562	0.193	0.401	5	5

*Change of slope (not a critical load); see Figure 9.6.

scheme and the value of n . Table 9.2 summarizes the most important results of the study for axially loaded unstiffened geometries.

The generated data that appear in Tables 9.1 and 9.2 are also presented in graphical form and a discussion of the various effects is presented. First, the results corresponding to $R/h = 1,000$ are presented and discussed. For this group, L/R is equal to one.

Figure 9.4 is a plot of \bar{N}_{xx} versus average end shortening for $\xi = 0.5$ (unstiffened geometry). These data are generated for several values of full waves, n , around the circumstance. From the figure it is clear that as the system is loaded quasi-statically from zero, the load-deflection curve is the same and independent of n . The limit point load, $\bar{N}_{xx,cr}$, is definitely dependent

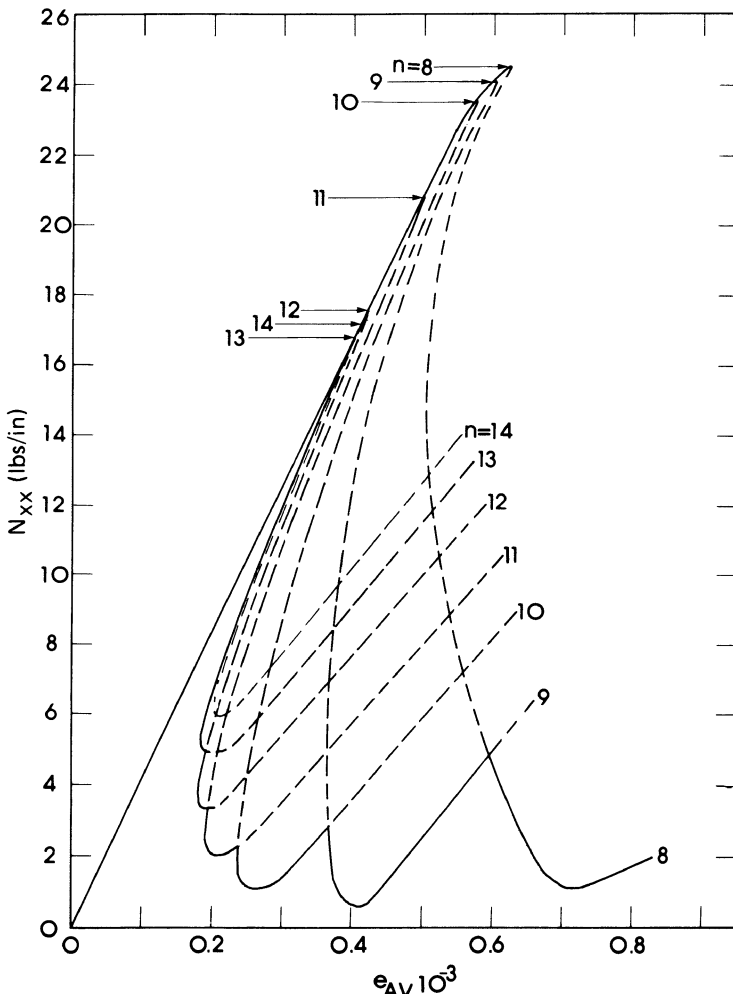


FIGURE 9.4. Response of unstiffened geometry ($R/h = 1,000$, $L/R = 1$, $\xi = 0.5$).

on n . It is observed that the value of the total potential corresponding to the lowest limit load and associated n is the smallest of all values corresponding to the same load and different n 's (at an equilibrium position). For this value of ξ (which corresponds to $w_{\max}^0 = 0.55h$), the limit point occurs at $\bar{N}_{xx} = 16.61 \text{ lb/in.}$ ($\lambda^l = \bar{N}_{xx_{cr}}/\bar{N}_{xx_{cl}} = 0.653$). In the post-limit point region, the unstable branch shows several changes from $n = 13$ to $n = 12$ to $n = 11$. These changes occur at the unstable portion of the curve. The change from $n = 11$ to $n = 10, \dots, n = 8$ occur at the stable portion of the curve. This implies that if one could transverse the post-limit point branches, one would move along the $n = 13$ curve (with decreasing load) and then along the $n = 12$ and $n = 11$ curves (with decreasing load). Then, along the $n = 11$ curve, the system moves with increasing load until it reaches the $n = 10$ curve. It then

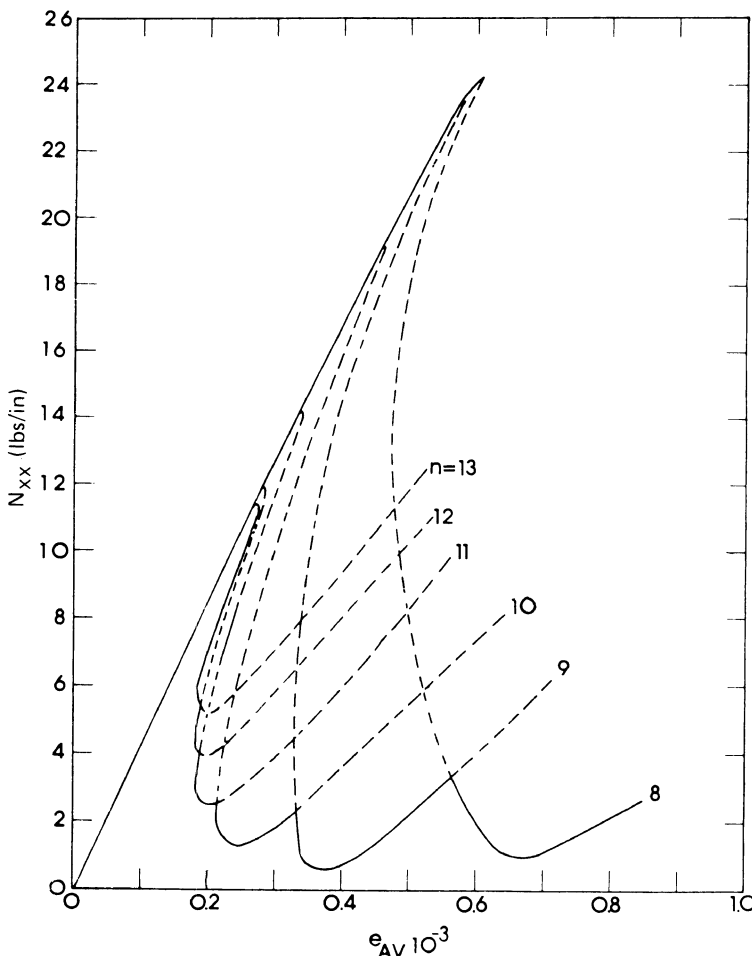


FIGURE 9.5. Response of unstiffened geometry ($R/h = 1,000$, $L/R = 1$, $\xi = 1.0$).

moves along the $n = 10$ curve until it intersects the $n = 9$ curve, etc. In reality, though, under dead weight loading, the system reaches the limit point and snaps through (violent buckling) toward far stable equilibrium positions. During the snapping process, it is clear from this figure that the shell experiences changes in the circumferential mode, corresponding to various n values. This phenomenon has been observed experimentally with high-speed photography for very thin and relatively short cylindrical shells.

Figure 9.5 presents data similar to those in Figure 9.4, but for $\xi = 1$. The behavior is very similar to that corresponding to $\xi = 0.5$. Note that curves corresponding to $n = 13, \dots, 8$ are shown. Data are generated for other n values but are not shown on the figure. Clearly, the same observations are made concerning violent buckling with changing circumferential mode. Moreover, data are generated for $\xi = 4$ and plotted on Figure 9.6. Note that for $n \geq 10$ there is no limit point instability, but for $n = 9, 8$, and 7 there exist limit points. The response, though, as the system is loaded quasi-statically

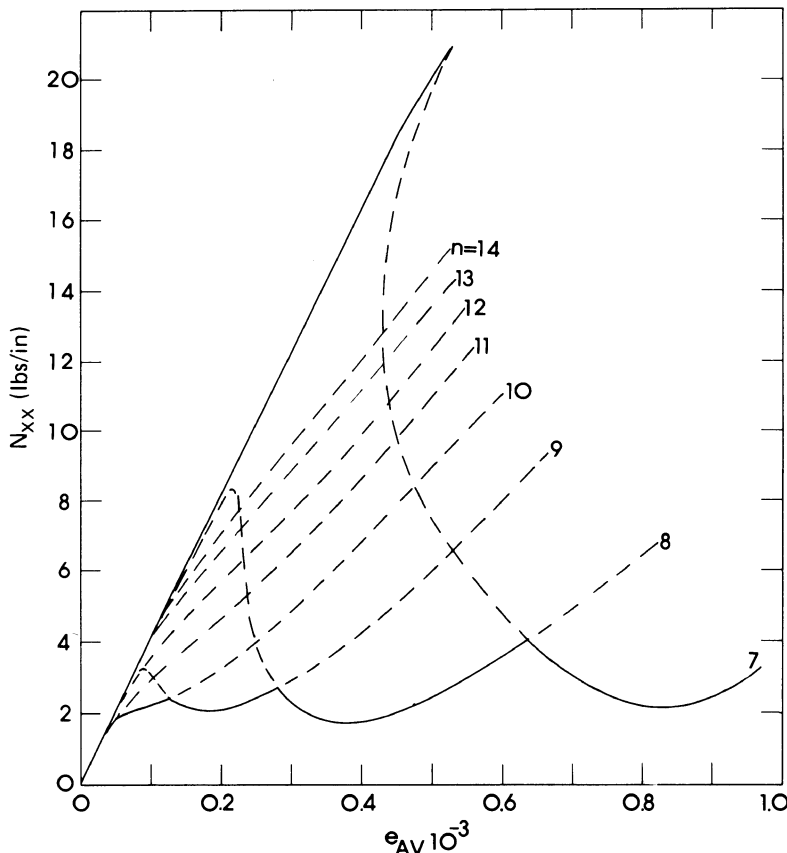


FIGURE 9.6 Response of unstiffened geometry ($R/h = 1,000$, $L/R = 1$, $\xi = 4.0$).

from zero, is along the $n = 10$ path and snapping takes place at the load level corresponding to unstable bifurcation (the $n = 10$ and $n = 9$ paths cross). Even for this imperfection amplitude ($\xi = 4$), violent buckling is predicted with change in circumferential mode. Finally, for the unstiffened geometry, Figure 9.7 presents the effect of the imperfection amplitude ξ on the limit point load $\lambda^l = \bar{N}_{xx_{cr}}/\bar{N}_{xx_{cl}}$ and on the minimum load $\lambda^m = \bar{N}_{xx_{min}}/\bar{N}_{xx_{cl}}$. It also presents the effect of imperfection amplitude on the dynamic critical load λ^d for the case of constant load of infinite duration. This effect is discussed in a later section. Note that $\bar{N}_{xx_{min}}$ corresponds to the minimum equilibrium load in the post-limit point region. As it can be seen from Figure 9.7, the shell is extremely sensitive to initial geometric imperfections (of virtually axisymmetric shape). Note that at $\xi = 0.48$, λ^l is equal to one-half. Since $w_{\max}^0 = 1.1\xi h$, $\lambda^l = 0.5$ when $w_{\max}^0 = 0.924h$. At $\xi = 3.5$, $\lambda^l = 0.1$, and at $\xi = 4$ the values of λ^l and λ^m are almost the same. This means that for $\xi \geq 4$, there is no possibility of snap-through buckling. The cylindrical shell simply deforms, with bending, from the initial application of the load. Finally, Fig-

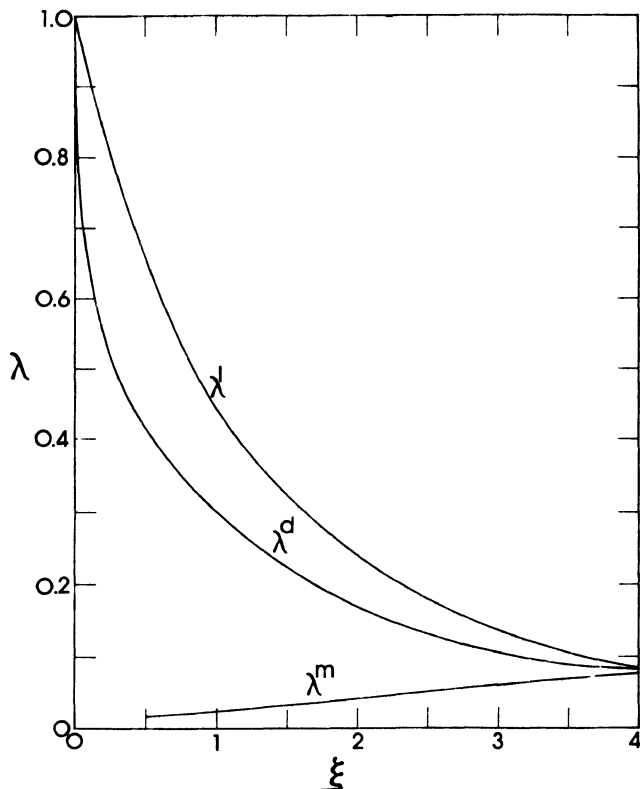


FIGURE 9.7. Plots of load parameters (λ^l , limit point; λ^d , critical dynamic; λ^m minimum post-limit point) versus imperfection amplitude parameter.

ure 9.8 presents a composite of Figures 9.4 to 9.6, and it includes pre-limit point and post-limit point behavior for $\xi = 0.5, 1.0$, and 4.0 .

Figure 9.9 is similar to Figure 9.5 but for $R/h = 500$. Figures 9.10 and 9.11 fall in the same category. These geometries correspond to examples 22 to 40 in Table 9.1, which along with Examples 8–13 study the effect of R/h on the shell response characteristics. Note that for all of these examples, $\xi = 1.0$ and $L/R = 1$.

Clearly, from Figure 9.9 it is seen that the response characteristics of the shell are very similar to those corresponding to $R/h = 1,000$ (Figure 9.5). The only difference is that the wave number n corresponding to both the limit point ($n = 11$) and the minimum post-limit point equilibrium load ($n = 8$) is smaller than that for $R/h = 1,000$. According to Figure 9.5, these wave numbers are $n = 13$ and $n = 9$, respectively. Note from Figure 9.10 that this trend continues as R/h decreases, and for $R/h = 80$, $n = 5$ corresponds to both loads. The composite response is shown on Figure 9.12.

Next, the effect of L/R is examined through examples 30–36, 41–49, and

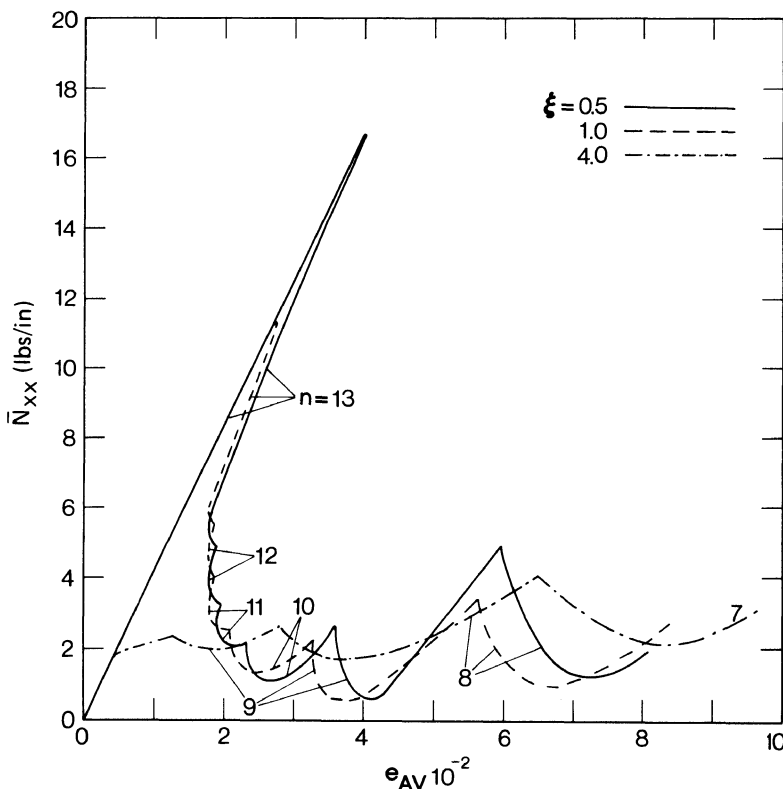


FIGURE 9.8. Pre- and post-limit point response of unstiffened geometry ($R/h = 1,000$, $L/R = 1$).

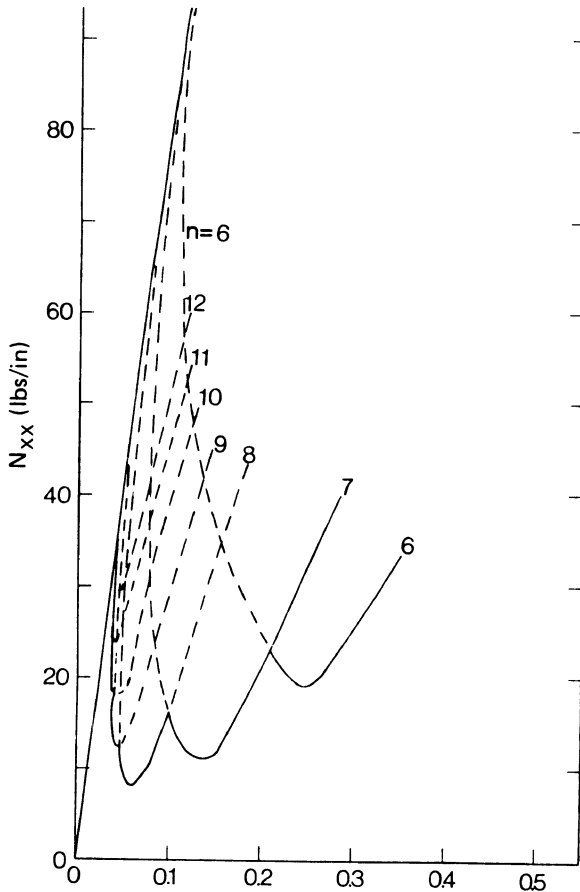


FIGURE 9.9. Response of unstiffened geometry ($R/h = 500$, $L/R = 1$, $\xi = 1.0$).

53–57 (see Table 9.1). All of these geometries correspond to $\xi = 1$ and $R/h = 250$, and L/R varies from 1 to 10. Then results of this study are presented graphically on Figure 9.10, 9.13, and 9.14 and in the composite of Figure 9.15. It is seen from these figures that as L/R increases, the entire static equilibrium response corresponds to one wave number ($n = 4$ for $L/R = 5$, $n = 3$ for $L/R = 8$ and 10). Note also that the n value decreases as L/R increases. This result seems reasonable. In addition, the sensitivity of the shell decreases as L/R increases. The latter effect is better shown on Figure 9.16. The dynamic results are discussed in a later section.

Finally, Figure 9.17 presents the effect of R/h on the limit point load, minimum post-limit point load, and dynamic critical load. There are two sets of curves, one set solid and the other set dashed. The solid curves

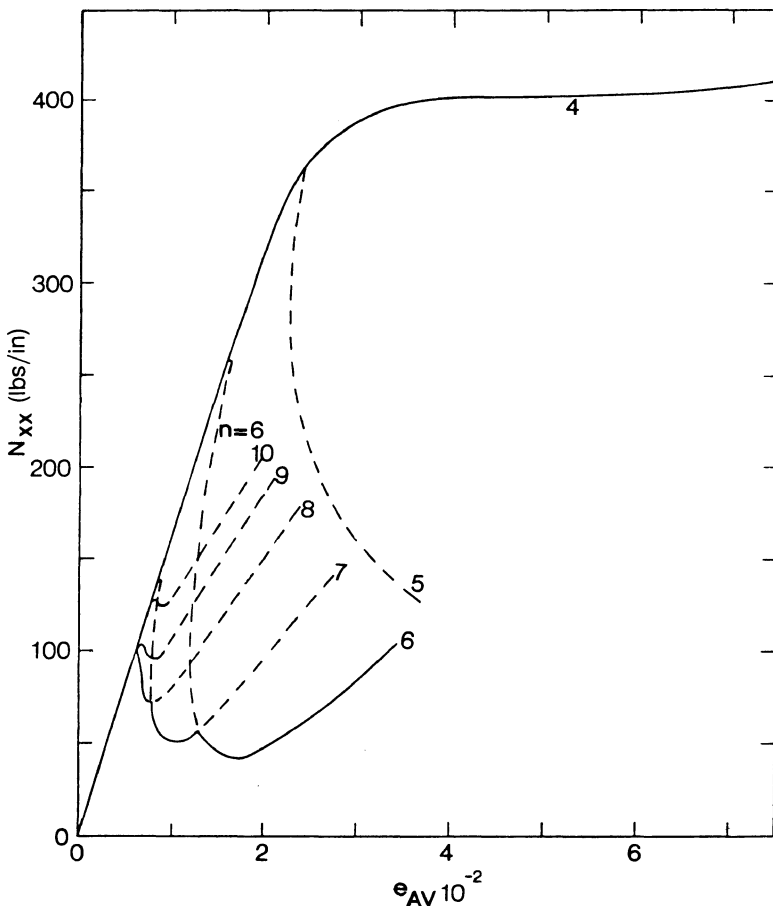
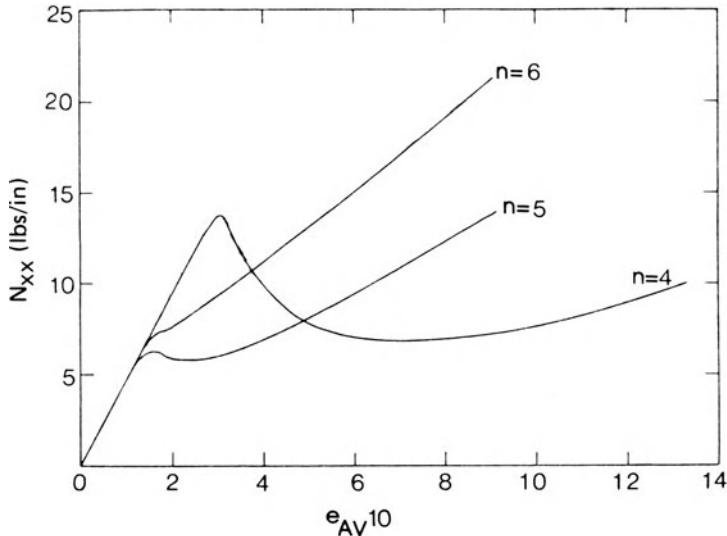
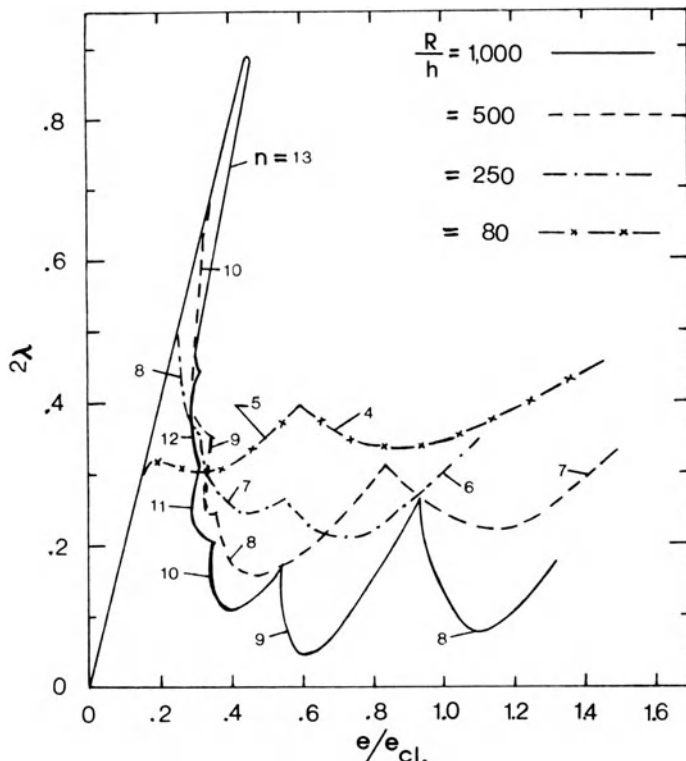


FIGURE 9.10. Response of unstiffened geometry ($R/h = 250$, $L/R = 1$, $\xi = 1.0$).

correspond to $\xi = 1$ and they imply change in the imperfection amplitude as R/h changes, since the data are generated for a constant R value (4 in.). The dashed curves correspond to the same imperfection amplitude, regardless of the value of the thickness. Note that, when $R/h = 1,000$, $h = 0.004$ in., since $R = 4$ in. From the amplitude of the imperfection, one may relate the solid curve to $\xi = 0.016/0.004 = 4$. Thus, it is very reasonable that λ^l corresponding to $\xi = 4$ is much smaller than λ^l corresponding to $\xi = 1$. On the other end of the curve, say $R/h = 100$, the opposite is true. For this value of R/h , $h = 0.04$ in. Then the dashed curve corresponds to $\xi = 0.016/0.040$, or $\xi = 0.4$, and λ^l corresponding to $\xi = 0.4$ is expected to be and is larger than λ^l corresponding to $\xi = 1.0$ (solid curve).

FIGURE 9.11. Response of unstiffened geometry ($R/h = 80$, $L/R = 1$, $\xi = 1.0$).FIGURE 9.12. Effect of R/t on the response of unstiffened geometry ($L/R = 1$, $\xi = 1.0$).

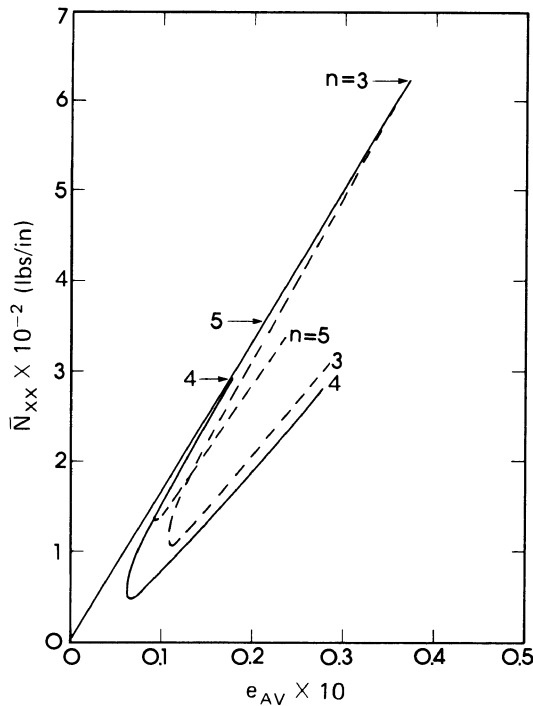


FIGURE 9.13. Response of unstiffened geometry ($R/h = 250$, $L/R = 5$, $\xi = 1.0$).

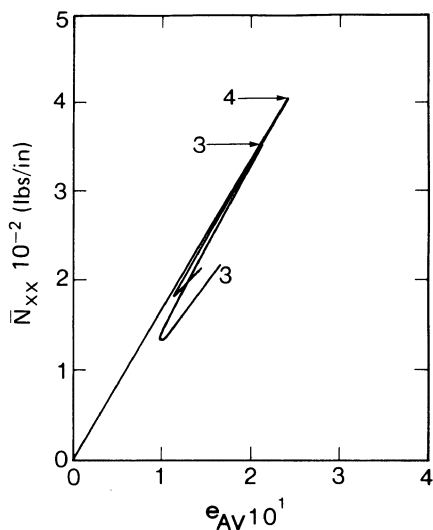


FIGURE 9.14. Response of unstiffened geometry ($R/h = 250$, $L/R = 8$, $\xi = 1.0$).

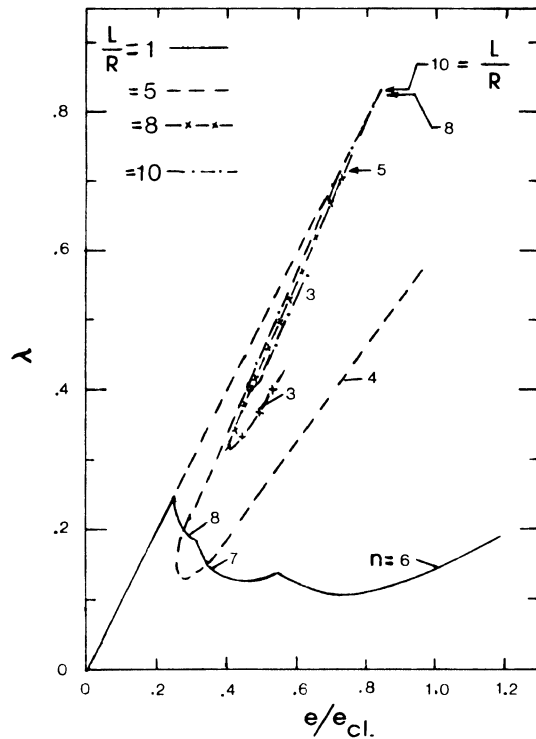


FIGURE 9.15. Effect of L/R on the response of unstiffened geometry ($R/h = 250$, $\xi = 1.0$).

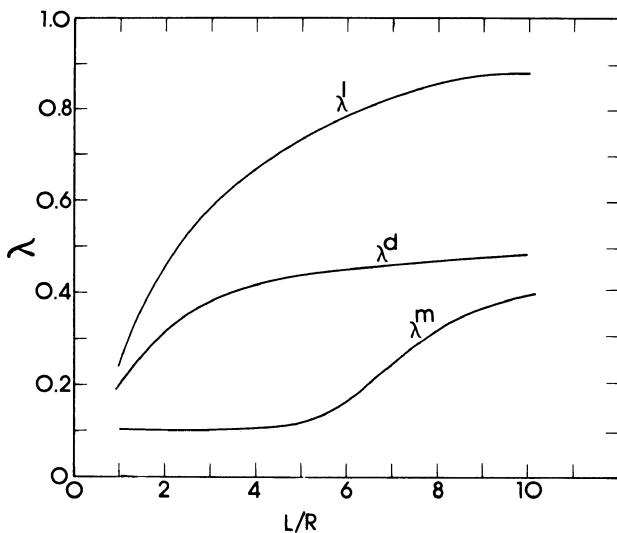


FIGURE 9.16. Plots of load parameters (λ^l , λ^d , λ^m) versus L/R ($R/h = 250$, $\xi = 1$).

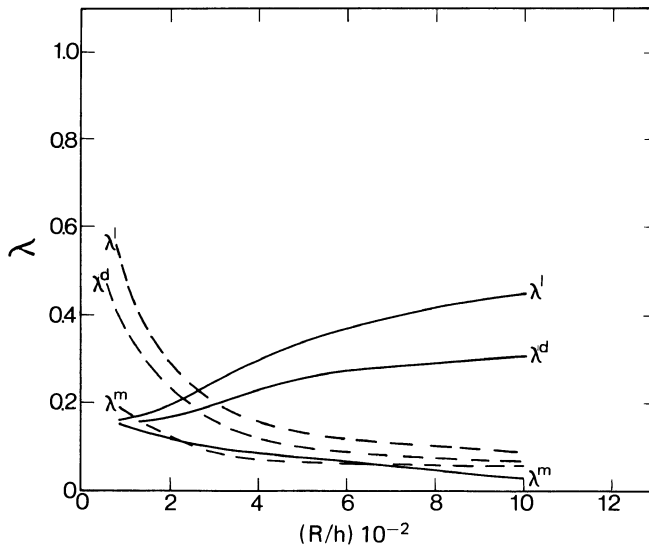


FIGURE 9.17. Plots of load parameters ($\lambda^l, \lambda^d, \lambda^m$) versus L/h ($L/R = 1$; solid curves, $\xi = 1$; dashed curves, constant imperfection amplitude, $\xi = 0.016/h$).

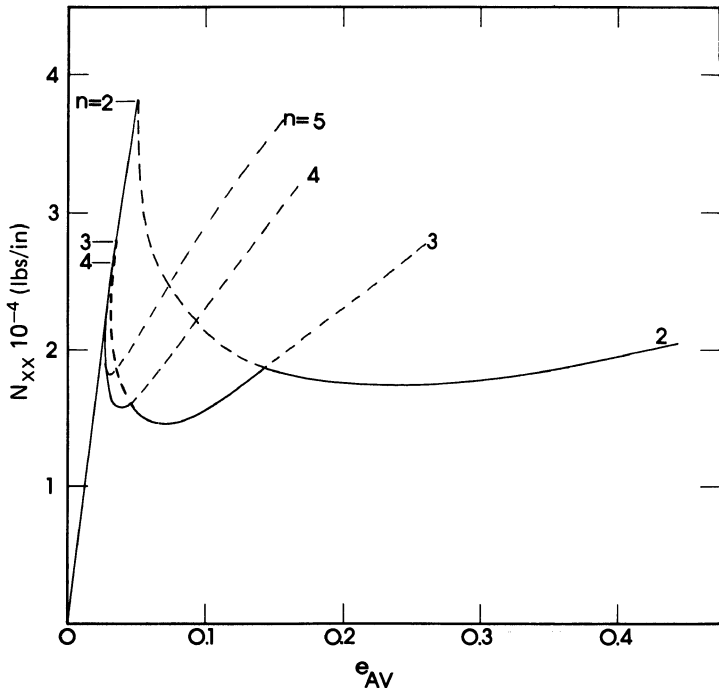
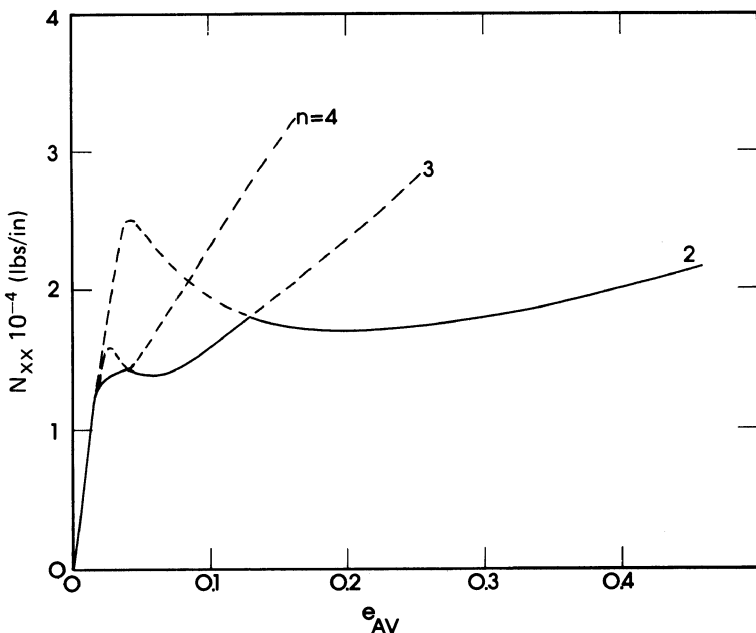
9.5.2 Ring and Stringer Stiffened Shell Geometries—Static

The stiffened geometries correspond to examples 14, 16, 18, 19 and 21 of [39]. Again, note that in [39] only limit point loads are reported. Moreover, for the data presented here, SS-3 boundary conditions are employed, as depicted by eqs. (41).

For the stiffened geometries, the results are presented on Figures 9.18–9.20.

The classical values for $\bar{N}_{xx_{cr}}$ are 35,220 lb/in. for external positioning of the stiffeners and 19,790 lb/in. for internal positioning. The geometric imperfection for the stiffened geometries is not axisymmetric but is symmetric with respect to y . This shape is similar to the classical buckling mode, provided that $n = 4$.

The results for the external positioning of the stiffeners are presented on Figures 9.18 and 9.19 for ξ equal to 1 and 4, respectively. It is seen from these two figures that the response is similar to that for the unstiffened geometry (Figures 9.4–9.6), but the number of full circumferential waves is smaller (this is an effectively much thicker thin shell). Note that the lowest limit point corresponds to $n = 4$ for $\xi = 1$. On the other hand, for $\xi = 4$ the mode changes from $n = 4$ to $n = 3$, and snapping occurs because of the existence of an unstable bifurcational branch. In this case also, a change in mode is observed during snap-through buckling. Another important similarity to the unstiffened-shell behavior is that this configuration is sensitive to initial geometric imperfections. Note that when $\xi = 1$ (which means that $w_{max}^0 = h$), $\bar{N}_{xx_{cr}} = 26,200$ lb/in. or $\lambda^l = 0.74$. The externally stiffened shell is not as

FIGURE 9.18. Response of externally stiffened geometry ($\xi = 1$, axial load).FIGURE 9.19. Response of externally stiffened geometry ($\xi = 4$, axial load).

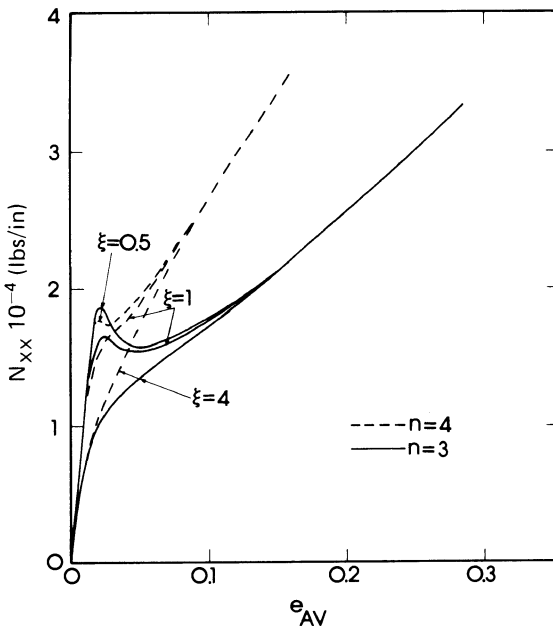


FIGURE 9.20. Response of externally stiffened geometry (axial load).

sensitive as the unstiffened thinner shell, but it is sensitive to initial geometric imperfections.

The results for the internally stiffened configuration are shown on Figure 9.20. The dashed lines correspond to $n = 4$ and the solid lines to $n = 3$. Data for other n values need not to be shown. The three sets of curves correspond to $\xi = 0.5, 1$, and 4 . Note that for $\xi = 0.5$, limit point instability occurs at $\bar{N}_{xx} = 17,800 \text{ lb/in.}$ with $n = 4$. Also note that during snap-through buckling, a change of circumferential mode occurs (to $n = 3$). The minimum equilibrium load in the post-limit point region corresponds to $n = 3$. On the other hand, for $\xi = 1$ snap-through buckling occurs at $\bar{N}_{xx} = 16,400 \text{ lb/in.}$ because of the existence of an unstable bifurcated branch (corresponding to $n = 3$). The minimum equilibrium load for $\xi = 1$ also corresponds to $n = 3$. Finally, there is no possibility of a snapping phenomenon for $\xi = 4$, neither through the existence of a limit point nor through the existence of an unstable bifurcated branch. This configuration is not very sensitive to initial geometric imperfections. For $\xi = 0.5$, $\lambda^1 = 0.90$, and for $\xi = 1$, $\lambda^1 \times 0.83$. The primary reason for the high values of λ is that internally stiffened configurations are less sensitive than externally stiffened ones, and stiffened configurations in general are less sensitive than unstiffened ones, to initial geometric imperfections.

9.5.3 Laminated Shell Geometries—Static

The primary reason for choosing these five configurations is to show the effect of lamina stacking on the critical (limit point) load for symmetric shape imperfections.

The results are presented in both tabular (Table 9.3) and graphical (Figures 9.21–9.24) forms.

For this study, the load is applied through the reference surface (which is the midsurface of the laminate) and the boundary conditions are SS-3 (classical simply supported). The imperfection shape is symmetric.

Table 9.3 shows critical loads \bar{N}_{xx}^l (limit point loads) for each geometry and various values of the imperfection amplitude parameter ξ . It also presents the range of n values used in finding critical loads and the n value corresponding to the critical condition. These results are also presented graphically on Figure 9.21.

Geometry I-1 is the one reported in [38]. According to this reference, the classical (linear theory) critical load is 165 lb/in. ($\bar{N}_{xx_{cl}}$) and the experimental value is 106 lb/in. Note from Figure 9.21 that through extrapolation \bar{N}_{xx}^l at $\xi = 0$ is approximately equal to 148 lb/in., which is 10% lower than the reported classical value.

The results for geometries I-2 and I-3 are identical. Both geometries are antisymmetric. This is reasonable since (1) the imperfection shape is symmetric with respect to a diametral plane and (2) the axially loaded cylinder does not distinguish between a positive 45° direction and a negative 45° direction.

TABLE 9.3. Critical loads.

Geometry	ξ	\bar{N}_{xx}^l (lb/in.)	n Range of n	n at \bar{N}_{xx}^l
I-1	0.05	145.55	5–7	6
	0.50	136.0		6
	1.00	123.0		6
	2.00	98.3		6
I-2, 3	0.05	138.80	5–7	6
	0.50	130.0		6
	1.00	118.7		6
	2.00	92.2		6
I-4	0.01	243.1	7–9	8
	0.05	232.03		8
	0.50	178.0		8
	1.00	137.2		8
	2.00	90.0		8
I-5	0.05	233.25	7–9	8
	0.50	191.0		8
	1.00	150.0		8
	2.00	109.5		8

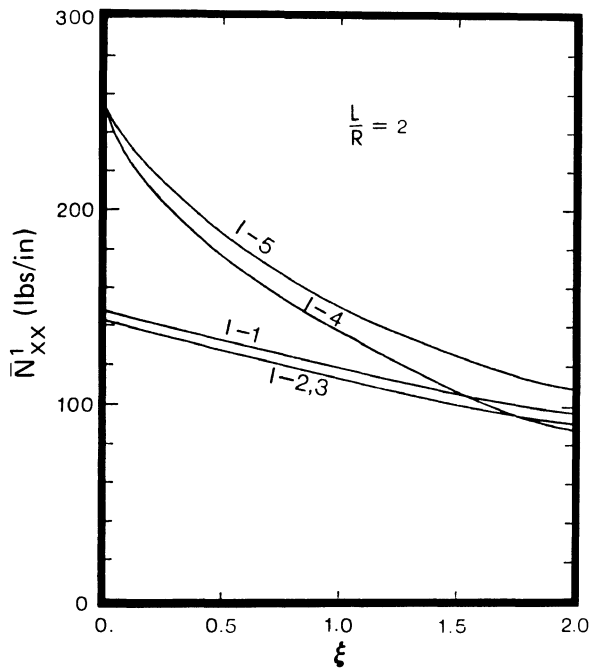


FIGURE 9.21. Imperfection sensitivity of the various configurations.

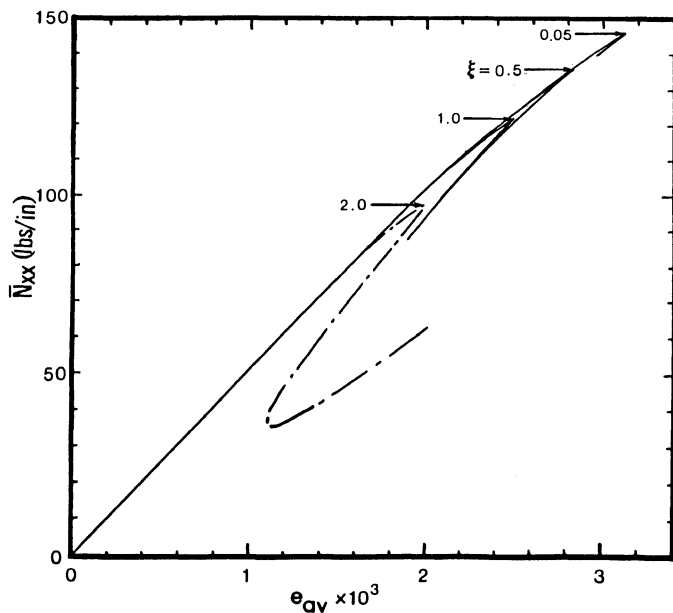
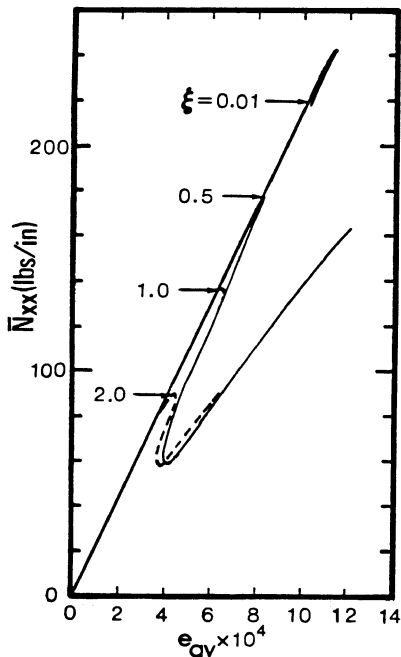
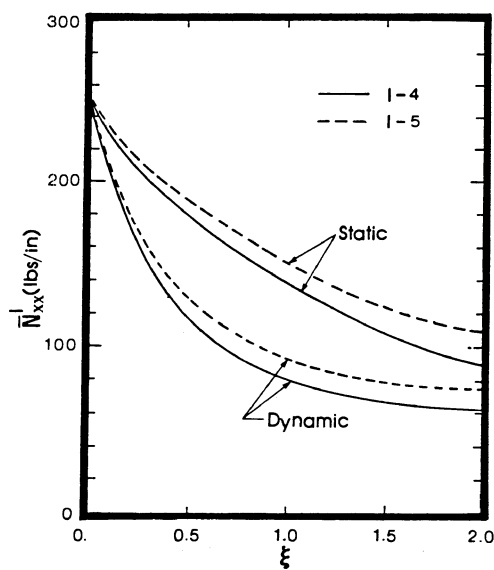


FIGURE 9.22. Axial load N_{xx} versus average end shortening e_{av} (configuration I-1).

FIGURE 9.23. Axial load N_{xx} versus average end shortening e_{av} (configuration I-4).FIGURE 9.24. Static and dynamic critical loads versus imperfection amplitude ξ (configuration I-4 and I-5).

Moreover, for virtually the entire range of ξ values considered, the I-2(3) geometry seems to be the weakest configuration, while the asymmetric configuration corresponding to I-5 is the strongest. The order of going from the weakest to the strongest is I-2(3), I-1, I-4, and I-5. Note that I-5 is a geometry for which the 0° ply is on the outside. Since buckling occurs in an inward transverse displacement mode (w is positive), the outside layer is in compression and it is reasonable to expect the strongest configuration to correspond to I-5 (the fibers of the outer ply are in the longitudinal direction).

Furthermore, the difference between the I-4 and I-5 geometries is the order of stacking (one is the reverse of the other). Their behavior, then, can be compared to the behavior of orthogonally stiffened metallic shells with outside and inside stiffening. Geometry I-5 is comparable to outside stiffening and geometry I-4 to inside stiffening.

Figures 9.22 and 9.23 present typical equilibrium paths for all geometries. Figure 9.22 corresponds to geometry I-1 and Figure 9.23 to geometry I-4. As seen, the response is in terms of plots of applied load \bar{N}_{xx} versus average end shortening e_{av} . Pre-limit point behavior, limit points, and post-limit point behavior are included for each ξ value. The entire curves correspond to the same wave number n . This n value is the one that yields critical conditions (the one at the instant of buckling). If a clear picture of post-limit point behavior is desired, one should show the plots that correspond to other wave numbers. This might reveal that the post-limit point curves cross each other, as in the case of isotropic shells (Section 9.5.1).

Critical (limit point) loads are plotted versus the imperfection amplitude parameter ξ on Figure 9.24 for the two asymmetric configurations, I-4 and I-5. On the same figure, critical dynamic loads are shown (suddenly applied with infinite duration) for the same configurations. Results for the dynamic case are discussed in the next section.

9.5.4 Critical Conditions for Sudden Application of the Loads

By employing the methodology described in Section 9.4, critical conditions for all three construction groups are presented in this section. The expression for the modified total potential is eq. (111) and it can be specialized for each construction by using the proper expression for a_{ij} [see eqs. (19)].

For the axially loaded unstiffened geometry, the results are presented in both tabular form (Tables 9.1 and 9.2) and graphical form (Figures 9.7, 9.16, and 9.17).

It is seen from Tables 9.1 and 9.2 that when a limit point exists and the difference between the limit point load and the minimum post-limit point load is distinct, a clear dynamic load exists. On the other hand, if there is no limit point (examples 17–21 of Table 9.1), there is no critical dynamic load. Similarly, if the value of the limit point load is very close to that of the

minimum post-limit point load, it is difficult to compute a critical dynamic load (see examples 35, 36, and 39 of Table 9.1). Figure 9.7, among others, shows a plot of λ^d versus the imperfection amplitude parameter, ξ . On the basis of the definition of critical dynamic load, λ^d starts from one and decreases to the common value of λ^l and λ^m at $\xi = 4$. Since the static behavior for $\xi > 4$ is not one of limit point instability, there is no critical dynamic load for these ξ values, according to the Hoff–Simitses concept and criterion discussed in Chapter I.

The effect of L/R is shown on Figure 9.16. The value of λ^d is very low for L/R equal to one ($\lambda^d = 0.2$) and it increases rapidly with increasing L/R values to $\lambda^d = 0.48$ at $L/R = 10$. This, of course, holds true only for ξ values for which the static behavior is the same as for $\xi = 1.0$ (see Figures 9.4 and 9.5 but not Figure 9.6).

For the axially loaded stiffened configuration, the results are presented on Figure 9.25. It is seen from this figure that the internally stiffened geometry (under static conditions) is not as sensitive as the externally stiffened one. Moreover, the ratio of the dynamic to the static load (λ^d/λ^l) is higher for the internally stiffened geometry. Note that the results for the internally stiffened geometry do not extend past $\xi = 1.0$. This is so because the static behavior will soon ($\xi = 1.5$ or so) cease to be of the limit point instability. On the other hand, the results for external stiffening extend to $\xi = 4$.

It is seen that the largest difference (or smallest ratio λ^d/λ^l) between the static and dynamic critical loads occurs at $\xi \approx 1.0$ (see Figures 9.7 and 9.25) for axially loaded geometries.

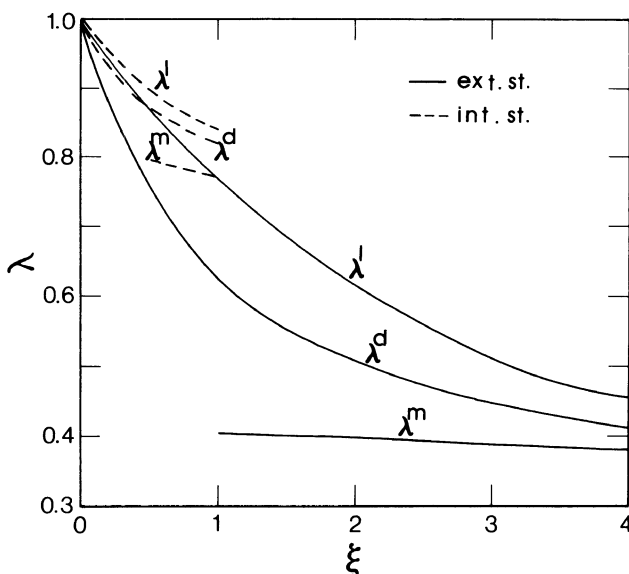


FIGURE 9.25. Plots of load parameters ($\lambda^l, \lambda^d, \lambda^m$) versus ξ for the stiffened geometries (axial load).

Finally, for the two laminated asymmetric configurations, I-4 and I-5, critical dynamic loads are calculated for the entire ξ range (see Figure 9.24). The trend is the same as that for the other two constructions. For these configurations, the critical dynamic load is never smaller than 60% of the corresponding static load.

For all constructions (see Figures 9.7, 9.24, and 9.25), it appears that at $\xi = 0$ the critical load is the same for both the static case and sudden application of the load. These values (at $\xi = 0$) are obtained through extrapolation and therefore their accuracy must be questioned.

References

1. Agamirov, V.L., and Vol'mir, A.S. Behavior of cylindrical shells under dynamic loading by hydrostatic pressure or by axial compression. *J. Am. Rocket Soc.* 31, 1, 1961, 98–101 (English translation from *Bull. Acad. Sci. USSR Div. Tech. Sci. Mech. Machine Construct.* 3, 1959 78–83).
2. Kadashevich, V.I. and Pertsev, A.K. Loss of stability of a cylindrical shell under dynamic loads. *J. Am. Rocket Soc.*, 32, 1, 1962, 140–142 (English translation from *Bull. Acad. Sci. USSR Div. Tech. Sci. Mech. Machine Construct.*, 3, 1960, 30–33).
3. Roth, R.S., and Klosner, J.M. Nonlinear response of cylindrical shells subject to dynamic axial loads. *AIAA J.*, 2, 10, 1964, 1788–1794.
4. Humphreys, J., and Bodner, S.R. Dynamic buckling of shallow shells under impulsive loads. *J. Eng. Mech. Div. ASCE*, 88, 2, 1962, pp. 17–36.
5. Goodier, J.N., and McIvor, I.K. The elastic cylindrical shell under nearly uniform radial impulse. *J. Appl. Mech.*, 31, 2, 1964, 259–266.
6. Budiansky, B., and Hutchinson, J.W. Dynamic buckling of imperfection-sensitive structures. *Proc. 11th International Congress of Applied Mechanics*, Munich (edited by H. Goler), pp. 636–651. Springer-Verlag, Berlin, 1964.
7. Budiansky, B. Dynamic buckling of elastic structures: Criteria and estimates. *Dynamic Stability of Structures* (edited by G. Herrmann), pp. 83–106. Pergamon Press, Oxford, 1966.
8. Hutchinson, J.W., and Budiansky, B. Dynamic buckling estimates. *AIAA J.*, 4, 3, 1966, 525–530.
9. Danielson, D.A. Dynamic buckling loads of imperfection-sensitive structures from perturbation procedures. *AIAA J.*, 7, 8, 1969, 1506–1510.
10. Lindberg, H.E., and Herbert, R.E. Dynamic buckling of a thin cylindrical shell under axial impact. *J. Appl. Mech.* 33, 1, 1966, 105–112.
11. Maymon, G., and Libai, A. Dynamics and failure of cylindrical shells subjected to axial impact. *AIAA J.*, 15, 9, 1977, pp. 1624–1630.
12. Zimcik, D.G., and Tennyson, R.C. Stability of circular cylindrical shells under transient axial impulsive loading. *AIAA J.*, 18, 5, 1980, 691–699.
13. Sunakawa, M., and Kibe, S. A critical value and behavior of cylindrical shells under axial step loading. *Proc. 9th Canadian Congress of Applied. Mechanics*, University of Saskatchewan, Saskatoon, May 1983, pp. 207–208.
14. Abramowicz, W., and Jones, N. Dynamic axial crushing of circular tubes. *Int. J. Impact Eng.*, 2, 4, 1984, 263–281.
15. Abramowicz, W., and Jones, N. Dynamic progressive buckling of circular and square tubes. *Int. J. Impact Eng.*, 4, 4, 1986, 247–270.

16. Lindberg, H.E., Rubin, M.B., and Schwer, L.E. Dynamic buckling of cylindrical shells from oscillating waves following axial impact. *Int. J. Solids Struct.*, 23, 6, 1987, 669–692.
17. Kirkpatrick, S.W., and Holmes, B.S. Structural response of thin cylindrical shells subjected to impulsive external loads. *AIAA J.*, 26, 1, 1988, 96–103.
18. Hubka, W.F. Dynamic buckling of the elastic cylindrical shell subjected to impulsive loading. *J. Appl. Mech.*, 41, 2, 1974, 401–405.
19. Lovell, E.G., and McIvor, I.K. Nonlinear response of a cylindrical shell to an impulsive pressure. *J. Appl. Mech.*, 36, 2, 1969, 277–284.
20. Almroth, B.O., Meller, E., and Brogan, F.A. Computer solutions for static and dynamic buckling of shells. *Buckling of Structures*, IUTAM Symposium (edited by B. Budiansky), pp. 52–66. Springer-Verlag, Berlin, 1976.
21. Tamura, Y.S., and Babcock, C.D. Dynamic buckling of cylindrical shell under step loading. *J. Appl. Mech.*, 42, 1, 1975, 190–194.
22. Lockhart, D., and Amazigo, J.C. Damped externally pressurized imperfect cylindrical shells. *J. Appl. Mech.*, 42, 2, 1975, 316–320.
23. Lockhart, D. Dynamic buckling of a damped externally pressurized imperfect cylindrical shell. *J. Appl. Mech.*, 46, 2, 1979, 372–376.
24. Lockhart, D.F. Post-buckling dynamic behavior of periodically supported imperfect shells. *Int. J. Nonlinear Mech.*, 19, 3, 1982, 165–174.
25. Simitses, G.J., and Sheinman, I. Dynamic buckling of shell structures: Concepts and applications. *Acta Astronaut.*, 9, 3, 1982, 179–182.
26. Simitses, G.J. Effect of static preloading on the dynamic stability of structures. *AIAA J.*, 21, 8, 1983, 1174–1180.
27. Sheinman, I., Shaw, D., and Simitses, G.J. Nonlinear analysis of axially loaded laminated cylindrical shells. *Comput. Struct.*, 16, 1, 1983, 131–137.
28. Simitses, G.J., and Sheinman, I. Static and Dynamic buckling of pressure-loaded, ring-stiffened cylindrical shells. *J. Ship. Res.*, 27, 2, 1983, 113–120.
29. Svalbonas, V., and Kalnins, A. Dynamic buckling of shells: Evaluation of various methods. *Nucl. Eng. Des.*, 44, 1977, 331–356.
30. Simitses, G.J. Instability of dynamically loaded structures, *Appl. Mech. Rev.*, 40, 10, 1987, 1403–1407.
31. Ray, H., and Lovell, E.G. Dynamic instability of suddenly heated cylindrical shells. *Nucl. Eng. Des.*, 61, 1980, 237–243.
32. Sheinman, I., and Simitses, G.J. Buckling analysis of geometrically imperfect stiffened cylinders under axial compression. *AIAA J.*, 15, 3, 1977, 374–382.
33. Jones, R.M. *Mechanics of Composite Materials*. McGraw-Hill, New York, 1975.
34. Simitses, G.J., and Sheinman, I. Dynamic Stability of Structures: Application to Frames, Cylindrical Shells and Other Systems. Technical Report AFWAL-TR-81-3155, Wright-Patterson Air Force Base, Ohio, February 1982.
35. Thurston, G.A. Newton's method applied to problems in nonlinear mechanics. *J. Appl. Mech.*, 32, 2, 1965, 383–388.
36. Tene, Y., Epstein, M., and Sheinman, I. A generalization of Potter's method. *Comput. Struct.*, 4, 6, 1974, 1099–1103.
37. Sheinman, I., and Simitses, G.J. A modification of Potter's method for diagonal matrices with common unknown, *Comput. Struct.*, 18, 2, 1985, 273–275.
38. Wilkins, D.J., and Love, T.S. Combined compression-torsion buckling tests of laminated composite cylindrical shells. *Proc. AIAA/ASME 15th Structures, Structural Dynamics and Materials Conference*, Las Vegas, Nevada, April 1974.

10

Other Structural Systems

As explained in Chapter 1, it is possible to extend the concept of dynamic buckling to all structural systems regardless of their behavior under static application of the loads (see Figures 1.6–1.10). This extension is discussed in Section 1.3, and it is based on limiting the deflectional response of a structure (when loaded suddenly), which is in agreement with requiring boundedness of deflectional response. One should observe that in limiting the deflectional response, boundedness is automatically satisfied (in some cases enforced), while the reverse is not true.

Some examples are presented in this chapter to clarify this extension of the concept of dynamic stability. Part of Section 1.3 is repeated here for the sake of self-containment.

10.1 The Mass–Spring System

Consider the mass–spring (linear) system shown on Figure 10.1. Consider a suddenly applied load $P(t)$ applied at $t = 0$. This load may, in general, include the weight (mg). In the case of finite duration, consider the weight to be negligible.

First, the problem of constant load suddenly applied with infinite duration is considered. For this case, one may write the equation of motion and solve for the response by imposing the proper initial conditions:

$$\ddot{x} + \frac{k}{m}x = \frac{P}{m} \quad (1)$$

subject to

$$\dot{x}(0) = x(0) = 0 \quad (2)$$

where the dot denotes differentiation with respect to time.

By changing the dependent variable to

$$y = x + C \quad (3)$$

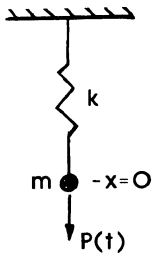



FIGURE 10.1. The mass-spring system.

where C is a constant, the equation of motion and initial conditions become

$$\ddot{y} + \frac{k}{m}y = 0, \quad (4)$$

$$y(0) = -\frac{P}{k} \quad \text{and} \quad \dot{y}(0) = 0. \quad (5)$$

The solution is

$$y = -\frac{P}{k} \cos \sqrt{\frac{k}{m}}t \quad (6)$$

and

$$x = \frac{P}{k} \left(1 - \cos \sqrt{\frac{k}{m}}t \right). \quad (6)$$

Note that

$$x_{\max} = \frac{2P}{k}, \quad (7)$$

and it occurs at

$$\sqrt{\frac{k}{m}}t = \pi \quad \text{or at} \quad t = \pi \sqrt{\frac{m}{k}} = T/2 \quad (8)$$

where T is the period of vibration.

Note that if the load is quasistatically, then

$$P_{st} = kx_{st}. \quad (9)$$

From eqs. (7) and (9), it is clear that if the maximum dynamic response x_{\max} and maximum static deflection $x_{st,\max}$ are to be equal and no larger than a specified value X (deflection-limited response), then

$$P_{st} = 2P_{dyn}. \quad (10)$$

Because of this, many systems for which the design loads are dynamic in

nature (suddenly applied of constant magnitude and infinite duration) are designed in terms of static considerations but with design (static) loads twice as large as the dynamic loads, eq. (10). Note that both loads (P_{st} , P_{dyn}) correspond to the same maximum deflection X .

Next, the same problem is viewed from energy considerations. First, the total potential U_T for the system is given by

$$U_T = \frac{1}{2}kx^2 - Px, \quad (11)$$

and the kinetic energy T by

$$T = \frac{1}{2}m(\dot{x})^2. \quad (12)$$

Note that the system is conservative, the kinetic energy is a positive definite function of the velocity (for all t), and $U_T = 0$ when $x = 0$. Then

$$U_T + T = 0, \quad (13)$$

and motion is possible only in the range of x values for which U_T is nonpositive (see shaded area of Figure 10.2).

It is also seen from eq. (11) that the maximum x value corresponds to $2P/k$.

Note that the static deflection is equal to P/k [eq. (9) and point A on Figure 10.2]. Therefore, if the maximum dynamic response and maximum static deflection are to be equal to X , eq. (10) must hold.

Now one may develop a different viewpoint for the same problem. Suppose that a load P is to be applied suddenly to the mass-spring system with the condition that the maximum deflectional response cannot be larger than a specified value X . If the magnitude of the load is such that

$$\frac{2P}{k} < X, \quad (14)$$

we shall call the load dynamically subcritical.

When the inequality becomes an equality, we shall call the corresponding load dynamically critical. This implies that the system cannot withstand a

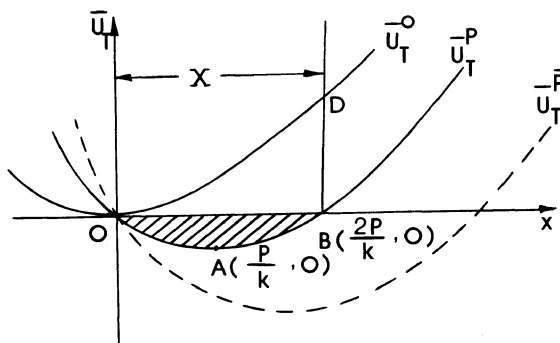


FIGURE 10.2 Total potential curves (suddenly loaded mass-spring system).

dynamic load $P > kX/2$ without violating the kinematic constraint. Therefore,

$$P_{\text{dyn,cr}} = \frac{kX}{2}. \quad (15)$$

This extension of the energy concept of dynamic stability was first introduced and discussed in Section 1.3.

Moreover, on the basis of this concept, one may find a critical ideal impulse. The question, in this load case, is to find the ideal impulse such that the system response does not exceed a prescribed value X . From Figure 10.2 and conservation of energy

$$U_T^0 + T = T_i \quad (16)$$

and T_i is critical if the system can reach position D with zero velocity (kinetic energy). Thus,

$$T_{i,cr} = U_T^0(D) = U_T^0(X). \quad (17)$$

From the impulse-momentum theorem, the ideal impulse, Imp , is related to the initial velocity and consequently to the initial kinetic energy:

$$\text{Imp} = \lim_{t_0 \rightarrow 0} (Pt_0) = m\dot{x}_i \quad (18)$$

where \dot{x}_i is the initial velocity magnitude (unidirectional case) and t_0 is the duration time of a square pulse.

From eq. (18)

$$\dot{x}_i = \frac{\text{Imp}}{m}, \quad (19)$$

and use of eqs. (5.12) yields

$$\dot{x}_i = \left(\frac{2T_i}{m} \right)^{1/2} \quad (20)$$

Since the critical initial kinetic energy is given by eq. (17)

$$\text{Imp}_{cr} = (mk)^{1/2}X. \quad (21)$$

Next, the following nondimensionalized parameters are introduced:

$$p = \frac{2P}{kX}, \quad \xi = \frac{x}{X}, \quad \tau = t \sqrt{\frac{k}{m}}, \quad (22)$$

$$\bar{U}_T = \frac{2U_T}{kX^2}, \quad \bar{T} = \frac{2T}{kX^2}, \quad \bar{\text{Imp}} = \frac{2\text{Imp}}{X\sqrt{km}}. \quad (23)$$

On the basis of this, eq. (21) becomes

$$\bar{\text{Imp}}_{cr} = 2. \quad (24)$$

Finally, the concept of dynamic stability is next applied to the general case of a suddenly applied load of constant magnitude but finite duration t_0 . The precise statement of the problem is: find the load P for a given duration time t_0 (or vice versa) such that the maximum deflection is no larger than a prescribed value X . Note that the extreme cases of $t_0 \rightarrow 0$ and ∞ have been dealt with separately and that for this case P must be greater than $P_{\text{dyn,cr}}$ [see eq. (15)].

For this load case and system, conservation of energy yields

$$U_T^P + T^P = 0, \quad 0 \leq t \leq t_0 \quad (25)$$

and

$$U_T^0 + T^0 = C, \quad t \geq t_0 \quad (26)$$

where C is a constant. This constant can be expressed in terms of U_T^P and U_T^0 values at the instant of release, t_0 . Since there exists kinematic continuity at t_0 , $T^P(t_0) = T^0(t_0)$, then

$$C = U_T^0(t_0) - U_T^P(t_0) \quad (27)$$

and

$$U_T^0 + T^0 = U_T^0(t_0) - U_T^P(t_0). \quad (28)$$

A critical condition exists if position X can be reached with zero velocity (kinetic energy). Thus, from eqs. (26) and (11)

$$\frac{1}{2}kX^2 = Px(t_0) = Px_{\text{cr}} \quad (29)$$

where x_{cr} is the x position at the instant of release.

From eqs. (25), (11), and (12) one may write

$$\frac{1}{2}kx^2 - Px + \frac{1}{2}m(\dot{x})^2 = 0, \quad 0 \leq t \leq t_0 \quad (30)$$

or

$$\dot{x} = \left(\frac{2P}{m}x - \frac{k}{m}x^2 \right)^{1/2}. \quad (31)$$

From this one may write

$$dt = \frac{dx}{((2P/m)x - (k/m)x^2)^{1/2}}. \quad (32)$$

Integration from zero to t_0 yields an equation that relates t_0 , $x(t_0)$, and P :

$$t_0 = \int_0^{x_{\text{cr}}} \frac{dx}{((2P/m)x - (k/m)x^2)^{1/2}}. \quad (33)$$

Equations (33) and (29) are two equations that relate P , x_{cr} , and t_0 . A critical condition is expressed in terms of either P_{cr} for a given t_0 or $t_{0,\text{cr}}$ for a given P value.

Computationally, it is simpler to assign values of ξ_{cr} from zero up to X and solve for the corresponding P from eq. (29) and for t_0 from eq. (33).

Use of the nondimensionalized parameters, eqs. (23), yields the following system of governing equation:

$$p\xi_{cr} = 1$$

and

$$\tau_0 = \int_0^{\xi_{cr}} \frac{d\xi}{(p\xi - \xi^2)^{1/2}}. \quad (34)$$

Note that the first of eqs. (34) corresponds to eq. (29) and the second to eq. (33). Moreover, the value of ξ_{cr} varies from zero to one.

The simultaneous solution of eqs. (34) yields

$$p = 1/\xi_{cr} \quad \text{and} \quad \tau_{0,cr} = \cos^{-1}(1 - 2\xi_{cr}^2). \quad (35)$$

Note that as ξ_{cr} approaches one, $\tau_{0,cr}$ is equal to half the period of oscillations and $p = 1$, which is the value that corresponds to the case of constant load suddenly applied, with infinite duration [see eq. (15)].

The results are shown graphically on Figure 10.3 as plots of p versus t_0/T or $\tau_0/2\pi$.

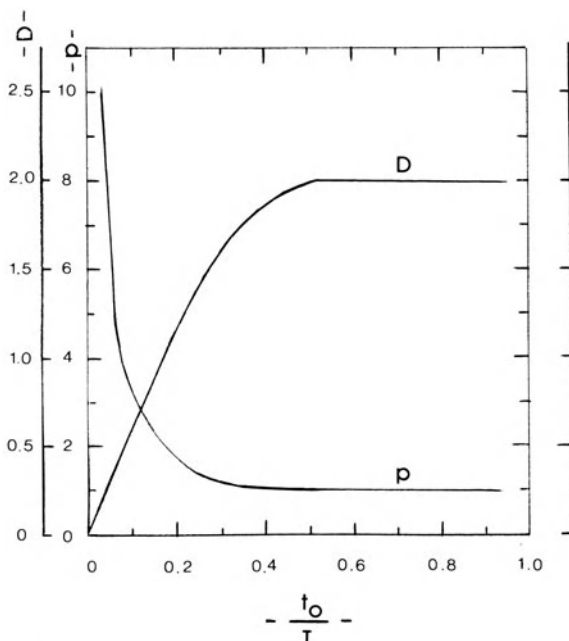


FIGURE 10.3. Critical load and dynamic magnification factor versus duration time (t_0/T or $\tau_0/2\pi$)

Parenthesis. Equation (29) may be interpreted in a different way. For instance, one may write

$$kX^2 = 2Px_{\text{cr}} \quad (36)$$

where x_{cr} is the position of the mass at the instant of release of the force P and X is the maximum amplitude of oscillations (maximum dynamic response). Moreover, P/k is a measure of the maximum static displacement $x_{\text{st,max}}$ (if P were applied quasi-statistically). Then eq. (36) may be written as

$$2 \frac{x_{\text{st,max}}}{X} \frac{x_{\text{cr}}}{X} = 1. \quad (37)$$

Next, $X/x_{\text{st,max}} = D$ is the dynamic magnification factor and $x_{\text{cr}}/X = \xi_{\text{cr}}$. Therefore, eq. (37) becomes

$$2\xi_{\text{cr}}/D = 1$$

or

$$\xi_{\text{cr}} = D/2. \quad (38)$$

Finally, the relation between $t_0/T (= \tau_0/2\pi)$ and the magnification factor D is obtained from the second of eqs. (35), or

$$\frac{\tau_0}{2\pi} = \frac{t_0}{T} = \frac{1}{2\pi} \cos^{-1} \left(1 - \frac{D^2}{2} \right), \quad (39)$$

from which

$$D = 2 \sin \left(\frac{\tau_0}{2} \right) = 2 \sin \frac{\pi t_0}{T}. \quad (40)$$

The dynamic magnification factor D (see [1], p. 94) is also plotted on Figure 10.3 and is identical to that shown on Figure 6.6 of [1].

Note that the parameters plotted on Figure 10.3 represent two different points of view. The plot of p versus t_0/T depicts the amount of a sudden load with finite duration t_0 that corresponds to a maximum amplitude X . On the other hand, the plot of D versus t_0/T shows the magnification of the maximum amplitude (compared to the static one) due to sudden application of the load with duration time t_0 . Note that in both cases, t_0 need not be larger than half the period of oscillation or $t_0/T \leq 2$.

Finally, before closing this section, one can see that the extreme case of $t_0 \rightarrow \infty$ and $t_0 \rightarrow 0$ are special cases of the finite-duration case.

From Figure 10.3, one sees that as $t_0/T \rightarrow \infty$, $p \rightarrow 1$, which is in agreement with eq. (15). The other extreme case is obtained from eqs. (34). If $t_0 \rightarrow 0$, then ξ_{cr} is an extremely small number and since $0 < \xi \leq \xi_{\text{cr}}$ then the second of eqs. (34) becomes

$$\tau_0 = \int_0^{\xi_{\text{cr}}} \frac{d\xi}{(\xi/\xi_{\text{cr}} - \xi^2)^{1/2}} \approx \int_0^{\xi_{\text{cr}}} \frac{d\xi}{(\xi/\xi_{\text{cr}})^{1/2}} = 2\xi_{\text{cr}}. \quad (41)$$

Then

$$(\text{Imp})_{\text{cr}} = (p\tau_0)_{\text{cr}} = \frac{1}{\xi_{\text{cr}}} 2\xi_{\text{cr}} = 2$$

which is identical to the result of eq. (24).

10.2 Suddenly Loaded Beams

A large class of structural problems that may be treated in a similar manner as the mass-spring system is that of Euler-Bernoulli beams. Under static application of the loads, these configurations exhibit unique stable equilibrium positions at each load level (see Figure 1.10).

Consider as an example the cantilever shown on Figure 10.4. The load $P(t)$ represents a sudden load with finite duration, in general.

If one assumes that the amplitude of the beam, at any point, is given by the static deflection curve multiplied by a time-dependent coefficient $y(t)$, then

$$w(x, t) = \frac{1}{2} y(t) \left[3 \left(\frac{x}{L} \right)^2 - \left(\frac{x}{L} \right)^3 \right]. \quad (42)$$

Note that under static application of the load P , y is the maximum (tip) deflection and it is related to the load by

$$y = \frac{PL^3}{3EI}. \quad (43)$$

The total potential for this case is

$$U_T = \frac{EI}{2} \int_0^L \left(\frac{\partial^2 w}{\partial x^2} \right)^2 dx - Pw(L, t) \quad (44)$$

or

$$U_T = \frac{3EI}{2L^3} y^2 - Py. \quad (45)$$

Note that the stiffness k at the free end becomes $k = 3EI/L^3$. With this value for the stiffness k , eq. (45) is identical to eq. (11) or

$$U_T = \frac{1}{2} ky^2 - Py. \quad (46)$$

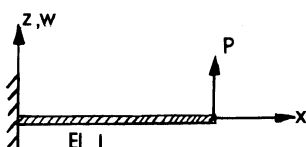


FIGURE 10.4. The cantilever beam.

Moreover, the kinetic energy for the cantilever problem is

$$T = \frac{1}{2} \int_0^L \rho \left(\frac{\partial w}{\partial t} \right)^2 dx \quad (47)$$

where ρ is the linear mass density. Substitution of eq. (42) into eq. (47) yields

$$T = \frac{1}{2} \left(\frac{33\rho L}{140} \right) \dot{y}^2, \quad (48)$$

which is similar to eq. (12), provided that $m = 33\rho L/140$. Equation (48) indicates that for the assumed deflection curve, the continuous beam is equivalent to a spring-mass system with k and m given by

$$k = 3EI/L^3 \quad \text{and} \quad m = 33\rho L/140.$$

Moreover, the continuous beam is equivalent to a weightless beam with a concentrated mass of m units at the end (see Example 1.5-3 on p. 19 of [2]).

On the basis of the above analogy, the results for the spring-mass system are applicable to the cantilever. In summary, for a prescribed maximum tip deflection Y , the various critical conditions are given by

$$\begin{aligned} \text{Imp}_{\text{cr}} &= \lim_{t_0 \rightarrow 0} (Pt_0) = (mk)^{1/2} Y \\ &= \left(0.70714 \frac{EI}{L^2} \rho \right)^{1/2} Y, \end{aligned} \quad (49)$$

$$P_{\text{dyn,cr}} = \frac{kY}{2} = \frac{3EI}{2L^3} Y. \quad (50)$$

Finally, for the case of suddenly applied loads of constant magnitude and finite duration, the results of Figure 10.3 are applicable provided that the proper expression for p is used.

According to eqs. (23), p may be defined as

$$p = \frac{2P}{kY} = \frac{2PL^3}{3EIY} = \frac{P}{P_{\text{dyn,cr}}}. \quad (51)$$

Note also that the magnification factor D in this case is the maximum dynamic amplitude (\bar{Y}) divided by the maximum static response.

10.3 The Imperfect Column

The imperfect column, under sudden application of an axial load, typifies structural systems with static behavior shown on Figure 1.5. Note that such a system, when of perfect geometry, is subject to bifurcational buckling with stable postbuckling behavior (smooth buckling). On the other hand, if there exists an initial geometric imperfection (small initial curvature), the system

exhibits a unique stable equilibrium path. Moreover, this system has received the most attention, as far as dynamic buckling is concerned, when loaded axially either by sudden loads or by time-dependent loads. Two complete reviews (with respect to their date of publication) of this problem may be found in [3] and [4]. As mentioned in these references the problem dates back to 1933 with the pioneering work of Koning and Taub [5], who considered a simply supported, imperfect (half-sine wave) column subjected to an axial sudden load of specified duration. In their analysis, they neglected the effects of longitudinal inertia, and they showed that for loads higher than the static (Euler) load the lateral deflection increases exponentially while the column is loaded, and after the release of the load, the column simply oscillates freely with an amplitude equal to the maximum deflection. Many investigations followed this work with several variations. Some included inertia effects, others added the effect of transverse shear, and so forth. The real difficulty of the problem, though, lies in the fact that there was no clear understanding by some investigators of the concept of dynamic stability and the related criteria.

According to [4], definition of a dynamic buckling load is possible only if there are initial small lateral imperfections in the column. Instability then stems from the growth of these imperfections. "Buckling occurs when the dynamic load reaches a critical value, associated with a maximum acceptable deformation, the magnitude of which is defined in most studies quite arbitrarily" [4]. There is some truth to this, primarily because the elastic column does not exhibit limit point instability or any other violent type of buckling under static application of the load. There is need for a cautioning remark related to the above statement, though. Analytically it has been shown (see [6]) that if a perfect column is suddenly loaded in the axial direction, the fundamental state is one of axial wave propagation (longitudinal oscillations). For some combination of the structural parameters, this state can become unstable and transverse vibrations of increasing amplitude are possible. Therefore, for this perfect column there exists a possibility of parametric resonance, which is one form of dynamic instability. In spite of this, almost all columns are geometrically imperfect, and therefore it is reasonable to investigate the dynamic behavior of imperfect columns including all variations of different effects as reported in [7–17]. These effects include axial inertia, rotatory inertia, transverse shear, and various loading mechanisms. Moreover, experimental results have been generated to test the various theories and effects.

Finally, the criterion employed in [4] is the one developed by Budiansky and Roth (Section 1), and it is applicable only to imperfection-sensitive structural systems, such as shallow arches, shallow spherical caps, and axially loaded imperfect cylindrical shells. The reason why the application of the Budiansky–Roth criterion may yield reasonable results for imperfect columns lies in the fact that the corresponding perfect configuration (column) possesses a very flat postbuckling branch. This means that the corresponding imperfect

column can experience, at some level of the sudden load or impulse, very large-amplitude oscillations (change from small- to large-amplitude oscillations). Note that the static curve for the imperfect column (static equilibrium), if the load is plotted versus the maximum lateral deflection, yields small values for the maximum deflection for small levels of the load. As the load approaches the Euler load, the value of the corresponding maximum deflection increases rapidly. On the other hand, if the criterion were to be applied to an imperfect flat plate, it is rather doubtful that reasonable, or any, answers could be obtained. This is so because the slope of the static postbuckling curve for the perfect plate is positive, and the imperfect plate exhibits a continuous bending response with smoothly increasing amplitude.

Next, the concept of dynamic stability, as developed and discussed in Chapter 1, is applied to an imperfect column. Consider the column shown on Figure 10.5. The length of the column is L (distance between supports); the bending and extensional stiffnesses are uniform, EI and EA ; and the sudden load $P(t)$ is acting along the horizontal, x , direction. Let u be the horizontal displacement component and $w - w^0$ the vertical (transverse) displacement component. For the analysis presented here, the initial geometric imperfection w^0 is a half-sine wave, or

$$w^0(x) = w_0 \sin \frac{\pi x}{L}. \quad (52)$$

The kinematic relations and the relations between the axial force P and bending moment M , on the one hand, and the reference axis strain ε^0 and change in curvature κ , on the other, are

$$\varepsilon = \varepsilon^0 + z\kappa, \quad (53)$$

$$\begin{aligned} \varepsilon^0 &= \frac{du}{dx} + \frac{1}{2} \left(\frac{dw}{dx} \right)^2 - \frac{1}{2} \left(\frac{dw}{dx} \right)^2, \\ \kappa &= - \left(\frac{d^2 w}{dx^2} - \frac{d^2 w^0}{dx^2} \right), \end{aligned} \quad (54)$$

$$= EA\varepsilon^0, \quad M^* = EI\kappa \quad (55)$$

Moreover, the total potential, U_T^* , expression for the system, is given by

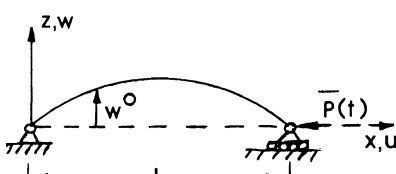


FIGURE 10.5. The imperfect column.

(for details, see Chapter 7 of [18])

$$U_T^* = \int_0^L \left(\frac{P^2}{2EA} + \frac{M^{*2}}{2EI} \right) dx + \bar{P}u(L). \quad (56)$$

Furthermore, the same nondimensionalization as in [18] is employed, or

$$\begin{aligned} \xi &= \frac{\pi x}{L}, & \eta(\xi) &= \frac{w(x)}{\rho}, & v(\xi) &= \frac{u(x)}{\rho}; \\ p &= \frac{P}{P_E}, & M &= \frac{M^*}{\rho P_E}, & U_T &= \frac{4U_T^*}{P_E \bar{\varepsilon}_E L} \end{aligned} \quad (57)$$

where

$$\rho^2 = \frac{I}{A}, \quad P_E = \frac{\pi^2 EI}{L^2}, \quad \bar{\varepsilon}_E = \left(\frac{\pi \rho}{L} \right)^2. \quad (58)$$

With these nondimensionalized parameters, one may write

$$p = \frac{1}{2} \left[2 \frac{v'}{\bar{\varepsilon}_E^{1/2}} + (\eta')^2 - (\eta'_0)^2 \right], \quad (59)$$

$$M = -(\eta'' - \eta'_0), \quad (60)$$

$$U_T = \frac{1}{\pi} \int_0^\pi \left[\frac{1}{2} \left\{ 2 \frac{v'}{\bar{\varepsilon}_E^{1/2}} + (\eta')^2 - (\eta'_0)^2 \right\} + 2(\eta'' - \eta''_0)^2 \right] + \frac{4}{\pi \bar{\varepsilon}_E^{1/2}} \bar{p} v(\pi) \quad (61)$$

where $(\)' = d/d\xi$.

From eq. (59), one may write

$$v' = -\bar{\varepsilon}_E^{1/2} \left[\frac{1}{2} \{ (\eta')^2 - (\eta'_0)^2 \} + \bar{p} \right] \quad (62)$$

and

$$\int_0^\pi v' d\xi = v(\pi) = -\bar{\varepsilon}_E^{1/2} \left[\frac{1}{2} \int_0^\pi [(\eta')^2 - (\eta'_0)^2] d\xi + \bar{p}\pi \right]. \quad (63)$$

Use of eq. (63) yields the following expression for the total potential:

$$U_T = \frac{1}{\pi} \int_0^\pi 2\bar{p}^2 d\xi + \frac{2}{\pi} \int_0^\pi (\eta'' - \eta''_0)^2 d\xi - \frac{4\bar{p}}{\pi} \left[\frac{1}{2} \int_0^\pi [(\eta')^2 - (\eta'_0)^2] d\xi + \bar{p}\pi \right]. \quad (64)$$

Note that in obtaining eqs. (62) and (64), use of in-plane static equilibrium is made, or

$$p = \text{const} = -\bar{p}. \quad (65)$$

For the dynamic case, this implies that the effect of in-plane inertia is being neglected.

Next, let us consider the case of suddenly loaded (by an axial force) half-sine

(imperfect) column. Then

$$w^0 = w_0 \sin \frac{\pi x}{L}, \quad \eta_0 = \frac{w_0}{\rho} \sin \xi = e \sin \xi. \quad (66)$$

Let the response η be of the form

$$\eta = [A(\tau) + e] \sin \xi. \quad (67)$$

The implication here is that at time $t = 0$, $\eta = e \sin \xi$.

Use of eqs. (66) and (67) in the expression for the total potential, eq. (64), yields

$$\bar{U}_T = -2\bar{p}^2 + A^2 - \bar{p}(A^2 + 2eA). \quad (68)$$

A modified potential $\bar{U}_{T_{mod}}$ is introduced, such that, regardless of the level of the applied load, the total potential is zero (modified) when $t = 0$ or when $A(0) = 0$. From eq. (68), it is clear that

$$\bar{U}_{T_{mod}} = \bar{U}_T + 2\bar{p}^2 = A^2 - \bar{p}(A^2 + 2eA). \quad (69)$$

The modified total potential is shown graphically on Figure 10.6 for $\bar{p} = 0$ and \bar{p} = specified value.

As in the case of the mass-spring system (note the similarity), critical dynamic conditions can be established if the maximum allowable amplitude is specified as X .

Only the case of a suddenly applied load of constant magnitude and infinite duration is presented here. From Figure 10.6 it is clear that $p_{cr,\infty}$ (load for which the system will not exceed the maximum allowable displacement $A(t) \leq X$) is given by

$$X = \frac{2e\bar{p}_{cr,\infty}}{1 - \bar{p}_{cr,\infty}} \quad \text{or} \quad \bar{p}_{cr,\infty} = \frac{X}{X + 2e}. \quad (70)$$

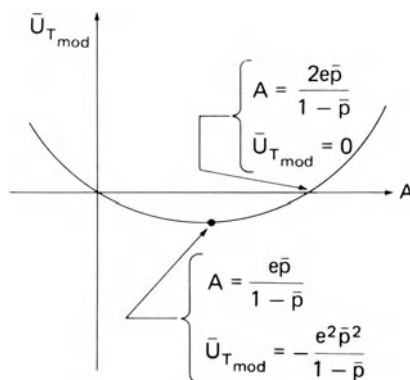


FIGURE 10.6. Total potential for a suddenly loaded half-sine column.

On the other hand, the static load required so that the maximum static deflection does not exceed the value X is

$$p_{\text{cr}_{\text{st}}} = \frac{X}{X + e}. \quad (71)$$

Note that eqs. (70) and (71) hold for $e \neq 0$.

The ratio ρ^d of $\bar{p}_{\text{cr}_{\infty}}$ to $\bar{p}_{\text{cr}_{\text{st}}}$ is given by

$$\rho^d = \frac{\bar{p}_{\text{cr}_{\infty}}}{\bar{p}_{\text{cr}_{\text{st}}}} = \frac{X + e}{X + 2e} = \frac{1 + (e/X)}{1 + 2(e/X)}. \quad (72)$$

This result is shown graphically on Figure 10.7.

Note that for very small values of e/X the ratio ρ^d is close to 1. For e/X equal to one, $\rho^d = 2/3$. Finally, as e/X becomes very large, ρ^d approaches the value of one-half.

Parenthesis. If load \bar{p} is applied quasi-statically the maximum deflection, $A_{\text{st}_{\text{max}}}$, is

$$A_{\text{st}_{\text{max}}} = \frac{e\bar{p}}{1 - \bar{p}}. \quad (73)$$

If load \bar{p} is applied suddenly the maximum amplitude $A_{\text{d}_{\text{max}}}$ is given by

$$A_{\text{d}_{\text{max}}} = \frac{2e\bar{p}}{1 - \bar{p}}. \quad (74)$$

On the basis of the above, the dynamic magnification factor for this case is

$$D = A_{\text{d}_{\text{max}}} / A_{\text{st}_{\text{max}}} = 2 \quad (75)$$

regardless of the value of e .

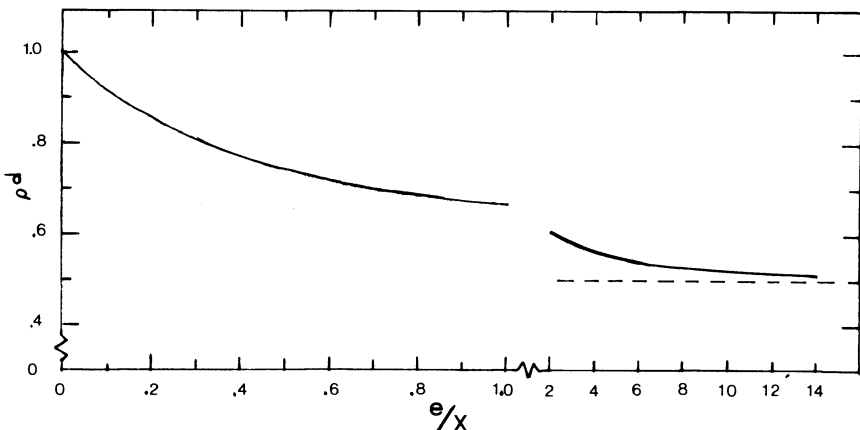


FIGURE 10.7. Ratio of dynamic to static load versus ratio of imperfection parameter to maximum allowable displacement (for the imperfect column).

References

1. Clough, R.W., and Renzien, J. *Dynamics of Structures*. McGraw-Hill Kogakusha Ltd., Tokyo, 1975.
2. Thomson, W.T. *Vibration Theory and Applications*, Prentice-Hall, Englewood Cliffs, N.J., 1965
3. Huffington, N.J., Jr. Response of elastic columns to axial pulse loading. *AIAA J.*, 1, 9, 1963, 2099–2104.
4. Ari-Gur, J., Weller, T., and Singer, J. Experimental Studies of Columns under Axial Impact. TAE No. 346, Department of Aeronautical Engineering, Technion-Israel Institute of Technology, December 1978.
5. Koning, C., and Taub, J. Impact buckling of thin bars in the elastic range hinged at both ends. *Luftfahrtforschung*, 10, 2, 1933, 55 (also translated as NACA TM 748 in 1934).
6. Wauer, J. Über Kinetische Verzweigungs Probleme Elastischer Strukturen unter Stossbelastung. *Ingenieur-Arch.*, 49, 1980, 227–233.
7. Meier, J.H. On the dynamics of elastic buckling. *J. Aero. Scie.* 12, 1945, 433–440.
8. Hoff, N.J., Nardo, S.V., and Erickson, B. The maximum load supported by an elastic column in a rapid compression test. In *Proc 1st U.S. National Congress of Applied Mechanics*, Chicago, 1951, pp. 419–423.
9. Hoff, N.J. The dynamics of the buckling of elastic columns. *J. Appl. Mech.*, 17, 1, 1953, 68–74.
10. Gerard, G., and Becker, H. Column behavior under conditions of impact. *J. Aero. Sci.*, 19, 1952, 58–65.
11. Lindberg, H.E. Impact buckling of a thin bar, *J. Appl. Mech.*, 32, 2, 1966, 241–247.
12. Davidson, J.F. Buckling of stunts under dynamic loading, *J. Mech. Phys. Solids*, 2, 1953, 54–66.
13. Hayashi, T., and Sano, Y. Dynamic buckling of elastic bars: 1st report; The case of low velocity impact. *Bull. Japanese Soc. Mech. Eng.*, 15, 1972, 1167–1175.
14. Hayashi, T., and Sano, Y. Dynamic buckling of elastic bars; 2nd report; The case of high velocity impact, *Bull. Japanese Soc. Mech. Eng.*, 15, 1972, 1176–1184.
15. Sevin, E. On the elastic bending of columns due to dynamic axial forces including effects of axial inertia. *J. Appl. Mech.*, 27, 1, 125–131.
16. Abrahamson, G.R., and Goodier, N.J. Dynamic flexural buckling of rods within an axial plastic compression wave. *J. Appl. Mech.*, 33, 2, 1966, 241–247.
17. Housner, J.M., and Knight N.F., Jr. The Dynamic collapse of a column impacting a rigid surface. *AIAA J.*, 21, 8, 1983, 1187–1195.
18. Simitses, G.J. *An Introduction to the Elastic Stability of Structures*. Prentice-Hall, Englewood Cliffs, N.J., 1976.

APPENDIX A

Parametric Resonance

A.1 Fundamentals

Resonance is a well-known and understood phenomenon in the field of oscillations. In a simple mass–spring system, if the forcing function is periodic and the frequency of the force is equal to the natural frequency of the system, the mass will oscillate with very large amplitudes (theoretically, the amplitude increases without bound) and the phenomenon is called resonance. It is important here to note that the forcing function causes the motion of the mass which is in the direction of the force. Moreover, this motion (oscillatory) is the primary and only state of the system.

Parametric resonance is a similar phenomenon with one important difference. The forcing function may cause a resonance in a secondary mode of vibration or a mode other than the one directly excited by its presence. For instance, consider an elastic column loaded in the axial direction by a periodic force. The primary motion consists of axial vibrations. It has been shown that, for certain relationship between the frequency of the axial periodic force and the natural frequency of free transverse (beam modes, secondary motion) vibrations, the bar will vibrate in the transverse direction with increasing (unbounded) amplitude. The phenomenon is called parametric resonance and the cause (forcing function) parametric excitation. According to [1], the terms parametric response and parametric behavior have also been used to describe the phenomenon.

Another example which further clarifies the phenomenon is the forced vibration of a thin ring by a periodic but uniform radial pressure. In general, the ring undergoes uniform radial vibrations (breathing mode) and, of course, the possibility of resonance exists. This means that the breathing mode may experience large-amplitude oscillations. Note also that the breathing mode corresponds to a periodic stretching (and therefore periodic hoop force) of the ring. Because of the dependence of the bending motion on the hoop force, the primary motion (breathing mode) may become dynamically unstable and bending vibrations with increasing amplitude may develop. This parametric resonance occurs for certain relationships between the parametric excitation frequency and the natural frequency of bending vibrations of the ring.

Similarly, shallow arches and shallow spherical caps can experience parametric resonance when acted by periodic, symmetric transverse loads.

So far, in describing the phenomenon of parametric resonance, the forcing function has been assumed to be periodic also. In a broader sense, though, the phenomenon of parametric resonance is possible for all dynamic loads which may cause oscillatory motion in the primary state. For example, a sudden axial load of finite duration will cause in-plane vibrations in a straight rod. The in-plane load is directly dependent on this oscillatory in-plane motion and therefore it is periodic itself. Then, because the bending motion is dependent on the in-plane load (which is periodic), large-amplitude bending vibrations are possible. Note that the net result is similar to having a periodic (axial) forcing function. Thus, parametric resonance is possible. The same can be said about suddenly loaded rings, shallow arches and spherical caps, and in general all systems which, when acted on by sudden loads, oscillate in a primary state (which in turn can become dynamically unstable and yield vibrations of increasing amplitude in a different state).

The number of structural systems which are subject to parametric resonance under either parametric excitation or other dynamic loads can increase to include flat thin plates under in-plane loads; thin, perfect-geometry, circular, cylindrical shells, with free ends and subjected to uniform lateral loading (periodic or sudden); and others. In general, parametric resonance is possible for all systems which under static loading are subject to bifurcational buckling, regardless of whether the postbuckling branch(es) is (are) stable or not. This is so because in bifurcational (static) buckling there exist a primary state and a secondary (buckling) state, through the appearance of which the primary state becomes unstable. Similarly, the parametric or sudden excitation causes oscillations in the primary state which can become dynamically unstable and admit unbounded oscillations in the secondary (buckling mode) state.

In spite of the oversimplified presentation of the phenomenon, it is a fairly accurate description of what has been presented in the literature concerning the analysis of systems under the heading of parametric resonance. There are a few questions that a skeptic might ask concerning the existence of parametric resonance, as suggested by the analytical (theoretical) treatment. These questions are similar to those concerning bifurcational (static) buckling. For instance, linear or nonlinear analysis of a perfect column reveals that there exists a primary state which is characterized by in-plane compression and no bending. Yet all tests on columns show that there is some bending at the onset of the axial load, and this bending remains very small until the load approaches the Euler buckling load. Then bending increases rapidly with very little increase in the applied load. This phenomenon occurs because the column is not free of small initial geometric imperfections and/or because the applied load is not necessarily coincident with the perfectly (?) straight column. This discussion may imply that the primary state is the combined bent-stretched state and not the bending-free state as suggested by the

analysis. Similarly, if the column is imperfect, parametric excitation or sudden application of the axial force cannot possibly cause in-plane (primary state) vibrations only, which may become dynamically unstable.

A.2 Short Historical Sketch

According to Evan–Iwanowski [1], the first observation of parametric resonance is attributed to Faraday [2] in 1831. The first mathematical explanation of the phenomenon was given by Lord Rayleigh [3] in 1883. Moreover, again according to [1] and Bolotin [4], the first analysis of parametric resonance of a structural configuration (the pinned perfect column) was presented by Beliaev [5]. Many studies started appearing in the open literature in the late 1940s and 1950s. Reviews on the subject, including excellent historical sketches, may be found in the works of Beilin and Dzhanelidze [6] and Evan–Iwanowski [1]. The reader is also referred to the books of Bolotin [4], Stoker [7], Hayashi [8], and Schmidt [9] for a more comprehensive and expanded treatment of the subject of parametric resonance. For more recent contributions on the subject, see [10–21]. Before closing this section, one should list the works of Mettler [22] and Ibrahim et al. [23]. Finally, since parametric resonance is possible when the excitation is sudden rather than periodic, the works of [24–26] are of importance and merit mentioning, especially the contribution of Wauer [26].

A.3 General Mathematical Model

In most applications, if one neglects the inertia in the primary state, uses linear theory to describe the motion in the secondary state, and neglects damping, and if the parametric excitation is harmonic, then the governing equation (of secondary state motion) is a second-order ordinary differential equation of the form

$$\frac{d^2w}{dt^2} + (\alpha - \beta \cos \theta t)w = 0 \quad (\text{A.1})$$

where w is the secondary state deformation component, α and β are constant related to the harmonic forcing function, and θ is the frequency of the forcing function. Equation (A.1) is called the Mathieu equation.

Parenthesis. In a more general case the periodic force is of the type

$$P(t) = P_0 + P_t \phi(t) \quad (\text{A.2})$$

where $\phi(t)$ is a periodic function of t with period T . In such a case the

governing equation becomes

$$\frac{d^2w}{dt^2} + [\alpha - \beta(t)]w = 0. \quad (\text{A.3})$$

This equation is called the Hill equation.

Mathieu–Hill equations have been investigated by many applied mathematicians [8, 27, 28]. The important characteristic of such equations is that in certain region of the parameters α and β the solution $w(t)$ is unbounded, while in others it is bounded. The concept of stability, then, associated with Mathieu–Hill equations is related to the boundedness of the solution. Critical conditions, in such cases, are related to the boundaries in the (α, β) space which separate the regions of stability and instability (bounded and unbounded solutions).

Figure A.1 shows typical results for the special case of

$$\frac{d^2w}{dt^2} + (\alpha - \beta \cos 2t)w = 0. \quad (\text{A.4})$$

The shaded areas correspond to regions of stability, while the clear areas correspond to regions of instability.

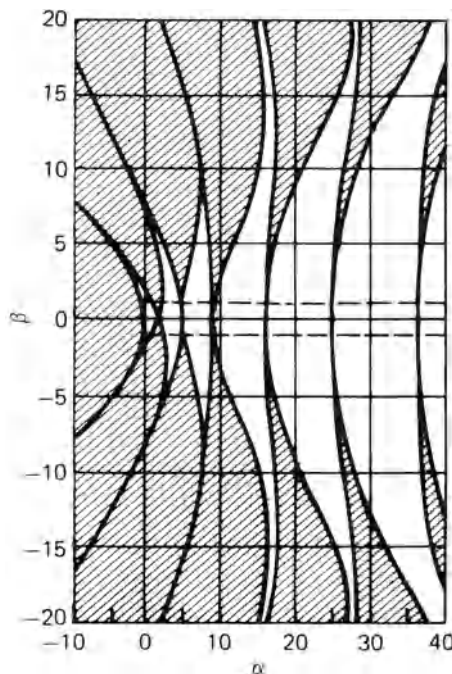


FIGURE A.1. Regions of stability and instability for a special Mathieu equation.

A.4 Simple Mechanical Model

Consider the rigid bar shown on Figure A.2. The bar is of length l and mass m , and it is subjected to a periodic force F at the free end:

$$F = P_0 + H \cos \theta t. \quad (\text{A.5})$$

The other end is immovable and its rotational spring of stiffness $\bar{\beta}$.

The equation of motion for the system is given by (for small ϕ ; $\sin \phi = \phi$)

$$\frac{ml^3}{3} \frac{d^2\phi}{dt^2} + (\bar{\beta} - Fl)\phi = 0 \quad (\text{A.6})$$

or

$$\frac{ml^2}{3} \frac{d^2\phi}{dt^2} + (\bar{\beta} - P_0 l - Hl \cos \theta t)\phi = 0. \quad (\text{A.7})$$

If $\theta = 2$ then eq. (A.7) becomes

$$\frac{d^2\phi}{dt^2} + \left(\frac{\bar{\beta} - P_0 l}{ml^3/3} + \frac{Hl \cos 2t}{ml^3/3} \right) \phi = 0. \quad (\text{A.8})$$

Equation (A.8) is identical to eq. (A.1), with

$$\phi = w, \quad \tau = t, \quad \alpha = \frac{3}{ml^3}(\bar{\beta} - P_0 l)$$

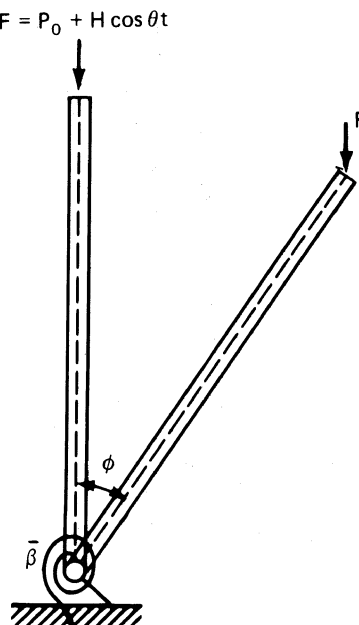


FIGURE A.2. A simple mechanical model. Geometry and sign convention.

and

$$\bar{\beta} = \frac{3H^2}{ml^2}.$$

Thus, the regions of stability and instability are given by those in Figure A.1.

A.5 The Euler Column

Consider the elastic column shown on Figure A.3. The length is L , the flexural stiffness EI , and the mass per unit length m . The equation of motion is given by

$$EI \frac{\partial^4 w}{\partial x^4} + F(t) \frac{\partial^2 w}{\partial x^2} + m \frac{\partial^2 w}{\partial t^2} = 0. \quad (\text{A.9})$$

The associated boundary conditions are

$$w(0, t) = \frac{\partial^2 w}{\partial x^2}(0, t) = w(L, t) = \frac{\partial^2 w}{\partial x^2}(L, t) = 0. \quad (\text{A.10})$$

The following series satisfies all boundary conditions:

$$w(x, t) = \sum_{n=1}^{\infty} f_n(t) \sin\left(\frac{n\pi x}{L}\right). \quad (\text{A.11})$$

Substitution of eq. (A.11) into eq. (A.9) yields

$$\sum_{n=1}^{\infty} \left[EI \left(\frac{n\pi}{L} \right)^4 f_n - F(t) \left(\frac{n\pi}{L} \right)^2 f_n + m \frac{\partial^2 f_n}{\partial t^2} \right] \sin \frac{n\pi x}{L} = 0. \quad (\text{A.12})$$

Because of the orthogonality of the trigonometric (sine),

$$m \frac{\partial^2 f_n}{\partial t^2} + \left[EI \left(\frac{n\pi}{L} \right)^4 - F(t) \left(\frac{n\pi}{L} \right)^2 \right] f_n = 0 \quad (\text{A.13})$$

for all n .

Since $F(t) = P_0 + H \cos 2\pi\theta t$, if a new time parameter is introduced, say $\tau = \pi\theta t$, then eq. (A.13) becomes

$$\frac{\partial^2 f_n}{\partial \tau^2} + (\alpha_n - \beta_n \cos 2\tau) f_n = 0 \quad (\text{A.14})$$

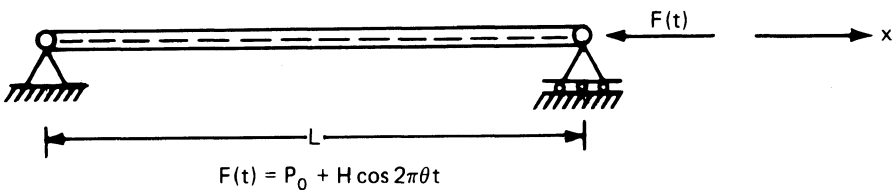


FIGURE A.3. The simply supported column.

where

$$\alpha_n = \frac{EI(n\pi/L)^4 - P_0(n\pi/L)^2}{m\pi^2\theta^2}$$

and

$$\beta_n = \frac{H(n\pi/L)^2}{m\pi^2\theta^2},$$

which is a Mathieu equation similar to eq. (A.4). For this case also, Figure A.1 gives the regions of stability and instability.

Note in this problem also that for the more general case of periodic loading, the axial force is given by

$$F(t) = P_0 + H_t\Phi(t) \quad (\text{A.15})$$

where $\Phi(t)$ is a periodic function of time with period T ,

$$\Phi(t + T) = \Phi(t). \quad (\text{A.16})$$

Substitution of this expression, eq. (A.15), into eq. (A.13) yields

$$\frac{\partial^2 f_n}{\partial \tau^2} + [\alpha_n - \beta_n \Phi(\tau)] f_n = 0 \quad (\text{A.17})$$

where

$$\alpha_n = \frac{EI(n\pi/L)^4 - P_0(n\pi/L)^2}{m\pi^2\theta^2}$$

$$\beta_n = \frac{H_t(n\pi/L)^2}{m\pi^2\theta^2} \quad \text{and} \quad \tau = \pi\theta t.$$

Regardless of whether the governing equation is a Mathieu or a Hill equation, the solution reveals that for certain combinations of the forcing function characteristics (magnitude, frequency, etc.) and system characteristics (natural frequencies, etc.), the amplitude of small oscillations starts to grow exponentially, and this yields the regions of stability or instability. For more details, including properties of the Mathieu–Hill equations and the construction of the regions of dynamic stability or instability, see Bolotin [4].

Several studies have removed some of the simplifying assumptions and examined the effect of certain parameters on the regions of stability or instability and the response of that system, in general. These parameters include viscous damping, transverse harmonic loading, in-plane motion, and attached masses.

Finally, there are several studies dealing with certain nonlinearities. For a summary of several results dealing with nonlinear effects, the interested reader is referred to the five reports of Ibrahim *et al.* (23).

References

1. Evan–Iwanowski, R.M. On the parametric response of structures. *Appl. Mech. Rev.*, 18, 9, 1965, 699–702.

2. Faraday, M. On a peculiar class of acoustical figures; and on certain forms assumed by a group of particles upon vibrating elastic surfaces. *Philos. Trans. R. Soc. London*, 121, 1831, 299–318.
3. Strutt, J.W. (Lord Rayleigh) On the crisscrosses of fluid resting upon a vibrating support. *Philos. Mat.*, 16, 1883, 50–53.
4. Bolotin, V.V. *The Dynamic Stability of Elastic Systems* (translated by V.I. Weingarten et al.). Holden Day, San Francisco, 1964.
5. Beliaev, N.M. Stability of prismatic rods subject to variable longitudinal forces. *Collection of Papers: Engineering Constructions and Structural Mechanics*, 149–167. Put', Leningrad, 1924.
6. Beilin, E.A., and Dzhanelidze, G.H. Survey of work on the dynamic stability of elastic systems. *Prikladnaia Matematika I Mekhanika*, 16, 5, 1952, 635–648. (Available in English as ASTIA No. AD-264148.)
7. Stoker, J.J. *Non-Linear Vibrations in Mechanical and Electrical Systems*, vol. II. Interscience, London, 1950.
8. Hayashi, C. *Nonlinear Oscillations in Physical Systems*. McGraw-Hill, New York, 1964.
9. Schmidt, G. *Parameterregte Schwingungen*. VEB Deutscher Verlage der Wissenschaften, Berlin, 1975.
10. Yao, J.C. Dynamic stability of cylindrical shells under static and periodic axial and radial loads. *AIAA J.*, 1, 6, 1963, 1391–1396.
11. Krajcinovic, D., and Herrmann, G. Parametric resonance of straight bars subjected to repeated impulsive compression. *AIAA J.*, 6, Nov. 10, 1968, 2025–2027.
12. Lovell, E.G., and McIvor, I.K. Nonlinear response of a cylindrical shell to an impulsive pressure. *J. Appl. Mech.*, 36, 2, 1969, 277–284.
13. Hsu, C.S. Impulsive parametric excitation: Theory. *J. Appl. Mech.*, 39, 1972, 551–558.
14. Dugundji, J., and Mukhopadhyay, V. Lateral bending-torsion vibrations of a thin beam under parametric excitation. *J. Appl. Mech., Trans. ASME, Ser. E*, 40, 3, 1973, 693–698.
15. Busby, H.R., Jr., and Weingarten, V.I. Dynamic stability of a nonlinear beam subjected to both longitudinal and transverse excitation. *Proc. Midwest Mechanics Conference, 13th*, University of Pittsburgh, August 1973, paper 27, pp. 367–382.
16. Carlson, R.L. Experimental study of the parametric excitation of a tensioned sheet with a cracklike opening. *Exp. Mech.*, 14, 11, 1974, 452–458.
17. Hsu, C.S. Some simple exact periodic responses for a nonlinear system under parametric excitation. *J. Appl. Mech., Trans. ASME, Ser. E*, 41, 4, 1974, 1135–1137.
18. Kounadis, A.N., and Belbas, S. On the parametric resonance of columns carrying concentrated masses. *J. Struct. Mech.*, 5, 4, 1977, 383–394.
19. Hsu, C.S., Cheng, W.H., and Yee, H.G. Steady state response of a non-linear system under impulsive periodic parametric excitation. *J. Sound Vibr.*, 50, 1, 1977, 95–116.
20. Sankar, T.S., and Rajan, G. Dynamic response of elastic rods under parametric excitations. *J. Eng. Ind. Trans. ASME, Ser. B*, 99, 1, 1977, 41–45.
21. Documaci, E. Pseudo-coupled bending-torsion vibrations of beams under lateral parametric excitation. *J. Sound Vibr.*, 58, 2, 1978, 233–238.
22. Mettler, E. Dynamic buckling. *Handbook of Engineering Mechanics* (editted by W. Flugge). McGraw-Hill, New York, 1962.

23. Ibrahim, R.A., Barr, A.D.S., and Roberts, J.M. Parametric resonance, Parts 1 to 5, *Shock Vibr. Dig.*, 10, 1–5, 1978.
24. McIvor, I.K., and Bernard, J.E. The dynamic response of columns under short duration axial loads. *J. Appl. Mech.*, 40, 3, 1973, 688–692.
25. Grybos, R. Impact stability of a bar. *Int. J. Eng. Sci.*, 13, 5, 1975, 463–478.
26. Wauer, J. Über Kinetische Verweigungs Probleme Elastischer Strukturen unter Stosseblastung. *Ingenieur-Arch.*, 49, 1980, 227–233.
27. McLachan, N.W. *Theory and Application of Mathieu Functions*. Oxford University Press, London, 1947.
28. Whittaker, E.T., and Watson, G.N. *A Course of Modern Analysis*, 4th ed. University Press, Cambridge, 1952.

APPENDIX B

Brachistochrone Problems

B.1 The Brachistochrone Problem

A statement of the brachistochrone problem and its solution can readily be found in virtually all texts on the calculus of variations (see [1–5]). The problem (the curve of quickest descent) was proposed by John Bernoulli in 1696 as a challenge to contemporary mathematicians. He challenged them to find the solution within 6 months. Independently, five mathematicians reported the correct solution. They were, of course, John Bernoulli himself, his brother Jacob Bernoulli, Newton, Leibniz, and de L'Hôpital.

Statement of the Problem. Given two points in space, A and B , with B being situated lower than A , find a smooth curve joining these points such that a material point of mass m subject to gravity only, compelled to travel on this curve and starting at A with a given initial velocity, shall reach point B in the shortest possible time.

The word brachistochrone originates from the Greek; *Brachistos* means shortest (quickest), while *chronos* means time. Moreover, note that the curve can be on any vertical plane containing points A and B ; therefore the problem can be defined in two dimensions, x (horizontal) and y (vertical, positive in the direction of gravity), characterizing a vertical plane.

Let the mass of the material point be m ; the coordinates of points A and B , respectively, $(0, 0)$ and (x, y) ; the time t , and the initial velocity \bar{v}_i .

Since the system is conservative, we may write

$$U + V = C \quad (\text{B.1})$$

where U is the potential of the external force (mg), V the kinetic energy, and C a constant. Note that since the particle is forced to travel on a curve, say $y = \phi(x)$, there exists a constraining force (on the particle) normal to the path of motion. But since the particle moves along curve $y = \phi(x)$, the work done by this force is zero. Thus, eq. (B.1) becomes

$$-gmy + \frac{m}{2} \left[\left(\frac{dx}{dt} \right)^2 + \left(\frac{dy}{dt} \right)^2 \right] = \frac{m\bar{v}_i^2}{2}. \quad (\text{B.2})$$

Note that $\bar{v}_i^2 = (dx/dt)_i^2 + (dy/dt)_i^2$, with i meaning initial state or values at $t = 0$. Further, note that the potential (energy level) is defined in such a way that it is zero at the origin, or the work done by mg is $mg(0 - y)$.

Equation (B.2) can be written as

$$\left[1 + \left(\frac{dy}{dx} \right)^2 \right] \left(\frac{dx}{dt} \right)^2 = \bar{v}_i^2 + 2gy \quad (\text{B.3})$$

or

$$dt = \left[\frac{1 + (dy/dx)^2}{2gy + \bar{v}_i^2} \right]^{1/2} dx. \quad (\text{B.4})$$

Integration of right-hand side from zero to x implies integration of the left-hand side, which gives the time T required to reach point B . Thus,

$$T = \int_0^x \left[\frac{1 + (dy/dx)^2}{2gy + \bar{v}_i^2} \right]^{1/2} dx. \quad (\text{B.5})$$

Clearly, the mathematical formulation of the brachistochrone problem is in the form of the simplest and most fundamental problem of the calculus of variations, that of extremizing

$$I = \int_a^b F \left(x, y, \frac{dy}{dx} \right) dx. \quad (\text{B.6})$$

Solutions to eq. (B.5) appear in the cited references. For the case of $\bar{v}_i = 0$, the solution is given on pp. 77–79 of [5] in parametric form as

$$\begin{aligned} y &= \frac{1}{2}b(1 + \cos 2\psi), \\ x &= a - \frac{1}{2}b(2\psi + \sin 2\psi). \end{aligned} \quad (\text{B.7})$$

According to eq. (B.7), the brachistochrone curves are arcs of cycloids described by a point on the circumference of a circle of radius $b/2$, which rolls on the x axis. For details, including uniqueness of solution, see [5].

B.2 The Brachistochrone as Applied to Model C (Constant Load of Infinite Duration)

As already mentioned in Section 3.5, for the case of finite duration, a critical condition depends on the path of motion during the application of the constant load ($0 \leq \tau \leq \tau_0$). A conservative answer can be obtained by requiring the path to be such that the time required is the shortest. Thus, the problem reduces to finding the brachistochrone path, starting from point $(r, s) = (\sqrt{\Lambda}, 0)$, and reaching the r position characterized by eq. (29) of Chapter 3. This position is termed r_{cr} in eq. (31) of Chapter 3, and its expression is

$$r = r_{cr} = \sqrt{\Lambda} - \frac{9}{4p}(\Lambda - 1) \quad (\text{B.8})$$

Since, from physical considerations, the motion in the interval $\sqrt{\Lambda - 3} \leq r \leq \sqrt{\Lambda}$ follows the steepest descent path, which is the symmetric path ($s = 0$), the brachistochrone problem will be restated as follows: find the path that requires the shortest time for the system to reach positions characterized by $r = r_{cr}$ and starting from $(r = \sqrt{\Lambda - 3}, s = 0)$ with $ds/dr = 0$.

The total potential energy of the system is given by eq. (58) of Chapter 2, or

$$\bar{U}_T^P = (r^2 + 9s^2 - 2\sqrt{\Lambda}r + \Lambda) + \frac{1}{2}(\Lambda - r^2 - 3s^2)^2 - 2p(\sqrt{\Lambda} - r). \quad (\text{B.9})$$

Since

$$\bar{U}_T^P + \bar{T}^P = 0 \quad \text{for } 0 \leq \tau \leq \tau_0 \quad (\text{B.10})$$

and

$$\bar{T}^P = \frac{1}{2}(1 + s'^2) \left(\frac{dr}{d\tau} \right)^2 \quad (\text{B.11})$$

according to eq. (28) of Chapter 3, with

$$(\cdot)' = \frac{d}{dr},$$

the brachistochrone problem reduces to extremizing the integral

$$I = \int_{\sqrt{\Lambda-3}}^{r_{cr}} \left(\frac{\sqrt{1 + s'^2}}{-2\bar{U}_T^P} \right) dr = \int_{\sqrt{\Lambda-3}}^{r_{cr}} X(r, s, s') dr \quad (\text{B.12})$$

by considering paths which start at $r = \sqrt{\Lambda - 3}$ and $s = 0$ with $s' = 0$ and reach positions characterized by $r = r_{cr}$ [constant; see eq. (B.8)].

The Euler–Lagrange equation and the associated boundary conditions for this brachistochrone problem, eq. (B.12), are (see [2])

$$\begin{aligned} \frac{\partial X}{\partial s} - \frac{d}{dr} \frac{\partial X}{\partial s'} &= 0, \\ \left. \frac{\partial X}{\partial s'} \right|_{r_{cr}} &= 0 \rightarrow \dot{s}|_{r_{cr}} = 0. \end{aligned} \quad (\text{B.13})$$

Note also that $s = s' = 0$ at $r = \sqrt{\Lambda - 3}$.

Since $X = \sqrt{(1 + s'^2)/(-2\bar{U}_T^P)}$, eq. (B.13) yields

$$\begin{aligned} s'' + (s' + s'^3) \frac{r + 9ss' - \sqrt{\Lambda} - (\Lambda - r^2 - 3s^2)(r + 3ss') + p}{-\bar{U}_T^P} \\ - (1 + s'^2)^2 \frac{9s - 3s(\Lambda - r^2 - 3s^2)}{\bar{U}_T^P} = 0. \end{aligned} \quad (\text{B.14})$$

One possible solution to eq. (B.14) that satisfies the boundary conditions is given by the path $s = 0$. However, there is no guarantee that path $s = 0$ is the unique extremal path of the variational problem. Suppose that the solution to eq. (B.13) bifurcates at a point ($r = r_b$, $s = 0$) where $r_{cr} \leq r_b \leq \sqrt{\Lambda - 3}$. Obviously, $s = 0$ at that point.

However, considering a closed domain $D = [r, s, s']$ such that $s < \delta$ and $s' < \delta$ where δ is a very small positive number ($\delta \ll 1$), with the point $(r_b, 0, 0)$ lying in the interior of D and $\bar{U}_T^P < -w$ ($w > 0$ any proper positive number) everywhere on D , the function

$$f(r, s, s') = -(s' + s'^3) \frac{r + 9ss' - \sqrt{\Lambda - (\Lambda - r^2 - 3s^2)(r + 3ss')} + p}{\bar{U}_T^P} - (1 + s'^2)^2 \frac{9s - 3(\Lambda - r^2 - 3s^2)}{\bar{U}_T^P} \quad (B.15)$$

is continuous and satisfies the following Lipschitz condition on D :

$$|f(r, \bar{s}, \bar{s}') - f(r, s, s')| < L_1 |\bar{s}' - s'| + L_2 |\bar{s} - s|. \quad (B.16)$$

Since higher-order terms in s and s' are canceled out, L_1 and L_2 are equal to

$$L_1 = \max \left| \frac{r - \sqrt{\Lambda - (\Lambda - r^2)r + p}}{\bar{U}_T^P} \right| = \max \Omega_1(r, s) \quad (B.17)$$

and

$$L_2 = \max \left| \frac{9 - (\Lambda - r^2)}{\bar{U}_T^P} \right| = \max \Omega_2(r, s). \quad (B.18)$$

The existence of L_1 and L_2 is guaranteed by the continuity of the functions Ω_1 and Ω_2 on D (see [6]).

Recalling the uniqueness theorem (Picard–Lindelöf) for a differential equation of second order (see [7]), the initial value problem composed of the differential equation (B.14) and the boundary conditions $s|_{r_b} = s'|_{r_b} = 0$, used as initial conditions in the mathematical sense, admits a unique continuous solution in the interior of D . Therefore, the solution to eq. (B.14), which is initially symmetric, does not bifurcate at any point on the r axis. Consequently, the symmetric ($s = 0$) solution is unique.

Since the total potential \bar{U}_T^P is symmetric with respect to the r axis, the extremal path, $s = 0$, cannot be a minimax. Moreover, around any path there always exists another path yielding a higher value for the time of motion [integral I expressed by eq. (B.12)]. Thus, the extremal path $s = 0$ cannot be a maximal path either. Therefore, $s = 0$ is the brachistochrone path of the problem.

Note that path $s = 0$ is not a fictitious path but a real one, since it satisfies the equations of motion

$$\frac{d^2r}{dt^2} - 2[4(\Lambda - 1 - r^2 - 3s^2) - p + \sqrt{\Lambda}] = 0 \quad (B.19)$$

and

$$\frac{d^2s}{dt^2} - 6s(\Lambda - 3 - r^2 - 3s^2) = 0 \quad (B.20)$$

for model C, under a suddenly applied constant load p . These two equations, eqs. (B.19) and (B.20), can easily be derived (see [8]).

References

1. Hancock, H. *Lectures on the CALCULUS OF VARIATIONS*. University of Cincinnati, Bulletin No. 1, 1904.
2. Weinstock, R. *Calculus of Variations*. McGraw-Hill, New York, 1952.
3. Courant, R., and Hilbert, D. *Methods of Mathematical Physics* (English edition), vol. I. Interscience, New York, 1953.
4. Gelfand, I.M., and Fomin, S.V. *Calculus of Variations*. Prentice-Hall, Englewood Cliffs, N.J., 1963.
5. Pars, L.A. *An Introduction to the Calculus of Variations*. Wiley, New York, 1962.
6. Apostol, T.M. *Mathematical Analysis*, Theorem 4-20. Addison-Wesley, Palo Alto, Calif., 1965.
7. Ince, L.E. *Ordinary Differential Equations*, Theorem 3-3, pp. 71–72. dover, New York, 1956.
8. Simitses, G.J. Dynamic stability of structural elements subjected to step-loads. *Proc. Army Symposium on Solid Mechanics, 1980; Designing for Extremes: Environment, Loading, and Structural Behavior*, South Yarmouth, Cape Cod, Mass., Sept. 30–Oct. 2, 1980.

APPENDIX C

The Influence of Small Damping

C.1 Damping

In many vibration experiments, we observe that oscillations decay and finally the system comes to rest. Examples of this include a cantilever beam, a mass hanging through an extensional spring (a real system, not a mass-spring model), and the simple pendulum. On the contrary, the mathematical representation for single-degree-of-freedom models leads to a simple harmonic function of time to describe the free vibration of the system (see [1–3]). The discrepancy lies in the fact that a mechanism for energy dissipation has not been incorporated in the analytical model. When it is in the form of a viscous damper, there is agreement between experiment and analysis.

Several types of damping and models thereof have been employed in predicting the oscillatory response of system.

In viscous damping, the damping force is proportional to the rate of extension, dq/dt . The constant of proportionality c between the force and the velocity is called the damping coefficient (see Section 3-1 of [2]). In this oversimplified but valuable modeling, the energy loss in typical mechanical systems is characterized by a dissipation function

$$U_F = \frac{1}{2}c\left(\frac{dq}{dt}\right)^2. \quad (\text{C.1})$$

Note that the dimensions of U_F are those of energy per unit of time, and of c are those of force per unit of speed.

Another type of damping is Coulomb damping (friction), where the damping force is constant and opposite to the direction of the velocity. Still another type of damping is structural damping as used in the modeling of aircraft vibration and flutter studies. This damping force is proportional to displacement but in phase with the velocity of a harmonically oscillating system (see [3]).

Viscous damping has a stabilizing effect on conservative systems. On the other hand, viscous damping may have a destabilizing effect in nonconservative elastic systems (see [4]).

In this appendix, the influence of small damping on the critical conditions for the case of constant load of finite duration is presented. Related work as applied to the shallow arch is presented in [5–7]. In [5] the authors use material viscous damping for energy dissipation, while the authors of [6] use a viscous foundation for the same purpose. Finally, the interested reader is referred to the review by Nicholson [8] on the stable response of damped mechanical systems.

C.2 General Approach

Small damping is introduced here through a viscous damper (dashpot) connected in parallel with the extensional springs in the three models analyzed in the first part of the text.

Since we are concerned with small damping, the trajectory of the damped system can be thought of as a perturbation about the trajectory of the undamped system. This is a key assumption in the estimation of critical loads. The critical load, on the basis of this assumption, appears as the sum of the critical load for the corresponding undamped system plus a product of the small (in magnitude) damping coefficient μ , times a quantity depending only on the model geometry.

Damping forces F are introduced by a dashpot and are equal to

$$F = \mu \dot{L}$$

where μ is the damping coefficient and L the trajectory of the dashpot.

A nondimensionalization $\bar{\mu}$ of the damping coefficient μ could be obtained by

$$\bar{\mu} = \frac{1}{\lambda k} \mu$$

where k is the elastic constant of the spring and λ a normalizing coefficient having the dimension of time.

Furthermore, the nondimensionalized dissipated energy \bar{D} is expressed by

$$\bar{D} = \bar{\mu} \oint_L \dot{L} dL \quad (C.2)$$

where $\oint_L \dot{L} dL$ stands for the nondimensionalized dissipated energy when $\bar{\mu} = 1$. The balance of energy is expressed by the equations

$$\bar{T}^p + \bar{U}_T^p + \bar{D} = 0 \quad \text{for } 0 < \tau < \tau_0 \quad (C.3)$$

and

$$\bar{T}^0 + \bar{U}_T^0 + \bar{D} = C \quad \text{for } \tau_0 < \tau \quad (C.4)$$

where C is a constant, eq. (C.3) characterizes the energy balance during the action of the load p , and eq. (C.4) characterizes the energy after the release of p .

Moreover, the continuity in both kinetic and dissipated energies at the

release of the load yields the constant coefficient C , equal to

$$C = \left[\bar{U}_T^0 - \bar{U}_T^p \right]_{\tau_0}.$$

With this value of C , eq. (C.4), the balance of energy after the action of the load p , becomes

$$\bar{T}^0 + \bar{U}_T^0 + \bar{D} + [\bar{U}_T^p - \bar{U}_T^0]_{\tau_0} = 0 \quad \text{for } \tau_0 < \tau. \quad (\text{C.5})$$

A system is called dynamically stable if it cannot reach the zero-load unstable equilibrium point, L_u^0 (with the least potential energy), with zero velocity (kinetic energy).

Consequently, the balance of energy for $\tau > \tau_0$ expressed by eq. (C.5) gives the critical condition, or

$$\bar{U}_T^0|_{L_u^0} = \bar{D}|_{L_u^0} - [\bar{U}_T^p - \bar{U}_T^0]|_{\tau_0}. \quad (\text{C.6})$$

Furthermore, since the nondimensionalized damping coefficient $\bar{\mu}$ is very small ($\bar{\mu} \ll 1$), the trajectory of the damped system could be thought of as a perturbation around the undamped one. Thus, the critical displacement L_{cr}^p , the displacement which guarantees stability as long as the applied force is released before the system reaches it, may be expanded in Taylor's series as

$$L_{cr}^p = {}_0 L_{cr}^p + \bar{\mu} {}_1 L_{cr}^p + O(\bar{\mu}^2) \quad (\text{C.7})$$

where ${}_0 L_{cr}^p$ is the critical displacement for the corresponding problem, without the influence of damping.

Use of eq. (C.2) in eq. (C.6) yields

$$\bar{U}_T^0|_{L_u^0} = -\bar{\mu} \int_0^{L_u^0} \dot{L} dL - [\bar{U}_T^p - \bar{U}_T^0]|_{L_{cr}^p}. \quad (\text{C.8})$$

Invoking the expression for L_{cr}^p from eq. (C.7), the quantity $[\bar{U}_T^p - \bar{U}_T^0]|_{L_{cr}^p}$ may also be expanded in Taylor's series

$$[\bar{U}_T^p - \bar{U}_T^0]|_{L_{cr}^p} = [\bar{U}_T^p - \bar{U}_T^0]|_{{}_0 L_{cr}^p} + \bar{\mu} \sum_{j=1}^J \frac{\partial [\bar{U}_T^p - \bar{U}_T^0]}{\partial L_j} \Big|_{{}_0 L_{cr}^p} ({}_1 L_{cr}^p) + O(\bar{\mu}^2) \quad (\text{C.9})$$

where J stands for the degrees of freedom of the model.

Introducing eq. (C.9) in eq. (C.8) and separating terms of the same order of magnitude yields two equations:

$$\bar{U}_T^0|_{L_u^0} = -[\bar{U}_T^p - \bar{U}_T^0]|_{{}_0 L_{cr}^p}; \quad (\text{C.10})$$

and for a one-degree-of-freedom trajectory,

$${}_1 L_{cr}^p = - \frac{\int_0^{L_u^0} \dot{\phi} f({}_0 \phi) d_0 \phi}{[\bar{U}_T^p - \bar{U}_T^0]|_{{}_0 L_{cr}^p}}. \quad (\text{C.11})$$

After evaluating ${}_1L_{\text{cr}}^p$, the critical time $\tau_{0,\text{cr}}$ for the release of the load p is found by the balance of energy equation [eq. (C.3)].

It is simply mentioned that eq. (C.10) gives the displacement estimate, ${}_0L_{\text{cr}}^p$, for the undamped system and it is the same as that given in Chapter 3.

On each model, eqs. (C.10) and (C.11) will be applied and the correction of the displacement ${}_1L_{\text{cr}}^p$ ($\bar{\mu} = 1$) will be found. Furthermore, corrections for the critical time $\tau_{0,\text{cr}}$ will also be computed.

C.3 Application to Model A

Consider model A, analyzed in Chapter 2, but under the influence of small damping. Damping is introduced by a dashpot connected with the spring as shown on Figure C.1. If $\bar{\mu}$ is the damping coefficient, the nondimensionalized dissipated energy \bar{D} is expressed by

$$\bar{D} = \frac{D}{kL^2} = \bar{\mu} \int_{\theta_0}^{\theta} \dot{\phi} \sin^2 \left(\frac{\pi}{4} - \frac{\phi}{2} \right) d\phi. \quad (\text{C.12})$$

It is assumed that the velocity of the dashpot is equal to that of joint B and that ϕ is the trajectory from θ_0 to θ .

Applying the nondimensionalization

$$\tau = \sqrt{\frac{2k}{m}} t, \quad \bar{\mu} = \frac{\sqrt{2}}{\sqrt{km}} \mu, \quad (\dot{\cdot}) = \frac{\partial}{\partial \tau} \quad (\text{C.13})$$

and recalling that the unstable position L_u^0 on the zero-load potential for

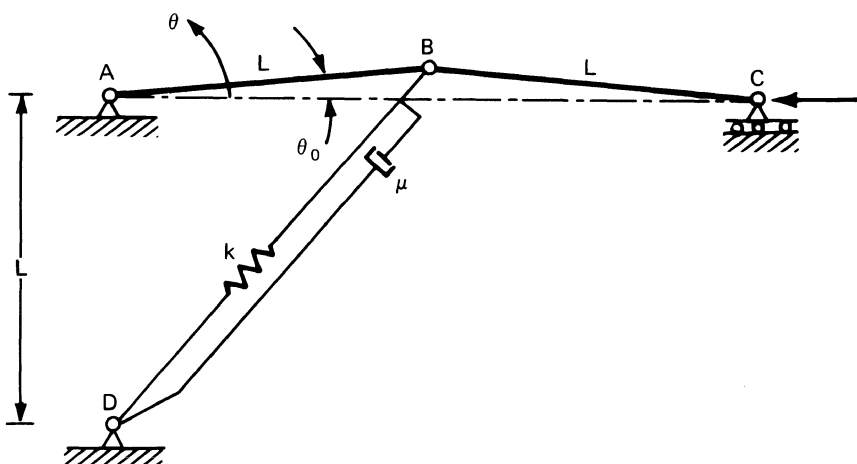


FIGURE C.1. Geometry of model A with damping.

the undamped system is given by $\theta = \pi/2$, then eqs. (C.10) and (C.11) yield

$$_0\theta_{cr}^p = \arccos \left[\cos \theta_0 - \frac{(\sqrt{2} - \sqrt{1 + \sin \theta_0})}{p} \right] \quad (C.14)$$

and

$$_1\theta_{cr}^p = \frac{\int_{\theta_0}^{\pi/2} _0\dot{\phi} \sin^2(\pi/4 - _0\phi/2) d_0\phi}{p \sin _0\theta_{cr}^p}. \quad (C.15)$$

The evaluation of the integral below is needed for (C.15), the evaluation of $_1\theta_{cr}^p$:

$$I = \int_{\theta_0}^{\pi/2} _0\dot{\phi} \sin^2 \left(\frac{\pi}{4} - \frac{_0\phi}{2} \right) d_0\phi. \quad (C.16)$$

Recalling the energy equation for the undamped system, eqs. (1) and (2) of Chapter 3, one may write (for this model)

$$_0\dot{\phi}^2 + [\sqrt{1 + \sin _0\phi} - \sqrt{1 + \sin \theta_0}]^2 - p(\cos \theta_0 - \cos _0\phi) = 0 \\ \text{for } \theta_0 < _0\phi < _0\theta_{cr} \quad (C.17)$$

and

$$_0\dot{\phi}^2 + [\sqrt{1 + \sin _0\phi} - \sqrt{1 + \sin \theta_0}]^2 = p(\cos \theta_0 - \cos _0\theta_{cr}^p) \\ \text{for } _0\theta_{cr} < \phi < \frac{\pi}{2}. \quad (C.18)$$

Hence integral I , eq. (C.16), becomes

$$I = \int_{\theta_0}^{_0\theta_{cr}^p} \sqrt{p(\cos \theta_0 - \cos _0\phi) - [\sqrt{1 + \sin _0\phi} - \sqrt{1 + \sin \theta_0}]^2} \sin^2 \left(\frac{\pi}{4} - \frac{_0\phi}{2} \right) d_0\phi \\ + \int_{_0\theta_{cr}^p}^{\pi/2} \sqrt{p(\cos \theta_0 - \cos _0\theta_{cr}^p) - [\sqrt{1 + \sin _0\phi} - \sqrt{1 + \sin \theta_0}]^2} \\ \times \sin^2 \left(\frac{\pi}{4} - \frac{_0\phi}{2} \right) d_0\phi. \quad (C.19)$$

The critical time $\tau_{0,cr}$ may be found by invoking eq. (C.3) for $0 < \tau < \tau_0$. Thus,

$$\tau_{0,cr} = \int_{\theta_0}^{_0\theta_{cr}^p} \frac{d\theta}{\sqrt{p(\cos \theta_0 - \cos \theta) - [\sqrt{1 + \sin \theta} - \sqrt{1 + \sin \theta_0}]^2} - \bar{\mu} \int_{\theta_0}^{\theta} _0\dot{\phi} \sin^2(\pi/4 - _0\phi/2) d_0\phi}. \quad (C.20)$$

Expanding $\tau_{0,cr}$ in power of $\bar{\mu}$, we have

$$\tau_{0,cr} = _0\tau_{0,cr} + \bar{\mu} _1\tau_{0,cr} + O(\bar{\mu}^2) \quad (C.21)$$

where

$$_0\tau_{0,cr} = \int_{\theta_0}^{_0\theta_{cr}^p} \frac{d\theta}{\sqrt{p(\cos \theta_0 - \cos \theta) - [\sqrt{1 + \sin \theta} - \sqrt{1 + \sin \theta_0}]^2}} \quad (C.22)$$

is the critical time for the undamped system, and

$$\begin{aligned} {}_0\tau_{0,\text{cr}} &= \left. \frac{\partial \tau_0}{\partial \bar{\mu}} \right|_{\bar{\mu}=0} \\ &= \frac{1}{2} \int_{\theta_0}^{{}_0\theta_{\text{cr}}^P} \frac{\left\{ \int_{\theta_0}^{\theta} {}_0\phi \sin^2(\pi/2 - {}_0\phi/2) d_0\phi \right\} d\theta}{[p(\cos \theta_0 - \cos \theta) - (\sqrt{2 + \sin \theta} - \sqrt{1 + \sin \theta_0})^2]^{3/2}} \\ &\quad + \frac{{}_1\theta_{\text{cr}}^P}{\sqrt{p(\cos \theta_0 - \cos {}_0\theta_{\text{cr}}^P) - [\sqrt{1 + \sin {}_0\theta_{\text{cr}}^P} - \sqrt{1 + \sin \theta_0}]^2}}. \end{aligned} \quad (\text{C.23})$$

Note that ${}_1\theta_{\text{cr}}^P$ is a function of parameters related to the undamped system only. The same holds true for ${}_1\tau_{0,\text{cr}}$.

The governing equations for finding critical conditions in the presence of small damping ($\bar{\mu} \ll 1$) are eqs. (C.14), (C.15), (C.22), and (C.23). Note that eq. (C.19) is employed in eq. (C.15). These four equations relate the given small damping coefficient $\bar{\mu}$, the applied load p , the time parameters ${}_0\tau_{0,\text{cr}}$ and ${}_1\tau_{0,\text{cr}}$, and the position parameters ${}_0\theta_{\text{cr}}^P$. Note that the range of p values (assigned) must be greater than the dynamic critical load values for the case of a suddenly applied constant load of infinite duration, without damping. The computational procedure involves the following steps: (1) assign a p value

TABLE C.1. Critical conditions for constant load of finite duration in the presence of damping (model A).

θ_0	p	${}_0\tau_{0,\text{cr}}$	${}_1\tau_{0,\text{cr}}$
0.0005	0.45	31.25	29.61
	0.50	19.55	11.15
	1.00	8.97	1.99
	3.00	3.42	0.55
	5.00	2.63	0.35
	10.00	2.11	0.20
	50.00	0.63	0.06
0.010	0.41	33.23	78.53
	0.45	21.14	12.85
	0.50	12.32	7.30
	1.00	7.78	1.64
	5.00	2.00	0.31
	10.00	1.24	0.18
	50.00	0.42	0.07
0.020	0.44	13.69	7.47
	0.55	9.98	3.62
	0.65	6.87	2.53
	1.00	5.85	1.30
	5.00	1.91	0.27
	10.00	0.96	0.16
	50.00	0.39	0.06

and compute ${}_0\theta_{cr}^P$ from eq. (C.14), (2) employ eq. (C.19) in eq. (C.15) and solve for ${}_1\theta_{cr}^P$, (3) from eq. (C.22) solve for ${}_0\tau_{0,cr}$, and finally (4) employ eq. (C.23) and solve for ${}_1\tau_{0,cr}$. A simple computer program can be written to accomplish the solution. Numerical results are generated for three values of the imperfection parameter θ_0 (0.005, 0.010, and 0.020). These results are presented in Table C.1.

Note that, since a critical condition corresponds to a set of $p, \tau_{0,cr}$ values, a small damping coefficient $\bar{\mu}$ has a stabilizing effect. This effect, though, is very small. For instance, at the high values of the load p (say for $\theta_0 = 0.05$, $p = 10$), the corresponding value for $\tau_{0,cr}$ (if $\bar{\mu} = 0.04$) is $2.110 + 0.008 = 2.118$. Remember that the $p-\tau_{0,cr}$ curve for the undamped system (see Figure 3.3) is very steep at the high p value and virtually flat at the low values of p . On the other hand, when $p = 0.45$ (a value close to $p_{cr,\infty} = 0.432$) the corresponding critical time is $\tau_{0,cr} = 31.25 + 1.184 + 32.434$. Since the curve is very flat at this load p value, one may conclude that the effect of small damping is virtually negligible.

C.4 Application to Model B

Consider model B, discussed in Chapter 3, but under the influence of small damping. Damping is introduced by a dashpot connected with the spring, as shown on Figure C.2.

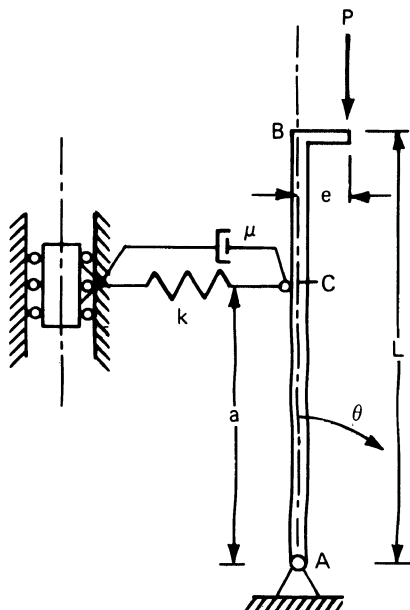


FIGURE C.2. Geometry of model B with damping.

If μ is the damping coefficient, the nondimensionalized dissipated energy \bar{D} is expressed by

$$\bar{D} = \frac{D}{\frac{1}{2}ka^2} = \frac{2\mu}{k} \int_0^\theta \dot{\phi} d\phi. \quad (\text{C.24})$$

It is assumed that the velocity of the dashpot is equal to that at joint C and ϕ is the trajectory from 0 to θ .

Applying the nondimensionalization

$$\tau = \frac{a}{L} \sqrt{\frac{k}{m}} t, \quad \bar{\mu} = \frac{2a}{L\sqrt{km}} \mu \quad \text{with } (\cdot) = \frac{\partial}{\partial \tau} \quad (\text{C.25})$$

and recalling that the unstable position L_u^0 for the “zero-load” potential of the undamped system is given by $\theta_u^0 = \pi/2$, then eqs. (C.10) and (C.11) yield

$$2p(1 - \cos \theta_{cr} + \bar{e} \sin \theta_{cr}) = 1 \quad (\text{C.26})$$

and

$$\theta_{cr} = \frac{\int_0^{\pi/2} \dot{\phi} d_0 \phi}{2p(\sin \theta_{cr} + \bar{e} \cos \theta_{cr})}. \quad (\text{C.27})$$

Thus for the evaluation of the integral

$$I = \int_0^{\pi/2} \dot{\phi} d_0 \phi \quad (\text{C.28})$$

the balance of the energy expressions for the undamped system, eqs. (1) and (2) of Chapter 3, are recalled. Hence

$$_0\dot{\phi}^2 + \sin^2 \theta_0 \phi - 2p(1 - \cos \theta_0 \phi + \bar{e} \sin \theta_0 \phi) = 0 \quad \text{for } 1 < \theta_0 \phi < \theta_{cr}, \quad (\text{C.29})$$

and

$$_0\dot{\phi}^2 + \sin^2 \theta_0 \phi - 2p(1 - \cos \theta_{cr} + \bar{e} \sin \theta_{cr}) = 0 \quad \text{for } \theta_{cr} < \theta_0 \phi < \frac{\pi}{2}. \quad (\text{C.30})$$

Integral I becomes

$$\begin{aligned} I = & \int_0^{\theta_{cr}} \sqrt{2p(1 - \cos \theta_0 \phi + \bar{e} \sin \theta_0 \phi) - \sin^2 \theta_0 \phi} d_0 \phi \\ & + \int_{\theta_{cr}}^{\pi/2} \sqrt{2p(1 - \cos \theta_{cr} + \bar{e} \sin \theta_{cr}) - \sin^2 \theta_0 \phi} d_0 \phi. \end{aligned} \quad (\text{C.31})$$

The critical time $\tau_{0,cr}$ may be found by invoking eq. (C.3). Thus,

$$\tau_{0,cr} = \int_0^{\theta_{cr}^P} \frac{d\theta}{\sqrt{2p(1 - \cos \theta + \bar{e} \sin \theta) - \sin^2 \theta - \bar{\mu} \int_0^\theta \dot{\phi} d_0 \phi}}. \quad (\text{C.32})$$

Expanding $\tau_{0_{cr}}$ in power series of $\bar{\mu}$ ($\bar{\mu} \ll 1$), one obtains

$$\tau_{0_{cr}} = {}_0\tau_{0_{cr}} + \bar{\mu}_1 \tau_{0_{cr}} + O(\bar{\mu}^2) \quad (\text{C.33})$$

where

$${}_0\tau_{0_{cr}} = \int_0^{{}_0\theta_{cr}^P} \frac{d\theta}{\sqrt{2p(1 - \cos \theta + \bar{e} \sin \theta) - \sin^2 \theta}} \quad (\text{C.34})$$

is the critical time for the undamped system, and

$$\begin{aligned} {}_1\tau_{0_{cr}} &= \left. \frac{\partial \tau_0}{\partial \bar{\mu}} \right|_{\bar{\mu}=0} = \frac{1}{2} \int_0^{{}_0\theta_{cr}^P} \frac{\int_0^\theta {}_0\dot{\phi} d_0 \phi}{[2p(1 - \cos \theta + \bar{e} \sin \theta) - \sin^2 \theta]^{3/2}} d\theta \\ &+ \frac{{}_1\theta_{cr}^P}{\sqrt{2p(1 - \cos {}_0\theta_{cr} + \bar{e} \sin {}_0\theta_{cr}) - \sin^2 {}_0\theta_{cr}}}. \end{aligned} \quad (\text{C.35})$$

Note that ${}_1\theta_{cr}^P$ is a function of parameters related to the “undamped system” parameters only. The same holds true for ${}_1\tau_{0_{cr}}$.

The governing equations for finding critical conditions in the presence of small damping ($\bar{\mu} \ll 1$) are eqs. (C.26), (C.27), (C.34), and (C.35). Note that eq. (C.31) is employed in eq. (C.27). These four equations relate the given small damping coefficient $\bar{\mu}$, the applied load p , the time parameters ${}_0\tau_{0_{cr}}$ and ${}_1\tau_{0_{cr}}$, and the position parameters ${}_0\theta_{cr}^P$ and ${}_1\theta_{cr}^P$. A critical condition is expressed in terms of a load level p and the corresponding time, $\tau_{0_{cr}} = {}_0\tau_{0_{cr}} + \bar{\mu}_1 \tau_{0_{cr}}$. Thus, a critical condition may be found by posing the problem as follows: for a given small damping coefficient $\bar{\mu}$ and load level p , find (through the simultaneous solution of the four governing equations) the corresponding critical time parameters, ${}_0\tau_{0_{cr}}$, and ${}_1\tau_{0_{cr}}$, and position parameters, ${}_0\theta_{cr}^P$ and ${}_1\theta_{cr}^P$. Note that the range of p values (assigned) must be greater than the dynamic critical load values for the case of a suddenly applied constant load of finite duration, without damping. The computational procedure involves the following steps: (1) assign a p value and compute ${}_0\theta_{cr}^P$ from eq. (C.26), (2) employ eq. (C.31) in eq. (C.27) and solve for ${}_1\theta_{cr}^P$, (3) from eq. (C.34) solve for ${}_0\tau_{0_{cr}}$, and finally (4) employ eq. (C.35) and solve for ${}_1\tau_{0_{cr}}$.

A simple computer program can be written to accomplish a solution. Numerical results are generated for three values of the eccentricity parameter \bar{e} (0.005, 0.010, and 0.020). These results are presented in Table C.2.

Note that, since a critical condition corresponds to a set of $p, \tau_{0_{cr}}$ values, a small damping coefficient $\bar{\mu}$ has a stabilizing effect. This effect though, is very small. For instance, at the high values of the load p (say for $\bar{e} = 0.005$, $p = 10$) the corresponding value for $\tau_{0_{cr}}$ (if $\bar{\mu} = 0.04$) is $0.16 + 0.0064 = 0.1664$. Remember that the $p-\tau_{0_{cr}}$ curve for the undamped system (see Figure 3.5) is very steep at the high p value and virtually flat at the low value of p . On the other hand, when $p = 0.95$ (a value close to $p_{cr_\infty} = 0.948$), the corresponding critical time is $\tau_{0_{cr}} = 1.93 + 0.005 = 1.985$. Since the curve is

TABLE C.2. Critical conditions for constant load of finite duration in the presence of damping (model B).

\bar{e}	p	${}_0\tau_{0\text{cr}}$	${}_1\tau_{0\text{cr}}$
0.005	0.95	1.930	1.39
	1.20	1.280	1.04
	1.50	0.750	0.80
	5.00	0.230	0.27
	10.00	0.160	0.16
	100.00	0.029	0.04
	0.01	1.15	1.220
		1.70	0.650
		5.00	0.270
		10.00	0.180
0.02	20.00	0.110	0.07
	100.00	0.024	0.06
	0.02	1.10	0.780
		1.50	0.460
		5.00	0.160
		10.00	0.092
		30.00	0.048
		75.00	0.022
			0.02

very flat at this load p value, one may conclude that the effect of small damping is virtually negligible.

C.5 Application to Model C

In this article, the effect of small damping on a two-degree-of-freedom model (model C) is investigated. Damping is introduced through a dashpot connected with the extensional spring, as shown on Figure C.3. The damping coefficient is denoted by μ .

The contraction in the spring (and dashpot) is given by

$$w^* = L(\cos \theta - \cos \alpha + \cos \phi - \cos \alpha - [1 - \cos \psi]).$$

For small angles θ and ϕ and in a nondimensionalized form, the expression for w^* becomes [use of eq. (54) of Chapter 2 was made]

$$w = w^*/L\bar{\beta} = \Lambda - r^2 - 3s^2. \quad (\text{C.36})$$

The rate of change of w is then given by

$$\frac{dw}{d\tau} = -2\dot{r}r - 3\dot{s}s. \quad (\text{C.37})$$

If

$$\bar{\mu} = \frac{1}{(\bar{\beta}_k/2m)^{1/2}k}\mu$$

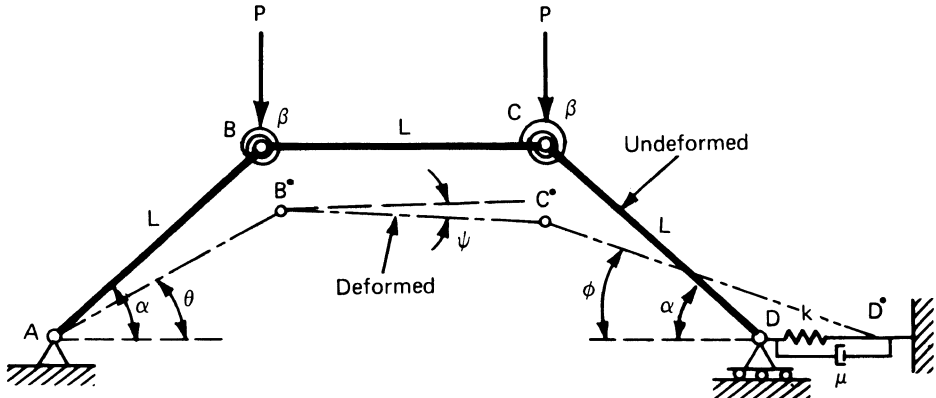


FIGURE C.3. Geometry of model C, including damping.

is the nondimensionalized damping coefficient, and \bar{D} , the nondimensionalized dissipated energy, then

$$\bar{D} = \bar{\mu} \int \frac{dw}{d\tau} dw, \quad (\text{C.38})$$

and with the right-hand sides of eqs. (C.36) and (C.37), the nondimensionalized dissipated energy becomes

$$\bar{D} = \bar{\mu} \oint (2\dot{r}\dot{r} + 6\dot{s}\dot{s})(2r dr + 6s ds) \quad (\text{C.39})$$

where \oint stands for the line integral along the trajectory of the system in the $r-s$ plane. Furthermore, the lowest-potential unstable equilibrium position of the zero-load potential is the saddle point with

$$\bar{U}_T^0 = \frac{9}{2}(\Lambda - 1). \quad (\text{C.40})$$

Recalling that for the undamped system the trajectory which must be followed for maximizing the added energy when p is acting lies on the r axis, and recalling eq. (C.10) it is found that

$$_0 r_{cr}^P = \frac{9}{4p}(\Lambda - 1) + \sqrt{\Lambda}. \quad (\text{C.41})$$

However, the trajectory that the system follows from the release of the load until it reaches the unstable saddle point ($r = \sqrt{\Lambda} - \frac{3}{2}$, $s = \pm [\sqrt{\Lambda} - \frac{7}{4}]^{1/2}$) is not known. Since eq. (C.39) gives the dissipated energy during this period of time as

$$\bar{D} = \bar{\mu} \oint_{_0 r_{cr}^P}^{\sqrt{\Lambda} - 3/2} (2r + 6s)^2 \dot{r} dr$$

where the prime denotes differentiation with respect to r . A lower bound for the absolute value of \bar{D} may be found if one considers the path, $s \equiv 0$, for $\sqrt{\Lambda} - \frac{2}{3} \leq r < \sqrt{\Lambda}$. Note that $r = \sqrt{\Lambda}$ is the starting point and $r = \sqrt{\Lambda} - \frac{3}{2}$ is the r coordinate of the saddle point on the zero-load potential.

Following the same steps as in the brachistochrone problem (see Appendix B), it is proved that the symmetric path $s = 0$ is the minimizing path. Then from eq. (C.11)

$${}_1r_{\text{cr}}^P = -\frac{1}{2p} \int_{\sqrt{\Lambda}}^{\sqrt{\Lambda}-3/2} 4\dot{r}r^2 dr \quad (\text{C.42})$$

where ${}_1r_{\text{cr}}^P$ is the parameter shown in the equation

$$r_{\text{cr}}^P = {}_0r_{\text{cr}}^P + \bar{\mu} {}_1r_{\text{cr}}^P + O(\bar{\mu}^2). \quad (\text{C.43})$$

Furthermore, recalling that the total energy for the undamped system, along the r axis ($s = 0$), is expressed by

$$\frac{1}{2}(\dot{r})^2 + (r - \sqrt{\Lambda})^2 + \frac{1}{2}(\Lambda - r^2)^2 - 2p(\sqrt{\Lambda} - r) = 0, \quad (\text{C.44})$$

then

$$\dot{r} = \sqrt{4p(\sqrt{\Lambda} - r) - (\Lambda - r^2)^2 - 2(r - \sqrt{\Lambda})^2}. \quad (\text{C.45})$$

Hence, eq. (C.42) becomes

$$\begin{aligned} {}_1r_{\text{cr}}^P &= -\frac{2}{p} \int_{\sqrt{\Lambda}}^{{}_0r_{\text{cr}}^P} r^2 \sqrt{4p(\sqrt{\Lambda} - r) - (\Lambda - r^2)^2 - 2(r - \sqrt{\Lambda})^2} dr \\ &\quad - \frac{2}{p} \int_{{}_0r_{\text{cr}}^P}^{\sqrt{\Lambda}-3/2} r^2 \sqrt{4p(\sqrt{\Lambda} - r) - (\Lambda - r^2)^2 - 2(r - \sqrt{\Lambda})^2} dr. \end{aligned} \quad (\text{C.46})$$

In addition, the critical time τ_0 may be found by invoking eq. (C.3), which expresses the balance of energy for $0 < \tau < \tau_0$. Thus,

$$\tau_{0,\text{cr}} = \int_{\sqrt{\Lambda}}^{{}_0r_{\text{cr}}^P} \frac{dr}{\sqrt{4p(\sqrt{\Lambda} - r) - (\Lambda - r^2)^2 - 2(r - \sqrt{\Lambda})^2 - 8\bar{\mu} \int_{\sqrt{\Lambda}}^r \dot{x}x^2 dx}}, \quad (\text{C.47})$$

and expanding τ_0 in power series of $\bar{\mu}$ ($\bar{\mu} \ll 1$), one may write

$${}_0\tau_{0,\text{cr}} = {}_0\tau_{0,\text{cr}} + \bar{\mu} {}_1\tau_{0,\text{cr}} + O(\bar{\mu}^2) \quad (\text{C.48})$$

where

$${}_0\tau_{0,\text{cr}}^P = \tau_{0,\text{cr}}|_{\bar{\mu}=0} = \int_0^{{}_0r_{\text{cr}}^P} \frac{dr}{\sqrt{4p(\sqrt{\Lambda} - r) - (\Lambda - r^2)^2 - 2(r - \sqrt{\Lambda})^2}} \quad (\text{C.49})$$

and

$$\begin{aligned} {}_1\tau_{0_{cr}} = \frac{\partial \tau_{0_{cr}}}{\partial \mu} \Big|_{\bar{\mu}=0} &= \int_{\sqrt{\Lambda}}^{{}_0r_{cr}^P} \frac{8 \int_r^{{}_0r_{cr}^P} x^2 \sqrt{4p(\sqrt{\Lambda}-x) - (\Lambda-x^2)^2 - 2(x-\sqrt{\Lambda})^2} dx}{[4p(\sqrt{\Lambda}-r) - (\Lambda-r^2)^2 - 2(r-\sqrt{\Lambda})^2]^{3/2}} dr \\ &- \frac{{}_1r_{cr}^P}{\sqrt{4p(\sqrt{\Lambda}-{}_0r_{cr}) - (\Lambda-{}_0r_{cr}^2)^2 - 2({}_0r_{cr} - \sqrt{\Lambda})^2}}. \end{aligned} \quad (C.50)$$

Note that ${}_1r_{cr}^P$ is a function of undamped-system parameters only. The same holds true for ${}_1\tau_{0_{cr}}$.

The governing equations for finding critical conditions in the presence of small damping ($\bar{\mu} \ll 1$) are eqs. (C.41), (C.46), (C.49), and (C.50). These four equations relate the given small damping coefficient $\bar{\mu}$, the applied load p , the time parameters ${}_0\tau_{0_{cr}}$ and ${}_1\tau_{0_{cr}}$, and the position parameters ${}_0r_{cr}^P$ and ${}_1r_{cr}^P$.

TABLE C.3. Critical conditions for constant load of finite duration in the presence of damping (model C).

Λ	p	${}_0\tau_{0_{cr}}$	${}_1\tau_{0_{cr}}$
5.0	4.15	1.320	79.66
	4.20	1.290	33.11
	4.30	1.130	16.50
	5.00	0.780	4.12
	8.00	0.390	1.10
	10.00	0.320	0.74
	30.00	0.110	0.10
	70.00	0.410	0.03
	100.00	0.290	0.02
6.0	5.25	1.700	131.11
	5.50	1.520	5.12
	7.00	0.600	2.94
	10.00	0.390	1.57
	12.00	0.340	0.78
	20.00	0.180	0.31
	30.00	0.130	0.16
	50.00	0.078	0.06
	80.00	0.042	0.03
	7.75	0.710	56.31
8.0	8.50	0.650	6.12
	9.00	0.550	4.34
	15.00	0.230	0.99
	20.00	0.210	0.68
	30.00	0.140	0.34
	50.00	0.089	0.11
	80.00	0.052	0.05
	150.00	0.018	0.01

A critical condition is expressed in terms of a load level p and the corresponding time, $\tau_{0,cr} = {}_0\tau_{0,cr} + \bar{\mu} {}_1\tau_{0,cr}$. Thus, a critical condition may be found by posing the problem as follows: for a given small damping coefficient $\bar{\mu}$ and load level p , find (through the simultaneous solution of the four governing equations) the corresponding critical time parameters, ${}_0\tau_{0,cr}$ and ${}_1\tau_{0,cr}$, and position parameters, ${}_0r_{cr}^P$ and ${}_1r_{cr}^P$. Note that the range of p values (assigned) must be greater than the dynamic critical load values for the case of a suddenly applied (constant) load of infinite duration, without damping. The computational procedure involves the following steps: (1) assign a p value and compute ${}_0r_{cr}^P$ from eq. (C.41), (2) employ eq. (C.46) and solve for ${}_1r_{cr}^P$, (3) from eq. (C.49) solve for ${}_0\tau_{0,cr}$, and finally (4) employ eq. (C.50) and solve for ${}_1\tau_{0,cr}$.

A simple computer program can be written to accomplish a solution. Numerical results are generated for three values of the parameter Λ ($\Lambda = 5.0, 6.0, 8.0$).

These results are presented in Table C3. Note that, since a critical condition corresponds to a set of $(p, {}_0\tau_{0,cr})$ values, a small damping coefficient $\bar{\mu}$ has a stabilizing effect. This effect, though, is very small. For instance, at the high values of the load p (say for $\Lambda = 5$, $p = 10$), the corresponding value for $\tau_{0,cr}$ (if $\bar{p} = 0.04$) is $0.32 + 0.029 = 0.349$. Remember that the $(p - \tau_0)_{cr}$ curve for the undamped system (see Figure 3.7) is very steep at the high p value and virtually flat at the low values of p . On the other hand, when $p = 4.15$ (a value close to $p_{cr} = 3.71$) the corresponding critical time is $\tau_{0,cr} = 1.32 + 3.18 = 4.50$. Since the curve is very flat at this load value, one may conclude that the effect of small damping is virtually negligible.

References

1. McGill, D.J., and King, W.W. *Engineering Mechanics: An Introduction to Dynamics*. Brooks/Cole Engineering Division, Wadsworth, Inc., Monterey, Calif., 1984.
2. Crafton, P.A., *Shock and Vibration in Linear Systems*. Harper and Brothers, New York, 1961.
3. Scanlan, R.H., and Rosenbaum, R. *Aircraft Vibration and Flutter*. Macmillan, New York, 1951.
4. Herrmann, G. Stability of equilibrium of elastic systems subjected to nonconservative forces. *Appl. Mech. Rev.*, 20, 2, 1967, 103–108.
5. Huang, N.C., and Nachbar, W. Dynamic snap-through of imperfect viscoelastic shallow arches. *J. Appl. Mech.*, 35, 2, 1968, 289–296.
6. Hegemier, G.A., and Tsung, F. Influence of damping on the snapping of a shallow arch under a step pressure load. *AIAA J.*, 7, 8, 1969, 1494–1499.
7. Johnson, E.R. The effect of damping on dynamic snap-through, *J. Appl. Mech.*, 47, 3, 1980, 601–606.
8. Nicholson, D.W. Stable response of nonclassically damped mechanical systems. *Appl. Mech. Rev.*, 40, 6, 1987, 733–740.

Index

- Approaches to dynamic stability**
equations of motion, 6, 38–41
total energy-phase plane, 6, 36–38
total potential energy, 6–20, 24–36,
41–51
- Arches**
arch model, 41–51
critical dynamic loads, 143, 144, 150,
152
dynamic stability analysis
clamped arch, 148–152
effect of static preloading, 140–142
pinned arch, 129–142
historical review, 117
static stability analysis, 118–121
clamped arch, 144–148
pinned arch, 122–129
- Beams**
static beam response, 15, 16
suddenly loaded, 252, 253
- Brachistochrone problem**, 58, 71, 269
- Buckled motion**, *see* Motion
- Buckling**
bifurcational, 10, 16, 45, 110, 115, 253
dynamic, 5, 16, 95, 117
smooth, 95
snap-through, 26, 127, 152, 237
violent, 16, 26
- Columns**
parametric resonance of, 265, 266
suddenly loaded, 253–258
- Conservative forces**, 4
- Conservative system**, 6
- Constant load**
of finite duration, 13, 54, 74, 80, 87,
136
of infinite duration, 5, 10, 29, 35, 38,
39, 48, 73, 79, 86, 129
- Critical loads, dynamic**
minimum guaranteed (MGCL), 5, 9,
31, 35, 47, 48, 50
minimum possible (MPCL), 5, 9, 31,
35, 47, 48, 50
- Critical loads, static**, 33, 45, 109, 111,
127, 128, 147, 148, 169, 222–224
- Cylindrical shells**, *see* Thin cylindrical
shells
- Damping**, 10, 274–287
- Dynamic magnification factor**, 250, 251,
258
- Dynamic stability**
of beams, 252, 253
criteria and estimates, 3–21, 95–100
extension of concepts, 13
of the imperfect column, 253–258
of the mass–spring system, 245–252
of the shallow arch, 117–153
of the shallow spherical cap, 154–175
of simple mechanical models, 24
of suddenly loaded systems, 5
of thin cylindrical shells, 176–244
of the two-bar frame, 101–116
- Finite difference equations**, 209

- Finite duration problems**
 criterion for stability, 54
 low arch results, 136–140
 mechanical model results, 58–67
- Flow-induced vibrations**, 4
- Fluid–structure interaction**, 5
- Flutter (aeroelastic)**, 3
- Frames (two-bar)**
 critical loads, 114
 dynamic analysis, 111–116
 static analysis, 101–111
- Galerkin's procedure**, 195, 198
- Geometric imperfections**, 24, 111, 178, 219, 220, 255
- Ideal impulse**, 5, 6, 26, 33, 36, 45, 72, 78, 85, 132
- Imperfection amplitude**, 219–221, 228
- Imperfection-sensitive systems**, 5, 16, 24, 31, 111, 220–241
- Limit point instability**, 16, 31, 45, 108, 110
- Load eccentricity**, 31, 101
- Mass–spring system**
 dynamic analysis, 245–248
 dynamic stability, 248–252
- Mathieu–Hill equation**, 263
- Mechanical model**
 geometrically imperfect, 24, 58, 73
 load imperfection, 31, 61, 78
 snap-through, 41, 64, 82
- Motion**
 buckled, 7, 9, 11, 13, 27, 38, 51, 97, 116
- escaping**, 9, 16, 20, 34, 38, 95
oscillatory, 20, 97, 99
unbuckled, 7, 27, 38, 54, 68, 97, 99
- Newton's method**, 201
- Nonconservative systems**, 4
- Parametric excitation**, 3, 260, 262
- Parametric resonance**, 3, 20, 260
 of the Euler column, 265
 fundamentals of, 260
 short history of, 262
 of a simple mechanical model, 264
- Shallow spherical caps**
 comparison with other results, 172–174
 dynamic analysis, 167–172
 historical review, 154–156
 static analysis, 156–166
- Stability**
 dynamic, 16, 24, 54, 56, 95
 static, 31, 43
- Static preloading**, 68–91, 140
- Thin cylindrical shells**
 dynamic solution, 218, 219
 mathematical formulation, 177–190
 numerical results
 laminated (dynamic), 240, 243
 laminated (static), 238–241
 stiffened (dynamic), 242
 stiffened (static), 235–237
 unstiffened (dynamic), 222–224, 228, 234, 235, 242
 unstiffened (static), 220–235
 static solution, 190–218